Modeling Alveolar Epithelial Cell Behavior In Spatially Designed Hydrogel Microenvironments

by

Katherine Jean Reeder Lewis

B.A., Whitman College, 2008

M.S., University of Colorado at Boulder, 2012

A thesis submitted to the

Faculty of the Graduate School of the

University of Colorado in partial fulfillment

of the requirement for the degree of

Doctor of Philosophy

Department of Chemical and Biological Engineering

2016

This thesis entitled:
Modeling Alveolar Epithelial Cell Behavior in Spatially Designed Hydrogel Microenvironments
written by Katherine Jean Reeder Lewis
has been approved for the Department of Chemical and Biological Engineering

_____
Kristi Anseth

_____
Stephanie Bryant

Date_____

The final copy of this thesis has been examined by the signatories, and we find that both the content and the form meet acceptable presentation standards of scholarly work in the above mentioned discipline.

IACUC protocol # 1412.01

Abstract

Lewis, Katherine J. R. (Ph.D., Chemical Engineering)
Department of Chemical and Biological Engineering, University of Colorado

Modeling Alveolar Epithelial Cell Behavior in Spatially Designed Hydrogel Microenvironments

Thesis directed by Professor Kristi S. Anseth

The alveolar epithelium consists of two cell phenotypes, elongated alveolar type I cells (AT1) and rounded alveolar type II cells (ATII), and exists in a complex three-dimensional environment as a polarized cell layer attached to a thin basement membrane and enclosing a roughly spherical lumen. Closely surrounding the alveolar cysts are capillary endothelial cells as well as interstitial pulmonary fibroblasts. Many factors are thought to influence alveolar epithelial cell differentiation during lung development and wound repair, including physical and biochemical signals from the extracellular matrix (ECM), and paracrine signals from the surrounding mesenchyme. In particular, disrupted signaling between the alveolar epithelium and local fibroblasts has been implicated in the progression of several pulmonary diseases. However, given the complexity of alveolar tissue architecture and the multitude of signaling pathways involved, designing appropriate experimental platforms for this biological system has been difficult. In order to isolate key factors regulating cellular behavior, the researcher ideally should have control over biophysical properties of the ECM, as well as the ability to organize multiple cell types within the scaffold.

This thesis aimed to develop a 3D synthetic hydrogel platform to control alveolar epithelial cyst formation, which could then be used to explore how extracellular cues influence cell behavior in a tissue-relevant cellular arrangement. To accomplish this, a poly(ethylene glycol) (PEG) hydrogel network containing enzymatically-degradable crosslinks and bioadhesive

pendant peptides was employed as a base material for encapsulating primary alveolar epithelial cells. First, an array of microwells of various cross-sectional shapes was photopatterned into a PEG gel containing photo-labile crosslinks, and primary ATII cells were seeded into the wells to examine the role of geometric confinement on differentiation and multicellular arrangement. Aggregate formation in these microwells motivated us to develop a templating technique to create hollow cyst-like epithelial structures within PEG hydrogels. Photodegradable microspheres were used to form spherical epithelial layers, which were then encapsulated in a PEG hydrogel followed by template erosion with cytocompatible light. With these model alveoli, we investigated the interplay between the epithelium and mesenchyme by co-encapsulating healthy and diseased pulmonary fibroblasts with healthy and diseased epithelial cysts and measuring important cellular behaviors (*i.e.* proliferation, migration, and protein expression). This model of alveolar tissue represents a significant advance in culture platforms available to researchers interested in identifying the mechanisms involved in disease progression and for testing potential therapeutics in a controlled, tissue-appropriate setting.

To Parker James Lewis

Acknowledgements

This thesis would not have been possible without the help and support of so many people. First, I would like to thank my advisor, Kristi Anseth, for her support and guidance over the last five years. I have learned so much from her, and I appreciate her dedication to helping me succeed both academically and personally. Next, I would like to acknowledge the incredible guidance of my collaborator, Vivek Balasubramaniam, who has been an enthusiastic supporter of my research since our very first meeting. I would also like to thank my other committee members, Stephanie Bryant, Joel Kaar, and Jeffrey Stansbury, for their insightful feedback and encouragement.

I have had the pleasure of working with many talented and friendly collaborators, post-docs, graduate students, and undergraduate students during my time here. First, a heartfelt thank you to April Kloxin and Mark Tibbitt who took me under their wing and taught me all about cell culture and hydrogels. Thank you to my undergraduate mentees, Yi Zhao, Laura Stevens, Emi Kiyotake, and Jessica Hall, who performed many of these experiments and showed exceptional dedication and enthusiasm for this research. Thank you to my collaborators at the Anschutz Medical Campus, Sharon Ryan and Greg Seedorf. Thank you to the lab at the University of Queensland, who welcomed me into their group for two months and taught me a completely new skill set: Justin Cooper-White, Nick Glass, Jane Kenna, Li-yen Wong, Clementine Pradal, and Jess Frith. Lastly, thank you to all the Anseth lab members past and present who made this such an enjoyable workplace and helped me figure out this thing called research, especially Cole DeForest, Daniel Alge, Jen Leight, Mellissa Pope, William Wan, Adrianne Rosales, Steven Santana, Joseph Grim, Abby Bernard, Chun Yang, Kyle Kyburz, Emi Tokuda, Kelly Shekiro, and Kelly Mabry.

Finally, I would like to thank my friends and family for their love and encouragement throughout this journey. Thank you to my Boulder friends for being there every step of the way with good food, games, and wine: Kelly and Josh Mabry, Katherine and Will McDanel, Shannon and Matthias Young, Hilary (Marsh) Feier, and Jennie Jorgenson. Thank you to my extended family on both the Reeder and Lewis sides for believing in me and encouraging me to reach my full potential. A big warm thank you goes to my parents, Paul and Rachel Reeder, for all their support over the years and for taking an interest in my research, reading at least the abstract of every paper. Most importantly, I would like to thank my husband, Ryan Lewis, for being my best friend, my travel buddy, my chef, my confidant, my coach, and my rock, especially during this pregnancy. I could not have done this without you.

Contents

Figures

Chapter 1

Introduction and Background

Sections as published in *MRS Bulletin*, **38**, 260-268 (2013)

1.0 Overview

Lung disease and injury affect millions of Americans, many of them with chronic symptoms, and grouped together they are the number three killer in the United States.[1] Stiffening and scarring of lung tissue is a common pathological feature in many of these diseases, including lung cancer and idiopathic pulmonary fibrosis.[2–5] Understanding alveolar morphogenesis and repair mechanisms, as well as the exchange between the mesenchyme and the epithelium during these processes, could lead to valuable discoveries of treatment options for such diseases. Of particular interest to this thesis research is gaining a better understanding of the differentiation process of type II alveolar epithelial cells (ATII) into type I alveolar epithelial cells (ATI) in response to matrix cues, how these cell populations reform after wounding, and how cross talk with fibroblasts during wound repair can lead to diseased phenotypes. Understanding how alveolar epithelial cells respond to environmental cues in the normal and diseased lung may provide important clues in the development of potential therapies to reverse disease or even in the engineering of functional lung tissue.

Culturing alveolar epithelial cells inherently demands a 3D environment to recreate cyst-like structures that are physiologically relevant. Ideally, 3D scaffolds for studying alveolar morphogenesis would allow spatial and temporal control of the matrix structure, as well as the regulated presentation of growth factors and other biochemical cues. While naturally derived gels are the most commonly used substrates for lung epithelial studies *in vitro,* the properties of

these matrices cannot be easily controlled or modified, nor can the identity or amount of proteins within them be precisely defined by the user. Since several environmental signals are important for alveoli formation including extracellular matrix (ECM) proteins, growth factors, and matrix geometry, having precise control over these signals is critical and necessary for understanding essential developmental and restorative cues.

Our laboratory has previously developed poly(ethylene glycol) (PEG)-based, peptide-functionalized hydrogels that can undergo light-mediated or cell-initiated degradation, and can be used to create highly tunable, cytocompatible scaffolds for 3D cell culture. The advantage of these synthetic mimics of the ECM over natural protein matrices is the ability to control precisely the presentation of ECM epitopes, growth factors, and topographies/physical geometries. This thesis employs these photosensitive biomaterials to explore the role of matrix structure and tissue architecture on alveolar epithelial cell differentiation and behavior, both alone and in co-culture with fibroblasts. The overall goal of this work is to develop an *in vitro* model alveoli system in which environmental signals can be varied to explore key processes involved in the transition from healthy to diseased tissue. Specifically, this model facilitates testing of hypotheses about the role of matrix elasticity, composition, and cell-cell signaling on the differentiation and function of lung cells

1.1 Alveolar biology

1.1.1 Alveolar epithelial cells

Lung architecture follows an increasingly complex network of connected tubes starting from a single trachea that branches into bronchi, bronchioles, and finally ends in millions of hollow air sacs called alveoli. The major components of alveolar tissue include the single cell

layer epithelium attached to the basement membrane and surrounded by a fine mesh of capillaries. There are two types of alveolar epithelial cells: ATI cells, which have an elongated morphology, form 95% of the alveolar surface area, and facilitate gas exchange between the lung and the blood stream;[6] and ATII cells, which exhibit a cuboidal morphology, produce lung surfactants, and are the progenitor cells for both the ATII and ATI cell populations in the alveoli (Fig. 1.1).[7,8] There is a fundamental interest in better understanding alveolar homeostasis,[9–12] the interplay between the epithelium and the mesenchyme during lung development[13–15] and wound healing,[16–20] and how these processes might go awry in diseased states.

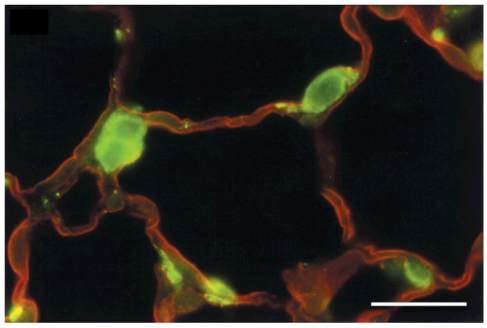

Figure 1.1 Alveolar epithelial cell phenotype arrangement. A rat lung section illustrates that cuboidal ATII cells (surfactant protein D, green) localize to points where neighboring alveoli meet, while ATI cells (*Lycopersicon esculentum* lectin, red) spread out along the curves of the alveolus. Scale bar = 20 μm. Adapted from Reference 8.

Several growth factors and extracellular matrix (ECM) proteins have been implicated in the proliferation and differentiation process during both lung morphogenesis and repair. Throughout early embryonic development soluble signals from the mesenchyme determine the fate of the epithelium with which it is associated, and it was shown that tracheal epithelium can be reprogrammed to express a distal epithelial phenotype by grafting onto distal mesenchyme and vice versa.[13,14,21] In particular, FGF-7 has been shown to be necessary for ATII proliferation, as well as differentiation into and maintenance of the ATII phenotype, both *in vivo* and *in vitro*.[17–19,21,22] It has also been demonstrated that the specific arrangement of ECM proteins, such

as laminin and collagen IV, determine the sites at which ATI and ATII cells localize and may play a role in migration and differentiation.[23,24] Interestingly, the transition of ATII into ATI has proved to be reversible *in vitro*, regulated by culture conditions such as the addition of soluble factors and changes in substrate adhesion proteins.[10,25,26]

1.1.2 Epithelial-to-mesenchymal transition (EMT) in the lung

Epithelial cells are typified by close contacts with neighboring cells and polarization of the epithelial layer through the arrangement of adherens junctions (protein complexes that join neighboring cells' cytoskeletons, located basally) and tight junctions (similar to adherens junctions, but their main function is to provide an impermeable barrier between epithelial cells, located apically). These cells are normally non-migratory and are separated from the surrounding tissue by a thin layer of basement membrane, which is primarily composed of collagen, elastin, and laminin. Mesenchymal cells like fibroblasts, on the other hand, are loosely distributed throughout the 3D ECM bordering the epithelium (Figure 1.2).[11] Epithelial-to-mesenchymal transition (EMT) is the conversion of epithelial cells into a mesenchymal phenotype, which is characterized by the loss of cell junction-associated proteins (*e.g.*, E-cadherin), addition of mesenchymal markers (*e.g.*, vimentin), and often increased motility. EMT is an important

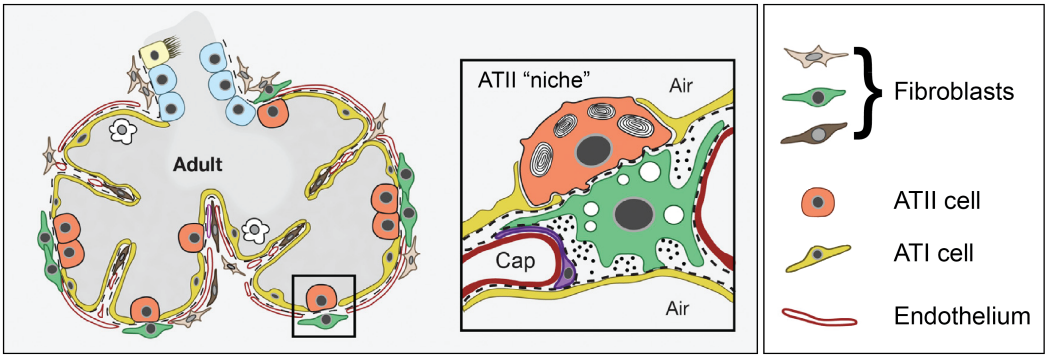

Figure 1.2 Schematic of adult mouse alveoli. The epithelium consists of ATI and ATII phenotype cells attached to a thin basement membrane. Surrounding the epithelium are loosely distributed fibroblasts as well as capillary endothelial cells. In the ATII cell niche, gaps in the basement membrane allow for direct contact with fibroblasts. Adapted from Reference 11.

mechanism in normal organ development and wound repair processes; however, misregulation of EMT can lead to pathological conditions like tissue fibrosis and cancer metastisis.[27]

One prominent disease of alveolar tissue is idiopathic pulmonary fibrosis (IPF), which is characterized by an increase in activated fibroblasts (*i.e.*, myofibroblasts) that lay down connective tissue, such as collagen, that results in stiffening of the tissue and destruction of normal alveolar architecture.[2] Growing evidence suggests that abnormal communication between pulmonary fibroblasts and the alveolar epithelium causes this increase in myofibroblasts, although it is still unknown what percentage of these activated fibroblasts comes from recruitment of local fibroblasts by the epithelium and how much EMT contributes to this pool (Figure 1.3).[2,27,28] Recent studies have recognized the importance of mesenchymal-epithelial crosstalk in IPF pathophysiology and have identified alterations in gene expression between normal and IPF fibroblasts.[20,29]

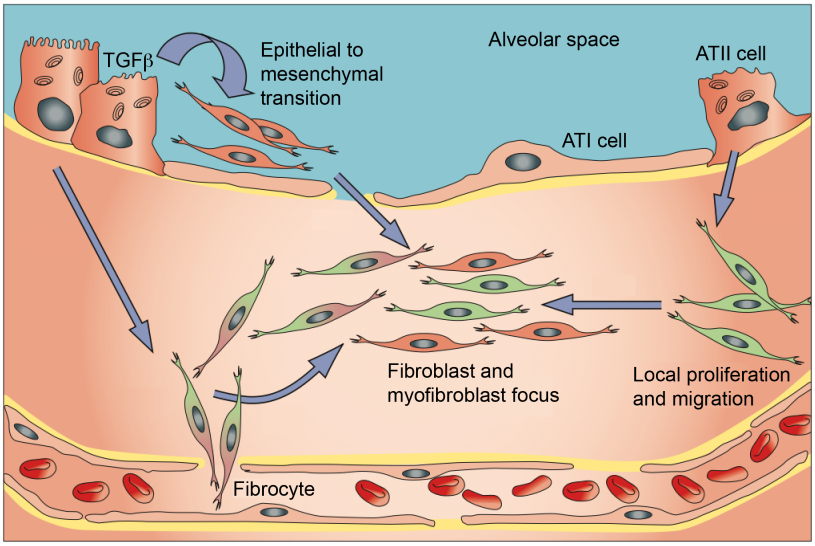

Figure 1.3 Potential sources of myofibroblasts during idiopathic pulmonary fibrosis development. Activated alveolar epithelial cells secrete chemotactic and mitogen growth factors, which induce recruitment of circulating mesenchymal cells (fibrocytes) from the peripheral blood to the wound site, as well as migration and proliferation of resident fibroblasts. In addition, factors such as TGFβ may stimulate epithelial-to-mesenchymal transition (EMT) of the alveolar epithelium. Clusters of fibroblasts (foci) differentiate to myofibroblasts, which are more aggressively profibrotic. Adapted from Reference 2.

EMT also plays a key role in cancer progression, allowing tumor cells to detach from the main tumor, migrate into the surrounding stroma, and eventually enter the bloodstream leading to metastases into other organs (Figure 1.4).[27,30] The tumor microenvironment has been shown to be a key regulator in tumor formation and invasion, and several studies have begun to tease out the signaling pathways between pulmonary fibroblasts and lung cancer cells.[3,4,31–33] For example, a lung adenocarcinoma cell line, A549, has been shown to increase alpha smooth muscle actin (α-SMA) expression in normal fibroblasts, indicating activation to the myofibroblast phenotype.[31] Tumor cells can also cause fibroblasts to increase their matrix metalloproteinase

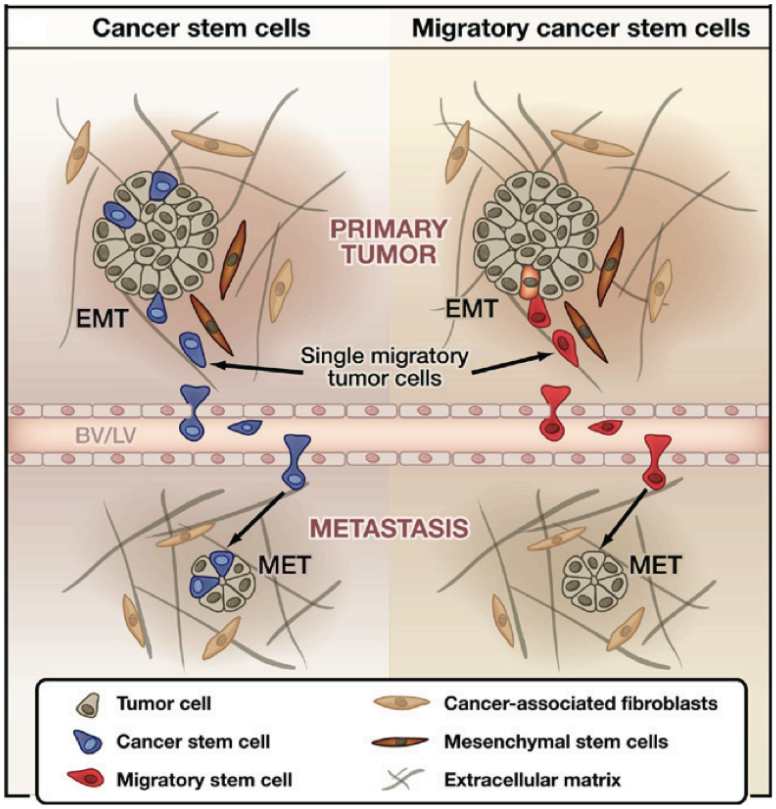

Figure 1.4 Tumor progression and metastasis formation may depend on epithelial-to-mesenchymal transition (EMT). During metastasis, single cells detach from the main tumor and migrate along the extracellular matrix to the blood stream or lymph vessel (BV/LV). Active research is investigating the contributions of cancer-associated fibroblasts to inducing this event. An ongoing question is whether the migratory cells arise from cancer stem cells (blue cells) or somatic epithelial tumor cells that have undergone EMT (red cells). Adapted from Reference 27.

(MMP) production, which in turn can influence matrix remodeling and tumor invasion.[3] In addition, paracrine signaling from cancer-associated fibroblasts can cause an increase in epithelial tumor proliferation, migration, and even drug resistance.[4,33]

1.2 Previous alveolar *in vitro* models

Over the last forty years, the development of effective procedures for isolating nearly pure populations of primary ATII cells[34] has led to numerous methods for culturing these cells *in vitro*. Much of the *in vitro* work with alveolar epithelial cells has been done as 2D monolayers grown on protein-coated substrates that are unphysiologically stiff, such as glass coverslips,[24] tissue culture polystyrene (TCPS),[35] and transwell membranes,[36] but in some reports they have also been seeded on top of soft gels of ECM-derived proteins.[18,25,37,38] While 2D studies have demonstrated the tendency for ATII cells to differentiate into ATI-like cells within 3-5 days of culture,[25] this work has provided valuable information about matrix interactions, such as important ECM binding peptides.[37] Furthermore, 3D tissue structure has been shown to be important to normal cellular function.[39–41] Therefore, encapsulating cultured alveolar epithelial cells within ECM-mimicking scaffolds is required if one wishes to more closely recapitulate the fully 3D nature of the cyst-like alveolar structure and its environment.

Previous 3D cultures of alveolar epithelial cells have primarily made use of naturally derived gels, such as type I collagen[42,43] and Matrigel,[39,44] a basement membrane produced by Engelbreth-Holm-Swarm (EHS) mouse cancer cells. These studies have demonstrated the ability of cultured ATII cells to spontaneously form alveolus-like structures consisting of a central hollow cavity (a lumen) surrounded by polarized cells exhibiting microvilli on the cell surface facing the lumen (apical side), resembling native lung tissue (Figure 1.5).[39,42–44] The addition of

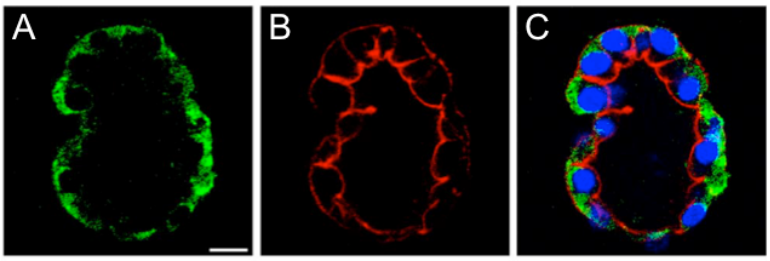

Figure 1.5 Spontaneous cyst formation of human primary ATII cells when cultured in Matrigel for 5 days. (a) Green immunostaining for surfactant protein C. (b) Red staining for actin with phalloidin. (c) Merged image of a and b with nuclei stained blue with Hoechst. Scale bar = 10 μm. Adapted from Reference 44.

growth factors (*e.g.*, FGF-7 and FGF-10) to the culture medium induced proliferation, sacculation, and branching of the alveolus-like epithelial structures within these gels.[39,43] One study compared rat ATII cells cultured on human lung alveolar matrix to those cultured on amniotic basement membrane, and results demonstrated that different basement membranes provide significantly different signals to cells that direct different phenotype expression.[45] This finding highlights the primary difficulty when using naturally derived matrices for studying the effects on ATII cells of growth factors, ECM proteins, and other biochemical cues already present in these substrates.

Ideally, an *in vitro* scaffold should provide the user with the ability to modulate the presentation of biochemical and physical signals in space and time, and this control enables highly defined experiments to elucidate the effect of each individual cue on cell phenotype and function. Using a metastatic lung carcinoma cell line, which is genetically quite different from healthy ATII cells, one group was able to demonstrate spontaneous cyst formation in a photopolymerized, enzymatically-degradable PEG-acrylate hydrogel.[46] However, alveolar cyst formation with primary cells has not been accomplished within synthetic hydrogels, where the researcher has a high level of control over matrix properties and biochemical signaling. Instead,

the field is left with the natural matrices and 'watching' spontaneous evolution of cysts for their primary cell culture methods.

With this motivation, numerous groups are interested in developing more physiologically relevant models for culture of alveolar epithelial cells, especially in the context of culture with other lung cells. In one example, Carterson, *et al.,* employed an interesting technique by growing A549 cells, a human adenocarcinoma cell line with similarities to the ATII phenotype, on commercial microcarrier beads in suspension culture in a rotating wall vessel reactor to create a 3D alveolar cyst model.[47] While the method is robust, the end result is a cyst that polarizes the epithelium with the basolateral side facing in towards the sphere and the apical side facing out towards the medium, thus inverting the typical hollow cyst architecture. While the approach enables easy access to the apical surface, it limits the researchers ability to modify the matrix properties of the adhesive surface and does not allow for co-cultures with cell types found on the basolateral side of the epithelium, such as fibroblasts and endothelial cells.

1.3 Hydrogel scaffolds as models to study cell biology in four dimensions

Hydrogels represent a robust material system for answering fundamental biological questions relating to three-dimensional cell culture and have been especially effective in investigating the question: How do cells receive and exchange information with their extracellular environment? In living tissues, cells are surrounded by an extracellular matrix (ECM), a network of various protein fibers (e.g., collagen and fibrin) interlaced with glycosaminoglycan chains that provide support and signaling essential for proper development and maintenance of the tissue. The native ECM is actively involved in providing cues that influence cellular processes; for example, adhesion proteins bind to cell-surface receptors that

prevent cell death,[48] facilitate attachment,[49] and influence motility[50] in a manner that depends on their concentration and composition (Figure 1.6).[51] In addition, the ECM serves as a reservoir for important cytokines and chemokines, often sequestering growth factors in both latent and active forms.[52] Rapid proteolytic release and activation of these factors enables localized signaling that is important in promoting wound healing, dictating development, or even furthering cancer progression.[53–55] From a general perspective, the ECM is enzymatically degradable to allow for local cellular remodeling.[56] These proteinaceous matrices have a high water content and resist mechanical stresses, both of which are properties thought to influence chemical signaling between and within cells through mechanotransduction and diffusion of paracrine, autocrine, and hormone signaling molecules.[57]

More recent work has focused on de-convoluting the complex roles that mechanical and chemical signals play in dictating cellular development. Diverse tissues in the body have an ECM environment with different compositions and different stiffnesses. For example, the

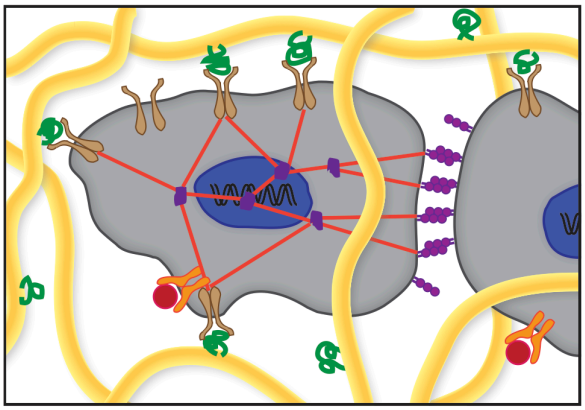

Figure 1.6 Schematic of cells within a native extracellular matrix (ECM). Cells (grey) bind specific ECM proteins (green) with cell-surface receptors, such as integrins (brown), to form adhesions important in cell viability, migration, and mechanotransduction. Cell-cell junctions (purple) in addition to cell-ECM adhesions allow the cell to feel mechanical forces in its environment through cytoskeletal stress fibers (red). The ECM is also a reservoir for important soluble cytokines and chemokines (red), which bind to specific cell-surface receptors (orange). The structural fibers of the ECM (yellow) can be cleaved by proteinases secreted by the cells, allowing for localized matrix remodeling. Adapted from Reference 51.

elasticity of various mammalian tissues ranges from about 10 Pa in soft tissues, such as the brain, up to hundreds of kPa in cartilage.[58] The mechanical properties of the surrounding cellular environment have been shown to greatly influence cell fate. For example, matrix elasticity is known to affect cytoskeletal tension, which can translate to intracellular signals and has been shown to direct stem cell differentiation.[59] In addition, tumor microenvironments are often described as much stiffer than healthy tissue, a fact supported by the familiar cancer screening technique of inspection for a hard mass within a compliant tissue. In a striking example of mechanical signaling, mammary epithelial cells cultured on substrates with an elastic modulus comparable to that of malignant breast tissue took on cancer-like traits, whereas soft substrates promoted normal tissue growth.[60] Clearly, there is much still to be learned about mechanotransduction processes and how mechanical and chemical cues work in concert to regulate cell function and fate, and the design of tunable material culture systems will be important in advancing the field.

Animal models have provided an important approach to test some of these complex signals and can illuminate the effects of the introduction of small molecules or macromolecular signals in the context of the entire body. This approach can be particularly useful, for example, in the drug development process when potential damage to off-target organs needs to be discovered. For fundamental research, however, animal models have the obvious drawback of being complicated systems with countless signaling pathways, redundancies, and environmental influences that can confound experimental variables. Therefore, many studies *in vitro* have aimed to mimic aspects of the native ECM, creating more biologically relevant models, through the use of natural and synthetic hydrogels.[61,62] At the most basic definition, hydrogels are three-dimensional networks of hydrophilic polymers that are rendered water swellable, but insoluble,

because of chemical or physical interactions between the polymer chains. The high water content imparts tissue-like elastic properties and facilitates rapid transport of small molecules, as well as gradients in cell-secreted growth factors and matrix molecules.[63]

From the applied perspective, gels used for three-dimensional cell culture *in vitro* should allow for cell migration, matrix degradation, and distribution of evolving tissue. However, numerous challenges with engineering the properties of these hydrogels remain; state-of-the-art tissue-engineered cartilage is still weak and inferior compared to native cartilage, and regenerating complex tissues from multiple cell sources continues to be elusive. Beyond basic structural and mechanical function, it is often challenging to define a minimum functionality for the encapsulating matrix (i.e., decide what chemical signals to include at relevant doses) and to work with cells that must perform metabolic functions. As a result, the field has much to learn, starting with the basic understanding of how cells receive signals from their ECM and progressing toward strategies to dynamically alter this environment in a cellularly appropriate manner. Thus, many research groups are revisiting advances in material science and engineering to develop highly controlled cellular microenvironments to improve our understanding and apply this knowledge toward the manipulation and engineering of critical cellular functions.

Ideally, an *in vitro* scaffold should provide the user with the ability to modulate the presentation of biochemical and physical signals in space and time in order to elucidate the effect of each individual cue, as well as their synergies, on desired cell fates. The following sections illustrate some of our perspectives on critical advances and recent progress toward the development of cytocompatible chemistries and their applications in synthesizing cell-laden material matrices. In a simplified sense, this might be described as understanding biology in four

dimensions, where experimenters control the cellular niche in three-dimensional space *and* the fourth dimension of time.

1.3.1 PEG hydrogels as ECM mimics for cell culture

From a fundamental perspective, synthetic materials provide a basic platform to engineer cell culture matrices with defined mechanical properties, transport properties, and even degradation rates. In such systems, poly(ethylene glycol) or PEG is a frequent choice as the base material for synthetic hydrogel matrices because of its low level of protein adsorption, which prevents nonspecific interactions between cells and the network, providing a "blank slate" that can be easily modified to present chemical and physical cues in a defined manner. For example, the photoinitiated solution polymerization of PEG-diacrylate (PEGDA) in the presence of cells creates a cell-laden network of polyacrylate kinetic chains crosslinked by elongated PEG chains (Figure 1.7a-b).[64] Cytocompatible reaction conditions and monomer formulations have been identified for PEGDA hydrogels, which enable both 2D culture on preformed materials as well as 3D encapsulation and cell culture within a minimal ECM.[65,66]

While synthetic systems, such as crosslinked PEG, have numerous advantages, a major limitation of this material chemistry is the lack of biochemical signals that cells recognize. Thus, encapsulated cells generally adopt a rounded morphology (Figure 1.7c), and tissue engineering approaches rely on the ability of cells to rapidly and appropriately remodel their local matrix environment. Such minimal systems are permissive to cell function and can be suitable for the long-term culture of cells with low metabolic activities or a natural rounded morphology (e.g., cartilage cells, aka chondrocytes[64,67]) or alternatively when one wishes to promote cell-cell interactions (e.g., islets[68], neurospheres[69]). However, a significant drawback of purely synthetic

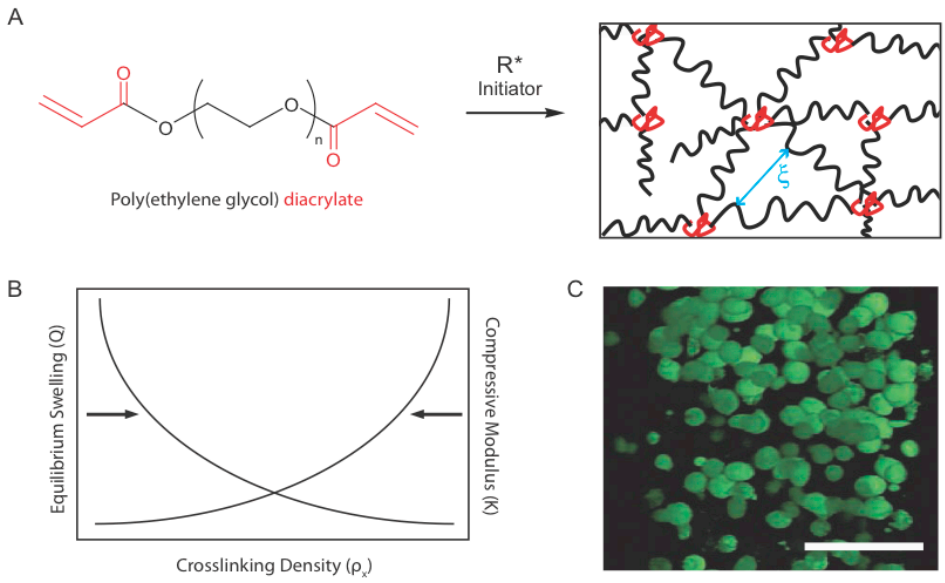

Figure 1.7 (a) Poly(ethylene glycol) diacrylate (PEGDA), of varying number of repeat units (n), can be chain polymerized in the presence of a radical initiator (R*) to form a network of polyacrylate chains (red) crosslinked by PEG (black). Mesh size (ξ) is a measure of the distance between crosslinks and inversely related to crosslinking density. (b) Generic plot showing the relationship between equilibrium swelling and compressive modulus as a function of crosslinking density. As crosslinking density increases, compressive modulus of the hydrogel increases while swelling decreases. (c) Chondrocytes encapsulated within a PEGDA hydrogel, stained with LIVE/DEAD®. Live cells fluoresce green. In this "blank slate" hydrogel, cells do not form attachments to the matrix and maintain a rounded morphology. Scale bar = 50 μm. Adapted from Reference 64.

and non-degradable extracellular matrix analogs is the inability of cells to spread or migrate, which can severely limit the broad utility of such a system.

To enable cell motility through these materials, network crosslinks must be cleaved. As a result, researchers have explored methods to integrate and control degradation in cell-laden matrices. These approaches range from pre-engineered hydrolytic degradation[70–72] to cell-dictated degradation through secretion of enzymes[73,74] to emerging paradigms in user-dictated degradation[75]. Systems that depend on hydrolytic degradation often employ the cleavage of ester bonds, and the rate at which these materials degrade can be tuned to allow for cell proliferation and ECM deposition. The degradation kinetics of ester hydrolysis can be controlled by changing

either the monomer chemistry or the number of cleavable links in the macromolecular backbone.[76] Because of the high water content of hydrogels, the degradation kinetics and mass loss can be engineered to proceed in a predictable and homogeneous manner (i.e., bulk degradation).[77] However, correctly timing the exchange of newly synthesized ECM with the degrading synthetic scaffold requires a precise understanding of both the material degradation kinetics and the rate of tissue deposition, time scales that are not always well-characterized. Therefore, many researchers have moved to enzymatically degradable hydrogels for 3D cell culture, where scaffold degradation is caused by cellular activity (i.e., the production of active proteinases). This localized degradation allows cells to modify and migrate through their immediate surroundings, which limits the need for *a priori* knowledge of the appropriate degradation kinetics. However, in these materials the researcher is a passive observer of cell function and is often unaware of how the material is being altered locally.

While scaffolds with cell-dictated and pre-engineered degradation have certainly provided robust solutions to numerous tissue engineering applications, there has also been an evolution in thought toward the development of material platforms that respond to user-dictated inputs, which enable systematic and external modification of the cellular environment. Such systems allow the experimenter to test how cells react to these dynamic and controlled changes in matrix material properties. These user-controlled techniques are often combined with cell-dictated degradation mechanisms to both observe and manipulate cell function in a more native-like culture environment. Through appropriate chemical modifications, researchers can spatially and temporally vary both biophysical properties (stiffness, shape) and biochemical signals (adhesive ligands, growth factors) incorporated in cellular matrices, progressing the field toward a dynamic niche for culturing encapsulated cells.

1.3.2 User control over environmental signals presented to cells

To provide insight as to how cells respond to specific matricellular cues, researchers have recently pursued ways to actively manipulate the cellular microenvironment.[78] One convenient and versatile method is to initiate chemical reactions with light. A hallmark advantage of photochemical reactions is that they provide the user with precise spatial and temporal control over bond formation and cleavage, allowing for directed network formation and degradation as well as pendant ligand tethering and release. In photoinitiated processes reaction only occurs where light is present. Light can be controlled in space by using standard techniques such as photomasks and focused lasers, and controlled in time by turning the switch on and off. One specific example of a photolabile functionality employed to create cell culture matrices relies on a nitrobenzyl ether moiety (Figure 1.8a) that exhibits high photolytic efficiency.[75]

Acrylated nitrobenzyl ether has been attached to both ends of PEG-*bis*-amine through a pendant carboxylic acid, creating a photocleavable crosslinking molecule, PEGdiPDA (PEG di-photodegradable acrylate, Figure 1.8b). This macromer is readily copolymerized with PEG monoacrylates or other monomers to create photodegradable hydrogels. Upon irradiation with single photon light between 365-420 nm or multiphoton light centered at 740 nm, the ester bond connecting the nitrobenzyl ether to the rest of the network is cleaved, forming a carboxylic acid and a ketone (Figure 1.8c). As the PEGdiPDA segments are detached from the network, the overall crosslinking density decreases until complete degradation is achieved. This process is fully controlled by the intensity and wavelength of light dictated by the photophysical properties of the linker, giving the user spatio-temporal control over gel modulus and network geometry. Figure 1.8d illustrates that irradiating with either a lower intensity of the same wavelength of light *or* with a different wavelength of light that corresponds to a lower molar absorptivity for

nitrobenzyl ether will result in a longer degradation time.[75,79] Network degradation only occurs during exposure to light, so the gel modulus can be softened to a specific value, remaining constant while the light source is shuttered, and then it can be decreased again at a later point in time (Figure 1.8e).

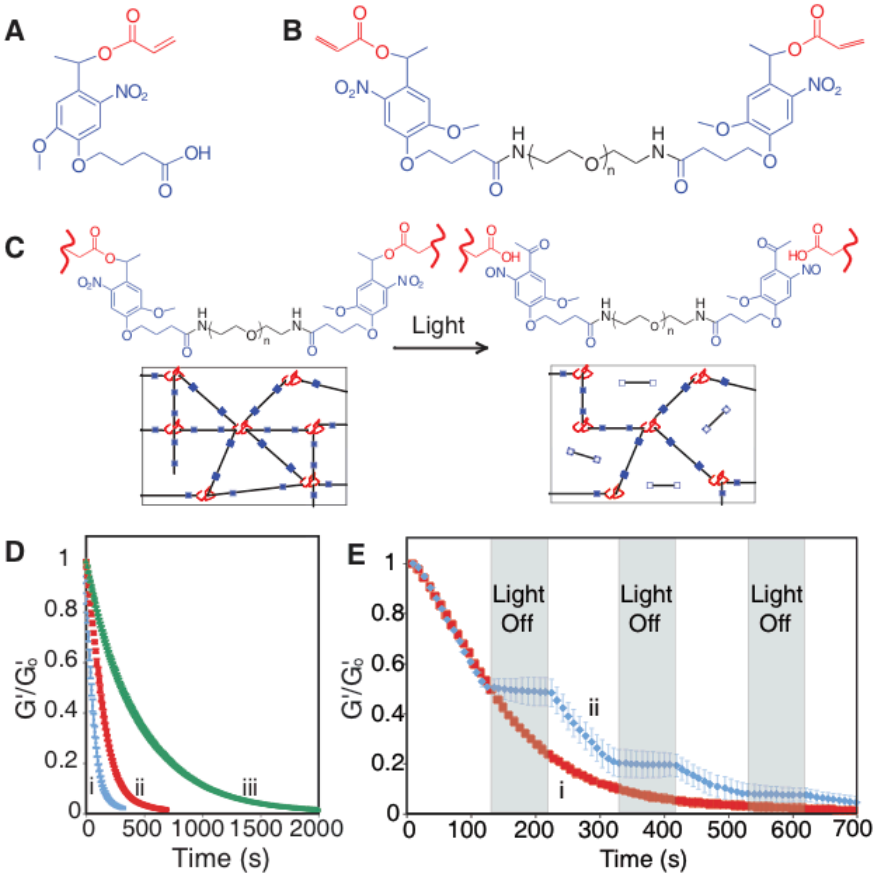

Figure 1.8 (a) Photolabile nitrobenzyl ether acrylic monomer. (b) Poly(ethylene glycol) di-photodegradable acrylate (PEGdiPDA) macromer, composed of PEG (black), photolabile moieties (blue), and acrylate end groups (red), polymerizes to form a gel. (c) Irradiation with specific wavelengths of light cleaves the nitrobenzyl ether moiety, degrading network crosslinks. (d) Wavelength and intensity of the light controls degradation time, as determined by *in situ* rheometry to measure elastic modulus (G') normalized to initial modulus (G'_n), which is directly proportional to crosslinking density. (i) 365 nm at 20 mW/cm^2, (ii) 365 nm at 10 mW/cm^2, and (iii) 405 nm at 25 mW/cm^2. (e) Degradation only proceeds during exposure to light. (i) Continuous or (ii) periodic irradiation with 365 nm at 10 mW/cm^2. Adapted from Reference 75.

This controlled degradation technique has been used to study the differentiation of the resident cell population found in heart valves, valvular interstitial cells (VICs), into activated myofibroblasts, a process that has been shown to be correlated with substrate stiffness.[80–82] VICs become activated from a quiescent fibroblast phenotype to an active myofibroblast phenotype in response to injury, and these activated myofibroblasts assist with the process of wound healing and valve homeostasis. Little is known about the fate of myofibroblasts after healing, but their persistence is often linked to the progression of fibrotic diseases. Since elasticity of the culture platform has been shown to influence VIC activation, matrices that allow fine-tuning of the modulus during culture are uniquely qualified to investigate thresholds and reversibility of activation *in vitro*.

Thus, the light-tunable properties of these PEG materials were harnessed to investigate questions related to the fibroblast-myofibroblast transition in VICs.[83,84] First, it was asked whether there was a critical threshold in matrix elasticity above which VIC activation would be promoted and below which VICs would remain quiescent. By passing a mask over a photodegradable hydrogel during irradiation, a modulus gradient was achieved, in this case ranging from ~7-32 kPa for Young's modulus (Figure 1.9a).[83] VICs were seeded on top of these gradient gels, and after three days, the number of myofibroblasts at each position on the gel was counted, as determined by the presence of α-smooth muscle actin (αSMA) organized into stress fibers (Figure 1.9b). Significantly more cells were activated on the stiff side of the gel than on the soft side, and the activation threshold was determined to be approximately 15 kPa.

While there are numerous materials and approaches to create hydrogels of varying elasticity, either through the preparation of discrete gels or the formation of gradient systems,[85–87] photodegradable gels allow unique experiments to be performed where the gels can be

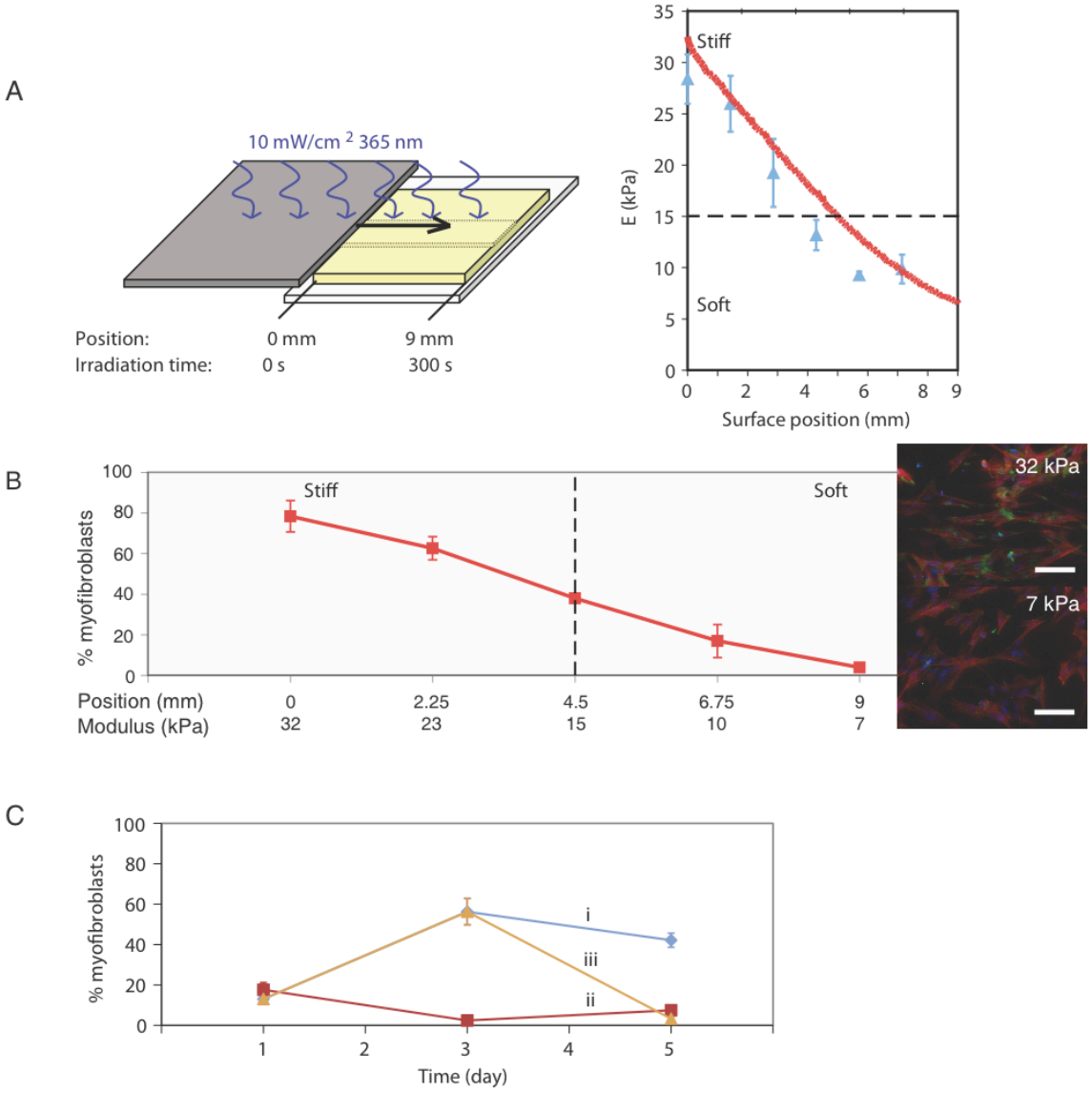

Figure 1.9 Valvular interstitial cell (VIC) activation on gradient and stiff-to-soft gels. (a) Modulus gradient across a gel created by moving a mask over the surface during irradiation (left). Modulus (*E*) measured by atomic force microscopy (blue triangles) and rheometric measurements (red line) as a function of position. (b) The stiff side of the gel promoted VIC activation, whereas cells grown on the soft side remained quiescent on day 3. Percentage of myofibroblasts determined by counting the fraction of cells with α-smooth muscle actin (αSMA) stress fibers, a classic marker for myofibroblasts. Inset: fluorescent images of VICs on stiff (32 kPa) and soft (7 kPa) sides of the gel on day 3, immunostained for αSMA (green), f-actin (red) and nuclei (blue). Scale bar = 100 μm. (c) By softening stiff gels during culture, VICs can be de-activated. (i) 32 kPa "stiff gels", (ii) 7 kPa "soft gels", and (iii) 32 kPa - 7 kPa "stiff-to-soft gels". Adapted from Reference 83.

softened *in situ* and the influence of this softening on cell fate can be observed. Specifically, the cytocompatible nature of the photodegradation reaction was exploited to soften gels that were initially stiff at later time points during culture of VICs to determine if de-activation of the myofibroblast state is possible. VICs cultured on ~32 kPa gels became activated over three days, then were exposed to 365 nm light to soften the underlying gel to ~7 kPa and cultured for another two days (Figure 1.9c). This temporal change in substrate modulus caused de-activation of the myofibroblasts, without cell death[84], highlighting the importance of substrate stiffness in tissue engineering applications and informing strategies for potential therapies to treat fibrosis.

The biomechanics of material culture systems are not the only environmental signals that can be modulated with this user-controlled photodegradable functionality; one can also dynamically present biochemical ligands to cells.[88–90] Typically, the amino acid sequence derived from fibronectin, arginine-glycine-aspartic acid-serine (RGDS), is pendantly incorporated into synthetic matrices to promote cell adhesion and survival.[91–93] However, biochemical signal presentation is not static *in vivo*, and sometimes a ligand used for one purpose can inhibit other important functions. In general, there is a complex exchange of signals between cells and the ECM, and materials-based strategies can be exploited to better understand the influence of key signals on cellular fates.

In vivo, differentiating human mesenchymal stem cells (hMSCs) initially secrete high levels of fibronectin, which is later down regulated between days 7-10 followed by up-regulation of glycosaminoglycans (GAGs), an early marker for chondrogenesis (i.e. differentiation toward cartilage-forming cells, chondrocytes).[94,95] While RGDS is necessary for cell viability in these PEG hydrogels during the first week of culture, the question is whether its persistence is necessary or detrimental after a certain period of time. To provide an illustrative example of

biochemical control of matricellular signaling, pendant peptides (Figure 1.10a, black) were tethered to the hydrogel network through the acrylated nitrobenzyl ether group (Figure 1.10a, blue and red), allowing for removal of the signal at a defined place and time. In this instance, RGDS was attached to a PEGDA hydrogel and photoreleased to study the influence of dynamic RGDS presentation on chondrogenesis of encapsulated hMSCs.[75] When RGDS was photoreleased from the gels on day 10 and diffused out of the network, GAG production was found to increase four-fold over gels persistently presenting RGDS for the full three weeks of culture, indicating a significant increase in an important chondrogenic marker in the photoreleasable gels (Figure 1.10b). This example provides one simple demonstration where the dynamic nature of biochemical signal presentation can be mimicked to influence cellular functions and hints at the potential need for multiple aspects of control over the cell microenvironment for *in vitro* culture systems.

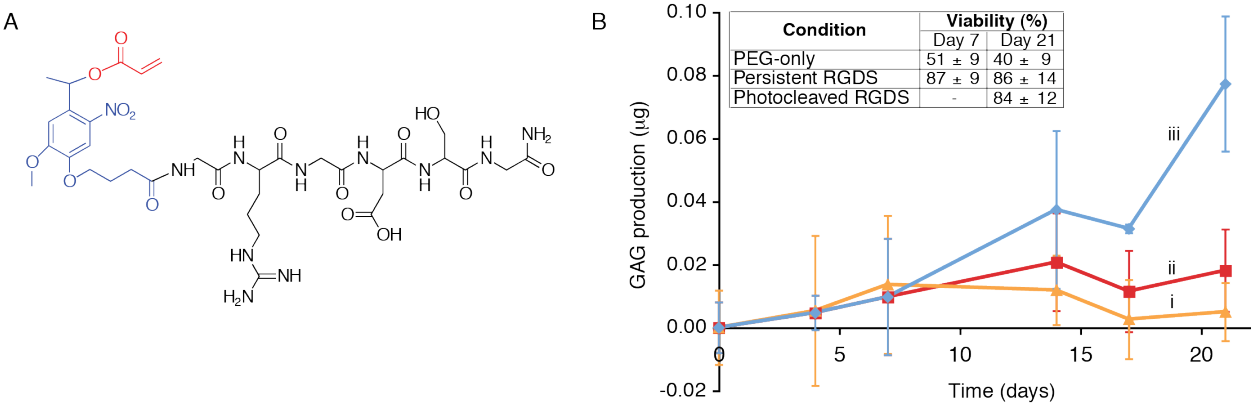

Figure 1.10 (a) Structure of the photoreleasable adhesion peptide monomer, arginine-glycine-aspartic acid-serine (RGDS) in black, photolabile moiety in blue, acrylate in red. (b) RGDS presentation maintains human mesenchymal stem cell viability within PEG-based gels (inset table). A chondrogenic marker (glycosaminoglycan, GAG, production) is increased four-fold by day 21 when the adhesive ligand RGD is photoreleased on day 10. (i) PEG-only gels. (ii) Persistently presented RGDS. (iii) Photolytic removal of RGDS on day 10. Adapted from Reference 75.

1.3.3 Cellular remodeling of their environment

While materials with user-controlled properties are beneficial in performing certain types of experiments, there are many other instances when one may wish to be a passive observer, watching cells in a more physiologically relevant environment. In this case, materials researchers have sought to develop methods to formulate hydrogel environments that promote specific cellular interactions, such as survival cues, degradable sequences, and growth factor binding functionalities. In the context of PEG hydrogels, one way in which a more advanced synthetic ECM can be realized is to apply the cytocompatible, photoinitiated, step-growth, thiol-ene polymerization.[96,97] In this example, a multi-arm PEG-norbornene is reacted with dicysteine-peptide crosslinkers with or without monocysteine-peptide pendant groups (Figure 1.11a-c). This approach exploits certain aspects of the biochemical properties of peptides, as mimics of their full protein counterparts, and builds from the pioneering early work of Hubbell *et al.* to create peptide functionalized PEG hydrogels using a complementary type of step-growth polymerization based on Michael-type addition reactions.[98–101]

As with the PEGDA system, the photoinitiation technique provides both spatial and temporal control over network formation. However, the thiol-ene reaction has the extra advantages of rapid gelation and ideal network formation, maintaining uniform physical properties throughout the gel. Moreover, biochemical signals can easily be tethered to the network through the same thiol-ene reaction between excess PEG-norbornene or other ene functionalities pendant to the PEG backbone and cysteine-containing proteins or peptides either during the initial network formation for uniform signal distribution or in a post-gelation step allowing for spatial patterning within the gel (Figure 1.11d).[96,102] For example, the commercially available protecting group allyloxycarbonyl (alloc) used during peptide synthesis contains a

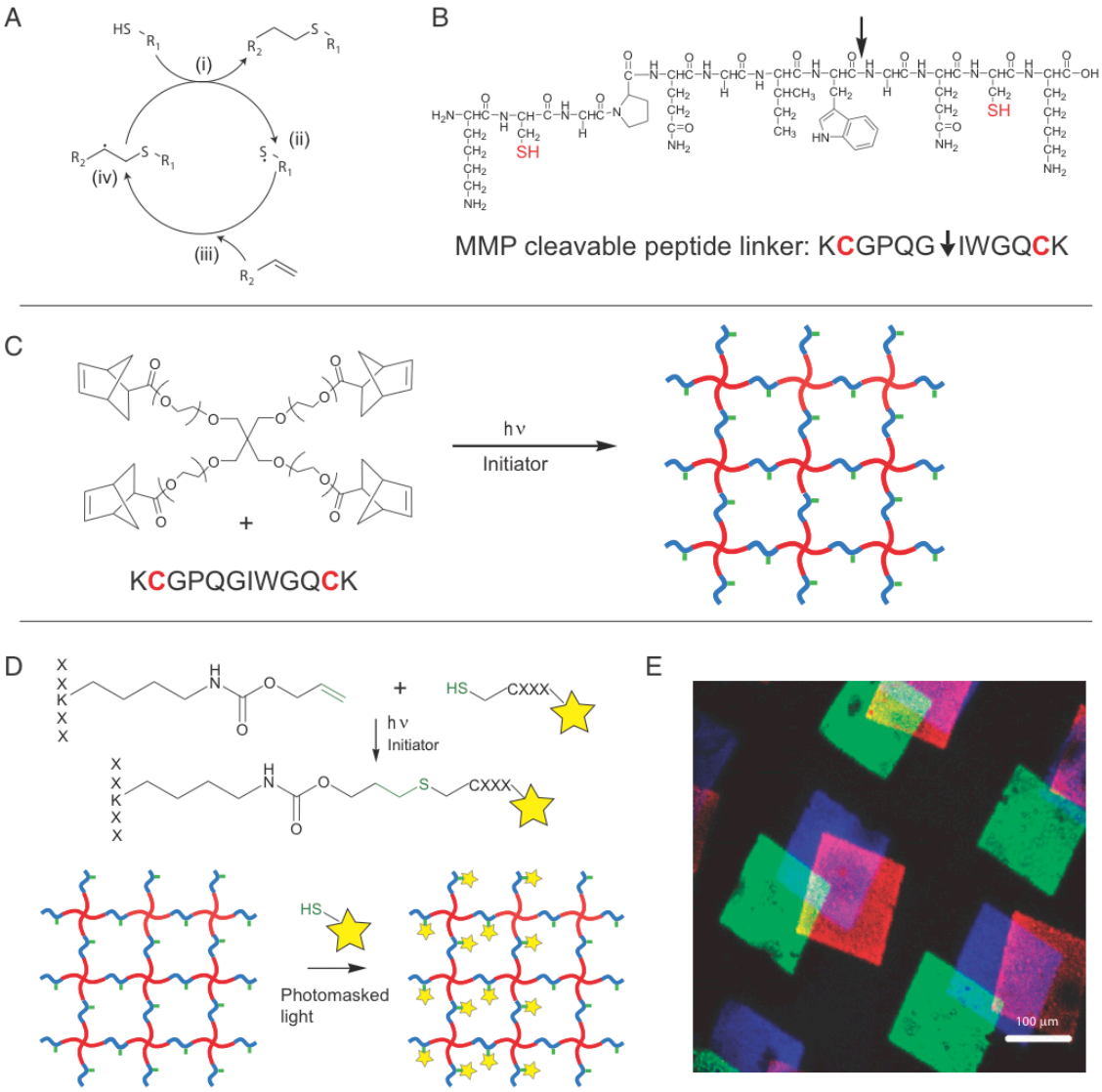

Figure 1.11 (a) Thiol-ene reaction cycle. An initiator abstracts a proton from a thiol (i), forming a thiyl radical (ii), which then reacts with a carbon-carbon double bond (iii). The resulting carbon radical (iv) abstracts a proton from another thiol, completing the thio-ether bond and regenerating a thiyl radical. (b) Di-cysteine polypeptide monomer, chemical structure (top) and amino acid abbreviation (bottom). This sequence, derived from collagen I, is cleavable by cell-secreted matrix metalloproteinases (MMPs), cleavage site indicated by arrow, and is often used as a cellularly degradable crosslinker. (c) PEG-tetranorbornene and di-cysteine peptides react via the thiol-ene reaction cycle to form a step-growth network. Note: PEG (red), peptide crosslinker (blue), pendant peptide (green). (d) Peptide tethering with the thiol-ene reaction. Using photomasked light or focused laser light, cysteine-containing peptides can be covalently attached to pendant ene groups on the polymer network exclusively in user-defined regions. Fluorescent label on pendant peptide is indicated by a star. (e) Three different fluorescently labeled peptides (blue, green, and red) are sequentially attached at user-defined locations and times using photomasks and radical-initiated thiol-ene coupling reactions. Adapted from References 103, 107, and 108.

terminal vinyl group that can be employed as a handle for covalently attaching cysteine-containing peptides to an existing peptide network crosslink post-gelation. Gels are swollen with the desired peptide and a photoinitiator, and then exposed to light. Since radicals are only formed in irradiated areas of the gel, these ligands can be patterned into the gel using a photomask. Typically, low concentrations of pendant peptides are used, leaving plenty of vinyl handles available for the addition of other peptides at later times (Figure 1.11e). In this way the permissive "blank slate" PEG gel becomes a promoting environment, presenting cells with biologically relevant cues from the native ECM and promoting specific cell functions through cell-matrix interactions.

These peptide-functionalized PEG hydrogels are readily tuned to permit cellular remodeling of their surroundings. Specifically, enzymes naturally produced by cultured cells can be exploited to create a flexible milieu in which network crosslinks are locally cleaved. As part of many physiologic and pathologic processes, numerous cell types produce matrix metalloproteinases (MMPs), a family of enzymes that cleave proteins found in the ECM, causing degradation of the matrix and allowing for cell migration and remodeling of the matrix composition or geometry. An oligopeptide sequence derived from collagen I (Figure 1.11b) has been shown to be efficiently cleaved by several MMPs[73] and has been incorporated into hydrogels to facilitate migration of many cell types during 3D cell culture.[103–105] This designer peptide contains a cysteine on one or both ends to enable thiol-ene reactions with ene-functionalized PEG monomers and create enzymatically-cleavable pendant groups or crosslinks. A noteworthy advantage of this thiol-ene reaction is that any cysteine-containing peptide can be used and requires no post-synthetic modifications.

Cells encapsulated within these promoting scaffolds are able to form attachments to the hydrogel network, as integrins found on the cell surface will bind to many peptide sequences. These cell-material interactions allow the cell to adhere and spread (Figure 1.12a), which is very different from cells encapsulated in the PEGDA "blank slate" gels. In addition, enzymatically-cleavable crosslinks allow for local remodeling of the hydrogel matrix, which enables cell migration through the material. Individual cell paths can be tracked using real-time microscopy, and such quantitative data allows researchers to better understand how matricellular cues influence parameters, including cell speed and persistence, both of which are important to fields such as cancer biology and wound healing (Figure 1.12b). Peptide functionalized gels can provide a minimal mimic of the extracellular matrix, and thiol-ene chemistry is one easy avenue to synthesize materials decorated with these biologically functional molecules and represents a significant advance toward more native-like material platforms for culturing encapsulated cells.

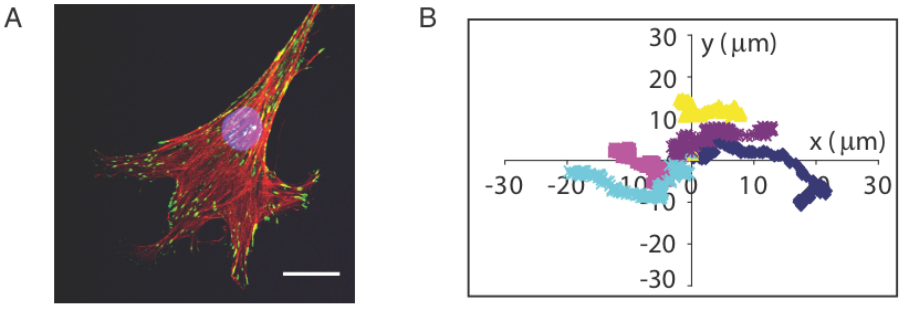

Figure 1.12 Cells attach, proliferate and migrate in MMP-degradable thiol-ene hydrogels. (a) human mesenchymal stem cells exhibit a spread morphology that depends on the degradability and integrin binding motifs in thiol-ene gels. Single cell immunostained for nucleus (blue), actin (red), and vinculin (green, focal adhesions). Scale bar = 25 μm. Image courtesy of Chelsea Kirschner. (b) Plot of five different cell migration paths of valvular interstitial cells encapsulated within the same MMP-degradable gel. When the enzymatically-cleavable crosslink is used for gel formation, cells are able to degrade the surrounding isotropic material and migrate freely in a random walk. Cells were imaged and tracked on a real-time microscope. Adapted from Reference 104.

1.3.4 Sequential and orthogonal reactions create dynamic material niches for 3D cell culture

When combined into one system, the techniques and reactions described previously empower the user to design a highly tunable scaffold for 3D cell cultures that can evolve in real time through both cell- and user-dictated processes (Figure 1.13a-e). Namely, one can envision strategies where one reaction is used to form a cell-laden gel, while bio-orthogonal reactions are used to introduce or remove biochemical signals or to erode the matrix. Bio-orthogonal reactions, which are chemical reactions that do not interfere with native biochemical processes, are of growing interest in numerous applications. Here, we show one recent example where a strain-promoted azide-alkyne cycloaddition (SPAAC) between cyclooctyne-functionalized PEGs and azide-functionalized peptides is used to encapsulate live cells.[106–109] Next, an orthogonal photoinitiated thiol-ene reaction between a cysteine-containing peptide or protein and a pendant ene functionality incorporated in the hydrogel backbone is used to pattern cues in a spatially defined manner.[107–109] Third, enzymatically-cleavable peptides are incorporated to enable cell migration or serve as reporters for local cell behavior.[107] Lastly, the photolabile nitrobenzyl ether moiety described earlier is included to allow user-directed softening or complete degradation of the material upon irradiation.[109]

To demonstrate the potential for this type of multifunctional and responsive material system, two different biochemical cues were sequentially patterned within a gel containing hMSCs to create a three-dimensional culture environment with spatially distinct biochemical regions (Figure 1.14a-b).[109] Later, columns of user-defined cross-section were eroded through the gel with two-photon microscopy to remove cells from selected niches (Figure 1.14c). The recovered cells were then plated, expanded, and further processed to provide more detailed molecular characterization, all processes that are difficult to do in typical three-dimensional

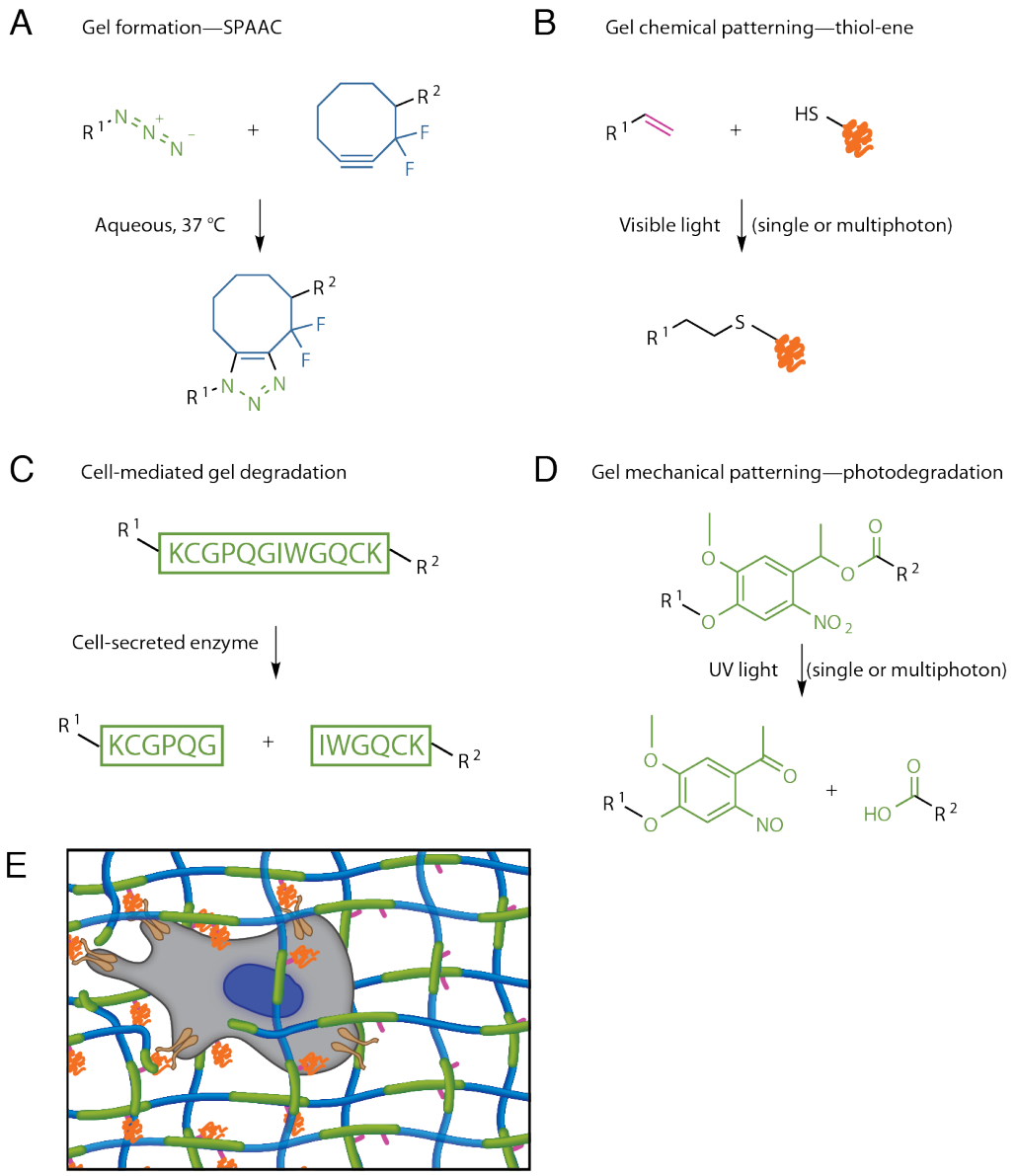

Figure 1.13 Sequential and orthogonal reactions. (a) Gels can be formed via a strain-promoted azide-alkyne cycloaddition (SPAAC) between cyclooctyne-functionalized PEGs (blue) and azide-functionalized peptides (green). (b) Peptide ligands can be patterned into the gel through the photoinitiated thiol-ene reaction between a cysteine-containing peptide (orange) and a free carbon-carbon double bond (pink) from the alloc protecting group located on the peptide crosslinker. (c) By choosing an enzymatically-cleavable peptide sequence for the di-azide crosslinker (green), the gel can be locally degraded by cells. (d) User-dictated degradation can be accomplished by incorporating a photolabile moiety (green) within the crosslinker. (e) In this synthetic scaffold, the cell (grey) can attach to the PEG matrix (blue) through integrins (brown) binding to adhesive peptides (orange), which are covalently linked to the network through a pendant ene functionality (pink) during a post-gelation photoinitiated reaction, enabling spatial patterning of the peptide. Enzymatically-degradable peptide sequences and/or photolabile groups form the crosslinks (green), allowing for cellular and/or user remodeling of the microenvironment. Adapted from Reference 109.

culture.[109] Alternatively, using the same techniques, channels were degraded within SPAAC gels and used to direct fibroblasts and their migration down user-directed paths by patterning the adhesive peptide RGD only in the desired channels (Figure 1.14d).[109] Such advanced patterning in three-dimensions may eventually address technical challenges in guiding formation of complex tissue structure involving multiple cell types.

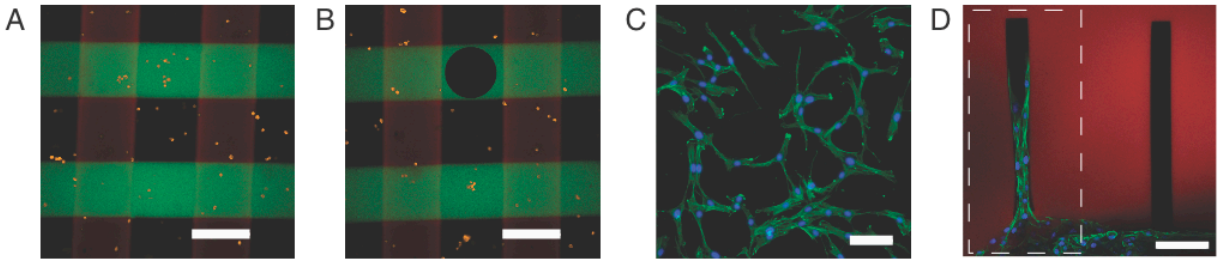

Figure 1.14 (a) Fluorescently-labeled arginine-glycine-aspartic acid-serine-cysteine (RGDSC, green) was swollen into cell-laden gels along with a photoinitiator and exposed to UV light through a photolithography mask, causing radical-mediated addition of a thiol across an olefin and creating stripes of the adhesive ligand in the gel. After swelling in fresh media to remove unreacted RGDSC, fluorescently-labeled proline-histidine-serine-arginine-asparagine-cysteine (PHSRNC, red) was similarly patterned in perpendicular stripes, creating an array of four unique environments in a single cell-laden gel: blank, RGD-only, PHSRN-only, and RGD plus PHSRN. Cells encapsulated within the gel are labeled orange. Scale bar = 200 μm (b) Circle-shaped columns were degraded to remove cells from a certain environmental niche. Scale bar = 200 μm (c) Those cells were then plated on TCPS and grown to show continued viability. Immunostained for F-actin (green) and cell nuclei (blue). Scale bar = 50 μm (d) Fibroblast outgrowth is directed by degrading channels in the SPAAC gel and tethering RGD only in the desired path by using focused laser light only in the channel enclosed by the dotted line. Scale bar = 100 μm Adapted from Reference 109.

1.3.5 Adaptability for studying alveolar tissue structures

By designing poly(ethylene glycol) hydrogel systems with the functionalities described, researchers can easily control and observe cell behavior with precise spatial and temporal resolution. Cytocompatible photochemistries allow the synthesis of versatile 3D cell culture material systems in which users can dictate material stiffness, matrix geometry, and biochemical signal presentation. Employing multiple orthogonal chemistries within a single scaffold greatly

improves our ability to mimic the biophysical and biochemical cues present in the native ECM environment and to study and direct cell function. These dynamic environments have been used to investigate complex biological processes, and are ideally suited to engineering tissue-relevant multicellular structures. By exploiting the photochemistries described here, spatial patterning of cells within hydrogels becomes possible, with the added advantage of being able to control organization of different cell types within the scaffold. This spatial control is especially important for studying the complex 3D alveolar epithelial microenvironment, in which epithelial cells form hollow cyst-like structures surrounded by extracellular matrix containing endothelial and mesenchymal cells.

1.4 Approach of this thesis

The overall goal of this thesis is to develop a physiologically-relevant *in vitro* model of the alveolar epithelium, which can be used to explore the effects of extracellular cues on epithelial cell phenotype and disease progression. Typical *in vitro* culture platforms for primary alveolar epithelial cells consist either of flat 2D surfaces, or 3D matrices composed of naturally-derived protein fibers. The hollow, cyst-like alveolus inherently exists as a three dimensional object, and we postulate that this complex tissue structure is essential for *in vitro* studies. Moreover, maintaining strict control over the cyst structure and the physical and biochemical components of the supporting matrix enables researchers to probe more precisely which elements are influencing the cell behavior. In this thesis, we aim to exploit the spatial and temporal control over the photo-cleavable materials developed in this laboratory to create defined 3D tissue structures with primary lung epithelial cells to study cellular behavior in response to external

cues. The global objective, specific hypotheses, and the aims to test these hypotheses are discussed in detail in Chapter 2.

To explore the influence of matrix geometry on alveolar epithelial cell differentiation, Chapter 3 describes the process of eroding microwells of defined shapes and sizes into a photo-cleavable hydrogel scaffold using standard photo-lithography techniques. Primary alveolar epithelial cells can be seeded into these wells, covered with a second layer of hydrogel to create a 3D environment, and cultured for extended periods of time. Experiments are designed to assess cell phenotype by immunostaining for phenotype-specific proteins (surfactant protein C, SPC, for ATII cells; T1α protein for ATI cells) and subsequent image collection with confocal microscopy. Since the microwell geometry is highly regular, heat maps averaging over multiple wells can be generated to examine the spatial arrangement of each phenotype marker within the well. With this method, results revealed that spontaneous hollow cyst formation was not observed with the microfabricated hydrogel well scaffolds, thereby motivating the methods described in Chapter 4.

Specifically, a templating procedure was envisioned to study the establishment of epithelial cysts within a synthetic hydrogel platform. First, photodegradable microspheres are polymerized in appropriate size ranges for alveoli (50-200 μm) and contain pendant peptides (RGDS) that allow for epithelial cell attachment to the outer surface. An alveolar epithelial cell line (A549) is used to test the process: cells are incubated with microspheres on an orbital shaker and monitored with time until they form a confluent layer on the microsphere surface; next, these pre-cysts are readily encapsulated in a synthetic hydrogel; finally, the microsphere templates are eroded with light (15 min of exposure to 10 mW/cm^2 of 365 nm light), leaving hollow epithelial cysts suspended in a hydrogel network that are cultured for up to 6 days after template erosion.

To assess functional properties, primary alveolar epithelial cells isolated from mice are also used in this process and analyzed for cell phenotype (SPC, T1α) and the presence of cell junction markers (β-catenin, ZO-1) by immunostaining and confocal microscopy.

Once methods were established for cyst formation, the model was used to test hypotheses about epithelial-mesenchymal paracrine signaling (Chapter 5). Specifically, co-culture models enable study of the interactions between pulmonary fibroblasts with epithelial cysts in both healthy and diseased states. Pulmonary epithelial cysts formed either from healthy cells isolated from mice or from a cancer cell line (A549) are co-cultured with pulmonary fibroblasts, either from a healthy cell line (CCL-210) or from an idiopathic pulmonary fibrosis cell line (CCL-134). The fibroblasts are distributed singly throughout the hydrogel surrounding the epithelial cysts at 1.6 million cells/mL. Signs of epithelial-to-mesenchymal transition (EMT) are assessed by immunostaining for key EMT protein markers (vimentin, α-SMA, ZO-1 and E-cadherin) and imaging with confocal microscopy. Proliferation rates of both cell types are analyzed by incorporation of a fluorescent nucleoside (EdU), followed by image analysis with confocal microscopy and quantification with automated object detection. Fibroblast motility is assessed with live cell confocal microscopy and 3D object tracking software to calculate fraction migrating, speed, and directionality. Finally, Chapter 6 summarizes the major conclusions of this work and recommends future research directions for this project.

1.5 References

1. Centers for Disease Control and Prevention. *National Vital Statistics Reports, Deaths: Final Data for 2004*. (2007).

2. King, T. E., Pardo, A. & Selman, M. Idiopathic pulmonary fibrosis. *Lancet* **378,** 1949–61 (2011).

3. Fromigué, O., Louis, K., Dayem, M., Milanini, J., Pages, G., Tartare-Deckert, S., *et al.* Gene expression profiling of normal human pulmonary fibroblasts following coculture with non-small-cell lung cancer cells reveals alterations related to matrix degradation, angiogenesis, cell growth and survival. *Oncogene* **22,** 8487–97 (2003).

4. Wang, W., Li, Q., Yamada, T., Matsumoto, K., Matsumoto, I., Oda, M., *et al.* Crosstalk to stromal fibroblasts induces resistance of lung cancer to epidermal growth factor receptor tyrosine kinase inhibitors. *Clin. Cancer Res.* **15,** 6630–8 (2009).

5. Puig, M., Lugo, R., Gabasa, M., Gimenez, A., Velasquez, A., Galgoczy, R., *et al.* Matrix Stiffening and 1 Integrin Drive Subtype-Specific Fibroblast Accumulation in Lung Cancer. *Mol. Cancer Res.* **13,** 161–173 (2015).

6. Williams, M. C. Alveolar type I cells: molecular phenotype and development. *Annu. Rev. Physiol.* **65,** 669–95 (2003).

7. Mason, R. J. Biology of alveolar type II cells. *Respirology* **11,** S12–S15 (2006).

8. Fehrenbach, H. Alveolar epithelial type II cell: defender of the alveolus revisited. *Respir. Res.* **2,** 33–46 (2001).

9. Guillot, L., Nathan, N., Tabary, O., Thouvenin, G., Le Rouzic, P., Corvol, H., *et al.* Alveolar epithelial cells: master regulators of lung homeostasis. *Int. J. Biochem. Cell Biol.* **45,** 2568–73 (2013).

10. Uhal, B. D. Cell cycle kinetics in the alveolar epithelium. *Am. J. Physiol. Cell. Mol. Physiol.* **272,** L1031–1045 (1997).

11. Hogan, B. L. M., Barkauskas, C. E., Chapman, H. A., Epstein, J. A., Jain, R., Hsia, C. C. W., *et al.* Repair and regeneration of the respiratory system: complexity, plasticity, and mechanisms of lung stem cell function. *Cell Stem Cell* **15,** 123–38 (2014).

12. Barkauskas, C., Cronce, M., Rackley, C., Bowie, E., Keene, D., Stripp, B., *et al.* Type 2 alveolar cells are stem cells in adult lung. *J. Clin. Invest.* **123,** 3025–3036 (2013).

13. Park, W. Y., Miranda, B., Lebeche, D., Hashimoto, G. & Cardoso, W. V. FGF-10 is a chemotactic factor for distal epithelial buds during lung development. *Dev. Biol.* **201,** 125–34 (1998).

14. Bellusci, S., Grindley, J., Emoto, H., Itoh, N. & Hogan, B. L. Fibroblast growth factor 10 (FGF10) and branching morphogenesis in the embryonic mouse lung. *Development* **124,** 4867–78 (1997).

15. Tang, N., Marshall, W. F., McMahon, M., Metzger, R. J. & Martin, G. R. Control of Mitotic Spindle Angle by the RAS-Regulated ERK1/2 Pathway Determines Lung Tube Shape. *Science* **333,** 342–345 (2011).

16. Perl, A.-K. T. & Gale, E. FGF signaling is required for myofibroblast differentiation during alveolar regeneration. *Am. J. Physiol. Lung Cell. Mol. Physiol.* **297,** L299–308 (2009).

17. Yano, T., Mason, R. J., Pan, T., Deterding, R. R., Nielsen, L. D. & Shannon, J. M. KGF regulates pulmonary epithelial proliferation and surfactant protein gene expression in adult rat lung. *Am. J. Physiol. Lung Cell. Mol. Physiol.* **279,** L1146–58 (2000).

18. Sugahara, K., Tokumine, J., Teruya, K. & Oshiro, T. Alveolar epithelial cells: differentiation and lung injury. *Respirology* **11,** S28–31 (2006).

19. Crosby, L. M. & Waters, C. M. Epithelial Repair Mechanisms in the Lung. *Am. J. Physiol. Lung Cell. Mol. Physiol.* **298,** 715–731 (2010).

20. Prasad, S., Hogaboam, C. M. & Jarai, G. Deficient repair response of IPF fibroblasts in a co-culture model of epithelial injury and repair. *Fibrogenesis Tissue Repair* **7,** 7 (2014).

21. Shannon, J. M., Gebb, S. A. & Nielsen, L. D. Induction of alveolar type II cell differentiation in embryonic tracheal epithelium in mesenchyme-free culture. *Development* **126,** 1675–88 (1999).

22. Steiling, H. & Werner, S. Fibroblast growth factors: key players in epithelial morphogenesis, repair and cytoprotection. *Curr. Opin. Biotechnol.* **14,** 533–537 (2003).

23. Warburton, D., Wuenschell, C., Flores-Delgado, G. & Anderson, K. Commitment and differentiation of lung cell lineages. *Biochem. cell Biol.* **76,** 971–995 (1998).

24. Isakson, B. E., Seedorf, G. J., Lubman, R. L. & Boitano, S. Heterocellular cultures of pulmonary alveolar epithelial cells grown on laminin-5 supplemented matrix. *In Vitro Cell. Dev. Biol. Anim.* **38,** 443–9 (2002).

25. Wang, J., Edeen, K., Manzer, R., Chang, Y., Wang, S., Chen, X., *et al.* Differentiated human alveolar epithelial cells and reversibility of their phenotype in vitro. *Am. J. Respir. Cell Mol. Biol.* **36,** 661–8 (2007).

26. Herzog, E. L., Brody, A. R., Colby, T. V, Mason, R. & Williams, M. C. Knowns and unknowns of the alveolus. *Proc. Am. Thorac. Soc.* **5,** 778–82 (2008).

27. Thiery, J. P., Acloque, H., Huang, R. Y. J. & Nieto, M. A. Epithelial-mesenchymal transitions in development and disease. *Cell* **139,** 871–90 (2009).

28. Willis, B. C. & Borok, Z. TGF-beta-induced EMT: mechanisms and implications for fibrotic lung disease. *Am. J. Physiol. Lung Cell. Mol. Physiol.* **293,** L525–34 (2007).

29. Marchand-Adam, S., Marchal, J., Cohen, M., Soler, P., Gerard, B., Castier, Y., *et al.* Defect of hepatocyte growth factor secretion by fibroblasts in idiopathic pulmonary fibrosis. *Am. J. Respir. Crit. Care Med.* **168,** 1156–61 (2003).

30. Kumarswamy, R., Mudduluru, G., Ceppi, P., Muppala, S., Kozlowski, M., Niklinski, J., *et al.* MicroRNA-30a inhibits epithelial-to-mesenchymal transition by targeting Snai1 and is downregulated in non-small cell lung cancer. *Int. J. Cancer* **130,** 2044–53 (2012).

31. Amann, A., Zwierzina, M., Gamerith, G., Bitsche, M., Huber, J. M., Vogel, G. F., *et al.* Development of an innovative 3D cell culture system to study tumour--stroma interactions in non-small cell lung cancer cells. *PLoS One* **9,** e92511 (2014).

32. Horie, M., Saito, A., Mikami, Y., Ohshima, M., Morishita, Y., Nakajima, J., *et al.* Characterization of human lung cancer-associated fibroblasts in three-dimensional in vitro co-culture model. *Biochem. Biophys. Res. Commun.* **423,** 158–63 (2012).

33. Bhowmick, N., Neilson, E. & Moses, H. Stromal fibroblasts in cancer initiation and progression. *Nature* **432,** 332–337 (2004).

34. Dobbs, L. G. Isolation and culture of alveolar type II cells. *Am. J. Physiol.* **258,** L134–47 (1990).

35. Bhaskaran, M., Kolliputi, N., Wang, Y., Gou, D., Chintagari, N. R. & Liu, L. Trans-differentiation of Alveolar Epithelial Type II Cells to Type I Cells Involves Autocrine Signaling by Transforming Growth Factor beta1 through the Smad Pathway. *J. Biol. Chem.* **282,** 3968–3976 (2006).

36. Qiao, R., Yan, W., Clavijo, C., Mehrian-Shai, R., Zhong, Q., Kim, K.-J., *et al.* Effects of KGF on alveolar epithelial cell transdifferentiation are mediated by JNK signaling. *Am. J. Respir. Cell Mol. Biol.* **38,** 239–46 (2008).

37. Matter, M. L. & Laurie, G. W. A novel laminin E8 cell adhesion site required for lung alveolar formation in vitro. *J. Cell Biol.* **124,** 1083–90 (1994).

38. Umino, T., Wang, H., Zhu, Y., Liu, X., Manouilova, L. S., Spurzem, J. R., *et al.* Modification of type I collagenous gels by alveolar epithelial cells. *Am. J. Respir. Cell Mol. Biol.* **22,** 702–707 (2000).

39. Mondrinos, M. J., Koutzaki, S., Jiwanmall, E., Li, M., Dechadarevian, J.-P., Lelkes, P. I., *et al.* Engineering three-dimensional pulmonary tissue constructs. *Tissue Eng.* **12,** 717–28 (2006).

40. Bissell, M. J., Kenny, P. A. & Radisky, D. C. Microenvironmental regulators of tissue structure and function also regulate tumor induction and progression: the role of extracellular matrix and its degrading enzymes. *Cold Spring Harb. Symp. Quant. Biol.* **70,** 343–56 (2005).

41. Griffith, L. G. & Swartz, M. A. Capturing complex 3D tissue physiology in vitro. *Nat. Rev. Mol. Cell Biol.* **7,** 211–24 (2006).

42. Sugihara, H., Toda, S., Miyabara, S., Fujiyama, C. & Yonemitsu, N. Reconstruction of alveolus-like structure from alveolar type II epithelial cells in three-dimensional collagen gel matrix culture. *Am. J. Pathol.* **142,** 783–92 (1993).

43. Mondrinos, M. J., Koutzaki, S., Lelkes, P. I. & Finck, C. M. A tissue-engineered model of fetal distal lung tissue. *Am. J. Physiol. Lung Cell. Mol. Physiol.* **293,** L639–50 (2007).

44. Yu, W., Fang, X., Ewald, A., Wong, K., Hunt, C. A., Werb, Z., *et al.* Formation of cysts by alveolar type II cells in three-dimensional culture reveals a novel mechanism for epithelial morphogenesis. *Mol. Biol. Cell* **18,** 1693 (2007).

45. Lwebuga-Mukasa, J. S., Ingbar, D. H. & Madri, J. A. Repopulation of a Human Alveolar Matrix by Adult Rat Type II Pneumocytes In Vitro. *Exp. Cell Res.* **162,** 423–435 (1986).

46. Gill, B. J., Gibbons, D. L., Roudsari, L. C., Saik, J. E., Rizvi, Z. H., Roybal, J. D., *et al.* A synthetic matrix with independently tunable biochemistry and mechanical properties to study epithelial morphogenesis and EMT in a lung adenocarcinoma model. *Cancer Res.* **72,** 6013–23 (2012).

47. Carterson, A., Bentrup, K. zu, Ott, C., Clarke, M., Pierson, D., Vanderburg, C., *et al.* A549 Lung Epithelial Cells Grown as Three-Dimensional Aggregates : Alternative Tissue Culture Model for Pseudomonas aeruginosa Pathogenesis. *Infect. Immun.* **73,** 1129–1140 (2005).

48. Reginato, M. J., Mills, K. R., Paulus, J. K., Lynch, D. K., Sgroi, D. C., Debnath, J., *et al.* Integrins and EGFR coordinately regulate the pro-apoptotic protein Bim to prevent anoikis. *Nat. Cell Biol.* **5,** 733–40 (2003).

49. Magnusson, M. K. & Mosher, D. F. Fibronectin : Structure, Assembly, and Cardiovascular Implications. *Arterioscler. Thromb. Vasc. Biol.* **18,** 1363–1370 (1998).

50. Parsons, J. T., Martin, K. H., Slack, J. K., Taylor, J. M. & Weed, S. A. Focal adhesion kinase: a regulator of focal adhesion dynamics and cell movement. *Oncogene* **19,** 5606–13 (2000).

51. Tibbitt, M. W. & Anseth, K. S. Hydrogels as extracellular matrix mimics for 3D cell culture. *Biotechnol. Bioeng.* **103,** 655–63 (2009).

52. Taipale, J. & Keski-Oja, J. Growth factors in the extracellular matrix. *FASEB J.* **11,** 51–59 (1997).

53. Jorma, A., Taipale, J. & Keski-Oja, J. Growth factors in the extracellular matrix. *FASEB J.* **11,** 51–59 (1997).

54. Kim, S.-H., Turnbull, J. & Guimond, S. Extracellular matrix and cell signalling: the dynamic cooperation of integrin, proteoglycan and growth factor receptor. *J. Endocrinol.* **209,** 139–51 (2011).

55. Bacac, M. & Stamenkovic, I. Metastatic cancer cell. *Annu. Rev. Pathol.* **3,** 221–47 (2008).

56. Daley, W. P., Peters, S. B. & Larsen, M. Extracellular matrix dynamics in development and regenerative medicine. *J. Cell Sci.* **121,** 255–64 (2008).

57. Ingber, D. Tensegrity: the architectural basis of cellular mechanotransduction. *Annu. Rev. Physiol.* **59,** 575–599 (1997).

58. Levental, I., Georges, P. C. & Janmey, P. A. Soft biological materials and their impact on cell function. *Soft Matter* **3,** 299–306 (2007).

59. Engler, A. J., Sen, S., Sweeney, H. L. & Discher, D. E. Matrix elasticity directs stem cell lineage specification. *Cell* **126,** 677–89 (2006).

60. Paszek, M. J., Zahir, N., Johnson, K. R., Lakins, J. N., Rozenberg, G. I., Gefen, A., *et al.* Tensional homeostasis and the malignant phenotype. *Cancer Cell* **8,** 241–54 (2005).

61. Rosso, F., Marino, G., Giordano, A., Barbarisi, M., Parmeggiani, D. & Barbarisi, A. Smart materials as scaffolds for tissue engineering. *J. Cell. Physiol.* **203,** 465–70 (2005).

62. Lutolf, M. P. & Hubbell, J. A. Synthetic biomaterials as instructive extracellular microenvironments for morphogenesis in tissue engineering. *Nat. Biotechnol.* **23,** 47–55 (2005).

63. Peppas, N. A., Hilt, J. Z., Khademhosseini, A. & Langer, R. Hydrogels in Biology and Medicine: From Molecular Principles to Bionanotechnology. *Adv. Mater.* **18,** 1345–1360 (2006).

64. Cushing, M. C. & Anseth, K. S. Materials science. Hydrogel cell cultures. *Science* **316,** 1133–4 (2007).

65. Sawhney, A., Pathak, C. & Hubbell, J. Bioerodible Hydrogels Based on Photopolymerized Poly(ethylene glycol)-co-poly(a-hydroxy acid) Diacrylate Macromers. *Macromolecules* **26,** 581–587 (1993).

66. Bryant, S. J., Nuttelman, C. R. & Anseth, K. S. Cytocompatibility of UV and visible light photoinitiating systems on cultured NIH/3T3 fibroblasts in vitro. *J. Biomater. Sci. Polym. Ed.* **11,** 439–57 (2000).

67. Bryant, S. J. & Anseth, K. S. Hydrogel properties influence ECM production by chondrocytes photoencapsulated in poly(ethylene glycol) hydrogels. *J. Biomed. Mater. Res.* **59,** 63–72 (2002).

68. Weber, L. M., He, J., Bradley, B., Haskins, K. & Anseth, K. S. PEG-based hydrogels as an in vitro encapsulation platform for testing controlled beta-cell microenvironments. *Acta Biomater.* **2,** 1–8 (2006).

69. Cordey, M., Limacher, M., Kobel, S., Taylor, V. & Lutolf, M. P. Enhancing the reliability and throughput of neurosphere culture on hydrogel microwell arrays. *Stem Cells* **26,** 2586–94 (2008).

70. Rice, M. A. & Anseth, K. S. Encapsulating chondrocytes in copolymer gels: bimodal degradation kinetics influence cell phenotype and extracellular matrix development. *J. Biomed. Mater. Res. A* **70,** 560–8 (2004).

71. Nuttelman, C. R., Henry, S. M. & Anseth, K. S. Synthesis and characterization of photocrosslinkable, degradable poly(vinyl alcohol)-based tissue engineering scaffolds. *Biomaterials* **23,** 3617–26 (2002).

72. Bryant, S. J. & Anseth, K. S. Controlling the spatial distribution of ECM components in degradable PEG hydrogels for tissue engineering cartilage. *J. Biomed. Mater. Res. A* **64,** 70–9 (2003).

73. Lutolf, M. P., Lauer-Fields, J. L., Schmoekel, H. G., Metters, A. T., Weber, F. E., Fields, G. B., *et al.* Synthetic matrix metalloproteinase-sensitive hydrogels for the conduction of tissue regeneration: engineering cell-invasion characteristics. *Proc. Natl. Acad. Sci. U. S. A.* **100,** 5413–8 (2003).

74. Salinas, C. N. & Anseth, K. S. The enhancement of chondrogenic differentiation of human mesenchymal stem cells by enzymatically regulated RGD functionalities. *Biomaterials* **29,** 2370–7 (2008).

75. Kloxin, A. M., Kasko, A. M., Salinas, C. N. & Anseth, K. S. Photodegradable hydrogels for dynamic tuning of physical and chemical properties. *Science* **324,** 59–63 (2009).

76. Bryant, S. & Anseth, K. in *Scaffolding Tissue Eng.* (Ma, P. X. & Elisseeff, J.) 71–90 (CRC Press, 2005). doi:10.1201/9781420027563.ch6

77. Metters, A. & Hubbell, J. Network formation and degradation behavior of hydrogels formed by Michael-type addition reactions. *Biomacromolecules* **6,** 290–301 (2005).

78. Tibbitt, M. W. & Anseth, K. S. Dynamic Microenvironments: The Fourth Dimension. *Sci. Transl. Med.* **4,** 160ps24–160ps24 (2012).

79. Kloxin, A. M., Tibbitt, M. W., Kasko, A. M., Fairbairn, J. A. & Anseth, K. S. Tunable Hydrogels for External Manipulation of Cellular Microenvironments through Controlled Photodegradation. *Adv. Mater.* **22,** 61–66 (2010).

80. Benton, J. A., Kern, H. B. & Anseth, K. S. Substrate Properties Influence Calcification in Valvular Interstitial Cell Culture. *J Hear. Valve Dis* **17,** 689–699 (2008).

81. Yip, C. Y. Y., Chen, J.-H., Zhao, R. & Simmons, C. A. Calcification by valve interstitial cells is regulated by the stiffness of the extracellular matrix. *Arterioscler. Thromb. Vasc. Biol.* **29,** 936–42 (2009).

82. Wang, H., Tibbitt, M. W., Langer, S. J., Leinwand, L. a & Anseth, K. S. Hydrogels preserve native phenotypes of valvular fibroblasts through an elasticity-regulated PI3K/AKT pathway. *Proc. Natl. Acad. Sci.* **110,** 19336–19341 (2013).

83. Kloxin, A. M., Benton, J. A. & Anseth, K. S. In situ elasticity modulation with dynamic substrates to direct cell phenotype. *Biomaterials* **31,** 1–8 (2010).

84. Wang, H., Haeger, S. S. M., Kloxin, A. M. A., Leinwand, L. A. & Anseth, K. S. Redirecting Valvular Myofibroblasts into Dormant Fibroblasts through Light-mediated Reduction in Substrate Modulus. *PLoS One* **7,** e39969 (2012).

85. Engler, A., Bacakova, L., Newman, C., Hategan, A., Griffin, M. & Discher, D. Substrate compliance versus ligand density in cell on gel responses. *Biophys. J.* **86,** 617–28 (2004).

86. Tse, J. R. & Engler, A. J. Stiffness gradients mimicking in vivo tissue variation regulate mesenchymal stem cell fate. *PLoS One* **6,** e15978 (2011).

87. Zaari, N., Rajagopalan, P., Kim, S. K., Engler, A. J. & Wong, J. Y. Photopolymerization in Microfluidic Gradient Generators: Microscale Control of Substrate Compliance to Manipulate Cell Response. *Adv. Mater.* **16,** 2133–2137 (2004).

88. Kloxin, A. M., Kasko, A. M., Salinas, C. N. & Anseth, K. S. Photodegradable hydrogels for dynamic tuning of physical and chemical properties. *Science* **324,** 59–63 (2009).

89. DeForest, C. A. & Tirrell, D. A. A photoreversible protein-patterning approach for guiding stem cell fate in three-dimensional gels. *Nat. Mater.* **14,** 523–531 (2015).

90. Gandavarapu, N. R., Azagarsamy, M. A. & Anseth, K. S. Photo-Click Living Strategy for Controlled, Reversible Exchange of Biochemical Ligands. *Adv. Mater.* **26,** 2521–2526 (2014).

91. Ruoslahti, E. & Pierschbacher, M. D. New perspectives in cell adhesion: RGD and integrins. *Science* **238,** 491–7 (1987).

92. Hubbell, J. Biomaterials in Tissue Engineering. *Nat. Biotechnol.* **13,** 565–576 (1995).

93. Burdick, J. A. & Anseth, K. S. Photoencapsulation of osteoblasts in injectable RGD-modified PEG hydrogels for bone tissue engineering. *Biomaterials* **23,** 4315–23 (2002).

94. Tavella, S., Bellese, G., Castagnola, P., Martin, I., Piccini, D., Doliana, R., *et al.* Regulated expression of fibronectin, laminin and related integrin receptors during the early chondrocyte differentiation. *J. Cell Sci.* **110,** 2261–70 (1997).

95. DeLise, A. M., Fischer, L. & Tuan, R. S. Cellular interactions and signaling in cartilage development. *Osteoarthr. Cartil.* **8,** 309–34 (2000).

96. Fairbanks, B. D., Schwartz, M. P., Halevi, A. E., Nuttelman, C. R., Bowman, C. N. & Anseth, K. S. A Versatile Synthetic Extracellular Matrix Mimic via Thiol-Norbornene Photopolymerization. *Adv. Mater.* **21,** 5005–5010 (2009).

97. Hoyle, C. E. & Bowman, C. N. Thiol-ene click chemistry. *Angew. Chem. Int. Ed. Engl.* **49,** 1540–73 (2010).

98. Lutolf, M. P., Tirelli, N., Cerritelli, S., Cavalli, L. & Hubbell, J. A. Systematic modulation of Michael-type reactivity of thiols through the use of charged amino acids. *Bioconjug. Chem.* **12,** 1051–6 (2001).

99. Elbert, D. L. & Hubbell, J. A. Conjugate addition reactions combined with free-radical cross-linking for the design of materials for tissue engineering. *Biomacromolecules* **2,** 430–41 (2001).

100. Lutolf, M. P. & Hubbell, J. A. Synthesis and physicochemical characterization of end-linked poly(ethylene glycol)-co-peptide hydrogels formed by Michael-type addition. *Biomacromolecules* **4,** 713–22 (2003).

101. Lutolf, M. P., Raeber, G. P., Zisch, A. H., Tirelli, N. & Hubbell, J. A. Cell-Responsive Synthetic Hydrogels. *Adv. Mater.* **15,** 888–892 (2003).

102. Polizzotti, B. D., Fairbanks, B. D. & Anseth, K. S. Three-dimensional biochemical patterning of click-based composite hydrogels via thiolene photopolymerization. *Biomacromolecules* **9,** 1084–7 (2008).

103. Anderson, S. B., Lin, C.-C., Kuntzler, D. V & Anseth, K. S. The performance of human mesenchymal stem cells encapsulated in cell-degradable polymer-peptide hydrogels. *Biomaterials* **32,** 3564–74 (2011).

104. Benton, J. A., Fairbanks, B. D. & Anseth, K. S. Characterization of valvular interstitial cell function in three dimensional matrix metalloproteinase degradable PEG hydrogels. *Biomaterials* **30,** 6593–603 (2009).

105. Mann, B. K., Gobin, A. S., Tsai, A. T., Schmedlen, R. H. & West, J. L. Smooth muscle cell growth in photopolymerized hydrogels with cell adhesive and proteolytically degradable domains: synthetic ECM analogs for tissue engineering. *Biomaterials* **22,** 3045–51 (2001).

106. Codelli, J. A., Baskin, J. M., Agard, N. J. & Bertozzi, C. R. Second-generation difluorinated cyclooctynes for copper-free click chemistry. *J. Am. Chem. Soc.* **130,** 11486–93 (2008).

107. DeForest, C. A., Polizzotti, B. D. & Anseth, K. S. Sequential click reactions for synthesizing and patterning three-dimensional cell microenvironments. *Nat. Mater.* **8,** 659–64 (2009).

108. DeForest, C. A., Sims, E. A. & Anseth, K. S. Peptide-Functionalized Click Hydrogels with Independently Tunable Mechanics and Chemical Functionality for 3D Cell Culture. *Chem. Mater.* **22,** 4783–4790 (2010).

109. DeForest, C. A. & Anseth, K. S. Cytocompatible click-based hydrogels with dynamically tunable properties through orthogonal photoconjugation and photocleavage reactions. *Nat. Chem.* **3,** 925–931 (2011).

Chapter 2

Thesis Objectives

Two cell phenotypes reside in the lung alveolar epithelium: alveolar type I (ATI) cells, which are thin and elongated to facilitate gas exchange with the surrounding capillaries, and alveolar type II (ATII) cells, which are rounded and secrete surfactant proteins that line the inside of the hollow, spherical alveolus. These epithelial cells attach to a thin basement membrane that separates them from the surrounding capillary endothelial cells as well as interstitial pulmonary fibroblasts, which are especially common in the collagen- and elastin-rich septa separating the alveolar walls.[1] The long, thin ATI cells are the most susceptible to injury, while the ATII cells serve as stem cells for the alveolar epithelium, repopulating and differentiating after injury to reform the epithelial layer.[2] The ATII cell niche often contains gaps in the basement membrane through which epithelial cells can form direct connections to the resident fibroblasts, indicating an important role for epithelial-mesenchymal communication in healthy alveolar tissue.[3] Crosstalk between the alveolar epithelium and interstitial fibroblasts is thought to be influential in maintaining alveolar extracellular matrix (ECM) secretion and composition, survival and differentiation of both epithelial cells and fibroblasts, and the progression of fibrotic diseases.[4] Despite their important function, much remains to be understood and discovered about the extracellular cues necessary for epithelial cell differentiation and their dysregulation that leads to disease.

In vitro model systems are particularly useful for studying questions related to the lung alveolus, because these systems give the user control over the individual signals presented to the cells, such as matrix geometry, and enable the experimenter to co-culture multiple cell types to

study specific interactions not available to *in vivo* experimental designs. The cyst-like alveolus is an inherently three-dimensional tissue structure, and this organization necessitates an appropriate 3D matrix environment for culturing alveolar cells in a similarly complex multicellular arrangement. One particularly versatile material scaffold for culturing cells in three dimensions is based on peptide-functionalized poly(ethylene glycol) (PEG) hydrogels, where the PEG component limits non-specific protein adsorption and the peptide component allows controlled presentation of matrix signals to the cell.[5] Both Michael addition and thiol-ene photoclick reactions have been used to synthesize PEG-peptide matrices, using reaction conditions that are cytocompatible and enable primary cell encapsulation.[6,7]

By using light-based chemistries to initiate gelation and to incorporate biomolecules into PEG networks, dynamic niches can be created that facilitate the study of how cells respond to user-dictated or cell-dictated changes in environmental signals. For example, our group has demonstrated integration of photo-cleavable moieties into PEG hydrogel crosslinks, as well as pendant functional groups, to construct gel culture niches with biophysical and biochemical properties that are spatiotemporally tunable with light.[8] Complementary to this approach, an enzymatically cleavable peptide sequence can be introduced within PEG hydrogels through photoinitiated addition reactions (*e.g.*, the thiol-ene photoclick reaction), such as between thiol-containing biomacromolecules and ene-containing synthetic polymers.[7] These types of materials mimic aspects of the ECM by allowing cells to bind to the matrix through integrins and to locally remodel their surrounding microenvironment. With such tunable material platforms, researchers can employ a systematic approach for 3D cell culture experiments, spatially and temporally modulating physical properties (*e.g.*, stiffness, scaffold geometry), as well as biological signals

(*e.g.*, adhesive ligands, degradable sequences) to study cell behavior in response to environmental stimuli.

This thesis research aims to study how extracellular cues influence alveolar epithelial cells in the context of a biologically relevant cellular arrangement. In particular, the key features of alveolar tissue that we seek to recapitulate are the curved single layer alveolar epithelium attached to an ECM-like scaffold surrounding a hollow central lumen. Preferably, the model system would allow control over the cell-matrix interactions (*e.g.*, matrix composition and mechanics) while enabling co-culture with other cell types found in the alveolar interstitium at controlled densities and distances relevant to paracrine signaling. We hypothesize that tissue geometry, matrix properties, and paracrine signaling from neighboring interstitial cells influence epithelial cellular behavior, in terms of primary ATII cell differentiation, proliferation, migration, and epithelial-to-mesenchymal transition (EMT). We posit that the materials developed and used in this research are robust and versatile for manipulating the multi-cellular architecture of lung cells, and enable us to study epithelial-matrix and epithelial-mesenchymal interactions in a model alveolus-like microenvironment *in vitro*. Specifically, we exploit a photocleavable crosslinking PEG macromolecule described in the Introduction (Chapter 1), first to create microwells for confining epithelial cells to a defined shape, and second to template epithelial cyst structures using photodegradable microspheres. Finally, this new culture platform allows us to study the exchange between fibroblasts and the epithelium that is thought to influence the progression of diseases, such as lung fibrosis and cancer, within a complex tissue-relevant co-culture model. To test the hypothesis listed above, the specific aims of this thesis are to:

Aim 1. Examine and quantify the effects of geometric confinement on differentiation and spatial arrangement of primary lung epithelial cells cultured in 3D matrices.

During lung development, spatially-regulated cues from the mesenchyme determine branching sites for the emerging lung buds.[9] In the mature lung, the two alveolar epithelial cell phenotypes are spatially arranged in specific patterns with the elongated ATI phenotype stretched out along the curves of the alveolus and the cuboidal ATII phenotype localized to the points where neighboring alveoli meet.[4] Given this spatial specificity, we hypothesize that matrix geometry may play a role in determining differentiation of freshly isolated ATII cells and branching of cultured tissue structures. A photomask is used to erode wells of varying shapes (*i.e.*, circles to multi-lobed clusters) within a photodegradable PEG hydrogel, which are subsequently seeded with mouse ATII cells. After 7 days of culture, cell phenotype is assessed by immunostaining for cell-specific markers (*i.e.,* T1α membrane protein for ATI cells and surfactant protein C for ATII cells) and by quantifying the position of each cell type within the wells through image analysis and generation of heat maps. To demonstrate temporal control over matrix geometry and potentially influence tissue branching, focused two-photon light is used to erode channels connecting neighboring microwells midway through the cell culture time.

Aim 2. Develop and test a hydrogel platform to culture alveolar epithelial cells and characterize their evolution into cyst-like structures.

Typical culture platforms used for studying primary alveolar epithelial cells *in vitro* rely on unphysiologically stiff 2D plastic substrates (*i.e.,* > 6 orders of magnitude stiffer than lung tissue) or on matrices derived from native ECM proteins that can confound experiments studying the influence of biochemical signals on cell phenotype because of the inherent batch variability

of these materials and limited control over their composition and matrix properties. Moreover, the hollow cyst structure of an alveolus can be difficult to achieve reproducibly *in vitro,* and studies to date have primarily relied on spontaneous cyst formation when primary cells are embedded in naturally-derived protein gels.[10,11] This motivated our efforts to develop a technique to form model alveoli *in vitro*, using a highly tunable synthetic hydrogel scaffold to allow manipulation of complex epithelial structures in a precisely engineered environment. To accomplish this goal, cell-adhesive photodegradable microspheres (50-200 μm in diameter) are used as templates to direct epithelial cyst formation within PEG hydrogels containing pendant adhesive peptides (*i.e.,* fibronectin-derived, CRGDS) and enzymatically-cleavable crosslinks (*i.e.* a collagenase-based target, KCGPQG↓IWGQCK). An alveolar epithelial cell line (A549) is used to develop the templating process, followed by primary ATII cells to characterize the cysts for structural fidelity by immunostaining for cell junction proteins (*i.e.,* β-catenin, ZO-1) and cell phenotype markers (*i.e.,* T1α, SPC), as well as imaging by confocal microscopy and analyzing the geometric arrangement of cells.

Aim 3. Utilize an innovative co-culture model to investigate the complex interplay between the alveolar epithelium and interstitial pulmonary fibroblasts to better understand the role of paracrine signaling on cellular properties correlated with disease progression.

Convincing evidence points to the importance of epithelial and mesenchymal interactions in the progression of lung diseases, such as idiopathic pulmonary fibrosis (IPF) and cancer.[12,13] However, human studies are limited to comparisons between normal patients and those already presenting the diseased state of the alveolar tissue, and this approach precludes examination of the molecular mechanisms associated with how an injured or mutated epithelium influences the

surrounding healthy fibroblasts and *vice versa.* For example, the source of profibrotic myofibroblasts in IPF has been highly controversial in recent years; whether they originate from proliferation and activation of local fibroblasts or epithelial-to-mesenchymal transition (EMT) of an activated epithelium.[14,15] We hypothesize that diseased cell types, either epithelial or mesenchymal, will cause an increase in abnormal processes (*e.g.,* increased proliferation, motility, expression of activation-associated proteins like α-SMA) in healthy cells when the two are co-cultured in a physiologically-relevant *in vitro* model of alveolar tissue. To test this hypothesis, normal (CCL-210) and diseased (CCL-134, IPF) pulmonary fibroblast cell lines are co-cultured with cysts formed from normal primary epithelial cells (isolated from wild-type mice) and a diseased epithelial cell line (A549, cancer). All cells are embedded in a hydrogel matrix that allows control of the spatial proximity and density of the cells, and also exploits our cyst templating technique (Aim 2). Cell proliferation is measured by incorporation of a fluorescent nucleoside into the DNA of dividing cells, and cell-laden gels are subsequently imaged and counted. Further, cell migration is quantified using live cell microscopy and cell tracking software, and signs of EMT are characterized by immunostaining for key EMT protein markers (*e.g.*, vimentin, α-SMA, E-cadherin, and ZO-1) and imaging with confocal microscopy.

2.1 References

1. Hogan, B. L. M., Barkauskas, C. E., Chapman, H. A., Epstein, J. A., Jain, R., Hsia, C. C. W., *et al.* Repair and regeneration of the respiratory system: complexity, plasticity, and mechanisms of lung stem cell function. *Cell Stem Cell* **15,** 123–38 (2014).

2. Mason, R. J. Biology of alveolar type II cells. *Respirology* **11,** S12–S15 (2006).

3. Sirianni, F. E., Chu, F. S. F. & Walker, D. C. Human Alveolar Wall Fibroblasts Directly Link Epithelial Type 2 Cells to Capillary Endothelium. *Am. J. Respir. Crit. Care Med.* **168,** 1532–1537 (2003).

4. Herzog, E. L., Brody, A. R., Colby, T. V, Mason, R. & Williams, M. C. Knowns and unknowns of the alveolus. *Proc. Am. Thorac. Soc.* **5,** 778–82 (2008).

5. Tibbitt, M. W. & Anseth, K. S. Hydrogels as extracellular matrix mimics for 3D cell culture. *Biotechnol. Bioeng.* **103,** 655–63 (2009).

6. Lutolf, M. P. & Hubbell, J. A. Synthesis and physicochemical characterization of end-linked poly(ethylene glycol)-co-peptide hydrogels formed by Michael-type addition. *Biomacromolecules* **4,** 713–22 (2003).

7. Fairbanks, B. D., Schwartz, M. P., Halevi, A. E., Nuttelman, C. R., Bowman, C. N. & Anseth, K. S. A Versatile Synthetic Extracellular Matrix Mimic via Thiol-Norbornene Photopolymerization. *Adv. Mater.* **21,** 5005–5010 (2009).

8. Kloxin, A. M., Kasko, A. M., Salinas, C. N. & Anseth, K. S. Photodegradable hydrogels for dynamic tuning of physical and chemical properties. *Science* **324,** 59–63 (2009).

9. Warburton, D., Schwarz, M., Tefft, D., Flores-Delgado, G., Anderson, K. D. & Cardoso, W. V. The molecular basis of lung morphogenesis. *Mech. Dev.* **92,** 55–81 (2000).

10. Yu, W., Fang, X., Ewald, A., Wong, K., Hunt, C. A., Werb, Z., *et al.* Formation of cysts by alveolar type II cells in three-dimensional culture reveals a novel mechanism for epithelial morphogenesis. *Mol. Biol. Cell* **18,** 1693 (2007).

11. Sugihara, H., Toda, S., Miyabara, S., Fujiyama, C. & Yonemitsu, N. Reconstruction of alveolus-like structure from alveolar type II epithelial cells in three-dimensional collagen gel matrix culture. *Am. J. Pathol.* **142,** 783–92 (1993).

12. King, T. E., Pardo, A. & Selman, M. Idiopathic pulmonary fibrosis. *Lancet* **378,** 1949–61 (2011).

13. Thiery, J. P., Acloque, H., Huang, R. Y. J. & Nieto, M. A. Epithelial-mesenchymal transitions in development and disease. *Cell* **139,** 871–90 (2009).

14. Kim, K. K., Kugler, M. C., Wolters, P. J., Robillard, L., Galvez, M. G., Brumwell, A. N., *et al.* Alveolar epithelial cell mesenchymal transition develops in vivo during pulmonary fibrosis and is regulated by the extracellular matrix. *Proc. Natl. Acad. Sci.* **103,** 13180–13185 (2006).

15. Rock, J. R., Barkauskas, C. E., Cronce, M. J., Xue, Y., Harris, J. R., Liang, J., *et al.* Multiple stromal populations contribute to pulmonary fibrosis without evidence for epithelial to mesenchymal transition. *Proc. Natl. Acad. Sci.* **108,** E1475–E1483 (2011).

Chapter 3

Responsive culture platform to examine the influence of microenvironmental geometry on cell function in 3D

As published in *Integr. Biol.*, **4**, 1540-1549 (2012)

3.1 Abstract

We describe the development of a well-based cell culture platform that enables experimenters to control the geometry and connectivity of cellular microenvironments spatiotemporally. The base material is a hydrogel comprised of photolabile and enzyme-labile crosslinks and pendant cell adhesion sequences, enabling spatially-specific, *in situ* patterning with light and cell-dictated microenvironment remodeling through enzyme secretion. Arrays of culture wells of varying shape and size were patterned into the hydrogel surface using photolithography, where well depth was correlated with irradiation dose. The geometry of these devices can be subsequently modified through sequential patterning, while simultaneously monitoring changes in cell geometry and connectivity. Towards establishing the utility of these devices for dynamic evaluation of the influence of physical cues on tissue morphogenesis, the effect of well shape on lung epithelial cell differentiation (i.e., primary mouse alveolar type II cells, ATII cells) was assessed. Shapes inspired by alveoli were degraded into hydrogel surfaces. ATII cells were seeded within the well-based arrays and encapsulated by the addition of a top hydrogel layer. Cell differentiation in response to these geometries was characterized over 7 days of culture with immunocytochemistry (surfactant protein C, ATII; T1α protein, alveolar type I (ATI) differentiated epithelial cells) and confocal image analysis. Individual cell clusters were further connected by eroding channels between wells during culture *via* controlled two-photon irradiation. Collectively, these studies demonstrate the development and utility of responsive

hydrogel culture devices to study how a range of microenvironment geometries of evolving shape and connectivity might influence or direct cell function.

3.2 Introduction

Extracellular matrix (ECM) signals, such as elasticity,[1] growth factor presentation,[2] and extracellular matrix protein assembly and binding,[3] are increasingly recognized as critical regulators of progenitor cell function and fate during development and tissue regeneration. For example, during lung development, spatiotemporally evolving growth factor gradients, basement membrane production and localized remodeling, and interactions between adjacent cells responding to the locally thinned and distended basement membrane are all part of the complex sequence of ECM signals that direct lung epithelium assembly, branching morphogenesis, and alveoli formation.[4] In particular, the geometry of the cell microenvironment, which regulates cell shape and cytoskeletal tension, polarization, receptor binding, and cell-cell communication,[4c, 5] in conjunction with biochemical factors, has been observed to direct cell differentiation and function in both tissue regeneration[6] and morphogenesis.[7] While many studies have demonstrated the importance of microenvironment geometry in guiding cell function within these biological processes, the native cell microenvironment contains a complex array of biophysical and biochemical signals that actively and reciprocally interact with cells.[8] A culture platform that more fully captures changes in microenvironment geometry in three dimensions would be useful to understand the transient role of cell shape in tissue development or regeneration. Here, we present a new culture platform based on photodegradable materials for spatiotemporally controlling cell geometry during culture and demonstrate its utility for probing

the role of shape in influencing progenitor cell fate, specifically alveolar type II (ATII) epithelial cell differentiation.

Cell microenvironment geometry has been controlled *in vitro* with micropatterned culture substrates. Both hard and soft materials have been patterned to control cell adhesion and shape within two-dimensional (2D) culture,[5, 9] where shape has been observed to regulate cell differentiation and fate.[6a, 10] Culture platforms that mimic native tissue geometry and architecture in three dimensions can be advantageous for recapturing *in vivo*-like cell response.[11] To control microenvironment geometry in three-dimensional (3D) culture, micropatterned well-based materials have been developed and utilized to examine mammary branching morphogenesis,[7b, 12] the epithelial-mesenchymal transition,[13] and MSC differentiation.[14] These well-based culture platforms are created using soft lithography to pattern arrays of wells within collagen hydrogels:[15] a PDMS stamp with 50-100 μm tall circular or rectangular posts is typically embedded within a liquid collagen mixture; the collagen mixture is crosslinked; and the stamp is removed, generating wells in which cells of interest are seeded. Subsequently, a second layer of collagen is added to encapsulate the cells within a spatially-defined 3D microenvironment. Cell function and fate in these micropatterned geometries are assessed using biochemical assays to quantify cell proliferation, apoptosis, or protein production and immunocytochemistry to examine cell phenotype, morphology and cytoskeletal organization, or cell-ECM/cell-cell interactions. In complementary approaches, 3D culture of cell aggregates has been achieved by using microwells and microengineering[16] or using micropatterning and electromagnetic fields to orient cell aggregates followed by photoencapsulation within a 3D polymer matrix.[17]

From these seminal contributions, the importance of 3D culture for examining the complex signaling involved in whole tissue development or regeneration is clearly demonstrated.

Cytoskeletal tension in conjunction with cell-secreted factors, cell-cell interactions, and cell-ECM binding has been observed to regulate morphogenesis in ECM-protein-based culture systems. Further, the relevant size and time scales for a geometrically defined 3D culture system have been identified, with geometries ranging from 50-250 μm in width for cylinders, rectangular prisms, and cubes while assessing cell fate decisions from days to weeks.[7]

A 3D culture platform that enables similar studies with temporally-evolving biophysical signals would offer further insight into the critical cues and mechanisms that drive tissue development and repair. The culture platform should afford (i) ease of handling throughout cell culture, (ii) accessible, facile generation of an array of microenvironment geometries, (iii) *in situ* biological assays for spatially-specific assessment of cell response, and (iv) spatiotemporal property manipulation to elucidate how evolving microenvironment geometry/connectivity influence cell fate.

In this contribution, we exploit a relatively unique and photodegradable material system by processing it into a microfabricated culture system and then studying how geometry temporally regulates lung epithelial cell function and fate. Inspired by prior 3D well-based culture platforms, we developed an approach for preparing devices with arrays of wells with varied shape and size and subsequently utilized them for 3D cell culture by seeding, encapsulation, and assessment of cells within the controlled shapes. A photolabile and enzymatically-degradable hydrogel was employed as the device foundation, and this base material was modified with integrin-binding peptides to promote cell adhesion and serve as an artificial, well-defined ECM. The photolabile functionality uniquely allowed the formation and later modification of well shapes, while the enzyme cleavage sites allowed cell-based remodeling of the matrix during long-term culture. Well shape, depth, and connectivity were controlled with

photolithography or focused two-photon irradiation using a confocal microscope. With this platform, we examined how geometry influences ATII epithelial cell fate, where ATIIs are the progenitor cells for both ATII and ATI cell populations in the alveolar epithelium.[18] In the native lung, ATII cells are also responsible for surfactant production and secretion, whereas ATI cells cover most of the alveolar surface area and promote gas exchange. Alveoli-inspired shapes were facilely created using photolithography, and cell phenotype in response to these geometries was characterized with *in situ* immunocytochemistry and confocal microscopy. The cell-laden wells were connected with channels by controlled photodegradation during culture to mimic branching and connectivity. This device system based on dynamically controlled hydrogel materials should prove useful for probing how many cell types respond to changes in microenvironment geometry and improve the field's understanding of the role of physical cues in directing tissue morphogenesis or regeneration.

3.3 Materials and methods

All reagents were purchased from Sigma Aldrich and used as received unless otherwise noted.

3.3.1 Synthesis of responsive monomers

A photolabile, enzyme-labile peptide functionalized with azides, N_3-RGK(alloc)GPQG↓IWGQRK(PL-ester-N_3)-NH_2, was synthesized according to previously published methods.[19] An *o*-nitrobenzyl ether photolabile group was incorporated to allow cleavage with externally-applied UV, visible, and two-photon irradiation.[20] A synthetic variant of an enzymatically degradable peptide sequence from collagen I was incorporated to allow directed degradation by many different cell types with a host of secreted matrix metalloproteinases (MMPs), including MMPs 1, 2, 3, 8, and 9.[21] A multi-arm poly(ethylene

glycol) (M_n ~ 10 kDa, JenKem Technology USA) modified with cyclooctyne end groups was synthesized according to previously published methods.[22] An azide-modified carboxylic acid was synthesized using previously published techniques[22] for subsequent attachment to amine-modified glass, as described in the following section.

3.3.2 Fabrication of hydrogel culture platform

Glass cover slips (#2; 22, or 18 mm diameter; Fisher Scientific) were cleaned with Piranha (30 min in freshly prepared 3:1 by volume concentrated sulfuric acid to 30% hydrogen peroxide solution, Fisher Scientific) rinsed with copious amounts of deionized water (DI) water, using appropriate safety precautions and personal protective equipment. After all Piranha waste was removed from the fume hood, the clean cover glass was rinsed with acetone and allowed to dry in the fume hood. This glass was modified with an amino-silane ((3-aminopropyl)-triethoxysilane, Gelest) based on a modified version of a published protocol.[23] Briefly, glass slides were immersed in 70 mM (3-aminopropyl)-triethoxysilane and 70 mM n-butyl amine in toluene and allowed to react 90 minutes at room temperature. They were then wiped with a toluene-wet kimwipe and dried overnight in an 80 °C oven. The amine-functionalized glass was subsequently reacted with the azide-modified carboxylic acid by immersing in 100 mM azide-butanoic acid, 100 mM HATU (ester activating agent, AnaSpec), and 100 mM *N*,*N*-diisopropylethylamine in dimethylformamide, reacting for 4^+ hours, rinsing with acetone and wiping dry, creating a thin, easy-to-handle base for hydrogel formation, patterning, and controlled cell culture. These azide-functionalized cover slides were kept at 4 ^oC in the dark until their use in hydrogel formation (typically used within 1 month of preparation).

Molds for hydrogel formation were assembled with an azide-functionalized cover slip, a 0.5 mm-thick, ~ 1-mm wide silicon rubber gasket on each side of this cover slip, and a cover slip

treated with an anti-adhesion agent (Rain-X) placed offset by ~ 1 mm on top, creating a ~ 15 mm x 15 mm area with two open sides for easy addition of the liquid monomer solution.

Monomer stock solutions were prepared under sterile conditions using sterile reagents: (1) 12.5 mM PEG-tetracyclooctyne in PBS (freshly prepared, containing 50 mM difluorinated cyclooctyne ($DIFO_3$)), (2) 25 mM azide-RGDS in PBS, and (3) 24 mM bis(azide)-functionalized peptide (containing 48 mM azide) dissolved first in minimal DMSO and diluted with PBS and azide-RGDS stock solution for 2 mM RGDS (typically 1:5 to 1:10 DMSO:PBS) (freshly prepared, containing 50 mM total azide). Note that these molar concentrations (mM) assume that the contribution of the solid to the solution volume is minimal upon dissolution. The sterile Dulbecco's phosphate buffered saline (PBS, Invitrogen) contained antibiotic (50 U/mL penicillin and 50 μg/mL streptomycin, Invitrogen) and antifungal (1 μg/mL amphotericin B, Invitrogen) agents. The final gel-forming solution was comprised of equal volumes of stock solution 1 and 3 for 6.7 wt% total monomer consisting of four-arm PEG-tetracyclooctyne in PBS, bis(azide)-functionalized peptide, and 1 mM azide-RGDS (total 25 mM $DIFO_3$ and 25 mM azide). For samples whose patterning would be characterized with confocal imaging, a small amount of azide-functionalized dye stock solution was added to the gel-forming monomer solution in place of PBS (Alexa Fluor® 594 Carboxamido-(6-Azidohexanyl), Invitrogen, dissolved per manufacturer instructions) for a final concentration of 0.1 mM within the hydrogels.

The mixed monomer solution was quickly centrifuged (Mini Centrifuge, Fisher Scientific) for ~ 15 s to remove air bubbles, and ~ 50 uL of gel-forming solution was pipetted into each mold. Owing to the fast reactivity of the copper-free click chemistry, no more than ~ 8 samples were prepared in parallel from a single Eppendorf tube, *i.e.*, additional tubes of monomer solutions could be mixed serially to achieve the desired number of samples for an

experiment. Hydrogels were allowed to polymerize in the dark for ~ 1 h, a time previously determined to allow complete polymerization.[19] Sterile PBS (with antifungal and antibiotic agents) was injected (26 gauge needle and syringe, BD) within the empty space surrounding the fully-formed gels, and the molds were fully submerged within a petri dish containing sterile PBS. The hydrogels were allowed to swell in this solution for 1 h, and the top Rain-X-treated cover slip was gently and carefully removed using a razor blade. The hydrogels were transferred to sterile 6-well plates, covered with fresh sterile PBS, sealed with Parafilm®, and stored at 4^{o}C overnight to allow any unreacted monomer to diffuse out.

3.3.3 Patterning of hydrogel devices

Photomasks were designed in Adobe Illustrator and emulsion printed on Mylar (Advance Reproductions, North Andover, MA). Shapes consisted of 200 μm diameter circles (Circle), two connected 100 μm diameter circles (Di), and four connected 100 μm diameter circles (Quad). Photomasks were bonded to glass slides (50 mm x 75 mm, Fisher Scientific) with the photopolymerization of a thin layer of urethane diacrylate and triethylene glycol diacrylate with I184 as the initiator to create an optically clear adhesive (40 mW/cm^2 of 320-500 nm irradiation centered at 365 nm for 15 min, mask aligner with collimated flood exposure source, Optical Associates, Inc., San Jose, CA).[24] Wells were photodegraded into the gels by placing a gasket around the gel coverslip, covering with sterile PBS, placing the photomask slide on top of the gasket, and irradiating with collimated 365 nm light at 9 ± 1 mW/cm^2 for up to 30 min (20 min irradiation used to pattern devices for cell seeding experiments; Omnicure S1000 with 365 nm filter, liquid filled light guide, and collimating lens, EXFO).[20g] Patterned gels were placed in sterile 12-well plates and swollen in sterile PBS containing antibiotics and antifungal overnight at 37 °C. Depths of the resulting wells were verified with profilometry (Stylus Profiler, Dektak

6M) and confocal microscopy (Zeiss 710, 10-20x water immersion objectives).[25] Irradiation intensities for all experiments were measured with a calibrated radiometer (Model IL1400A, International Light, Inc., Newburyport, MA).

3.3.4 Modeling of hydrogel patterning

A statistical-kinetic model of photodegradation recently was adapted to predict the depth of patterned features in these step growth hydrogels as a function of irradiation time.[25a, 26] The statistical-kinetic model accounted for the attenuation of light in the sample during irradiation, the kinetics of the photocleavage of the *o*-nitrobenzyl ether (NBE) moiety, reverse gelation of the hydrogel network, and diffusion of the degraded products after reverse gelation. Briefly, the Beer-Lambert Law and a first-order expression of the photocleavage reaction were solved numerically in 1-D over the space and time of the irradiation during patterning. The probability that a NBE moiety has been cleaved was solved at each point in space and time, $P(z,t) = 1 - [NBE]/[NBE]_0$. When $P(z,t) \geq P_{rg} = 0.67$, the critical extent of cleavage to induce reverse gelation based on the Flory-Rehner equation,[27] it was assumed that the gel disassembled into soluble components that diffused one-dimensionally, removing attenuators of the light from the light path. By numerically solving this system of equations using finite element methods (MATLAB, MathWorks®), the erosion depth as a function of time was predicted for this hydrogel system from t = 0 to 30 min. The diffusion coefficient for the degraded products was assumed to be 1×10^{-6} cm^2/s based on predicted hydrodynamic radii. The kinetic constant for photodegradation was taken from a previous analysis of the photolabile azide moiety.[19]

3.3.5 Cell isolation and expansion

Adenocarcinomic human alveolar basal epithelial cells (A549, ATCC) were used as a model lung epithelial cell to characterize cell seeding. A549 cells cultured per standard protocols

in growth media (Dulbecco's modified Eagle's medium (DMEM), 10% fetal bovine serum (FBS), 2% penicillin/streptomycin (100 U/mL), 0.4% fungizone (0.5 μg/mL), Invitrogen) at 37 °C with 5% CO_2 and successively passaged until use in experiments. To characterize cell seeding within the devices, plated A549s (~ 80% confluent) were labeled with Cell Tracker Green (CTG, Invitrogen) per the manufacturer's instructions using a minimal amount of 10 μM CTG in serum free media for 30 min during the labeling step. CTG labeled A549s were used immediately in cell seeding experiments.

3.3.6 Alveolar type II cell (AT2) isolation

Mice (6-8 weeks old) were euthanized by CO_2 asphyxiation. The thorax was opened and the pulmonary circulation flushed with sterile PBS. The lungs were excised and distal lung tissue was minced finely and digested in 1% collagenase (Worthington Biochemical, NJ) + 1 mg/ml DNase (GIBCO BRL, Carlsbad CA) for 30 minutes. An equal volume of 2 mg/ml typsin inhibitor (GIBCO BRL) + 2 mg/ml DNase was added and cell suspension was filtered through 10 μm pore diameter Nitex Filter. Cells were centrifuged at 430xg for 10 minutes at room air temperature. Cell pellet was washed with DMEM/F12 media and plated on non-tissue culture plates coated with IgG (6 mg/cm^2, Sigma) for one hour at 37°C. Non-adherent cells were recovered and centrifuged at 430xg for 10 minutes. Cell pellet was resuspended and cultured in DMEM/F12 + 10% FBS.

3.3.7 Study animals and protocols

All procedures and protocols were reviewed and approved by the Animal Care and Use Committee at the University of Colorado Denver Anschutz Medical Campus. Mice were obtained from The Jackson Laboratories and bred in-house.

3.3.8 Cell seeding and encapsulation within culture platform

To characterize the relationship between cell number and seeding density, CTG-labeled A549s were trypsinized, centrifuged (1000 rpm for 5 min), and suspended at varying concentrations in growth medium (0.25 to 2.5 x 10^6 cells/mL). Cells were seeded per a modified version of previously published protocols.[14a, 28] Growth medium was added to the patterned gels (1 gel per well of 12-well plate) and centrifuged at 3200 rpm for 1.5 minutes to force liquid into the wells. 2 mL of the cell suspension (0.5 to 5 x 10^6 cells/well) was added to each gel, followed by centrifugation at 1200 rpm for 2.5 minutes, rotation of the plate, and centrifugation at 1200 rpm for another 2.5 minutes. Plates were placed on an orbital shaker for 2 hours at 35 rpm and 37 °C. Media was changed and the cell-filled gels were incubated overnight.

For lung epithelial differentiation studies, freshly isolated primary adult mouse ATII cells (98-99% purity) were suspended at 1 x 10^6 cells/mL in DMEM containing 10% fetal bovine serum (FBS), antibiotic, and antimitotic. Media was added to the patterned gels and centrifuged at 3200 rpm for 1.5 minutes to force liquid into the wells. 2 mL of the cell suspension was added to each gel, followed by centrifugation at 1200 rpm for 2.5 minutes, rotation of the plate, and centrifugation at 1200 rpm for another 2.5 minutes. Plates were placed on an orbital shaker for 2 hours at 35 rpm and 37 °C. Media was changed, and the cell-filled gels were incubated overnight.

The next day, a second hydrogel layer was formed on top of the cell-seeded construct to encapsulate cells within individual wells. Media was removed from each sample. Monomer solutions were prepared as above. For each device, 25 μL of total monomer solution was mixed and allowed to react for 1 minute to increase the viscosity before adding it to the top of each cell-laden gel. In this manner, the infiltration of the top gel down into the wells was reduced creating

a cell and medium filled microwell in which cells experience matrix interactions at the periphery and cell-cell interactions within the aggregate. Samples were then allowed to fully polymerize for 20 minutes at 37 °C. To remove any unreacted monomer, media was added to each sample, incubated 1 hour, and then replaced with fresh media. This was considered day 0. Encapsulated cell clusters were cultured within these devices for up to 2 weeks. Culture medium contained FGF-7 (10 ng/mL) and FGF-10 (50 ng/mL) to promote proliferation and branching, respectively.[29] Culture medium was replaced daily.

3.3.9 Cell response assessment

Devices were harvested at time points of interest to observe cell morphology and cell phenotype. The devices were transferred to a new 12-well plate and fixed with 4% paraformaldehyde (PFA) in PBS for 15 min at room temperature (freshly diluted from 16% PFA stock, 1 mL per sample, Electron Microscropy Sciences), rinsed with PBS (3x of 2 mL per sample, gently rocking, 5 min), and stored in fresh PBS at 4 °C until samples for all time points were ready for staining.

Cells within the devices were labeled using immunocytochemistry for pro-surfactant protein C (an ATII cell marker in cell cytosol and secreted), T1-alpha protein (an ATI cell marker in the cell membrane), and DNA. After all samples were collected, fixed cells within devices were permeabilized in 1% TritonX-100 for 1 hour at room temperature. The samples were blocked with 40% goat serum (Invitrogen) in PBS overnight. Primary antibodies, rabbit anti-prosurfactant protein C (SPC, 1:100, Millipore AB3786) and hamster anti-mouse podoplanin (T1α, 1:100, eBioscience 14-5381-82), were added to samples with 5% polyvinylpyrrolidone (MW 10,000 g/mol), 0.3% Tween 20, and 10% goat serum in PBS and rocked overnight. Samples were rinsed, and then incubated with secondary antibodies, goat anti-

rabbit Alexa594 (1:200, Invitrogen) and goat anti-hamster Alexa488 (1:200, Invitrogen), in 4% goat serum, 0.1% Tween 20, and 0.1% bovine serum albumin in PBS for 16 hours. Samples were washed, followed by nuclei staining with DAPI (1:2000, Invitrogen) in PBS for 1 hour. The samples were washed with PBS twice before imaging.

All samples were imaged on a 710 LSM confocal microscope (Zeiss) with a 20x or 10x water immersion objective (NA = 1.0, Plan-Apochromat). Individual wells were centered in the imaging area and imaged from the top of the well down to the last visible cell with a z-stack slice step of 5 μm. Image analysis was done in Image J (NIH).

3.3.10 Frequency map generation

Based on an established protocol,[15] z-stack fluorescent images of each channel for each well were projected onto one image and converted to binary. These black-and-white images were added together to create a gray-scale image, and a HeatMap Histogram plugin (Authors: S. Pèan & M. Austenfeld, modified by K. Lewis) was used to convert the gray-scale image to a color-coded image (n=30 wells for each frequency map).

For side-view frequency maps, ZEN software with 3D rendering was used to slice through the middle of each well in the xz-plane and create a composite image of half the well. The same procedure was used to create frequency maps as described above.

3.3.11 *In situ* microenvironment modification during controlled cell culture

On day 4, rectangular channels were patterned between neighboring wells using two-photon techniques where a user-defined region within the hydrogel was selectively exposed to pulsed laser light (λ = 740 nm, 5 channels per sample, approximately 400 μm x 80 μm x 90 μm). Degraded monomer was removed by swelling in fresh media. These samples were then

incubated until day 7, when they were fixed and immunostained with the static culture, unmodified samples.

3.4 Results and discussion

We present the development of a culture platform that allows the experimenter to dictate the cell microenvironment geometry or connectivity and demonstrate its utility for controlled culture of lung epithelial cells (Figure 3.1). The photolabile and enzyme-labile hydrogel base material enables the creation of a wide range of well depths (50 to 200^{+} μm) and shapes using standard photolithographic techniques. Cells of interest can be facilely seeded within these wells and encapsulated to probe their response to a geometrically-defined environment, which is easily

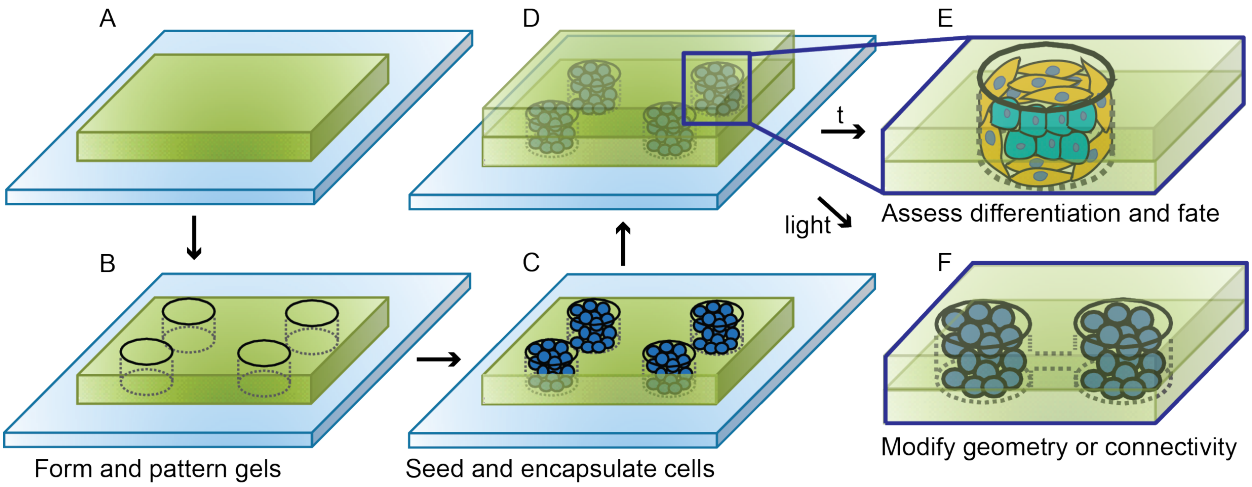

Figure 3.1 Platform fabrication for dynamic control of cell cluster shape and connectivity. (A) The photolabile, enzyme-labile hydrogel base material was formed on glass cover slips to enable ease of handling for subsequent patterning or cell seeding. (B) Hydrogel layers 0.5 mm in thickness were formed to enable the stable creation of a wide range of well depths (50 to 200 μm) and shapes with photolithography. (C) These wells were seeded with cells of interest, which could be used at this point in processing for microwell cultures, and (D) a second hydrogel layer was added to encapsulate cell clusters within 3D microenvironments that enable spatiotemporally controlled geometry. (E) Cell response to their geometrically-defined environments and cell-dictated remodeling was monitored over time with live or static imaging techniques, and (F) the geometry or connectivity of the local matrix was modified at any position and time during culture with the application of cytocompatible light.

assessed with imaging-based assays. As the patterning material can be degraded by cell-secreted proteases, cells can respond to and remodel their surrounding matrix. Further, the user can initiate changes to microenvironment shape or connectivity of the cell-laden wells through controlled, cytocompatible irradiation. We demonstrate the utility of these devices by examining how geometry regulates alveolar type II (ATII) epithelial cell fate. The versatile cell culture devices presented are a new tool for asking how geometry and connectivity dynamically regulate cell function and fate.

The base material for these devices is a light and enzyme degradable PEG hydrogel. The crosslinking monomer is a multi-arm PEG (4 arm, M_n ~ 10 kDa) modified with cyclooctyne end groups (Figure 3.2). A photolabile, enzyme-labile peptide functionalized with azides[19] was designed to allow cleavage either by externally-applied UV, visible, and two-photon irradiation or by cell-secreted matrix metalloproteinases, including MMPs 1, 2, 3, 8, and 9.[21] These MMPs

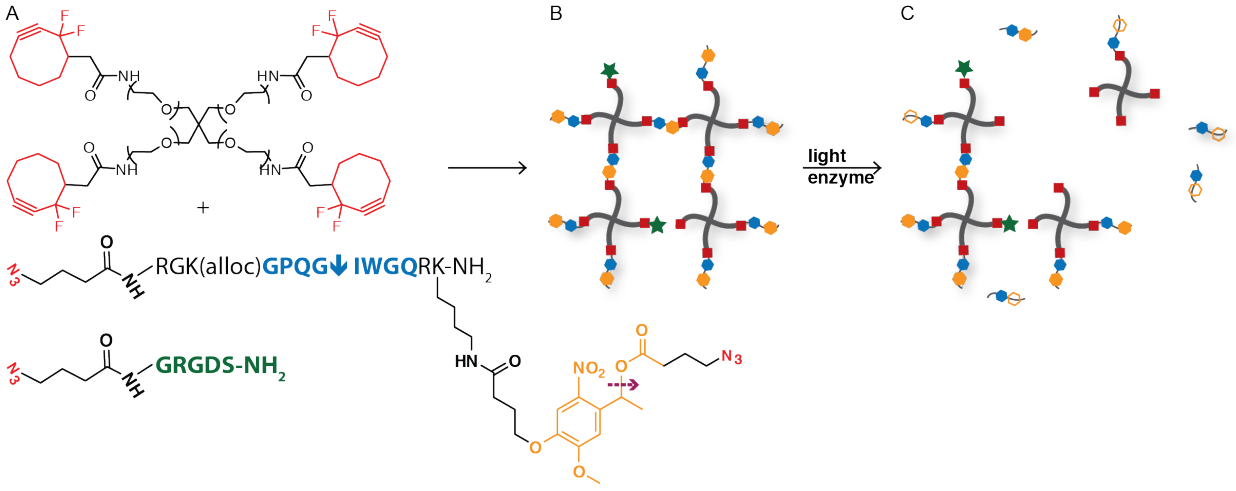

Figure 3.2 Hydrogel synthesis and degradation. (A) The hydrogel base material was comprised of poly(ethylene glycol) tetracycloctyne (M_n ~ 10 kDa, top); photolabile, enzyme-labile, diazide peptide (middle; enzymatically cleavable sequence in blue, light cleavable moiety in yellow, cleavage positions noted by arrows); and an azide-functionalized integrin-binding adhesive ECM mimic (bottom, integrin-binding sequence in green). (B) This combination of chemistries enabled copper-free 'click', bioorthogonal hydrogel formation (C) for subsequent experimenter-initiated *in situ* photolytic patterning (cytocompatible UV, visible, and two-photon irradiation), and cell-initiated enzymatic remodeling (various MMPs including 1, 2, 3, 8, and 9).

are secreted or present on the membranes of many cell types,[21c] including ATII cells which have been observed to secrete collagenase (MMP-1), gelatinase A (MMP-2), and gelatinase B (MMP-9) during *in vitro* culture.[30] Further, this enzymatically-degradable sequence derived from collagen I has been used within hydrogels for 3D culture of many cell types, including human dermal fibroblasts,[31] mesenchymal stem cells,[32] valvular interstitial cells,[33] osteoblast progenitor cells,[34] and smooth muscle cells.[35] Last, an integrin-binding ECM protein mimic, RGDS, functionalized on the N-terminus with an azide was added to the gel-forming monomer solution to promote general cell adhesion to the geometrically-defined synthetic ECM. This combination of chemistries allows copper-free click hydrogel formation and subsequent orthogonal light-based degradation and patterning or cell-driven enzymatic remodeling. While not shown here, the modulus of the base material can be easily manipulated by altering the weight percent of monomer in the hydrogel,[36] and biochemical moieties can be spatiotemporally added through radical-mediated photoaddition reactions of thiol-containing peptides with the allyl-protected lysine on the crosslinking peptide.[37]

One advantage of this system is the simplicity of the hydrogel patterning process, enabling the creation of wells of varied depth and shape *after* hydrogel formation. Shapes of interest on the micron scale can be drawn in a CAD or illustration program and printed onto transparent films for subsequent transfer with a low-intensity collimated light source. To demonstrate this practical approach, 200-μm circles individually, or in clusters as will be shown below, were drawn in Adobe Illustrator and the negative printed onto to a transparent film that was affixed to a microscope slide for patterning *via* photodegradation. Wells of the drawn shape were degraded into the hydrogel surface and subsequently seeded with cells (Figure 3.3A). Good

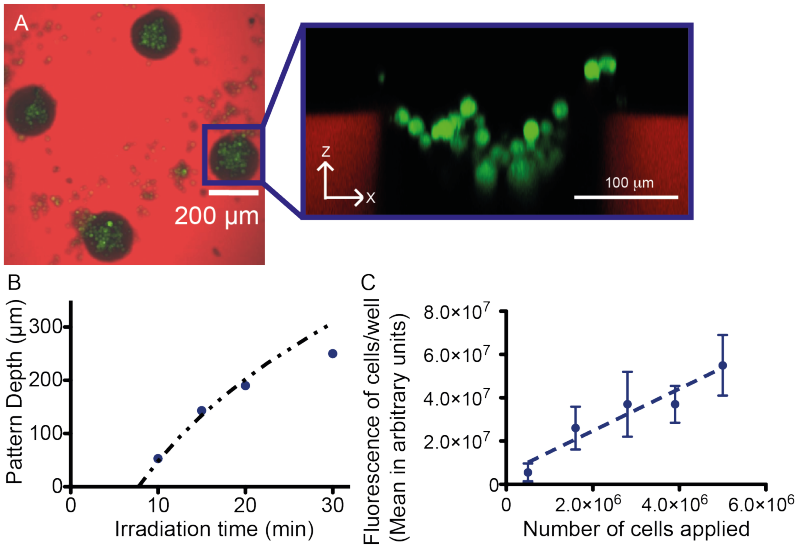

Figure 3.3 Culture platform well depth and cell seeding. (A) Micron-scale wells were patterned into the surface of the hydrogel base and seeded with cells (x-y left; x-z right). (B) Well depth, measured with profilometry, was controlled predictably with irradiation time (cytocompatible ~ 9 ± 1 mW/cm^2 at 365 nm). (C) For cell seeding, a well depth of ~ 200 µm was utilized, which was achieved with 20 min of irradiation. The total number of cells applied to each device (model lung epithelial cells, A549s, labeled with cell tracker green) linearly dictated the initial density of cells per well (measured as total green fluorescence per well). Data points are mean ± one standard deviation.

x-y pattern fidelity was observed, and well depth (≥ 50 µm) was controlled with irradiation time with a constant cytocompatible light intensity (9 ± 1 mW/cm^2 at 365 nm) (Figure 3.3B).

While the well depth did not increase linearly with irradiation time, this non-linear function was predicted by a statistical-kinetic model of photodegradation (Figure 3.3B). The complex interplay between the attenuation of light, diffusion of degraded products, and photodegradation results in a non-linear surface erosion rate. Owing to the attenuation of light in the hydrogel, the degrading light is initially limited to the near surface region of the gel. This confines degradation, and ultimately erosion, to the surface. Upon erosion, the degraded products of the gel become soluble and begin to diffuse out of the path of the light. This exposes subsequent regions of the gel to irradiation, allowing the erosion process to penetrate through the

material and generate patterns of increasing depth with irradiation time. Deviations between the statistical-kinetic model and experiment at later time points (t = 30 min) were likely due to slower diffusion rates in the experimental set-up than were assumed in the model, which would lead to a decreased extent of erosion. The pattern formation rate for this ideal network is rapid and occurs at much lower dosages of light than is required in similar chain polymerized photodegradable hydrogels. This is advantageous not only for the rapid generation of defined patterns, but also for subsequent patterning of the gel in the presence of cells.

Cells of interest are seeded within these wells using established techniques, where cells suspended in medium at a known concentration are applied to each device and centrifuged to facilitate seeding.[28] For a given device geometry and well depth, the total number of cells applied to each device dictates the initial density of cells per well (Figure 3.3C). These seeding experiments were performed with a model lung epithelial cell line (A549s labeled with cell tracker green for ease of imaging and quantification). While there is variation in cell seeding between individual wells, the overall average number of cells seeded per well is linear with the number of cells applied when averaged over the entire device (~ 30 wells). With a simple calibration experiment like this, the experimenter can determine the number of cells to apply to each device for the desired seeding density per well. Here, 2.75×10^6 cells/device was selected as a compromise between even well filling (see the inset Figure 3.3A) and total number of cells required per experiment, which can be limited by the availability of freshly isolated primary cells. Additionally, the number of cells per device can be scaled with device surface area, where preliminary experiments were performed with devices in 6-well plates and then scaled down to the final 12-well plate size and format to conserve cells (data not shown).

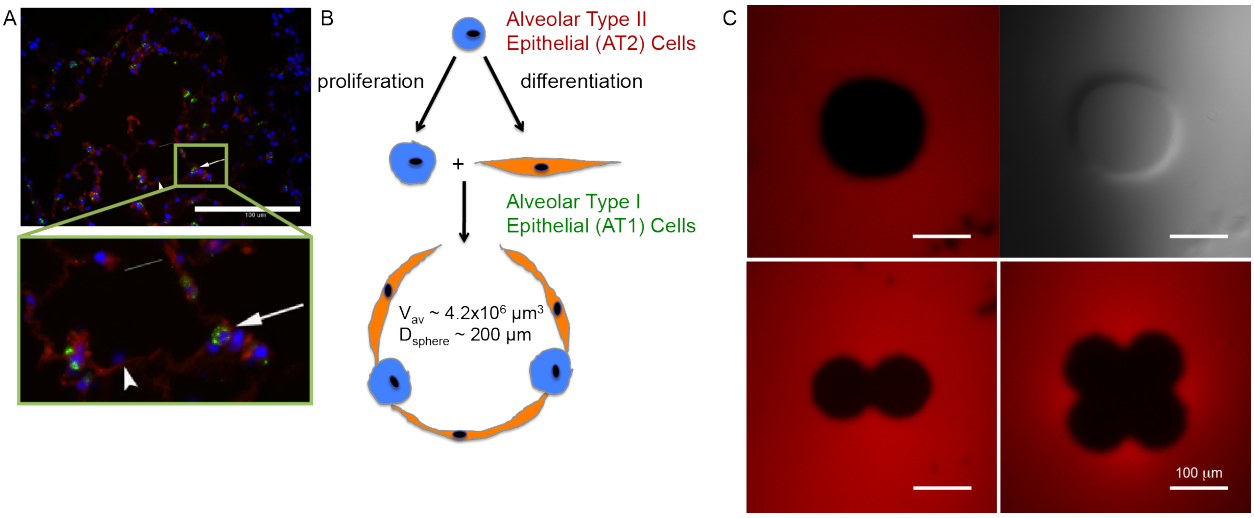

Figure 3.4 Alveolar-inspired shape wells and lung epithelial cell phenotypes. (A) ATII cells (green, noted by arrows) and ATI cells (red, noted with arrowhead) comprise the alveolar epithelium (mouse lung section, blue cell nuclei, and alveolar opening noted with white line). Scale bar = 100 µm. (B) ATI cells form the barrier between the airways and the capillaries, whereas ATII cells produce lung surfactants and can proliferate and differentiate to replenish both phenotypes after injury. The volume of an adult human alveolus is estimated to be about 4.2 million µm[3,40] which translates to a spherical diameter of about 200 µm. (C) Fluorescent and DIC images of the well shapes patterned into the gel. In this case a red fluorescent dye was incorporated into the hydrogel network so black areas are where the gel has been degraded. Given that native alveoli are not spherical, photolithographic masks were designed with an increasing number of circular lobes and an overall width of 200 µm to observe how changes in curvature affect cell fate.

We aimed to demonstrate the utility of these devices for probing the role of geometry in cell fate and focused on the hierarchically structured alveolar epithelium. Lung architecture follows an increasingly complex network of connected tubes starting from a single trachea that branches into bronchi, bronchioles, and finally ends in millions of hollow air sacs called alveoli (Figure 3.4A). The major components of alveolar tissue include the single cell layer epithelium attached to the basement membrane and surrounded by a fine mesh of capillaries. There are two types of alveolar epithelial cells: ATI cells, which have an elongated morphology, form 95% of the alveolar surface area, and facilitate gas exchange between the lung and the blood stream,[38] and ATII cells, which exhibit a cuboidal morphology, produce lung surfactants, and are the

progenitor cells for both the ATII and ATI cell populations in the alveoli[18] (Figure 3.4B). ATIIs are known to self renew and differentiate into ATIs during alveolar development and in response to injury; however, examining the complex milieu of signals involved in these processes *in vitro* can be difficult owing to rapid loss of the ATII phenotype during culture.[18, 39]

The size and shape chosen for the wells was inspired by human alveolar geometry. The average volume for an adult human alveolus has been measured to be 4.2 million cubic microns, which corresponds to a spherical diameter of 200 microns.[40] Alveoli *in vivo*, however, are not spherical;[40-41] therefore, well shapes consisting of an increasing number of circular lobes were designed with an overall diameter of 200 microns (Figure 3.4C). In native tissue, ATII cells are generally solitary and are found at the corners where neighboring alveoli meet, while ATI cells are adjacent to other ATI cells and are spread out along the curves of the alveoli.[42,43] Based on these observations, it was hypothesized that ATII phenotype cells would localize at the corners of the micropatterned wells where the curvature changes, while ATI phenotype cells would line the curved edges of the wells.

For this experiment we compared two sets of samples: one set fixed 1 day after encapsulation, and the other set fixed 7 days after encapsulation. To observe ATII differentiation within these devices, antibodies for pro-surfactant protein C (SPC, an ATII cell marker localized in the cell cytosol and potentially secreted) and T1-alpha protein (T1α, an ATI cell marker residing in the cell membrane) were used to label the two cell populations. Fluorescent images of the immunostained samples fixed on day 1 (Figure 3.5A) indicate that few cells were producing T1α, the ATI cell marker, which matches expectations given that 98-99% of the cells seeded into these wells were ATII phenotypic. After 7 days T1α production was relatively high (Figure 3.5B), with many elongated cells near the tops of the wells staining positive for both SPC and

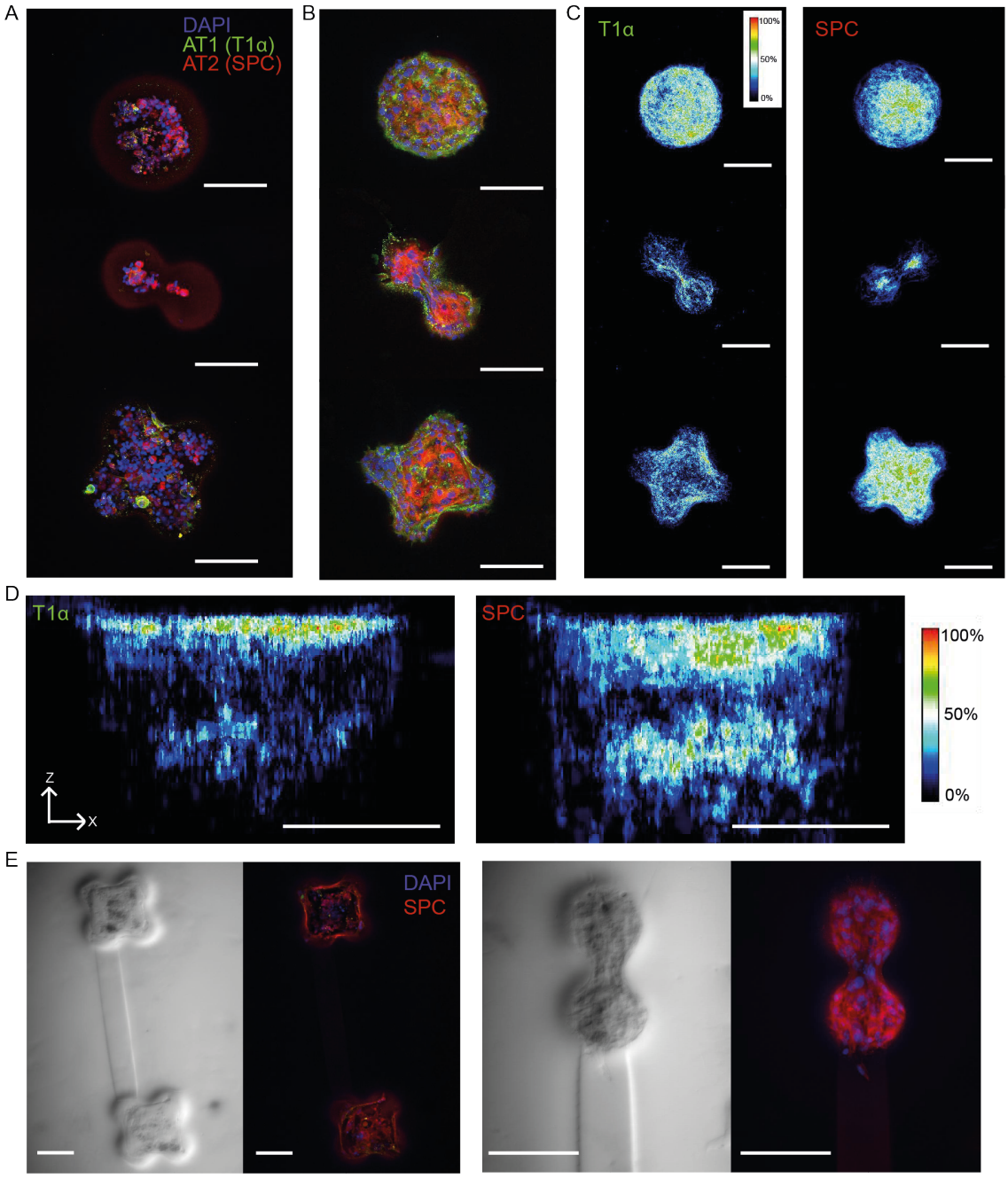

Figure 3.5 Lung epithelial cell response to alveolar-inspired geometries and connectivities. (A) Representative z-projections of the three well shapes fixed on day 1 after encapsulation showing immunostaining for ATI cell marker (T1α), ATII cell marker (SPC), and cell nuclei (DAPI). (B) Representative z-projections of the three well shapes fixed on day 7 after encapsulation showing the same immunostaining as in A. (C) Frequency maps of the three well shapes showing arrangement in the x-y plane of ATI cells in the left column and of ATII cells in the right column on day 7. n=30 (D) Frequency maps of a cross section of the circle wells showing arrangement in the x-z plane of ATI cells on the left and of ATII cells on the right on day 7. n = 30 (E) Bright field and fluorescent images of channels connecting pairs of wells patterned on day 4 after encapsulation. Samples were fixed and immunostained on day 7. All scale bars = 100 μm.

T1α, indicating an intermediate phenotype of alveolar epithelial cell that was transitioning from ATII to ATI. In addition, on day 7 most wells contained small, fragmented nuclei staining positive for SPC or neither marker deeper in the well, which likely maintained the ATII phenotype or were undergoing programmed cell death (apoptosis).

These initial qualitative observations were confirmed by analysis of frequency maps of SPC or T1α staining generated from 30 replicate wells of each shape (Figure 3.5C). DAPI frequency maps demonstrate that cells seeded in these wells initially clustered in the center of the well during seeding and then presumably proliferated and/or migrated towards the edges to fill the well by day 7 (data not shown). As seen in Figure 3.5C, after 7 days in culture SPC-positive cells tended to be located with increased frequency in the center of the well, whereas cells along the well edges tended to express T1α. These T1α-positive cells were not yet fully ATI phenotypic because they also stained positive for SPC, but given more time, they would likely continue differentiating and stop producing surfactant proteins. While in principle these experiments can be taken to longer time points, degradation of the synthetic extracellular matrix after 10 days in culture made handling of the gels during immunostaining and imaging extremely challenging and difficult to replicate.

The day 7 Quad frequency map is particularly interesting because there may have been some localization of T1α-positive cells along the inner curves of the shape. This is counter to the original hypothesis that ATII cells would prefer the corners where the curvature changes, based on lung histology. However, perhaps cells were localizing at those inner curves because they were the closest surfaces to the center of the well where the cells were initially seeded, and when the cells sensed the matrix surface, they spread out and began to differentiate. It may take additional time in culture for cells to reach the distant outer curves of the Quad shape.

By taking a cross-section of the circle wells and projecting in the y direction, frequency maps were generated to reveal the distribution in the x-z plane (Figure 3.5D). Clearly, the intermediate phenotype cells staining positive for both markers reside mainly near the tops of the wells, whereas a population of ATII cells (SPC-positive only) resided primarily lower down in the wells. This observation may be relevant to normal lung tissue in which neighboring alveoli share a progenitor ATII population at the bottom of the epithelium and present the ATI cells at the top surface. The retention of the ATII cell phenotype in some cells after 7 days in culture and the vertical distribution of the differentiating and non-differentiating cell populations are reminiscent of the *in vivo* pattern. However, the aggregates in these devices do not match the exact spatial arrangement of alveolar phenotypes observed *in vivo*, which could be influenced by the lack of other lung cell types, such as fibroblasts, macrophages, and endothelial cells in the culture system. Further work will focus on the effects of the co-culture of these cell types with alveolar epithelial progenitors and the temporal and spatial effects on their growth, survival and differentiation.

Channels were successfully eroded between wells using two-photon irradiation on day 4 after encapsulation (Figure 3.5E), demonstrating the ease with which matrix geometry and connectivity can be altered during cell culture. While 3T3 fibroblast cell migration has been demonstrated along channels eroded using the same techniques in equivalent gel materials,[19] almost no movement of the alveolar epithelial cells down these channels was observed by day 7. There are a few possible explanations for the absence of alveolar cell migration through these channels. RGD may be sufficient for alveolar epithelial cells to adhere to the matrix, but may not be useful for their migration, and a different peptide-based ECM mimic may be necessary for migration. Moreover, there was likely no impetus for these cells to become motile, as there was

no chemical signal attracting the cells, such as a growth-factor gradient. For example, FGF-10 has been shown to be a potent chemoattractant for alveolar epithelial cells during development, and without a gradient of it, there is no lung bud outgrowth.[29b, 44] The culture platform offers facile patterning of wells of varying shape, position, and connectivity at any time during cell culture, and combined with the presented quantitative imaging techniques, can be used to explore the dynamic interplay between these parameters in future experiments with alveolar epithelial cells, as well as other cell types of interest.

3.5 Conclusions

We have developed a dynamic, well-based cell culture platform to control the geometry and connectivity of the cell microenvironment spatiotemporally *in vitro*. Photolabile, enzyme-labile hydrogels were used as the base material, enabling the creation of wells with varied shape and depth in which primary cells were seeded and encapsulated. The utility of these devices for culturing ATII epithelial cells in defined geometries was demonstrated. This platform can be used to understand how static *or* evolving physical cues influence cell cluster shapes, cell-cell interactions, and ultimately function and fate in tissue development or regeneration.

3.6 Acknowledgements

The authors would like to thank Abigail Bernard for generously providing the urethane diacrylate and triethylene glycol diacrylate with I184 mixture for photomask adhesion and the cell seeding protocol; Balaji Sridhar for assistance with preliminary patterning and A549 seeding studies; Emily Roth, Sharon Ryan, and Liv Hoversten for assistance with preliminary A549 and ATII studies; and Ben Fairbanks for assistance with preliminary ATII 3D encapsulation studies.

The authors would like to acknowledge funding from the Howard Hughes Medical Institute and NSF (DMR 1006711); M.W.T. would like to thank the Teets Family Endowed Doctoral Fellowship for funding assistance; and V.B. is supported by NIH R01 HL089262.

3.7 References

1. (a) D. E. Discher, P. Janmey, Y. L. Wang, *Science* 2005, **310**, 1139; (b) V. Vogel, M. P. Sheetz, *Curr. Opin. Cell Biol.* 2009, **21**, 38; (c) M. A. Wozniak, C. S. Chen, *Nat. Rev. Mol. Cell Biol.* 2009, **10**, 34; (d) N. Wang, J. D. Tytell, D. E. Ingber, *Nat. Rev. Mol. Cell Biol.* 2009, **10**, 75; (e) A. J. Keung, S. Kumar, D. V. Schaffer, in *Annual Review of Cell and Developmental Biology, Vol 26*. Annual Reviews: Palo Alto, 2010, vol. 26, pp 533-556.

2. P. Tayalia, D. J. Mooney, *Adv. Mater.* 2009, **21**, 3269.

3. (a) R. A. Marklein, J. A. Burdick, *Adv. Mater.* 2010, **22**, 175; (b) M. P. Lutolf, P. M. Gilbert, H. M. Blau, *Nature* 2009, **462**, 433.

4. (a) D. Warburton, M. Schwarz, D. Tefft, G. Flores-Delgado, K. D. Anderson, W. V. Cardoso, *Mech. Dev.* 2000, **92**, 55; (b) S. Huang, D. E. Ingber, *Nat. Cell Biol.* 1999, **1**, E131; (c) N. Gjorevski, C. M. Nelson, *Birth Defects Res. Part C-Embryo Today-Rev.* 2010, **90**, 193.

5. F. Guilak, D. M. Cohen, B. T. Estes, J. M. Gimble, W. Liedtke, C. S. Chen, *Cell Stem Cell* 2009, **5**.

6. (a) R. McBeath, D. M. Pirone, C. M. Nelson, K. Bhadriraju, C. S. Chen, *Dev. Cell* 2004, **6**, 483; (b) S. Khetan, J. A. Burdick, *Biomaterials* 2010, **31**, 8228.

7. (a) C. M. Nelson, *Biochim. Biophys. Acta-Mol. Cell Res.* 2009, **1793**, 903; (b) C. M. Nelson, M. M. VanDuijn, J. L. Inman, D. A. Fletcher, M. J. Bissell, *Science* 2006, **314**.

8. (a) C. M. Nelson, M. J. Bissell, *Annu. Rev. Cell Dev. Biol.* 2006, **22**; (b) R. Xu, A. Boudreau, M. Bissell, *Cancer Metastasis Rev.* 2009, **28**.

9. (a) C. Moraes, Y. Sun, C. A. Simmons, *Integrative Biology* 2011, **3**; (b) D. H. Kim, P. K. Wong, J. Park, A. Levchenko, Y. Sun, in *Annu. Rev. Biomed. Eng.* Annual Reviews: Palo Alto, 2009, vol. 11, pp 203-233; (c) D. E. Ingber, *Int. J. Dev. Biol.* 2006, **50**, 255.

10. (a) C. S. Chen, M. Mrksich, S. Huang, G. M. Whitesides, D. E. Ingber, *Science* 1997, **276**, 1425; (b) C. M. Nelson, R. P. Jean, J. L. Tan, W. F. Liu, N. J. Sniadecki, A. A. Spector, C. S. Chen, *Proc. Natl. Acad. Sci. U. S. A.* 2005, **102**, 11594; (c) K. A. Kilian, B. Bugarija, B. T. Lahn, M. Mrksich, *Proc. Natl. Acad. Sci. U. S. A.* 2010, **107**, 4872.

11. (a) T. Gudjonsson, L. Ronnov-Jessen, R. Villadsen, M. J. Bissell, O. W. Petersena, *Methods* 2003, **30**, 247; (b) M. J. Bissell, A. Rizki, I. S. Mian, *Curr. Opin. Cell Biol.* 2003, **15**, 753; (c) G. Y. Lee, P. A. Kenny, E. H. Lee, M. J. Bissell, *Nat. Methods* 2007, **4**.

12. N. Gjorevski, C. M. Nelson, *Integrative Biology* 2010, **2**, 424.

13. E. W. Gomez, Q. K. Chen, N. Gjorevski, C. M. Nelson, *J. Cell. Biochem.* 2010, **110**, 44.

14. (a) S. A. Ruiz, C. S. Chen, *Stem Cells* 2008, **26**, 2921; (b) L. Gao, R. McBeath, C. S. Chen, *Stem Cells* 2010, **28**, 564.

15. C. M. Nelson, J. L. Inman, M. J. Bissell, *Nat. Protoc.* 2008, **3**.

16. (a) M. Nikkhah, F. Edalat, S. Manoucheri, A. Khademhosseini, *Biomaterials* 2012, **33**, 5230; (b) O. Z. Fisher, A. Khademhosseini, R. Langer, N. A. Peppas, *Accounts Chem. Res.* 2010, **43**.

17. (a) D. R. Albrecht, V. L. Tsang, R. L. Sah, S. N. Bhatia, *Lab Chip* 2005, **5**, 111; (b) D. R. Albrecht, G. H. Underhill, T. B. Wassermann, R. L. Sah, S. N. Bhatia, *Nat. Methods* 2006, **3**, 369.

18. R. J. Mason, *Respirology* 2006, **11**, S12.

19. C. A. DeForest, K. S. Anseth, *Nat. Chem.* 2011, **3**.

20. (a) C. P. Holmes, *Journal Of Organic Chemistry* 1997, **62**, 2370; (b) J. A. Johnson, J. M. Baskin, C. R. Bertozzi, J. T. Koberstein, N. J. Turro, *Chemical Communications* 2008, 3064; (c) M. Alvarez, A. Best, S. Pradhan-Kadam, K. Koynov, U. Jonas, M. Kreiter, *Adv. Mater.* 2008, **20**, 4563; (d) Y. R. Zhao, Q. Zheng, K. Dakin, K. Xu, M. L. Martinez, W. H. Li, *Journal Of The American Chemical Society* 2004, **126**, 4653; (e) D. Y. Wong, D. R. Griffin, J. Reed, A. M. Kasko, *Macromolecules* 2010, **43**, 2824; (f) A. M. Kloxin, A. M. Kasko, C. N. Salinas, K. S. Anseth, *Science* 2009, **324**, 59; (g) A. M. Kloxin, M. W. Tibbitt, K. S. Anseth, *Nat. Protoc.* 2010, **5**.

21. (a) M. P. Lutolf, J. L. Lauer-Fields, H. G. Schmoekel, A. T. Metters, F. E. Weber, G. B. Fields, J. A. Hubbell, *Proc. Natl. Acad. Sci. U. S. A.* 2003, **100**, 5413; (b) B. D. Fairbanks, M. P. Schwartz, A. E. Halevi, C. R. Nuttelman, C. N. Bowman, K. S. Anseth, *Adv. Mater.* 2009, **21**; (c) J. Patterson, J. A. Hubbell, *Biomaterials* 2010, **31**, 7836; (d) H. Nagase, G. B. Fields, *Biopolymers* 1996, **40**, 1996.

22. C. A. DeForest, B. D. Polizzotti, K. S. Anseth, *Nat. Mater.* 2009, **8**.

23. (a) D. M. Walba, C. A. Liberko, E. Korblova, M. Farrow, T. E. Furtak, B. C. Chow, D. K. Schwartz, A. S. Freeman, K. Douglas, S. D. Williams, A. F. Klittnick, N. A. Clark, *Liq. Cryst.* 2004, **31**, 481; (b) B. J. Adzima, Y. H. Tao, C. J. Kloxin, C. A. DeForest, K. S. Anseth, C. N. Bowman, *Nat. Chem.* 2011, **3**, 256.

24. H. A. Simms, C. A. Bowman, K. S. Anseth, *Biomaterials* 2008, **29**, 2228.

25. (a) A. M. Kloxin, M. W. Tibbitt, A. M. Kasko, J. F. Fairbairn, K. S. Anseth, *Adv. Mater.* 2010, **22**; (b) M. W. Tibbitt, A. M. Kloxin, K. U. Dyamenahalli, K. S. Anseth, *Soft Matter* 2010, **6**.

26. A. E. Rydholm, S. K. Reddy, K. S. Anseth, C. N. Bowman, *Polymer* 2007, **48**.

27. (a) P. J. Flory, J. Rehner, *J. Chem. Phys.* 1943, **11**, 512; (b) P. J. Flory, *Principles of Polymer Chemistry*. Cornell University: 1953; p 672.

28. A. B. Bernard, C. C. Lin, K. S. Anseth, *Tissue Eng.* 2012, **18**, 1.

29. (a) T. Yano, R. J. Mason, T. L. Pan, R. R. Deterding, L. D. Nielsen, J. M. Shannon, *Am. J. Physiol.-Lung Cell. Mol. Physiol.* 2000, **279**, L1146; (b) W. Y. Park, B. Miranda, D. Lebeche, G. Hashimoto, W. V. Cardoso, *Dev. Biol.* 1998, **201**, 125.

30. A. Pardo, K. Ridge, B. Uhal, J. Iasha Sznajder, M. Selman, *The International Journal of Biochemistry & Cell Biology* 1997, **29**, 901.

31. G. P. Raeber, M. P. Lutolf, J. A. Hubbell, *Biophys. J.* 2005, **89**, 1374.

32. S. B. Anderson, C. C. Lin, D. V. Kuntzler, K. S. Anseth, *Biomaterials* 2011, **32**.

33. J. A. Benton, B. D. Fairbanks, K. S. Anseth, *Biomaterials* 2009, **30**.

34. M. Ehrbar, A. Sala, P. Lienemann, A. Ranga, K. Mosiewicz, A. Bittermann, S. C. Rizzi, F. E. Weber, M. P. Lutolf, *Biophys. J.* 2011, **100**, 284.

35. B. K. Mann, A. S. Gobin, A. T. Tsai, R. H. Schmedlen, J. L. West, *Biomaterials* 2001, **22**.

36. C. A. DeForest, E. A. Sims, K. S. Anseth, *Chemistry Of Materials* 2010, **22**.

37. C. A. DeForest, K. S. Anseth, *Angew. Chem.-Int. Edit.* 2011, **51**, 1816.

38. M. C. Williams, *Annu. Rev. Physiol.* 2003, **65**, 669.

39. M. J. Mondrinos, S. Koutzaki, E. Jiwanmall, M. Y. Li, J. P. Dechadarevian, P. I. Lelkes, C. M. Finck, *Tissue Eng.* 2006, **12**, 717.

40. M. Ochs, L. R. Nyengaard, A. Lung, L. Knudsen, M. Voigt, T. Wahlers, J. Richter, H. J. G. Gundersen, *Am. J. Respir. Crit. Care Med.* 2004, **169**, 120.

41. A. Tsuda, N. Filipovic, D. Haberthur, R. Dickie, Y. Matsui, M. Stampanoni, J. C. Schittny, *J. Appl. Physiol.* 2008, **105**, 964.

42. E. L. Herzog, A. R. Brody, T. V. Colby, R. J. Mason, M. C. Williams, *Proceedings of the American Thoracic Society* 2008, **5**, 778.

43. H. Fehrenbach, *Respir. Res.* 2001, **2**, 33.

44. S. Bellusci, J. Grindley, H. Emoto, N. Itoh, B. L. M. Hogan, *Development* 1997, **124**, 4867.

Chapter 4

In vitro model alveoli from photodegradable microsphere templates

As published in *Biomater. Sci.*, **3**, 821-832 (2015)

4.1 Abstract

Recreating the 3D cyst-like architecture of the alveolar epithelium *in vitro* has been challenging to achieve in a controlled fashion with primary lung epithelial cells. Here, we demonstrate model alveoli formed within a tunable synthetic biomaterial platform using photodegradable microspheres as templates to create physiologically relevant, cyst structures. Poly(ethylene glycol) (PEG)-based hydrogels were polymerized in suspension to form microspheres on the order of 120 μm in diameter. The gel chemistry was designed to allow erosion of the microspheres with cytocompatible light doses (≤15 min exposure to 10 mW/cm^2 of 365 nm light) via cleavage of a photolabile nitrobenzyl ether crosslinker. Epithelial cells were incubated with intact microspheres, modified with adhesive peptide sequences to facilitate cellular attachment to and proliferation on the surface. A tumor-derived alveolar epithelial cell line, A549, completely covered the microspheres after only 24 hours, whereas primary mouse alveolar epithelial type II (ATII) cells took ~3 days. The cell-laden microsphere structures were embedded within a second hydrogel formulation at user defined densities; the microsphere templates were subsequently removed with light to render hollow epithelial cysts that were cultured for an additional 6 days. The resulting primary cysts stained positive for cell-cell junction proteins (β-catenin and ZO-1), indicating the formation of a functional epithelial layer. Typically, primary ATII cells differentiated in culture to the alveolar epithelial type I (ATI) phenotype; however, each cyst contained ~1-5 cells that stained positive for an ATII marker

(surfactant protein C), which is consistent with ATII cell numbers in native mouse alveoli. This biomaterial-templated alveoli culture system should be useful for future experiments to study lung development and disease progression, and is ideally suited for co-culture experiments where pulmonary fibroblasts or endothelial cells could be presented in the hydrogel surrounding the epithelial cysts.

4.2 Introduction

Epithelial cysts are important tissue structures in the body and recent work has employed *in vitro* models to investigate the mechanisms involved in cyst formation and function in many of these tissues, such as the lung,[1–5] mammary glands,[6–9] and kidneys.[10–12] In the lung, hollow epithelial cysts, or alveoli, are clustered at the distal end of bronchioles. Maturation of alveoli occurs postnatally, with secondary septa separating the smooth rudimentary alveoli into many open-sided polyhedra that share a common duct space.[13,14] The major components of alveolar tissue include the single cell layer epithelium attached to the basement membrane and surrounding a hollow central lumen. There are two alveolar epithelial cell phenotypes: ATI cells, which have an elongated morphology, form 95% of the alveolar surface area, and facilitate gas exchange between the lung and the blood stream;[15] and ATII cells, which exhibit a cuboidal morphology, produce lung surfactants, and are the progenitor cells for both the ATII and ATI cell populations in the alveoli.[16]

Many studies concerning alveoli have been focused on understanding alveolar homeostasis[17–20] and the interplay between the epithelium and the mesenchyme during lung development[21–23] and wound healing.[24–28] Much of the *in vitro* work with alveolar epithelial cells has been conducted with 2D monolayers grown on protein-coated stiff substrates such as glass

coverslips,[29] tissue culture polystyrene (TCPS),[30] and transwell membranes[31] or seeded on top of soft gels of extracellular matrix (ECM) such as Matrigel[4,26,32] and type I collagen.[33] Nonetheless, 3D tissue structure is critical to normal cellular function,[3,34,35] and therefore, recapitulating the curved cyst architecture is important when designing an *in vitro* alveolar model system. Previously, 3D hollow cysts have been formed from single-cell suspensions of primary alveolar epithelial cells trapped within ECM gels. For example, ATII cells isolated from juvenile rats and embedded within type I collagen gels underwent spontaneous cyst formation over the course of a few weeks in culture.[2] Similarly, adult human ATII cells encapsulated in Matrigel migrated towards each other to form polarized cysts within 5 days in culture.[1] Unfortunately, spontaneous alveolar cyst formation with primary lung epithelial cells has not been achieved in synthetic hydrogels, where the researcher has a high level of control over matrix properties and biochemical signaling. It should be noted that one example of lung epithelial cells spontaneously forming cysts in a polymer hydrogel has been published,[5] but the authors used a metastatic lung adenocarcinoma cell line, which has significant genetic modifications from a normal, healthy ATII cell. However, with spontaneous *in vitro* formation the final cyst size varies with time in culture, gel composition, and cell seeding density, and reported sizes range from 30 μm to 1 mm, whereas human alveolar size *in vivo* is believed to be on the order of 200 μm in diameter.[36] In order to study the influence of cyst size, matrix mechanics, and matrix signaling on alveolar cell behavior, a user-defined, tunable culture system can be useful to direct cyst formation and manipulate the cyst microenvironment.

Carterson *et al.* employed an interesting technique to create model alveoli by growing A549 cells, a human adenocarcinoma cell line with similarities to the ATII phenotype, on commercial microcarrier beads in suspension culture in a rotating wall vessel reactor.[37] This

approach inverts the typical hollow cyst architecture, polarizing the epithelium with the basolateral side facing in to the sphere and the apical side facing out to the medium. While it does allow for facile manipulation of the apical surface, it motivated us to develop a complementary method that would allow one to modify the matrix properties of the adhesive surface and allow for co-culture with cell types found on the basolateral side of the epithelium, such as fibroblasts and endothelial cells.

Synthetic hydrogels, such as those based on a poly(ethylene glycol) (PEG) backbone, exhibit many of the same biophysical qualities as ECM gels (e.g., high water content, tissue-relevant modulus range, as well as facile transport of oxygen and other nutrients) and they are readily modified using several cytocompatible reactions to introduce biochemical signals (i.e., adhesive ligands or growth factors).[38,39] Previous work from our lab has demonstrated the versatility of PEG hydrogels for 3D culture of many primary cell types,[40–43] in particular pioneering the use of the thiol-ene bio-click photoreaction between multi-arm PEGs functionalized with norbornene and cysteine-containing peptides.[44] Using a complementary photocleavage reaction, we also developed a PEG crosslinker that degrades upon exposure to single or two photon light, allowing for softening of the gel or its complete erosion on demand.[45,46] This photodegradable functionality has been incorporated into cell-sized microspheres for drug-delivery applications, allowing the user to completely erode the microspheres with light and release a payload on demand.[47] Building on the microcarrier concept, we aimed to use these photolabile microspheres in a new way, as templates for cyst formation.

Here, we demonstrate the formation and stability of *in vitro* model alveoli using A549 cells or primary ATII cells coated on photodegradable microspheres, serving as sacrificial

templates for the hollow cyst tissue structure, and encapsulated in a user-defined hydrogel network. The general procedure is depicted schematically in Figure 4.1. The diameters of the microspheres were increased to relevant *in vivo* alveolar sizes, and adhesive molecules were incorporated to promote cell attachment to the microspheres. A549 cells or primary ATII cells were incubated with adhesive microspheres to generate cell-coated pre-cysts. The thiol-ene chemistry established by our lab was then used to embed and stabilize these structures in a second hydrogel before erosion of the microsphere templates with cell-compatible light. This process was developed with the A549 cell line, and then expanded to use ATII cells isolated from wild-type mice as an *in vitro* model of healthy alveoli. After template erosion, the cysts maintained their architecture; cells did not infiltrate the central lumen even after 6 days of culture; and they expressed markers of cell junctions and both alveolar epithelial cell phenotypes.

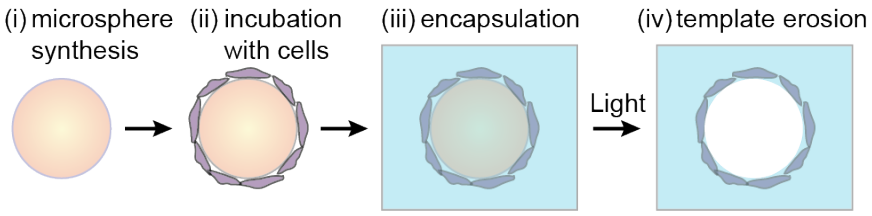

Figure 4.1 Schematic of the overall cyst-forming procedure, cross-sectional view. (i) Bioadhesive, photodegradable microspheres (orange) were (ii) incubated with epithelial cells (purple) to coat the surface of the microspheres with cells. The cell-microsphere pre-cyst structures were (iii) encapsulated in a second bioadhesive hydrogel (blue), followed by (iv) erosion of the microsphere template with 365 nm light, leaving a hollow epithelial cyst inside the encapsulating hydrogel.

4.3 Materials and methods

4.3.1 Photodegradable microsphere synthesis

Photodegradable crosslinker, poly(ethylene glycol) di-photodegradable acrylate (PEGdiPDA; M_n ~ 4070 Da) was synthesized as previously described.[46] Poly(ethylene glycol)

tetrathiol (PEG4SH; M_n ~ 5000 Da) was purchased from JenKem Technology USA. Microspheres were formed by inverse suspension polymerization as acrylates on PEGdiPDA underwent a base-catalyzed Michael addition with thiols on PEG4SH in aqueous droplets suspended in an organic phase, as published earlier.[47] Briefly, the organic phase consisted of sorbitan monooleate (Span 80, Sigma-Aldrich) and PEG-sorbitan monooleate (Tween 80, Sigma-Aldrich) in a 3:1 ratio dissolved in hexanes (EMD Millipore), with 30 mg surfactant per mL of hexanes. The aqueous phase was comprised of 6.9 wt% PEGdiPDA, 4.2 wt% PEG4SH, and 300 mM triethanolamine (Sigma-Aldrich) at pH 8.0 in phosphate buffered saline (PBS; Life Technologies), plus the desired adhesive ligand. The adhesive ligands selected here were ultrapure mouse laminin (Corning; 380 nM), fibronectin (BD Biosciences; 450 nM), and CRGDS peptide (American Peptide Company, Inc.; 1.5 mM). The full proteins were entrapped during network formation, whereas the peptide was covalently tethered to the network through the thiol functionality on cysteine. To achieve larger microsphere diameters, the aqueous phase was pipetted into the organic phase and triturated only twice, instead of vortexing the suspension as done previously. In addition, the suspension was stirred at a slower rate (~200 rpm vs. ~600 rpm; Thermolyne Cimarec 2 stir plate with 1 cm magnetic stir bar). Following polymerization, particles were recovered by centrifugation and washed with hexanes, isopropanol, and sterile PBS.

4.3.2 Microsphere size characterization

Microspheres were fluorescently tagged with AlexaFluor 488 C_5 maleimide (Life Technologies), which was pre-reacted with the PEG4SH before microsphere synthesis as above. The washed microspheres were diluted in PBS and loaded between a cover slip and a glass slide, separated by a 1 mm rubber gasket. The equilibrium swollen microspheres were then imaged

under an epifluorescent microscope (Nikon Eclipse TE2000-S). Images were analyzed using Image J software (NIH). After thresholding the image, microsphere area was measured using the Analyze Particles plug-in. Diameters of 3,087 microspheres were calculated and binned using Excel.

4.3.3 Microsphere photodegradation

A 0.8 mM solution of PEGdiPDA was prepared in PBS. An absorbance spectrum, 220-748 nm, was taken on a spectrophotometer (NanoDrop 1000; Thermo Scientific) with a path length of 1 mm. This spectrum matches previously published results for the photolabile nitrobenzyl ether (NBE) group.[47] From this spectrum, the molar absorptivity of a NBE group at 365 nm was calculated using Beer's Law, and subsequently used to estimate the time required to fully erode the microspheres using the equation published by Tibbitt *et al.*[48]:

$$\frac{z_c}{t_c} = \frac{-k_{\text{eff}} I_0}{2.3 \varepsilon_i C_i \ln(1 - P_{\text{rg}})} \qquad (1)$$

where z_c is the critical length scale of erosion, t_c is the critical time scale of surface erosion, k_{eff} is the effective kinetic constant of NBE photocleavage, I_0 is the intensity of the incident light, ε_i is the molar absorptivity of the NBE group, C_i is the concentration of the NBE group in the swollen gel, and P_{rg} is the critical fraction of cleaved NBE species, calculated from the Flory-Stockmayer equation.

Particle tracking was used as a method to characterize microsphere photodegradation. Photodegradable microspheres were prepared as above without the adhesive peptide, but containing 2 μm polystyrene beads (FluoSpheres; Life Technologies; 1:100 volume of beads to volume of monomer solution). These microspheres were then encapsulated in thiol-ene PEG gels (described below) and equilibrated in PBS overnight. Bright-field time-lapse images were taken with a confocal microscope (Zeiss LSM 710; every 30 seconds for 15 minutes) before and after

exposure of the samples to the 365 nm degrading light at ~10 mW/cm^2 for 15 minutes. MetaMorph software (Molecular Devices) was used to track the beads' positions over time (the solid case had 94 particle trajectories; the liquid case had 74 particle trajectories). These trajectories were corrected for frame drift and an ensemble mean squared displacement was calculated for each time interval using MATLAB. From this plot, an estimate of the particle diffusion coefficient was calculated as previously published, and used to determine the light dose needed to reach the gel to sol transition.[49–51]

4.3.4 Thiol-ene hydrogel synthesis

8-arm poly(ethylene glycol) norbornene (PEG-Nb; MW ~40,000 Da) was synthesized as previously described.[44,52] Enzymatically-cleavable di-cysteine peptide (KCGPQG↓IWGQCK) and adhesive peptide (CRGDS) were purchased commercially (American Peptide Company, Inc.). Photoinitiator lithium phenyl-2,4,6-trimethylbenzoylphosphinate (LAP) was synthesized as previously published.[53] To form gel precursor solution, PEG-Nb (10 wt%), peptide crosslinker (0.75 thiol:ene), CRGDS (1 mM), and LAP (0.05 wt%) in sterile PBS were mixed by vortex and the pH was adjusted to 6.8-7.2 by adding sterile-filtered 0.1 M sodium hydroxide. Pre-cysts or single-cell suspensions were added to this gel precursor solution and gently mixed with a pipette. Gels were formed by placing 30 μL of gel precursor solution onto a Sigmacote-treated glass slide, positioning a 1 mm thick rubber gasket around the droplet, and covering it with a second Sigmacote-treated glass slide. This mold was then exposed to 365 nm light at ~10 mW/cm^2 for 3 min to initiate the radical-mediated thiol-ene step-growth polymerization reaction. After gelation, the glass slides were separated and the free gel was transferred to an untreated 24-well plate with 1 mL appropriate growth medium. Gels were kept at 37 °C with 5% CO_2 for 1 day before microsphere template erosion.

4.3.5 A549 cell culture

A549 human adenocarcinoma cells (ATCC, CCL-185) were cultured in standard growth medium (Dulbecco's modified Eagle's medium (DMEM), 10% fetal bovine serum (FBS), 2% penicillin/streptomycin (100 U/mL), 0.4% fungizone (0.5 μg/mL), Invitrogen) at 37 °C with 5% CO_2 and passaged until use in experiments. For viability experiments, cells were trypsinized, centrifuged, and resuspended at 25 million cells/mL in PBS. For seeding on microspheres, cells were trypsinized, centrifuged, and resuspended at 1 million cells/mL in growth medium.

4.3.6 Viability experiments

A549 cells were encapsulated at 6.7 million cells/mL in thiol-ene gels as described above. The day after encapsulation, half the gels were exposed to 365 nm light at ~10 mW/cm^2 for 15 min, and half remained in the dark. A Live/Dead cell viability assay (Life Technologies) was performed an hour later, and one day later. Gels were immediately imaged on a confocal microscope (Zeiss LSM 710), and image stacks were analyzed for red cell count (dead) and green cell count (live) with MATLAB.

4.3.7 ATII isolation and culture

All procedures and protocols were reviewed and approved by the Animal Care and Use Committee at the University of Colorado Denver Anschutz Medical Campus. Mice were obtained from The Jackson Laboratories and bred in-house.

Primary ATII cells were isolated from FVB/NJ mice (6-8 weeks old) as previously described.[42] Briefly, mice were euthanized by CO_2 asphyxiation, the chest was opened, and sterile saline was injected into right ventricle to clear the blood from the pulmonary circulation. The heart lung block was then excised and distal lung tissue was trimmed away from the heart, trachea and other tissue and finely minced. Lung tissue was digested in 1% collagenase

(Worthington Biochemical) and 1 mg/mL DNase (Sigma) for 20 minutes at 37 °C. Then, trypsin (Fisher) was added (final concentration of 0.01%) and incubated for 20 minutes. Next, a solution of 1 mg/mL trypsin inhibitor and 1 mg/mL DNase was added and the mixture was passed through a 100 μm cell strainer to remove large undigested lung sections, followed by filtration through a Nitex Filter (10 μm pore diameter). The filtered lung solution was centrifuged for 8 min at 480 *g*, and the cell pellet was washed with DMEM/F12 media. Immune cells were separated from epithelial cells by adding the cell suspension to tissue culture plates coated with IgG (11 mg/cm^2) and incubating for 1 hour at 37 °C. Non-adherent cells were recovered and centrifuged at 480 *g* for 8 min. Cells were resuspended at 1 million cells/mL in growth medium supplemented with hepatocyte growth factor (HGF; R&D Systems; 50 ng/mL) and keratinocyte growth factor (KGF; Sigma; 10 ng/mL) prior to using in cyst experiments.

4.3.8 Cell-microsphere seeding

To seed photodegradable microspheres with cells, either A549 cells at 200,000 cells/mL or ATII cells at 500,000 cells/mL were placed in an ultra-low adhesion 24-well plate (Corning) with 40 μL microspheres in sterile PBS. The plate was placed on an orbital shaker at 45 rpm and incubated at 37 °C with 5% CO_2 overnight. A549 cells were incubated for 1 day to enable full coating of the microspheres, whereas ATII cells were incubated for 3 days before encapsulation in hydrogels. These cell-microsphere structures are referred to here as pre-cysts. Brightfield images of cell seeding were taken on an inverted epifluorescent microscope (Nikon Eclipse TE2000-S).

4.3.9 Template erosion

Cell-laden microspheres were encapsulated in thiol-ene gels and cultured for one day to enable formation of cellular attachments to the encapsulating gel. Gels were exposed to 365 nm

light at ~10 mW/cm^2 for 15 minutes to cleave the photodegradable moiety and completely erode the microsphere templates. The low molecular weight degradation products were allowed to swell out of the gels for 1 hour before the media was changed. Thereafter, media was changed daily, with the growth factor-supplemented media prepared fresh every other day for the primary cysts. Cysts were typically cultured for another 3-6 days after template erosion.

4.3.10 Immunostaining and imaging

At the completion of each experiment, samples were fixed in 4% paraformaldehyde in PBS for 15 minutes at room temperature and washed 3 times with PBS. Cells were subsequently permeabilized in 1% TritonX-100, and samples were blocked overnight with 40% goat serum in PBS. Primary antibodies used in these experiments were rabbit anti-prosurfactant protein C (SPC; 1:100; Millipore), hamster anti-mouse podoplanin (T1α; 1:100; eBioscience), mouse anti-β-catenin (1:100; Invitrogen), and rabbit anti-ZO-1 (1:100; Invitrogen). Secondary antibodies used in these experiments were goat anti-rabbit AlexaFluor 594 (1:200; Life Technologies), goat anti-hamster AlexaFluor 488 (1:200; Life Technologies), and goat anti-mouse AlexaFluor 488 (1:200; Life Technologies). For the whole mount gels, samples were incubated with primary antibodies overnight at 4 °C, followed by 3 wash steps (twice for 1 hour, and once overnight). Samples were then incubated with secondary antibodies overnight at 4 °C, followed by 3 wash steps (twice for 1 hour, and once overnight). Finally, nuclei were stained with DAPI (1:2000; Invitrogen) for 1 hour at room temperature, and samples were washed twice for 30 minutes and once overnight in PBS.

In one experiment, A549 cysts were fixed and permeabilized as before, followed by staining with DAPI (1:2000; Invitrogen) and TRITC-Phalloidin (1:200; Sigma) for 1 hour at room temperature to label the nuclei and actin cytoskeleton.

All samples were imaged on a confocal microscope (Zeiss LSM 710) with a 20x water-dipping objective (Plan Appochromat; NA=1.0). Image stacks were taken from the top of a cyst to the bottom (z step = 5 μm), and analyzed in ImageJ software (NIH).

4.3.11 Histological sectioning of cysts

To verify that the cysts' central lumen remained free of cells after template erosion, one set of primary cysts in gels was fixed as before and then prepared for cryosectioning. Gels were swollen in HistoPrep (Fisher) overnight at 4 °C, then flash frozen in liquid nitrogen for ~10 seconds. These were transferred to molds containing room temperature HistoPrep and covered with a small drop of HistoPrep. The molds were then flash frozen in liquid nitrogen and slowly warmed to -22 °C in a cryostat (Leica CM1850). 50 μm sections were cut and mounted onto microscope slides. These sections were then stained as before for T1α, SPC, and DAPI, and imaged on a confocal microscope (Zeiss LSM 710).

4.3.12 Histological sectioning of mouse lungs

Mouse lungs were fix inflated with 4% paraformaldehyde. Tissue sections of 75 μm thickness were prepared using a vibratome. Sections were stained with the following antibodies: rabbit anti-SPC (1:200; Seven Hills Bioreagents), Syrian hamster anti-T1alpha (1:100; Developmental Studies Hybridoma Bank) and goat anti-rabbit Cy3 or goat anti-syrian hamster FITC (1:200; Jackson ImmunoResearch Laboratories).

Labeled cells were observed with a confocal laser scanning microscope LSM 510 (Carl Zeiss, Germany) equipped with an argon laser (excitation 488 nm) and a DPS laser (excitation 561 nm). Serial optical sections were captured over a total depth of 50 um with a 0.5 um z-step. Three-dimensional reconstructions and rotating movies were generated using IMARIS analysis

software (Bitplane, Switzerland). Three-dimensional surface projections were shown for visualization of lung architecture.

4.4 Results and discussion

Alveoli in the native lung are roughly spherical, with an approximate diameter of 200 μm in human lungs.[36] The alveolar epithelium consists of flattened ATI cells interspersed with rounded ATII cells, typically found where neighboring alveoli meet.[54] To maintain a barrier between the airway and the vasculature, these epithelial cells form tight junctions and adherens junctions, as evidenced by expression of ZO-1 and β–catenin, respectively. To model this spherical epithelial arrangement *in vitro,* we developed a templating procedure with hydrogels, exploiting the photochemistry previously developed in our laboratory to create sacrificial spherical molds for the epithelial cells to adhere to. The general procedure is to form bioadhesive photodegradable microspheres, seed these microspheres with epithelial cells, encapsulate the cell-microsphere structures (referred to from here on as pre-cysts) inside a second hydrogel, and erode the microsphere template with light, leaving a hollow epithelial cyst attached to the surrounding hydrogel (Figure 4.1).

4.4.1 Microsphere synthesis and characterization

The microsphere template consisted of an 11.1 wt% PEG macromer solution formed as aqueous droplets suspended in an organic phase to make spherical particles. The polymer network was formed via spontaneous base-catalyzed Michael addition between the thiol groups on PEG4SH and the acrylate groups on PEGdiPDA (Fig. 4.2A). A small, commonly used peptide (CRGDS; Fig. 4.2A) that binds to integrin receptors on the cell surface was covalently tethered to the polymer network through the thiol group on the n-terminal cysteine. Many types

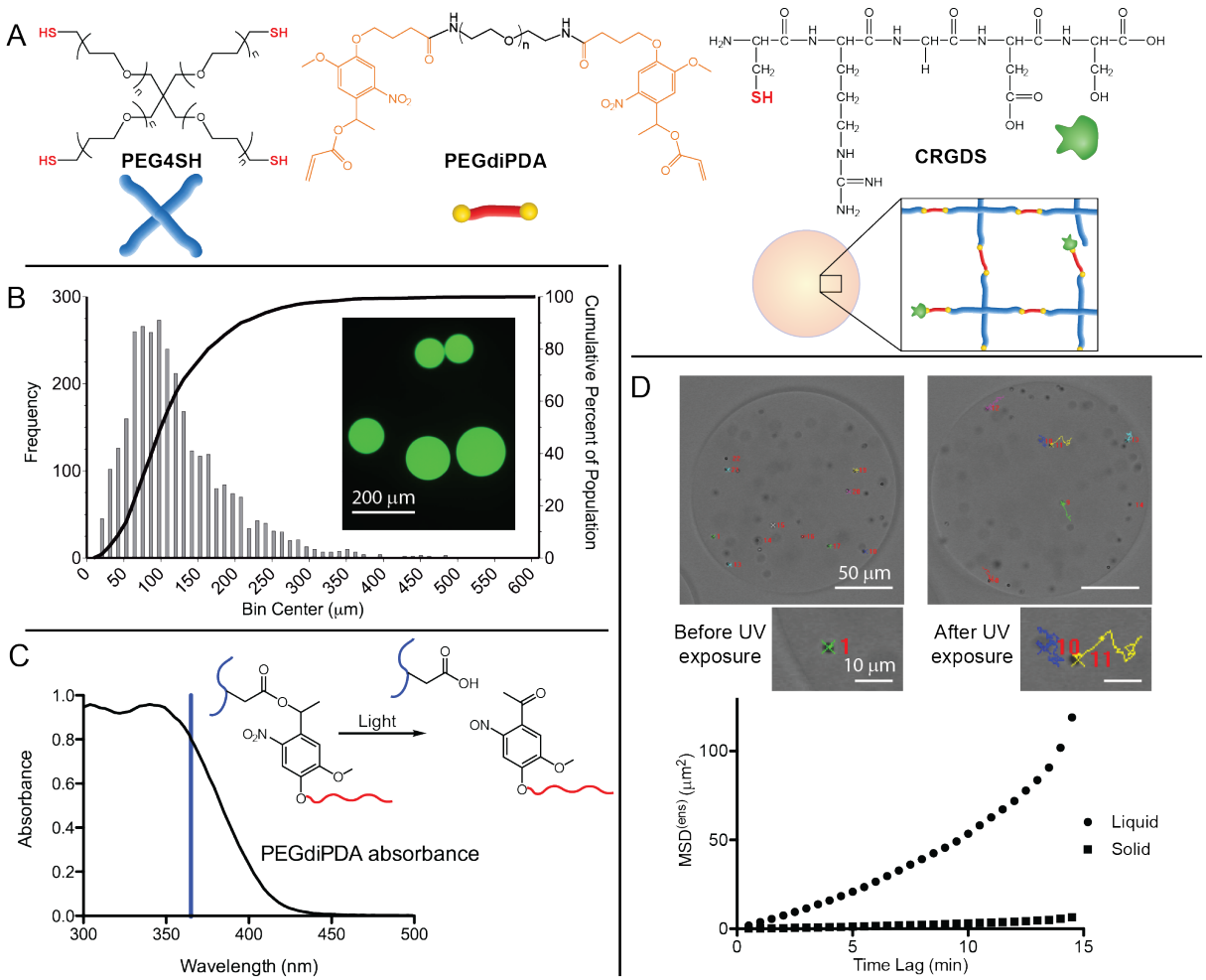

Figure 4.2 Microsphere synthesis and erosion. (A) The microsphere hydrogel network was composed of poly(ethylene glycol) tetrathiol (PEG4SH; M_n ~5 kDa) and poly(ethylene glycol) di-photodegradable acrylate (PEGdiPDA; Mn ~4.1 kDa), with the bioadhesive peptide CRGDS included at 1.5 mM. The monomers were reacted via an inverse suspension polymerization using a base-catalyzed Michael addition to form the microspheres. (B) Microspheres labeled with a green fluorescent dye were imaged and analyzed to determine the size distribution. Histogram shows distribution of microsphere diameters, and the black line indicates the cumulative percentage of the population. Inset shows representative fluorescent image of microspheres used for diameter measurement. n = 3087 (C) The chemical structure indicates the cleavage of the nitrobenzyl ether moiety with light. The absorbance spectrum is for the PEGdiPDA crosslinker (0.8 mM) in phosphate-buffered saline, where the blue line indicates 365 nm. The molar extinction coefficient at 365 nm for the nitrobenzyl ether moiety was calculated to be ~5,000 L mol^{-1} cm^{-1}. (D) Microspheres containing entrapped 2 μm diameter polystyrene beads were encapsulated in a second hydrogel and exposed to 365 nm light at an intensity of ~10 mW/cm^2 for 15 minutes to erode the microspheres. Images are of polystyrene bead tracks over 15 minutes before and after light exposure illustrating increased Brownian motion after microsphere erosion. The plot gives the ensemble mean squared displacement for the liquid and solid cases.

of adhesive ligands could be included in these microspheres, and early work with A549 cells presented here used full proteins (laminin or fibronectin) physically entrapped in the gel network during polymerization. Proteins larger than ~25 kDa are readily entrapped in the network and other thiol-containing peptides or thiolated proteins can be reacted into the polymer network, as desired.

A maleimide-conjugated AlexaFluor 488 dye was reacted into the microsphere network to measure the size distribution of the microspheres by image analysis (Fig. 4.2B; n = 3087 particles). The microspheres had an average diameter of 120 ± 70 μm with a polydispersity of 1.4, and 90% of the particles were <200 μm in diameter. This size range is relevant to mammalian alveoli *in vivo,* with human alveoli diameters on the order of 200 μm and mouse alveoli diameters on the order of 50 μm.[55]

The nitrobenzyl ether (NBE) groups in the PEGdiPDA crosslinker (yellow in Fig. 4.2A) are susceptible to cleavage by light, as depicted in Fig. 4.2C. The absorbance spectrum (Fig. 4.2C) of the crosslinker shows that the NBE moieties strongly absorb light between 300-400 nm, as has been previously reported.[45–47] Light at 365 nm was chosen for erosion of the microspheres because it has been shown many times to be cytocompatible and light sources are readily available. Beer's Law was used to calculate the molar absorptivity of the NBE moiety at 365 nm (ε_{365} = 5,000 L mol^{-1} cm^{-1}). Since the microspheres are optically thick (A > 0.1), erosion is limited to the top surface of the gel until the degradation products diffuse out of the light path and allow more light to reach deeper sections of the gel. Using the models published by Tibbitt *et al.,* a rate at which erosion progresses through the microspheres can be calculated with Equation 1.[48] Briefly, this rate depends on the effective rate of photocleavage of the NBE group, the intensity of the incident light, the molar absorptivity of the NBE group, the concentration of

NBE in the gel, and the critical fraction of cleaved NBE groups to reach reverse gelation. For this step growth network, reverse gelation occurs when 42% of the crosslinks have been cleaved. Using the calculated erosion rate (13.5 μm/min with 365 nm light at 10 mW/cm^2), we estimated that a 100 μm diameter microsphere would take 7.4 minutes to fully erode and a 200 μm diameter microsphere would take 15 minutes to fully erode.

To confirm these estimates and directly measure erosion, we characterized the gel to sol transition by entrapping 2 μm beads inside the hydrogel microspheres, encapsulating them inside thiol-ene hydrogels, and using time-lapse microscopy to look for Brownian motion of the beads (Fig. 4.2D). Before erosion of the microspheres, but after experiencing the 3-minute thiol-ene gel polymerization with 365 nm light, the beads were stationary, indicating the microspheres were still solid gels. After exposure to another 15 minutes of 365 nm light at ~10 mW/cm^2, the beads moved randomly through the space where the microsphere had been, indicating the microsphere had eroded to a liquid. By tracking bead position over time, the ensemble mean squared displacement curve was calculated for 94 beads in the solid case and 74 beads in the liquid case. From this plot, the diffusion coefficient was estimated to be 0.050 μm^2/min for the solid case and 0.94 μm^2/min for the liquid case. This corresponds to a viscosity of 0.13 Pa•s for the solid case and 0.0069 Pa•s for the liquid case. Since the eroded microspheres had a viscosity that is two orders of magnitude lower than that of the microspheres before exposure to light, we conclude that the gel network is completely degraded and no solid gel or surface remains to promote cell attachment. Further evidence that the microsphere network erodes with this light dose came from the observation that A549 cell layers attached to microspheres would swell as polymer crosslinks were cleaved and then collapse when the network reached reverse gelation (ESI Video 1).

Encapsulation in a second hydrogel was necessary to stabilize the cysts during and after template erosion (ESI Video 2).

4.4.2 Encapsulation of lung epithelial cells in thiol-ene hydrogels

Before encapsulating pre-cyst structures in the thiol-ene gels, the compatibility of the gel for permitting high survival of single cells was studied. The encapsulating hydrogel consisted of a norbornene-functionalized 8-arm PEG and a di-cysteine peptide crosslinker (KCGPQG↓IWGQCK) derived from a sequence known to be cleavable by cell-secreted matrix metalloproteinases (Fig. 4.3A).[56] The norbornene and thiol groups undergo photoinitiated radical polymerization to form a step-growth network.[44] Again, the adhesive peptide CRGDS was covalently bound to the network through the thiol on the cysteine. Here, too, the adhesive ligand can be varied easily with different cysteine-containing peptides, if desired. While not shown in this work, the elastic modulus of the encapsulating gel is also tunable by varying the weight percent of the PEG macromer or by changing the stoichiometric ratio of the thiol groups on the peptide crosslinker to the ene groups on the PEG.[41,43,52,57] For the specific formulation studied here, the elastic modulus was ~20 kPa, which is within the reported range of moduli for healthy lung tissue (*i.e.*, 5-30 kPa).[58,59]

This hydrogel system was shown to be cytocompatible by encapsulating a single-cell suspension of A549 cells, staining for the actin cytoskeleton to show typical rounded cell morphology (Fig. 4.3B), and performing a cell viability assay (Fig. 4.3C). Cell survival was high with 93 ± 3% cells staining positive with the live marker one day after encapsulation. To further probe cell viability during the cyst-making process, encapsulated A549 cells were exposed to 15 minutes of 365 nm light at ~10 mW/cm^2, the same light dose used to erode the microsphere

templates. Viability one hour and one day after light exposure were both 90 ± 4% live, which is not statistically different from the cells left in the dark.

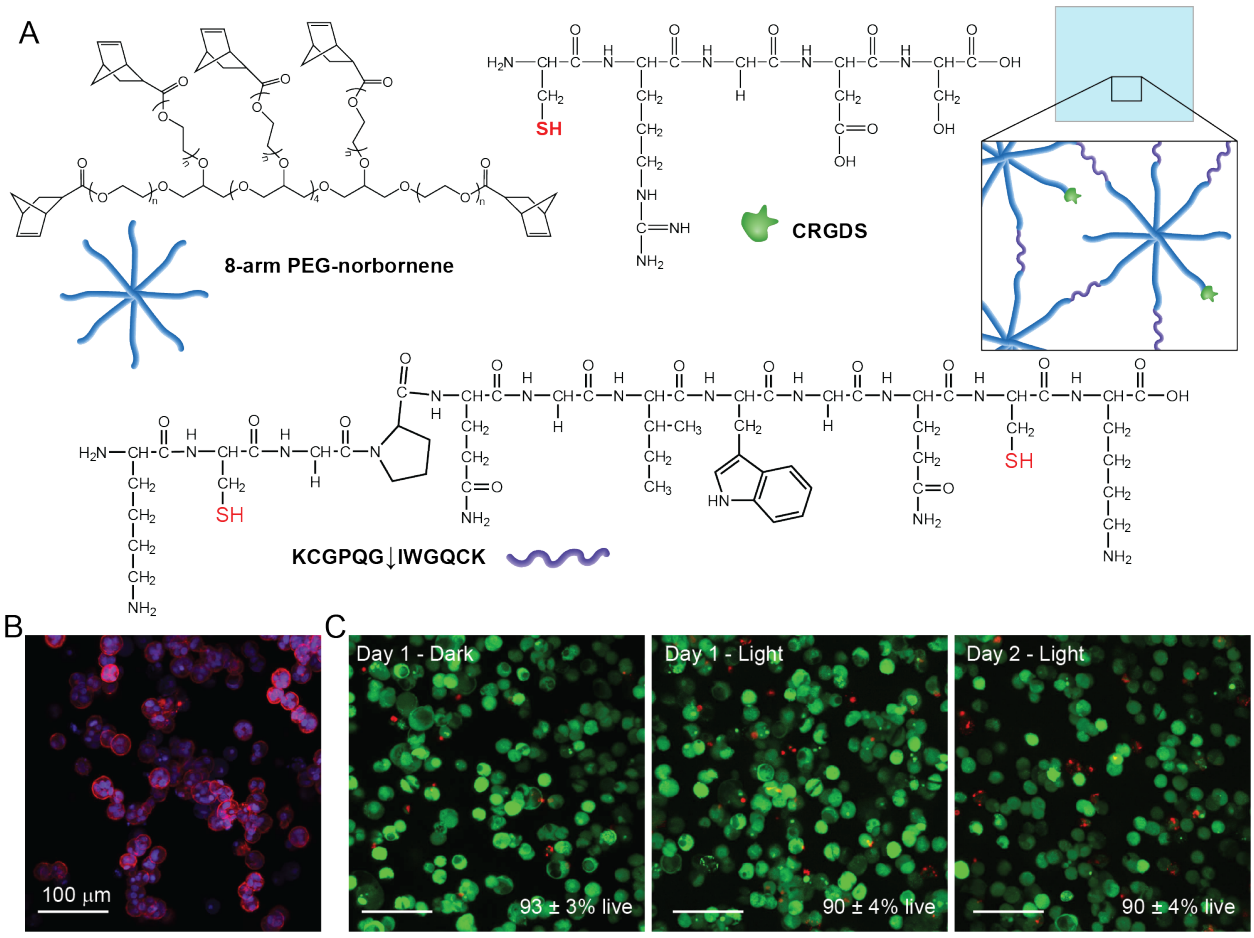

Figure 4.3 Encapsulating hydrogel formulation. (A) The encapsulating gel was composed of 8-arm poly(ethylene glycol) functionalized with norbornene end groups (M_n ~40 kDa) and an enzymatically-cleavable di-cysteine peptide crosslinker (KCGPQG↓IWGQCK), with the adhesive peptide CRGDS included at 1 mM. The arrow indicates the enzymatic cleavage site. Thiol groups (red) react with the -ene functionalities on the 8-arm PEG through a radical-initiated thiol-ene polymerization. (B) Single cell suspension of A549 cells encapsulated in the thiol-ene gel. The image is a z-projection of a 250 μm confocal stack showing healthy actin cytoskeleton (red) and cell nuclei (blue). (C) Single cell suspension of A549 cells encapsulated in thiol-ene gels. The images are z-projections of a 500 μm confocal stack with live cells stained green and dead cells stained red. The first is a representative image of a gel left in the dark and stained on day 1 after encapsulation (93 ± 3% live). The second is a representative image of a gel exposed to 15 minutes of 365 nm light at ~10 mW/cm^2 on day 1 after encapsulation and stained 1 hour later (90 ± 4% live). The third is a representative image of a gel exposed to 15 minutes of 365 nm light at ~10 mW/cm^2 on day 1 after encapsulation and stained 1 day later (90 ± 4% live).

4.4.3 Testing the procedure with A549 cells

Cyst-like structures were formed using the characterized, photodegradable microspheres and the cytocompatible, thiol-ene hydrogels. During the cyst-forming process, the cells experience three distinct matrix situations (Fig. 4.4). First, the cells attach to the RGD in the microsphere template and spread and proliferate to form a complete epithelial layer on the carrier hydrogel. Next, the pre-cysts are encapsulated in the thiol-ene hydrogel and the cells form additional attachments to the RGD in the second gel. Finally, the microsphere templates are eroded, leaving only the encapsulating gel for the cells to adhere to and a hollow central lumen where the microsphere had been. While polymer degradation products including CRGDS peptides are initially present after template erosion, fast integrin turnover and diffusion of small-molecule products through gaps in the epithelium contribute to the lack of ECM signaling inside the cyst lumen in the hours and days following erosion.

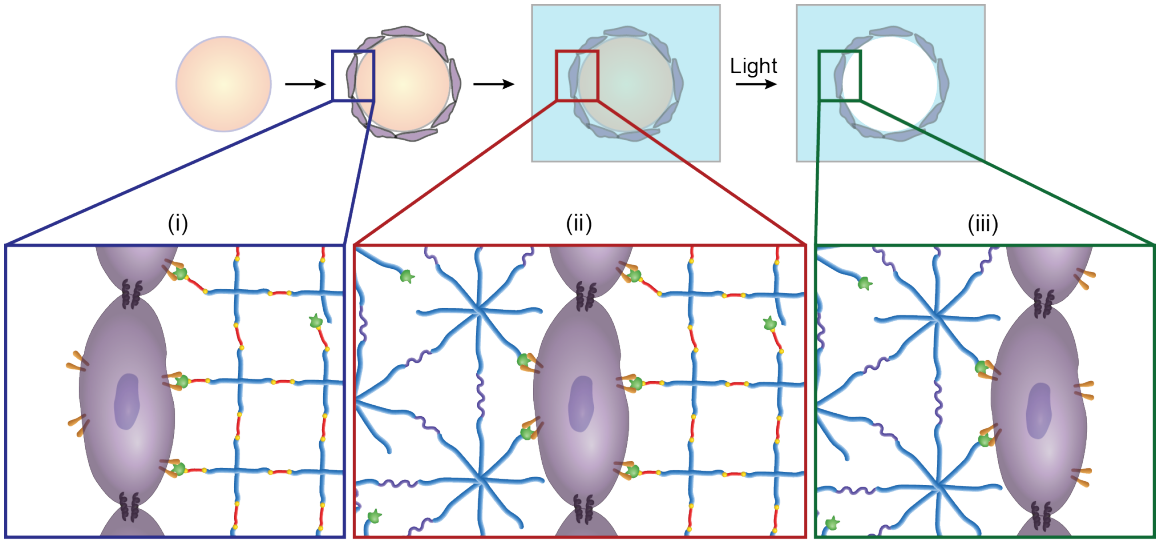

Figure 4.4 Schematic illustration of the three conditions that epithelial cells experience during the cyst-forming procedure, cross-sectional view. (i) First, cells form integrin binding sites with the CRGDS peptide in the microsphere network. (ii) Then, pre-cysts are encapsulated within the thiol-ene gel and cells form attachments to the CRGDS in the encapsulating gel. (iii) Finally, microspheres are eroded with light and with fast integrin turnover on the apical side only the integrins on the outside of the cyst retain their connections to the gel network.

First, the A549 cell line was employed to test the cyst templating procedure, because of its ease of culture, rapid proliferation, and previous use in the literature as a model cell line for the ATII phenotype.[28,37,60] To coat the microsphere templates with cells, A549s and fibronectin-loaded microspheres were combined in an ultra-low adhesion 24-well plate and incubated on an orbital shaker. The wells were monitored by bright field microscopy, and cells were shown to completely cover the microspheres within 24 hours (Fig. 4.5A). Interestingly, this coating time did not significantly change with several different adhesive proteins (laminin, fibronectin) or peptide adhesive ligands (RGD) that were examined (data not shown). After 24 hours of coating, the pre-cysts were encapsulated in the thiol-ene gel as described above and allowed to form attachments to this new substrate for another 24 hours. Next, the microsphere template was eroded with 365 nm light at ~10 mW/cm^2 for 15 minutes (Fig. 4.5B,C), as determined earlier. The cysts were cultured three more days after template erosion before being fixed and stained for

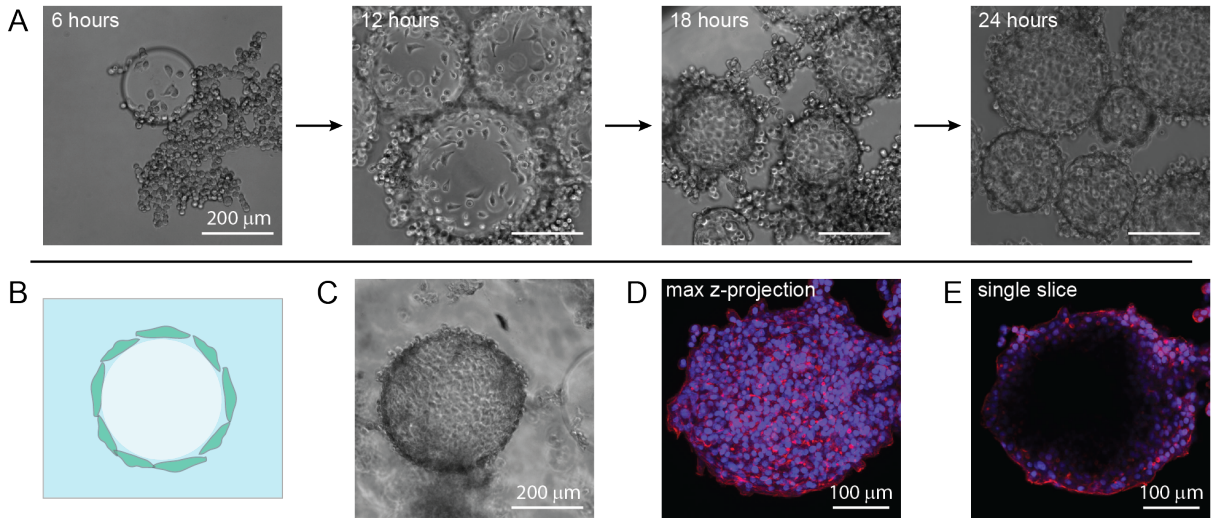

Figure 4.5 A549 cysts. (A) Bright field images of A549 cells progressively covering fibronectin-loaded microspheres. (B) Cross-section schematic illustrating the hollow cyst that remains in the hydrogel after erosion of the microsphere template. (C) Bright field image of an encapsulated A549 cyst after template erosion. (D) Maximum intensity projection of a confocal image stack of an A549 cyst, fixed 3 days after template erosion. Red is actin; blue is the cell nucleus. (E) Single confocal image through the center of the same A549 cyst demonstrating the hollow interior. Red is actin; blue is the cell nucleus.

the actin cytoskeleton and the cell nucleus (Fig. 4.5D,E). The A549 cysts remained roughly spherical in culture, and the confocal slice demonstrates that the central lumen remained free of cells after erosion of the microsphere template. The A549 cell line is limited in its use due to the rapid proliferation of this adenocarcinoma cell line and the lack of appropriate apical-basal polarity. Cysts formed utilizing this cell line have multiple cell layers and display rough edges, which is atypical of a healthy alveolus. However, the A549 cysts may be useful in studying cancer progression of the alveolar epithelium.

4.4.4 Primary alveolar epithelial cell cysts

ATII cells isolated from healthy mice were used in the same cyst templating procedure described above. In contrast with the highly proliferative A549 cell line, these primary cells took three days to spread and cover the microspheres completely (Fig. 4.6A). As before, the pre-cysts were encapsulated and the microsphere templates were eroded one day after encapsulation (Fig. 4.6B). The cysts were cultured another 3-6 days (7-10 days after isolation from the mice) and fixed and stained for cell phenotype markers (Fig. 4.6C,D). The primary cysts also remained spherical with empty central lumens. To confirm that no cells infiltrated the lumen and prove that imaging with the confocal microscope does not suffer from complete light attenuation in the center of these cysts, gels containing primary cysts were cryosectioned into 50 μm sections and stained and imaged as before (Fig. 4.6E). Sections of one half of a cyst are presented here to demonstrate that the cyst interior remained devoid of cells. The primary cysts were noticeably smoother than the A549 cysts and displayed an epithelium that was typically only one or two cells thick, which is more in keeping with the native alveolar architecture. Primary cysts had an average diameter of 180 ± 80 μm, which is in the size range relevant to human alveoli (~200

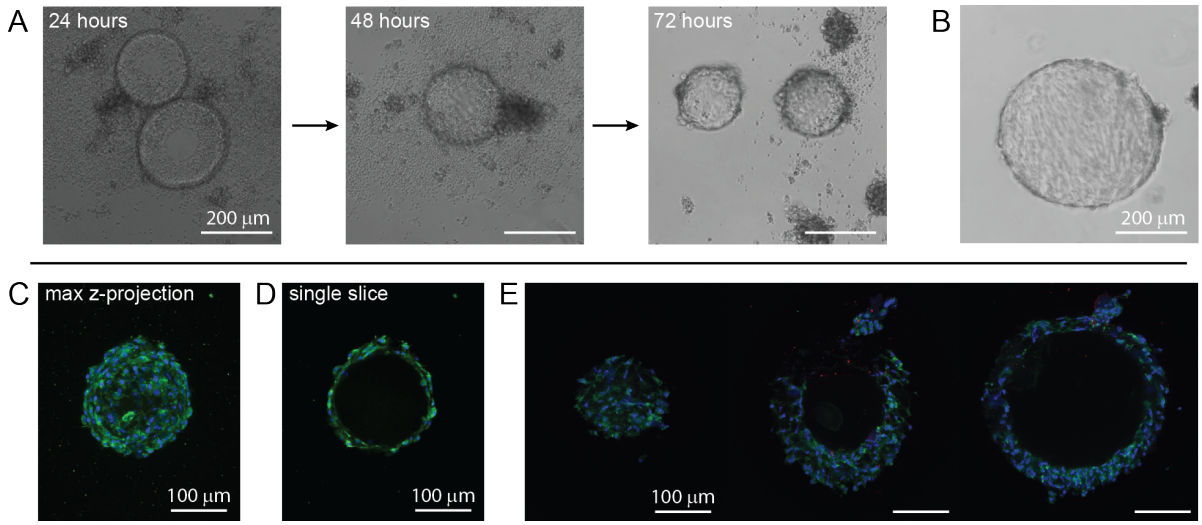

Figure 4.6 Primary cysts. (A) Bright field images of primary cells proliferating to cover the microspheres. (B) Bright field image of an encapsulated primary cell cyst after template erosion. (C) Maximum intensity projection of a confocal image stack of a primary cell cyst, fixed 3 days after template erosion. Green is T1α, a marker of the ATI cell phenotype; blue is the cell nucleus. (D) Single confocal image through the center of the same primary cell cyst demonstrating the hollow interior. Green is T1α, a marker of ATI cell phenotype; blue is the cell nucleus. (E) Maximum intensity projections of three 50 μm cryosections, documenting the absence of cells in the central lumen. Red is SPC, a marker of the ATII cell phenotype; green is T1α, a marker of the ATI cell phenotype; blue is the cell nucleus.

μm). The average cyst diameter was larger than that of the original microspheres, but that may have been caused by sampling bias when selecting cysts to image, or the smaller pre-cysts may have preferentially adhered to the well plate and been left behind when the pre-cysts were transferred to the gel precursor solution. One intriguing possibility for the increased luminal volume is that ATII cells may have secreted surfactant lipids and proteins into the central lumen, although we have not yet explored this option.

Hallmarks of any epithelial layer are the formation of adherens junctions to connect the cytoskeletons of neighboring cells and tight junctions between the cells to provide a barrier against passive solute diffusion. To further characterize the primary cysts, we stained for the cell junction proteins β-catenin (adherens junctions) and ZO-1 (tight junctions) (Fig. 4.7A,B). β-

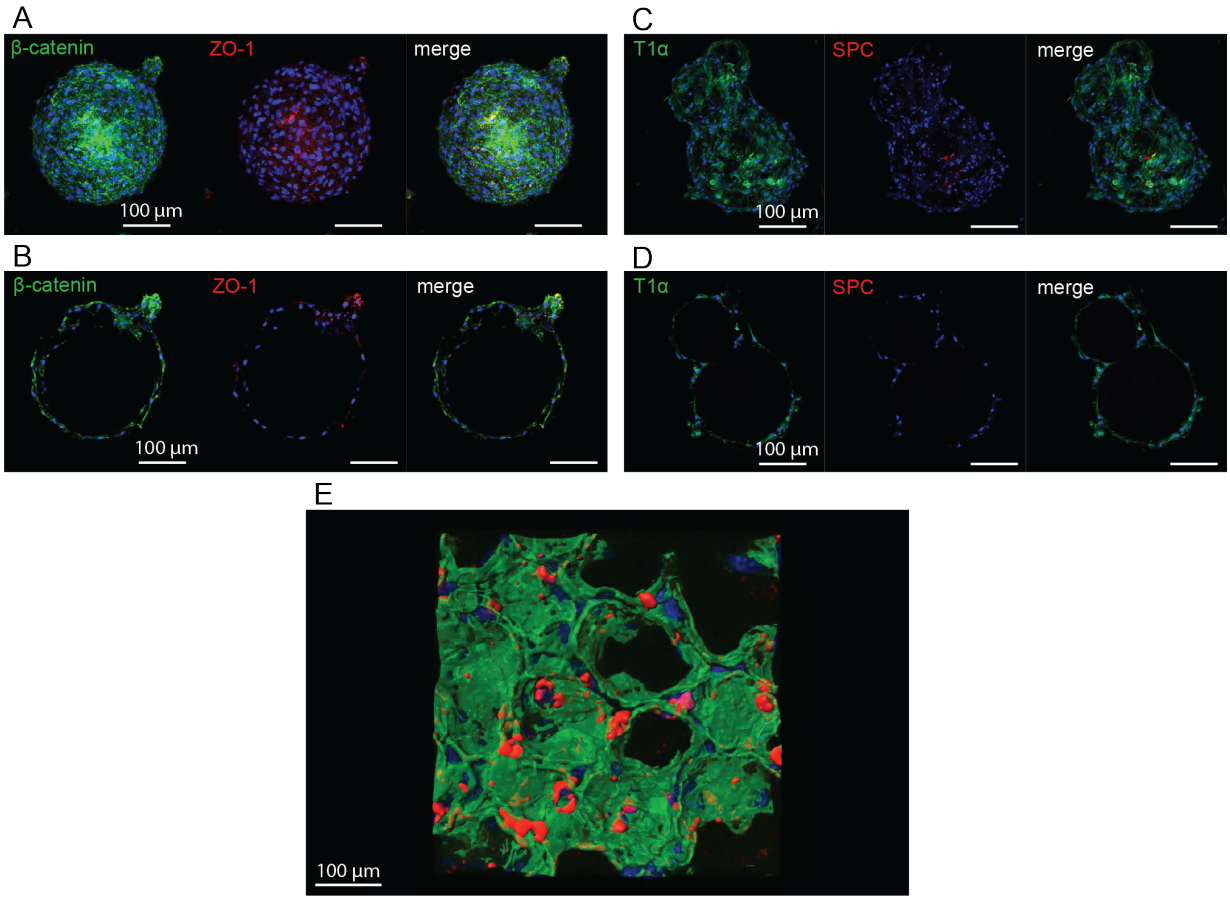

Figure 4.7 Immunostaining of Primary Cysts. (A) Maximum intensity projections of a confocal image stack of a primary cell cyst, fixed 3 days after template erosion. Green is β-catenin, a marker of adherens junctions; red is ZO-1, a marker of tight junctions; blue is the cell nucleus. (B) Single confocal image through the center of the same primary cell cyst. Colors are the same as in A. (C) Maximum intensity projections of a confocal image stack of a primary cell cyst, fixed 6 days after template erosion. Green is T1α, a marker of the ATI cell phenotype; red is SPC, a marker of the ATII cell phenotype; blue is the cell nucleus. (D) Single confocal image through the center of the same primary cell cyst. Colors are the same as in C. (E) 3D surface projection of a 50 µm mouse lung tissue section showing multiple cysts, with on average 2 ATII cells per cyst. Colors are the same as in C.

catenin was bright along the cell membranes throughout the cyst, indicating mature adherens junction formation between these epithelial cells. ZO-1 was less widely distributed, but it did appear in many of the cells, demonstrating at least partial formation of tight junctions in the cyst. Further development of these junctions may require more time in culture.

Finally, primary cysts were stained and analyzed for cell phenotype (Fig. 4.7C,D). Surfactant protein C (SPC) is produced by ATII cells and stored in the cell cytosol and is commonly used as a marker of ATII cell phenotype. T1α is located in the cell membrane of ATI cells and is a marker of the ATI cell phenotype. As is typically seen in culture *in vitro,*[30,61] the freshly isolated ATII cells quickly differentiated on the microspheres into ATI-like cells with an elongated morphology, positive staining for T1α, and almost no staining for SPC. The number of cells per cyst positive for SPC was very small (3 ± 2 per cyst). However, this number may be relevant to native alveoli, because the 3D surface reconstruction of a 50-micron section of mouse lung tissue shown in Figure 4.7E suggests that each mouse alveolus only contains 1 or 2 ATII cells (to view this reconstruction from multiple angles see ESI Video 3). When compared to the mouse cysts in the lung tissue section, the engineered cysts recreate the approximate size scale and small numbers of ATII cells, although the total number of cells in the engineered cysts is much higher. Collectively, the evidence presented indicates that the epithelial cysts developed here capture many aspects of the structure and cellular arrangement found in alveoli *in vivo,* and may be useful as *in vitro* models of the distal airway epithelium for future experiments.

4.5 Conclusions

We have developed an *in vitro* 3D model of the alveolar epithelium using photodegradable microspheres as sacrificial templates to form spherical multi-cellular structures with hollow interiors, cultured within a tunable hydrogel scaffold. This procedure was demonstrated with a tumor-derived alveolar epithelial cell line as well as primary mouse ATII cells, the majority of which differentiated into ATI-like cells. Given the size range, cellular arrangement, cell junction protein and phenotype marker expression demonstrated here, these

model alveoli captured several of the same biological aspects of alveoli *in vivo*. Recapitulating the native alveolar tissue architecture within an easily modifiable synthetic platform provides an avenue for numerous experiments previously unattainable *in vitro*. For instance, bulk matrix properties can be systematically varied to determine their influence on cell phenotype or cellular response to external signals such as inflammatory cytokines. Moreover, this model is particularly suited for co-culture experiments with epithelial cysts surrounded by a second cell type such as pulmonary fibroblasts or endothelial cells, both of which play key roles during lung development and disease progression. We believe that this cyst model will be a valuable tool for those studying the biology of the lung epithelium, as well as screening potential therapeutics for treating diseases, such as lung fibrosis.

4.6 Acknowledgements

The authors would like to thank Emi Kiyotake for histological sectioning, particle tracking, and image analysis and Sharon Ryan for mouse cell isolations. This work was supported in part by a grant from the National Science Foundation (CTS1236662) and the Howard Hughes Medical Institute.

4.7 Notes and references

Electronic Supplementary Information (ESI) available. See DOI: 10.1039/c5bm00034c

1. Yu, W., Fang, X., Ewald, A., Wong, K., Hunt, C. A., Werb, Z., *et al.* Formation of cysts by alveolar type II cells in three-dimensional culture reveals a novel mechanism for epithelial morphogenesis. *Mol. Biol. Cell* **18,** 1693 (2007).

2. Sugihara, H., Toda, S., Miyabara, S., Fujiyama, C. & Yonemitsu, N. Reconstruction of alveolus-like structure from alveolar type II epithelial cells in three-dimensional collagen gel matrix culture. *Am. J. Pathol.* **142,** 783–92 (1993).

3. Mondrinos, M. J., Koutzaki, S., Jiwanmall, E., Li, M., Dechadarevian, J.-P., Lelkes, P. I., *et al.* Engineering three-dimensional pulmonary tissue constructs. *Tissue Eng.* **12,** 717–28 (2006).

4. Matter, M. L. & Laurie, G. W. A novel laminin E8 cell adhesion site required for lung alveolar formation in vitro. *J. Cell Biol.* **124,** 1083–90 (1994).

5. Gill, B. J., Gibbons, D. L., Roudsari, L. C., Saik, J. E., Rizvi, Z. H., Roybal, J. D., *et al.* A synthetic matrix with independently tunable biochemistry and mechanical properties to study epithelial morphogenesis and EMT in a lung adenocarcinoma model. *Cancer Res.* **72,** 6013–23 (2012).

6. Sharp, J. A., Cane, K. N., Mailer, S. L., Oosthuizen, W. H., Arnould, J. P. Y. & Nicholas, K. R. Species-specific cell-matrix interactions are essential for differentiation of alveoli like structures and milk gene expression in primary mammary cells of the Cape fur seal (Arctocephalus pusillus pusillus). *Matrix Biol.* **25,** 430–42 (2006).

7. Montesano, R. & Soulié, P. Retinoids induce lumen morphogenesis in mammary epithelial cells. *J. Cell Sci.* **115,** 4419–4431 (2002).

8. Paszek, M. J., Zahir, N., Johnson, K. R., Lakins, J. N., Rozenberg, G. I., Gefen, A., *et al.* Tensional homeostasis and the malignant phenotype. *Cancer Cell* **8,** 241–54 (2005).

9. Bissell, M. J., Rizki, A. & Mian, I. S. Tissue architecture: the ultimate regulator of breast epithelial function. *Curr. Opin. Cell Biol.* **15,** 753–762 (2003).

10. Schumacher, K. M., Phua, S. C., Schumacher, A. & Ying, J. Y. Controlled formation of biological tubule systems in extracellular matrix gels in vitro. *Kidney Int.* **73,** 1187–92 (2008).

11. Martín-Belmonte, F., Yu, W., Rodríguez-Fraticelli, A. E., Ewald, A., Werb, Z., Alonso, M. A., *et al.* Cell-polarity dynamics controls the mechanism of lumen formation in epithelial morphogenesis. *Curr. Biol.* **18,** 507–13 (2008).

12. O'Brien, L., Zegers, M. & Mostov, K. Building epithelial architecture: insights from the three-dimensional culture models. *Nat. Rev. Mol. Cell* **3,** 531–537 (2002).

13. Burri, P. H. Structural aspects of postnatal lung development - Alveolar formation and growth. *Biol. Neonate* **89,** 313–322 (2006).

14. Kitaoka, H., Nieman, G. F., Fujino, Y., Carney, D., DiRocco, J. & Kawase, I. A 4-dimensional model of the alveolar structure. *J. Physiol. Sci.* **57,** 175–185 (2007).

15. Williams, M. C. Alveolar type I cells: molecular phenotype and development. *Annu. Rev. Physiol.* **65,** 669–95 (2003).

16. Mason, R. J. Biology of alveolar type II cells. *Respirology* **11,** S12–S15 (2006).

17. Guillot, L., Nathan, N., Tabary, O., Thouvenin, G., Le Rouzic, P., Corvol, H., *et al.* Alveolar epithelial cells: master regulators of lung homeostasis. *Int. J. Biochem. Cell Biol.* **45,** 2568–73 (2013).

18. Uhal, B. D. Cell cycle kinetics in the alveolar epithelium. *Am. J. Physiol. Cell. Mol. Physiol.* **272,** L1031–1045 (1997).

19. Hogan, B. L. M., Barkauskas, C. E., Chapman, H. A., Epstein, J. A., Jain, R., Hsia, C. C. W., *et al.* Repair and regeneration of the respiratory system: complexity, plasticity, and mechanisms of lung stem cell function. *Cell Stem Cell* **15,** 123–38 (2014).

20. Barkauskas, C., Cronce, M., Rackley, C., Bowie, E., Keene, D., Stripp, B., *et al.* Type 2 alveolar cells are stem cells in adult lung. *J. Clin. Invest.* **123,** 3025–3036 (2013).

21. Park, W. Y., Miranda, B., Lebeche, D., Hashimoto, G. & Cardoso, W. V. FGF-10 is a chemotactic factor for distal epithelial buds during lung development. *Dev. Biol.* **201,** 125–34 (1998).

22. Bellusci, S., Grindley, J., Emoto, H., Itoh, N. & Hogan, B. L. Fibroblast growth factor 10 (FGF10) and branching morphogenesis in the embryonic mouse lung. *Development* **124,** 4867–78 (1997).

23. Tang, N., Marshall, W. F., McMahon, M., Metzger, R. J. & Martin, G. R. Control of Mitotic Spindle Angle by the RAS-Regulated ERK1/2 Pathway Determines Lung Tube Shape. *Science* **333,** 342–345 (2011).

24. Perl, A.-K. T. & Gale, E. FGF signaling is required for myofibroblast differentiation during alveolar regeneration. *Am. J. Physiol. Lung Cell. Mol. Physiol.* **297,** L299–308 (2009).

25. Yano, T., Mason, R. J., Pan, T., Deterding, R. R., Nielsen, L. D. & Shannon, J. M. KGF regulates pulmonary epithelial proliferation and surfactant protein gene expression in adult rat lung. *Am. J. Physiol. Lung Cell. Mol. Physiol.* **279,** L1146–58 (2000).

26. Sugahara, K., Tokumine, J., Teruya, K. & Oshiro, T. Alveolar epithelial cells: differentiation and lung injury. *Respirology* **11,** S28–31 (2006).

27. Crosby, L. M. & Waters, C. M. Epithelial Repair Mechanisms in the Lung. *Am. J. Physiol. Lung Cell. Mol. Physiol.* **298,** 715–731 (2010).

28. Prasad, S., Hogaboam, C. M. & Jarai, G. Deficient repair response of IPF fibroblasts in a co-culture model of epithelial injury and repair. *Fibrogenesis Tissue Repair* **7,** 7 (2014).

29. Isakson, B. E., Seedorf, G. J., Lubman, R. L. & Boitano, S. Heterocellular cultures of pulmonary alveolar epithelial cells grown on laminin-5 supplemented matrix. *In Vitro Cell. Dev. Biol. Anim.* **38,** 443–9 (2002).

30. Bhaskaran, M., Kolliputi, N., Wang, Y., Gou, D., Chintagari, N. R., Liu, L., *et al.* Trans-differentiation of Alveolar Epithelial Type II Cells to Type I Cells Involves Autocrine Signaling by Transforming Growth Factor ␤1 through the Smad Pathway *. *J. Biol. Chem.* **282,** 3968 –3976 (2007).

31. Qiao, R., Yan, W., Clavijo, C., Mehrian-Shai, R., Zhong, Q., Kim, K.-J., *et al.* Effects of KGF on alveolar epithelial cell transdifferentiation are mediated by JNK signaling. *Am. J. Respir. Cell Mol. Biol.* **38,** 239–46 (2008).

32. Wang, J., Edeen, K., Manzer, R., Chang, Y., Wang, S., Chen, X., *et al.* Differentiated human alveolar epithelial cells and reversibility of their phenotype in vitro. *Am. J. Respir. Cell Mol. Biol.* **36,** 661–8 (2007).

33. Umino, T., Wang, H., Zhu, Y., Liu, X., Manouilova, L. S., Spurzem, J. R., *et al.* Modification of type I collagenous gels by alveolar epithelial cells. *Am. J. Respir. Cell Mol. Biol.* **22,** 702–707 (2000).

34. Bissell, M. J., Kenny, P. A. & Radisky, D. C. Microenvironmental regulators of tissue structure and function also regulate tumor induction and progression: the role of extracellular matrix and its degrading enzymes. *Cold Spring Harb. Symp. Quant. Biol.* **70,** 343–56 (2005).

35. Griffith, L. G. & Swartz, M. A. Capturing complex 3D tissue physiology in vitro. *Nat. Rev. Mol. Cell Biol.* **7,** 211–24 (2006).

36. Ochs, M., Nyengaard, J. R., Jung, A., Knudsen, L., Voigt, M., Wahlers, T., *et al.* The number of alveoli in the human lung. *Am. J. Respir. Crit. Care Med.* **169,** 120–4 (2004).

37. Carterson, A., Bentrup, K. zu, Ott, C., Clarke, M., Pierson, D., Vanderburg, C., *et al.* A549 Lung Epithelial Cells Grown as Three-Dimensional Aggregates : Alternative Tissue Culture Model for Pseudomonas aeruginosa Pathogenesis. *Infect. Immun.* **73,** 1129–1140 (2005).

38. Tibbitt, M. W. & Anseth, K. S. Hydrogels as extracellular matrix mimics for 3D cell culture. *Biotechnol. Bioeng.* **103,** 655–63 (2009).

39. Lewis, K. J. R. & Anseth, K. S. Hydrogel scaffolds to study cell biology in four dimensions. *MRS Bull.* **38,** 260–268 (2013).

40. Salinas, C. N. & Anseth, K. S. The enhancement of chondrogenic differentiation of human mesenchymal stem cells by enzymatically regulated RGD functionalities. *Biomaterials* **29,** 2370–7 (2008).

41. Benton, J. A., Fairbanks, B. D. & Anseth, K. S. Characterization of valvular interstitial cell function in three dimensional matrix metalloproteinase degradable PEG hydrogels. *Biomaterials* **30,** 6593–603 (2009).

42. Kloxin, A. M., Lewis, K. J. R., Deforest, C. A., Seedorf, G., Tibbitt, M. W., Balasubramaniam, V., *et al.* Responsive culture platform to examine the influence of microenvironmental geometry on cell function in 3D. *Integr. Biol.* **4,** 1540–1549 (2012).

43. McKinnon, D. D., Kloxin, A. M. & Anseth, K. S. Synthetic hydrogel platform for three-dimensional culture of embryonic stem cell-derived motor neurons. *Biomater. Sci.* **1,** 460 (2013).

44. Fairbanks, B. D., Schwartz, M. P., Halevi, A. E., Nuttelman, C. R., Bowman, C. N. & Anseth, K. S. A Versatile Synthetic Extracellular Matrix Mimic via Thiol-Norbornene Photopolymerization. *Adv. Mater.* **21,** 5005–5010 (2009).

45. Kloxin, A. M., Kasko, A. M., Salinas, C. N. & Anseth, K. S. Photodegradable hydrogels for dynamic tuning of physical and chemical properties. *Science* **324,** 59–63 (2009).

46. Kloxin, A. M., Tibbitt, M. W. & Anseth, K. S. Synthesis of photodegradable hydrogels as dynamically tunable cell culture platforms. *Nat. Protoc.* **5,** 1867–87 (2010).

47. Tibbitt, M. W., Han, B. W., Kloxin, A. M. & Anseth, K. S. SFB Student Award Winner in the Ph.D. Category: Synthesis and application of photodegradable microspheres for spatiotemporal control of protein delivery. *J. Biomed. Mater. Res. Part A* **100A,** 1647–1654 (2012).

48. Tibbitt, M., Kloxin, A., Sawicki, L. & Anseth, K. Mechanical Properties and Degradation of Chain and Step- Polymerized Photodegradable Hydrogels. *Macromolecules* **46,** 2785–2792 (2013).

49. Michalet, X. Mean square displacement analysis of single-particle trajectories with localization error: Brownian motion in an isotropic medium. *Phys. Rev. E* **82,** 041914 (2010).

50. Ernst, D. & Köhler, J. Measuring a diffusion coefficient by single-particle tracking: statistical analysis of experimental mean squared displacement curves. *Phys. Chem. Chem. Phys.* **15,** 845–9 (2013).

51. Shenoy, R., Tibbitt, M. W., Anseth, K. S. & Bowman, C. N. Formation of Core-Shell Particles by Interfacial Radical Polymerization Initiated by a Glucose Oxidase-Mediated Redox System. *Chem. Mater.* **25,** 761–767 (2013).

52. Gould, S. T., Darling, N. J. & Anseth, K. S. Small peptide functionalized thiol-ene hydrogels as culture substrates for understanding valvular interstitial cell activation and de novo tissue deposition. *Acta Biomater.* **8,** 3201–9 (2012).

53. Fairbanks, B. D., Schwartz, M. P., Bowman, C. N. & Anseth, K. S. Photoinitiated polymerization of PEG-diacrylate with lithium phenyl-2,4,6-trimethylbenzoylphosphinate: polymerization rate and cytocompatibility. *Biomaterials* **30,** 6702–7 (2009).

54. Herzog, E. L., Brody, A. R., Colby, T. V, Mason, R. & Williams, M. C. Knowns and unknowns of the alveolus. *Proc. Am. Thorac. Soc.* **5,** 778–82 (2008).

55. Soutiere, S. E., Tankersley, C. G. & Mitzner, W. Differences in alveolar size in inbred mouse strains. *Respir. Physiol. Neurobiol.* **140,** 283–91 (2004).

56. Lutolf, M. P., Lauer-Fields, J. L., Schmoekel, H. G., Metters, A. T., Weber, F. E., Fields, G. B., *et al.* Synthetic matrix metalloproteinase-sensitive hydrogels for the conduction of tissue regeneration: engineering cell-invasion characteristics. *Proc. Natl. Acad. Sci. U. S. A.* **100,** 5413–8 (2003).

57. Kyburz, K. A. & Anseth, K. S. Three-dimensional hMSC motility within peptide-functionalized PEG-based hydrogels of varying adhesivity and crosslinking density. *Acta Biomater.* **9,** 6381–92 (2013).

58. Cavalcante, F. S. A., Ito, S., Brewer, K., Sakai, H., Alencar, A. M., Almeida, M. P., *et al.* Mechanical interactions between collagen and proteoglycans: implications for the stability of lung tissue. *J. Appl. Physiol.* **98,** 672–9 (2005).

59. Levental, I., Georges, P. C. & Janmey, P. A. Soft biological materials and their impact on cell function. *Soft Matter* **3,** 299–306 (2007).

60. Foster, K. A., Oster, C. G., Mayer, M. M., Avery, M. L. & Audus, K. L. Characterization of the A549 cell line as a type II pulmonary epithelial cell model for drug metabolism. *Exp. Cell Res.* **243,** 359–66 (1998).

61. Isakson, B., Lubman, R., Seedorf, G. & Boitano, S. Modulation of pulmonary alveolar type II cell phenotype and communication by extracellular matrix and KGF. *Am J Physiol Cell Physiol* **281,** C1291–C1299 (2001).

Chapter 5

Epithelial-mesenchymal crosstalk influences cellular behavior in a 3D alveolus-fibroblast model system

5.1 Abstract

Interactions between lung epithelium and interstitial fibroblasts are increasingly recognized as playing a major role in the progression of several lung pathologies, including idiopathic pulmonary fibrosis (IPF) and cancer. Three-dimensional *in vitro* co-culture systems offer tissue-relevant platforms that spatially position cells at physiologically relevant distances for studying the signaling interplay between diseased and healthy cell types. Such systems provide a controlled environment in which to probe the mechanisms involved in epithelial-mesenchymal crosstalk. To recapitulate the native alveolar tissue architecture, we employed a cyst templating technique to culture alveolar epithelial cells on photodegradable microspheres and subsequently encapsulate the spheres within poly(ethylene glycol) (PEG) hydrogels containing dispersed pulmonary fibroblasts. Normal and IPF fibroblast cell lines were cultured with normal mouse alveolar epithelial primary cells and a cancerous alveolar epithelial cell line to probe the influence of diseased cell phenotypes on healthy cells and *vice versa*. Using this 3D co-culture model, cancerous epithelial cells and normal fibroblasts had significantly higher proliferation rates when co-cultured together (45% and 12%, respectively) compared to any other cell combination, indicating a potential reciprocal relationship between their signaling pathways. When examining fibroblast motility, IPF fibroblast migration was significantly faster when co-cultured with primary epithelial cysts (15 μm/h) compared to monoculture (7 μm/h), and their speed in this combination was also greater than the normal fibroblasts in co-culture with primary cysts (10 μm/h). Conversely, the normal fibroblasts migrated significantly faster when co-

cultured with cancerous A549 cells (15 μm/h). Finally, immunohistochemistry revealed a potential marker for epithelial-to-mesenchymal transition (EMT) in primary epithelial cells when co-cultured with fibroblasts, namely expression of alpha smooth muscle actin (α-SMA), a hallmark of the activated myofibroblast phenotype. Together, this evidence supports the idea that there is an exchange between the alveolar epithelium and surrounding fibroblasts during disease progression and points to particular cell combinations and potential signaling routes that merit further inspection to discover potential targets for therapeutic development.

5.2 Introduction

In the lungs, hollow, cyst-like alveoli consist of a polarized epithelial layer attached to a thin basement membrane and surrounded by capillaries and interstitial stromal cells, in particular a population of alveolar fibroblasts commonly found in the collagen- and elastin-rich septa dividing neighboring alveoli.[1,2] Gaps in the basement membrane allow for direct communication between the epithelium and these alveolar fibroblasts.[3] Normal epithelial-mesenchymal signaling is essential during lung development and is thought to play a role in adult alveolar homeostasis.[1,4] For example, during repair of the wounded alveolar epithelium, interstitial fibroblasts secrete extracellular matrix (ECM) proteins to enable migration of proliferating and differentiating epithelial cells, followed by matrix degradation and apoptosis of activated fibroblasts (*i.e.*, myofibroblasts).[5] However, disruption of this signaling has been implicated in the progression lung diseases, such as idiopathic pulmonary fibrosis (IPF) and cancer.[6,7]

IPF is characterized by clusters of myofibroblasts that deposit an excessively collagen-rich ECM that stiffens the tissue and destroys normal alveolar tissue architecture.[6] A growing body of evidence suggests that disrupted signaling within the alveolar epithelium may lead to

altered gene expression seen in IPF fibroblasts. For example, hepatocyte growth factor (HGF) secretion by fibroblasts is thought to protect the epithelium from fibrosis, but HGF production is reduced in IPF fibroblasts versus normal fibroblasts.[8] This decrease may be linked to reduced interstitial prostaglandin E-2 (PGE2), which is an anti-fibrotic signal normally secreted by alveolar epithelial cells that suppresses migration, proliferation, and collagen production of fibroblasts.[9] The source of the clustered myofibroblasts characteristic of IPF continues to be debated in the literature. One hypothesis is that activated epithelial cells undergo epithelial-to-mesenchymal transition (EMT), which is identified by loss of epithelial cell junction markers (*e.g.,* E-cadherin, ZO-1) and rise of fibroblast and myofibroblast markers (*e.g.,* vimentin, alpha smooth muscle actin; α-SMA) as well as increased motility.[6] In one study, clearly labeled epithelial cells appeared in the alveolar interstitium producing myofibroblast markers.[10] In direct contradiction, another lineage-tracing study showed no evidence of EMT; instead, myofibroblasts arose from other stromal cell populations.[11]

EMT is also thought to play a role in tumor metastasis, allowing separation and migration of epithelial-derived cancer cells away from the primary tumor.[7,12] In addition to influencing EMT in cancer, the local microenvironment has also been shown to be a key regulator in tumor formation and invasion, especially mesenchymal cells and the ECM proteins and cytokines that they secrete.[13] As in IPF, there appears to be a reciprocal exchange of signals between pulmonary fibroblasts and epithelial-derived lung cancer cells. On one hand, an alveolar epithelium-derived adenocarcinoma cell line (A549) has been shown to increase α-SMA production in normal fibroblasts and increase matrix metalloproteinase (MMP) production in fibroblasts, influencing matrix remodeling and tumor invasion.[14,15] On the other hand, an increase in paracrine signals secreted by cancer-associated fibroblasts has been shown to increase

epithelial tumor proliferation (HGF), migration (transforming growth factor β; TGFβ), and drug resistance (HGF).[13,16]

Much still remains to be discovered about the intricacies of epithelial-mesenchymal crosstalk during disease progression, and *in vitro* co-culture models have been proven to be useful tools for studying such questions.[14,17–22] One advantage of these systems is the researcher's ability to control the density and spatial proximity of healthy cell types in co-culture with diseased cell types to probe the influence of one on the other and propose mechanisms by which injury or mutations in one type may lead to progression of disease in the overall tissue. Given the three-dimensional architecture of alveolar tissue and tumor masses, more physiologically relevant models must employ ECM mimics that support the growth and culture of 3D multicellular tissue structures. While many techniques exist to form dense tumor spheroids (*e.g.,* the hanging drop method),[23,24] the cyst-like alveolus structure is notoriously difficult to achieve and manipulate *in vitro* with primary alveolar epithelial cells, especially in synthetic ECM mimics. Recently, our lab demonstrated the use of photolabile microspheres as templates for patterning hollow, spherical model alveoli within peptide-modified poly(ethylene glycol) (PEG) hydrogels.[25] These hydrogels capture several key features of the native ECM (*e.g.,* high water content; lung tissue appropriate elasticity; enzymatically degradable crosslinkers that enable local remodeling by cell-secreted proteases; introduction of integrin binding sites, such as the fibronectin-derived RGDS sequence), with the added advantage of precise user control over matrix properties (*e.g.*, elastic modulus, scaffold geometry, tethered biochemical cues).[26] To complement this approach, our lab has also developed a PEG crosslinker that cleaves upon exposure to selected light wavelengths (365-420 nm) under cytocompatible conditions. These materials have been used to synthesize microspheres of discrete size ranges that are completely

degradable upon exposure to light, and have found applications as depots for drug delivery (10-50 μm), as well as for templating of multicellular cyst-like structures (50-200 μm).[25,27,28]

In the work presented here, our cyst templating technique was used to create model epithelial alveoli that were subsequently encapsulated in a PEG hydrogel laden with pulmonary fibroblasts. This approach allowed the culture of two distinct lung cell types in a physiologically-relevant geometry where the density and distance of the cell types were readily controlled to test hypotheses related to paracrine signaling. The results report on two types of epithelial cells: primary mouse alveolar epithelial cells to represent a healthy epithelium and an adenocarcinoma cell line (A549) to represent lung tumor cellular structures. These epithelial cells were co-cultured with two different pulmonary fibroblast cell lines: normal fibroblasts (CCL-210), and IPF fibroblasts (CCL-134). The co-cultured cells were analyzed for signs of disease progression and EMT by measuring for proliferation, migration, and immunostaining for key protein markers. Our goal was to test whether a diseased epithelium would influence the surrounding fibroblasts by increasing their proliferation and migration, and whether diseased fibroblasts would cause an increase in epithelial proliferation and expression of mesenchymal protein markers. Interestingly, our results suggest a feedback loop between diseased and healthy cells, in which cancer cell proliferation is increased in the presence of healthy fibroblasts and IPF fibroblast migration is increased in co-culture with normal epithelial cysts.

5.3 Materials and methods

5.3.1 Microsphere synthesis

Photodegradable microspheres[28] were formed by inverse suspension polymerization via base-catalyzed Michael addition of a photodegradable diacrylate (PEGdiPDA; M_n~4070 Da)

with a poly(ethylene glycol) tetrathiol (PEG4SH; M_n~5000 Da). The PEGdiPDA was synthesized as previously described,[29] and PEG4SH was purchased from JenKem Technology. An aqueous phase consisting of 6.9 wt% PEGdiPDA, 4.2 wt% PEG4SH, CRGDS peptide (1.5 mM final concentration), 300mM triethanolamine (Sigma-Aldrich) in pH 8.0 phosphate buffered saline (PBS, Sigma-Aldrich) was pipetted and triturated twice into an organic phase comprised of 3:1 sorbitan monooleate (Span 80, Sigma-Aldrich) and PEG-sorbitan monooleate (Tween80, Sigma-Aldrich) dissolved at 30 mg surfactant per mL in hexanes (EMD Millipore). The aqueous droplet suspension was immediately stirred at a rate of ~200 rpm with a 1cm magnetic stir bar in a 20 mL glass scintillation vial overnight, protected from light. Polymerized particles were then retrieved via centrifugation and washed consecutively with hexanes, isopropanol, and sterile phosphate-buffered saline (PBS).

As a control and reference point for cell tracking calculations, non-degradable, fluorescently labeled microspheres were used in fibroblast migration experiments. Briefly, AlexaFluor-488 C_5 maleimide (Life Technologies; <1 mM) was pre-reacted with PEG4SH for ~30 minutes in the dark. Poly(ethylene glycol) diacrylate (PEGDA; M_n~4000) was synthesized as previously described.[30] Fluorescently tagged microspheres were synthesized as above with an aqueous phase consisting of 6.9 wt% PEGDA, 4.2 wt% AlexaFluor-488-labeled PEG4SH, 300 mM triethanolamine in pH 8.0 PBS.

5.3.2 Cell culture

A549 human adenocarcinoma cells (CCL-185, ATCC) were cultured in high glucose Dulbecco's modified Eagle's medium (DMEM, Life Technologies); human normal lung fibroblasts (CCL-210, ATCC) were cultured in low glucose DMEM; and human idiopathic pulmonary fibrosis lung fibroblasts (CCL-134, ATCC) were cultured in Kaighn's modification

of Ham's F-12 medium (F-12K, Life Technologies). All cell line growth medium was supplemented with 10% fetal bovine serum (FBS, Life Technologies), 1% penicillin/streptomycin (Life Technologies), and 0.2% fungizone (Life Technologies). Cells were cultured at 37 °C with 5% CO_2 and passaged until use in experiments.

5.3.3 Primary ATII cell isolation

All procedures and protocols were reviewed and approved by the Animal Care and Use Committee at the University of Colorado, Boulder. Primary mouse alveolar epithelial type II (ATII) cells were isolated as previously described.[31] Briefly, FVB/NJ mice (6 weeks old) were obtained from The Jackson Laboratories, immediately euthanized by CO_2 asphyxiation and the chest cavity was opened to expose the heart-lung block. Sterile heparin was injected into the left ventricle and the inferior vena cava was cut. The pulmonary vasculature was then flushed with 1% heparin in sterile PBS. The heart-lung block was excised, and lung tissue was carefully dissected from the heart, trachea, and connective tissue.

Lung tissue was minced and digested in 0.1% Type-1 collagenase (Worthington Biochemical) and 1 mg/mL DNase (Sigma) for 20 minutes at 37°C. Next, trypsin (Fisher, 0.01% final concentration) was added and the solution was incubated for another 20 minutes at 37°C. A solution containing 1mg/mL trypsin inhibitor (Life Technologies) and 1 mg/mL DNase was added, and this final mixture was filtered through 100 μm cell strainers and through a Nitex filter with 10 μm pore diameter. The filtered solution was then centrifuged for 5 minutes at 2000 rpm, and the resultant pellet was resuspended in DMEM/F-12 medium (Sigma). This cell suspension was added to tissue culture plates coated with IgG (11 mg/cm^2) and incubated for 1 hour at 37°C to separate immune cells from epithelial cells. Non-adherent cells were recovered, centrifuged for 5 minutes at 2000 rpm, resuspended in 1:1 Dulbecco's Modified Eagle Medium:Nutrient

Mixture F-12 (DEMEM/F12, Corning) supplemented with 10% FBS and 1% antibiotic/antimitotic (Life Technologies), and counted. Cells were then centrifuged once more at 2000 rpm for 5 minutes and resuspended at 500,000 cells/mL in DMEM/F-12 medium supplemented with 10% FBS, 1% antibiotic/antimitotic, hepatocyte growth factor (HGF; R&D Systems; 50 ng/mL), and Fibroblast Growth Factor 7 (FGF-7; Sigma; 10 ng/mL). Primary ATII cells were immediately used in cyst experiments.

5.3.4 Microsphere seeding

A549 cells at 150,000 cells/mL or primary ATII cells at 500,000 cells/mL in appropriate growth medium were combined with 40 μL of photodegradable microspheres in an ultra-low adhesion 24-well plate (Corning). Plates containing pre-cysts were incubated at 37°C with 5% CO_2 on an orbital shaker at 45 rpm. Prior to encapsulation in hydrogel formulations, A549 pre-cysts were incubated for 18-24 hours and primary pre-cysts were incubated for 3 days to allow for attachment and optimal microsphere coverage.[25]

5.3.5 Cell labeling

For Click-it Plus EdU assays, immunohistochemistry experiments, and co-culture migration experiments, fibroblasts were labeled with Cell Tracker Green CMFDA (Life Technologies) per manufacturer's instructions prior to encapsulation in hydrogels. Fibroblasts were resuspended in appropriate serum-free growth medium containing Cell Tracker Green (10 μM final concentration) and incubated at 37°C for 30 minutes after which they were centrifuged and resuspended in PBS at 5 million cells/mL for encapsulation in hydrogels. For fibroblast-only migration experiments, fibroblasts were labeled with Cell Tracker Red CMPTX (Life Technologies, 20 μM final concentration) as above.

For co-culture migration experiments epithelial pre-cysts were stained with Cell Tracker Red CMPTX (Life Technologies). Pre-cysts were carefully removed from 24 well plates after the appropriate incubation period, allowed to settle by gravity, and the supernatant was removed with a pipet. Appropriate serum-free growth medium containing Cell Tracker Red (20 μM final concentration) was added, and cells were incubated for 30 minutes at 37°C. Cell Tracker Red medium was removed, and cysts were resuspended in PBS for encapsulation in hydrogels.

5.3.6 Gel formation/cell encapsulation

8-arm poly(ethylene glycol) norbornene (PEG-Nb M_w ~40,000) and photoinitiator lithium phenyl-2,4,6-trimethylbenzoylphosphinate (LAP) were both synthesized as previously published.[32,33] An enzymatically-cleavable di-cysteine peptide (KCGPQG↓IWGQCK) and an integrin-binding peptide (CRGDS) were purchased commercially from American Peptide Company, Inc.

For Click-iT Plus EdU assays and immunohistochemistry experiments, 8-arm 40 kDa PEG-Nb (5 wt%) was combined with di-cysteine peptide crosslinker (0.85:1 thiol:ene), CRGDS (1mM), and LAP (0.05 wt%) in sterile PBS and mixed by vortex to form a gel precursor solution. The pH was adjusted to 6.8-7.2 with sterile, 0.1 M sodium hydroxide. A fibroblast cell suspension (final concentration 1.6 million cells/mL) and/or epithelial cysts were then added to the gel precursor solution and gently mixed with a pipette. 30 μL drops of this precursor solution were placed on a Sigmacote-treated glass slide and exposed to 365 nm light at ~2 mW/cm^2 for 3 minutes to initiate the radical-mediated thiol-ene polymerization reaction. Each polymerized gel was then transferred to an untreated 24-well plate (Corning) with 1 mL of DMEM/F-12 growth medium supplemented with 10% FBS and 1% antibiotic/antimitotic and incubated at 37 °C with 5% CO_2.

For migration experiments, each well in a 24-well glass-bottomed plate (Greiner Bio-One) was washed in 95% ethanol prior to surface functionalization with thiol groups in 0.5% (v/v) (3-mercaptopropyl)trimethoxysilane in 95% ethanol (pH ~5.5) for 5 minutes. Each well was then washed in 95% ethanol and allowed to air dry. To make the gel precursor solution, 8-arm 40kDa PEG-Nb (3 wt%), di-cysteine MMP-degradable crosslinker (0.75:1), CRGDS (1 mM), and LAP (0.05 wt%) in sterile PBS were combined and mixed by vortex. Sodium hydroxide (0.1 M) was used to adjust the pH of the pre-cursor solution to 6.8-7.2. A fibroblast cell suspension (final concentration 1 million cells/mL) and either epithelial cysts or fluorescently-labeled non-degradable microspheres were added to the gel precursor solution and gently pipetted to mix. Square 1 mm tall rubber gaskets, with a 6 mm diameter circle cut out from the center with a biopsy punch, were sealed to the bottom of the wells in the thiolated 24-well glass-bottom plate and filled with 30 μL drops of the precursor solution. To initiate the thiol-ene polymerization, the plate was exposed to 365 nm light at ~2 mW/cm^2 for 4 minutes. After polymerization, the rubber gaskets were carefully removed. To each of the wells, DMEM/F-12 growth medium supplemented with 10% FBS and 1% antibiotic/antimitotic was added and incubated at 37 °C with 5% CO_2.

5.3.7 Microparticle template erosion

Gels containing fibroblasts and/or cysts were cultured for one day to allow cell attachment to the encapsulating hydrogel. Following this 24-hour incubation period, all samples were exposed to 365 nm light at ~10 mW/cm^2 for 15 minutes to cleave the photo-labile moiety in the microspheres and fully erode the cyst templates. Gels were then incubated for ~1 hour at 37°C with 5% CO_2 before changing growth medium. Growth medium was then exchanged daily until completion of each experiment (between 1 and 7 days).

5.3.8 Click-iT EdU assay and quantifying proliferation

Three biological replicates of each cell combination were studied, and images of the proliferating nuclei were quantified using MATLAB. Cell proliferation was detected using a Click-iT Plus EdU AlexaFluor-594 imaging kit (Life Technologies). A copper-catalyzed covalent "click reaction" between a picolyl azide on an AlexaFluor dye and an alkyne on the thymidine nucleoside analog, 5-ethynyl-2'-deoxyuridine (EdU), allowed for fluorescent staining of proliferating nuclei. EdU was added to growth media at a final concentration of 10 μM on day 1 or day 4 after cell/cyst encapsulation. Samples were then incubated for 17 hours at 37°C with 5% CO_2 to allow for EdU incorporation into DNA during active DNA synthesis, per manufacturer instructions. Samples were then fixed with 4% paraformaldehyde in PBS for 15 minutes at room temperature and washed in 3% bovine serum albumin (BSA) in PBS. Cells were permeabilized in 1% TritonX-100 for one hour and washed with 3% BSA in PBS. Click-it Plus reaction cocktail containing the AlexaFluor 594 dye was prepared as per manufacturer instructions, added to each sample, and incubated for 3 hours at room temperature with rocking. Samples were then washed with 3% BSA in PBS. Finally, nuclei were stained with DAPI (1:2000, Life Technologies) for one hour and washed in PBS. All samples were imaged on a confocal microscope (Zeiss LSM 710) with a 20× water-dipping objective (Plan Appochromat; NA = 1.0). Image stacks (10 per condition) were taken from the top to bottom of individual cysts, or in the center of the gel for fibroblast-only conditions (z step = 10 μm, average stack size ~500 μm).

Four categories of cell nuclei were counted using MATLAB: fibroblast nuclei, epithelial nuclei, proliferating fibroblast nuclei, and proliferating epithelial nuclei. TIFF images of each z-slice in each of three channels: DAPI, AF-594, and Cell Tracker Green, were created in Image-J

and processed in MATLAB. Separate masks were made of objects (nuclei) in the DAPI channel and AlexaFluor 594 channels, and objects were dilated by two pixels with a Disk Structuring Element. The mean intensity within each dilated object in the Cell Tracker Green channel was evaluated. Objects with a mean intensity above a given threshold were counted as fibroblasts; if the mean intensity fell below this threshold, the object was counted as an epithelial cell. Cell nuclei centroids were tracked and checked for their appearance in successive slices to account for double counted nuclei. Double counts were subtracted to give final cell counts and the percent of proliferating cells. Object counts were pooled from all ten image stacks, and the mean percent positive for EdU was calculated from three biological replicates. Statistical analysis was performed using two-way ANOVA followed by Bonferroni posttests. All error bars represent standard error of the mean (SEM).

5.3.9 Tracking cell migration

The 3D migration of fibroblasts in co-culture hydrogels was observed with an Operetta High Content Imaging System (Perkin Elmer) using Harmony High Content Imaging and Analysis software (Perkin Elmer) for automated image collection in real-time. As mentioned previously, co-culture hydrogels were formed and allowed to swell for 24 hours before cyst templates were eroded and fresh growth medium was introduced. During each experiment, the 10x long WD objective was used with the optical model set to confocal. Two channels, AlexaFluor 594 and AlexaFluor 488, were selected and exposure times were adjusted for each experiment. The layout selection for the images taken in each well was defined as nine fields of view in a 3x3 square in the center of the well. 400 μm z-stacks beginning at a height of 25 μm from the glass surface were collected for each image. Images were taken at 30-minute intervals for 24 hours. A live cell chamber was used to maintain the temperature at 37 °C and 5% CO_2.

Fibroblast migration in 3D was analyzed with Volocity 3D Image Analysis Software (Perkin Elmer). The protocol tracked the fibroblasts in the appropriate channel (AlexaFluor 488 for cyst co-cultures, AlexaFluor 594 for fibroblast-only gels) within a spherical region of interest (ROI) around a cyst or microsphere with a radius of 125 μm greater than the object. This radius was chosen to limit ROI overlap between neighboring cysts/microspheres, which were spaced about 250 μm apart, on average. Either the epithelial cyst in the AlexaFluor 594 channel or the microsphere in the AlexaFluor 488 channel was tracked as a single object to be used as a reference point. The centroids of the tracked reference point and fibroblasts were exported for subsequent analysis in MATLAB to determine cell speeds, displacements, meandering indices, and the percent of cells that were migrating. To compensate for drift in each ROI analyzed, the fibroblast centroid data was normalized to the corresponding tracked reference point. Fibroblast speeds were calculated as the average of the individual speeds between subsequent time points on the cell path. Displacement (distance between start and end points) was used to determine if a fibroblast was migrating towards or away from a cyst, where a positive displacement was traveling towards a cyst and negative displacement was traveling away from a cyst relative to the centroid of the cyst. The directionality (displacement/total distance traveled) was a measure of the straightness of a cell path analogous to persistence time, with values close to 1 indicating a perfectly linear path.[34] The fraction of migrating cells was defined as the number of fibroblasts migrating divided by the total number of fibroblasts tracked, where a cell was deemed migrating if the maximum distance away from the starting position was greater than one cell body length (15 μm) at any point during the 24 hour period, a criterion used in previous migration studies.[34] Statistical analysis was performed using the Kruskal-Wallis test followed by Dunn's Multiple Comparison test. All error bars represent standard error of the mean (SEM).

5.3.10 Immunohistochemistry

Primary antibodies used in these experiments included: hamster anti-mouse podoplanin (T1α; 1:100; eBioscience), rabbit anti-prosurfactant protein C (SPC; 1:100; Millipore), mouse anti vimentin (1:200; Abcam), mouse anti alpha smooth muscle actin (α-SMA; 1:200, Abcam), rabbit anti E-cadherin (E-cad; 1:100; Abcam) and rabbit anti-ZO-1 (1:100; Life Technologies). Secondary antibodies included: goat anti-mouse AlexaFluor 594 (1:200; Life Technologies), goat anti-rabbit AlexaFluor 594 (1:200; Life Technologies), and goat anti-hamster AlexaFluor 647 (1:200; Life Technologies).

Samples were cultured for 1, 4, or 7 days before fixing and staining. At the completion of each experiment, samples that would be stained for phenotype (SPC, T1α) or mesenchymal markers (α-SMA, Vimentin) were fixed with 4% PFA in PBS at room temperature for 15 minutes, rinsed in PBS, permeabilized for 1 hour in TritonX-100 at room temperature and washed in PBS. Samples intended for cell junction staining (E-cad, ZO-1) were fixed with 1:1 methanol:acetone on ice for 40 minutes and washed with PBS; these samples were not permeabilized. All samples were then blocked overnight (>16 h) in 40% goat serum in PBS at 4°C. Samples were incubated with primary antibodies overnight, followed by three wash steps. Samples were then incubated with secondary antibody overnight, followed by three wash steps. Finally, samples stained for phenotype or mesenchymal markers were stained with DAPI (1:2000, Life Technologies) for one hour and washed in PBS. Samples stained for cell junction markers were incubated in Hoechst (1:2,000; Life Technologies) for 1 hour at room temperature to stain nuclei, and then washed in PBS. All samples were imaged on a Zeiss LSM 710 confocal microscope with a 20x water-dipping objective (Plan Appochromat; NA = 1.0). Image stacks

were taken from top to bottom of individual cysts, or in the center of the gel for fibroblast-only conditions, and analyzed in ImageJ software (NIH).

5.4 Results

Using a previously developed cyst-forming technique,[25] a physiologically-relevant 3D co-culture system for lung cells was created with alveolar epithelial cysts embedded in a synthetic polymer hydrogel and surrounded by low-density pulmonary fibroblasts (Fig. 5.1). This *in vitro* culture system enabled us to probe cellular behavior in response to co-culture with a diseased cell type in an attempt to elucidate the role of epithelial-mesenchymal crosstalk in disease progression. To accomplish this goal, four cell types were used: normal alveolar epithelial cells (primary mouse cells), lung tumor epithelial cells (A549 cell line), normal pulmonary fibroblasts (CCL-210 cell line), and IPF fibroblasts (CCL-134 cell line). While the

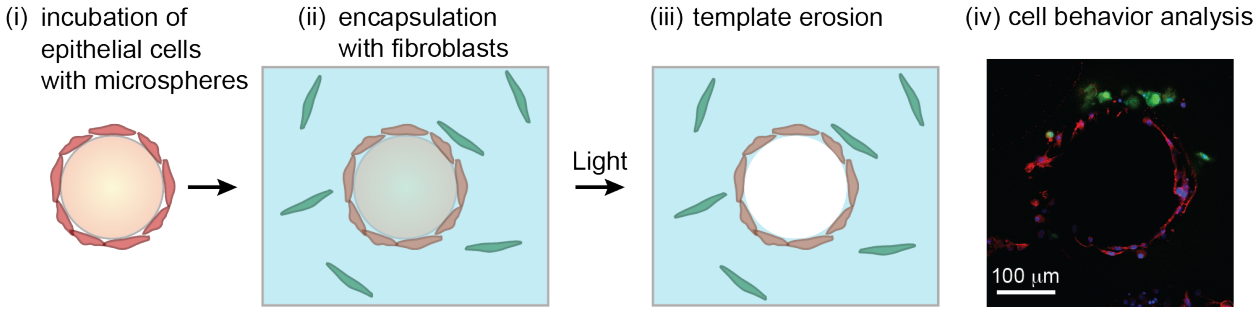

Figure 5.1 Cross-sectional schematic of the co-culture set-up. (i) Epithelial cells (red) were incubated on an orbital shaker with photodegradable microspheres (orange) containing RGDS peptides to allow for cellular attachment to the surface of the microsphere. (ii) Pre-cysts were co-encapsulated with a single cell suspension of fibroblasts (green) in a poly(ethylene glycol) (PEG) hydrogel (blue) containing pendant RGDS for cell adhesion and an enzymatically-degradable peptide crosslinker to allow for local matrix remodeling. (iii) One day after encapsulation, cytocompatible 365 nm light at ~10 mW/cm^2 for 15 minutes was applied to completely erode the microsphere templates, leaving a shell of epithelial cells surrounding a liquid-filled lumen. (iv) Cells were cultured for 1-7 days before being analyzed for proliferation, migration, or protein visualization. In this confocal image slice, normal fibroblasts labeled with Cell Tracker Green were co-cultured with primary epithelial cells, which were subsequently stained for an alveolar epithelial type 1 (ATI) phenotype marker. Green = Cell Tracker (fibroblasts), Blue = DAPI (nuclei), Red = T1α (ATI).

primary epithelial cells attached and spread to form single-cell layers on the microsphere templates, the cancerous A549 cells tended to form multilayered structures either on the microspheres or as detached aggregates, both of which were embedded in the encapsulating hydrogel. Therefore, the A549 results presented here include both the cyst-like structures, as well as the higher density aggregates, with no significant differences found between the two structure types in the assays studied here. We believe that this phenomenon is relevant to the tumor structures found in cancer progression, and many of the 3D model systems presented in the literature make use of tumor spheroids.[14,21,23,35] The advantage with the presented co-culture system is that we can study both normal alveolar epithelial cells in their native tissue structure, as well as tumor aggregates, and how they respond in the presence of fibroblasts distributed adjacent to and far from the epithelial surface.

5.4.1 Proliferation

An increase in proliferation in either epithelial cells or fibroblasts would indicate abnormal behavior potentially leading toward disease progression.[6,7] Here, we used a commercially available fluorescent EdU assay to measure the proliferation of each cell type after a 17-hour incubation period initiated on days 1 and 4 post-encapsulation. Automated analysis of confocal image slices (Fig. 5.2A) was performed to quantify the percent of nuclei positive for EdU.

The results for both epithelial cell types demonstrated a significant decrease in proliferation between day 1 and day 4, whether alone or in co-culture with fibroblasts (Fig. 5.2B). The primary epithelial cells had no difference in proliferation between the co-culture conditions and monoculture on either day, with ~28% positive on day 1 and ~15% positive on day 4. However, the A549 cancer cells showed a trend of slightly decreased proliferation on

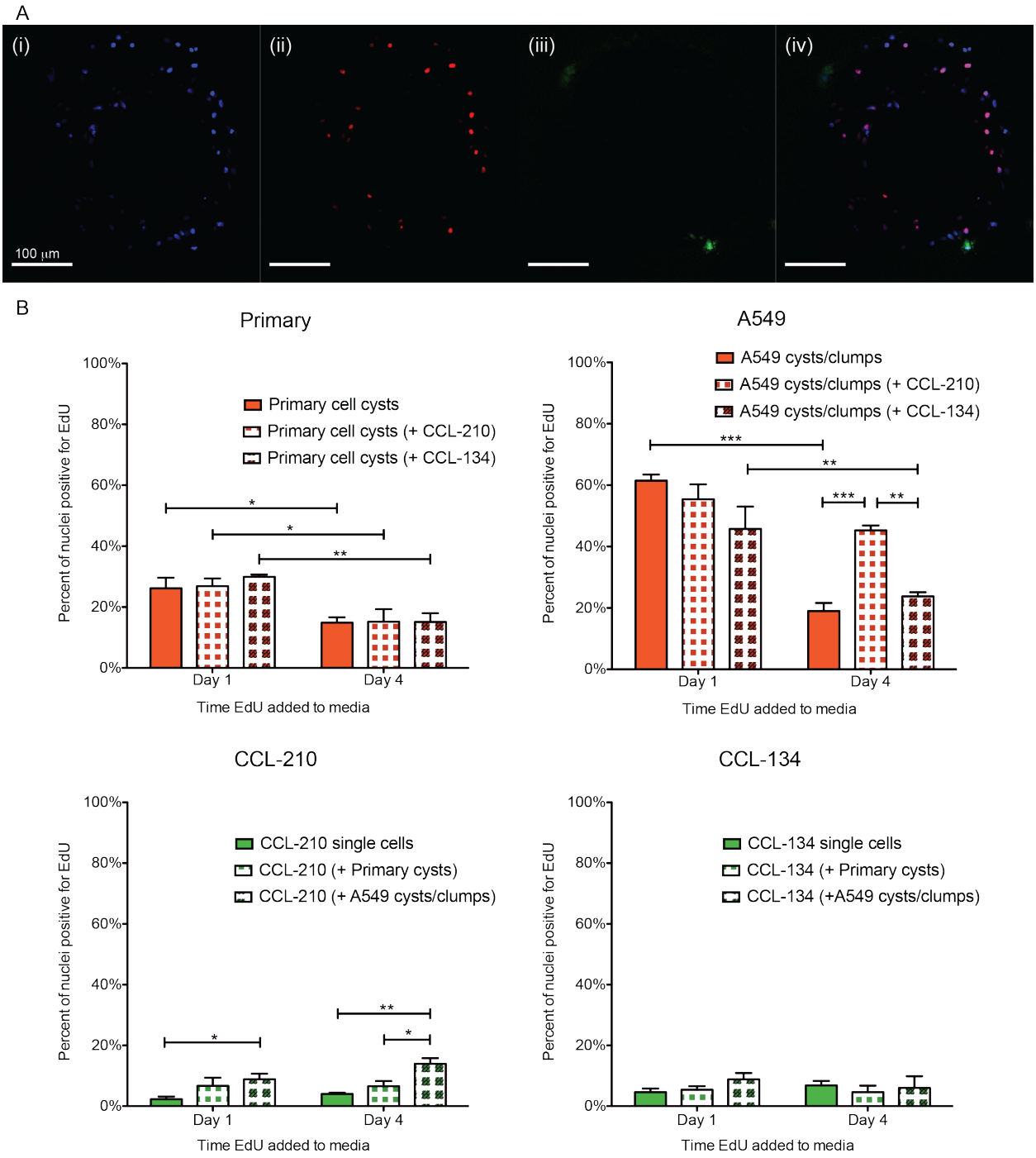

Figure 5.2 Click-iT Plus EdU proliferation assay. (A) Example confocal image slices used for automated nuclei counts. Each object found in the blue and red channels was measured for mean intensity in the green channel, and objects above a certain threshold were counted as fibroblasts. (i) Blue = DAPI (all nuclei). (ii) Red = EdU (proliferating nuclei). (iii) Green = Cell Tracker (fibroblasts). (iv) Merged image of previous three channels. (B) Plots depict percent of nuclei positive for EdU at the two time points in monoculture and both co-cultures, separated by cell type. Results are presented as means ± SEM of three biological replicates of each condition. *$p < 0.05$, **$p < 0.01$, ***$p < 0.001$

day 1 when co-cultured with either fibroblast cell line (55% and 46%) versus monoculture (61%), although this trend was not statistically significant in the present study due to variability between replicates. Interestingly, the A549 cells did exhibit significantly increased proliferation on day 4 when co-cultured with the normal fibroblasts (CCL-210, 45%) compared with monoculture (19%) and co-culture with IPF fibroblasts (CCL-134, 24%). When comparing primary epithelial cell proliferation to A549 proliferation, A549 cells had significantly higher percentages of EdU-positive nuclei on day 1 for monoculture and both co-culture conditions (Fig. 5.S1). On day 4, however, A549 proliferation was significantly higher only when co-cultured with normal fibroblasts (CCL-210).

The fibroblasts had a much lower proliferation rate than either epithelial cell type, and this rate did not appear to change over time (Fig. 5.2B). While the IPF fibroblast (CCL-134) proliferation (~6%) did not appear to be influenced by co-culture with epithelial cells, the normal fibroblasts (CCL-210) had a significantly higher percentage of EdU-positive nuclei when co-cultured with A549 cells on both days (~12%) compared to monoculture (~3%), and on day 4 when compared to co-culture with primary cysts (7%). When comparing the two fibroblast cell lines (Fig. 5.S1), the only significant difference in their proliferation was on day 4 when co-cultured with A549 cells, where the normal fibroblasts (CCL-210) had a higher percentage of EdU-positive nuclei (14%) compared with the IPF fibroblasts (CCL-134, 6%).

5.4.2 Fibroblast migration

Increased motility of both fibroblasts and epithelial cells has been used as an indicator of disease progression.[12,36–38] In the healthy adult lung, both cell populations remain quiescent until an injury occurs. Normal wound healing involves migration of interstitial fibroblasts to the wound site where they contribute to deposition of a provisional ECM.[5] ATII progenitor cells

then migrate along this provisional matrix to repopulate the wounded epithelium.[5,39] In the case of IPF, it is debated whether the characteristic myofibroblast foci arise from recruitment of nearby fibroblasts or migration of transformed epithelial cells away from the alveolar epithelium.[6,11] In cancer metastasis, it is thought that tumor cells undergo EMT, detach from the main tumor, and migrate through the surrounding matrix to reach the blood stream.[7] Therefore, an increase in fibroblast migration measurements would suggest activation of the wound repair response, which is overstimulated in diseases such as IPF, while epithelial migration would indicate either wound repair or EMT.

In this study, we fluorescently labeled each cell type and used live cell microscopy to record confocal image stacks every 30 minutes for 24 hours, starting one day post-encapsulation (Fig. 5.3A). Using automated software and analysis codes, we tracked cell position in three dimensions over time and calculated key migration measurements, namely the fraction of cells migrating per analyzed cyst, the fraction of cells migrating toward the reference cyst, the speed, and the directionality. While no significant movement was detected in the epithelial cells, we did observe fibroblast migration in these gels. Cells that traveled at least one cell body length away from their starting position at any point during the 24-hour experiment were considered to be migrating. All other measurements were calculated for the migrating cells only. Cells considered to be moving toward their reference cyst had final positions closer to the cyst than their starting positions.

The normal fibroblasts (CCL-210, Fig. 5.3B) had no statistically significant difference in cells migrating per cyst when co-cultured with either A549 cancer cells (44%) or primary cysts (52%) compared to monoculture (37%). Likewise, in all conditions the normal fibroblasts showed no directional preference toward or away from the reference cyst. Interestingly, the

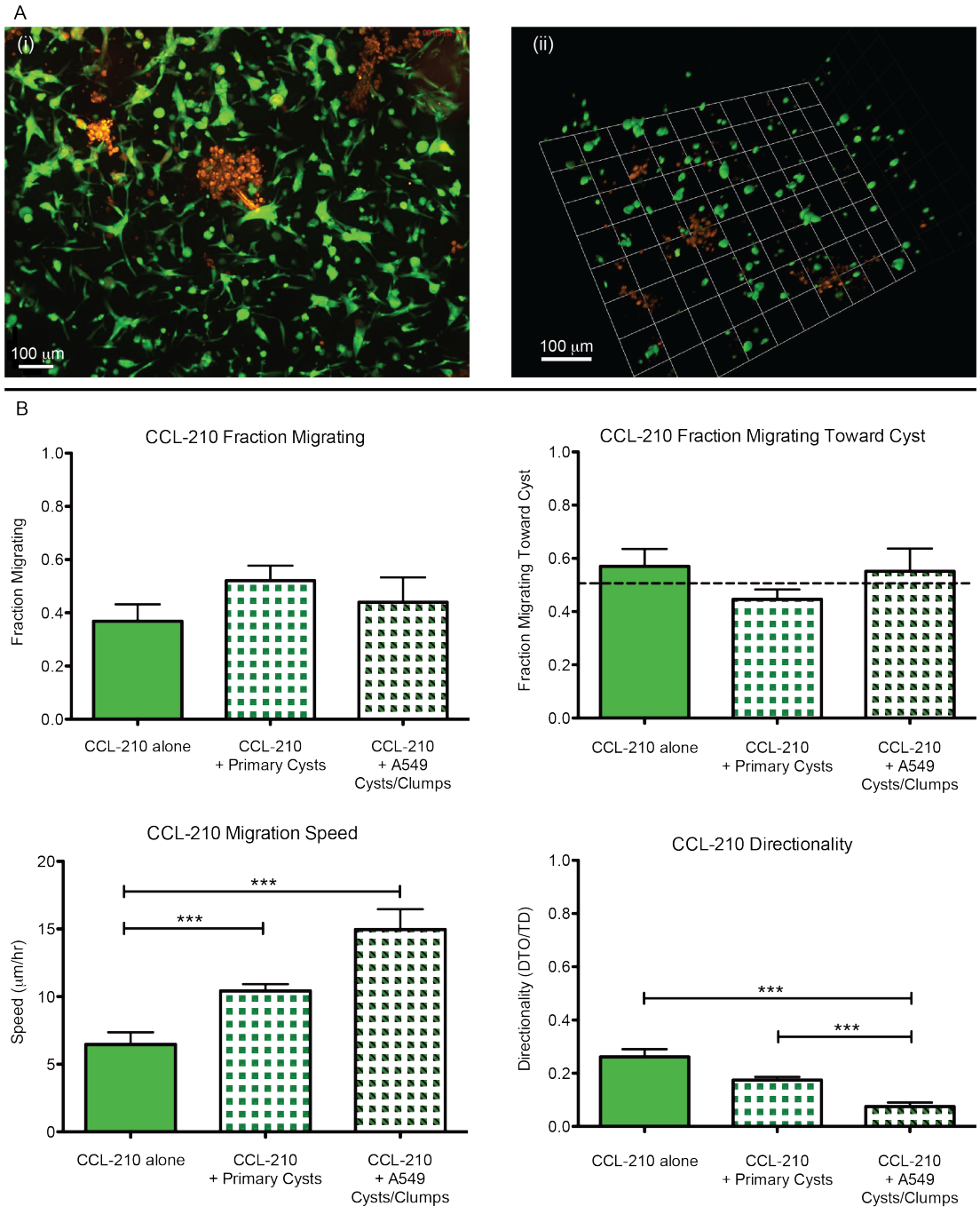

Figure 5.3 Normal fibroblast migration analysis. (A) Example images of fibroblasts (green) in co-culture with epithelial cysts (red) used in cell tracking. (i) Max z-projection of 400 µm confocal stack. (ii) 3D rendering of 200 µm confocal stack using Volocity (Perkin Elmer). (B) Plots show fraction migrating, fraction migrating toward cyst, migration speed, and directionality (Distance-To-Origin/Total Distance) of migrating normal fibroblasts (CCL-210) in monoculture and co-culture with both epithelial cell types. Data in fraction migrating plot represent means ± SEM of cells migrating per cyst. Data in the remaining plots represent means ± SEM of all migrating cells. ***$p < 0.001$

average speed of the migrating CCL-210 cells in monoculture was ~6 μm/h, while their speed in co-culture with either epithelial cell type was significantly faster (10 μm/h with primary cysts and 15 μm/h with A549 cells). These speeds are much slower than previously reported values for human dermal fibroblasts in similar hydrogels (~40 μm/h),[34] but fall in the same range reported for human mesenchymal stem cells (~5-20 μm/h, depending on RGD concentration and crosslinking density).[40] With regards to directionality (distance to origin/total distance), where a value of 1 represents a completely straight path, the normal fibroblasts in all conditions exhibited relatively random migration. However, co-culture with A549 cells resulted in significantly less persistent motion (0.07) than in monoculture (0.26) or in co-culture with primary cysts (0.17).

The IPF fibroblasts (CCL-134, Fig. 5.4) also had no statistically significant difference in cells migrating per cyst in any condition, although the fraction migrating appeared to be higher when co-cultured with primary cysts (70%) compared to monoculture (42%) and co-culture with A549 cells (40%). None of the CCL-134 conditions showed a directional preference either toward or away from the reference cyst, indicating isotropic migration. Interestingly, the average migration speed of the IPF fibroblasts when co-cultured with primary cysts (15 μm/h) was significantly faster than when co-cultured with A549 cells (10 μm/h), and both were significantly higher than in monoculture (7 μm/h). Again, the IPF fibroblasts displayed relatively random migration, with directionality values around 0.19 in all conditions.

When comparing each measurement between paired CCL-210 and CCL-134 culture conditions (*i.e.,* monoculture, co-culture with primary cysts, and co-culture with A549 cells; Fig. 5.S2), only a few statistically significant differences were found. First, in co-culture with primary cysts, the IPF fibroblasts moved significantly faster than the normal fibroblasts (15 μm/h vs. 10 μm/h). This finding was reversed in co-culture with A549 cells, where the IPF fibroblasts moved

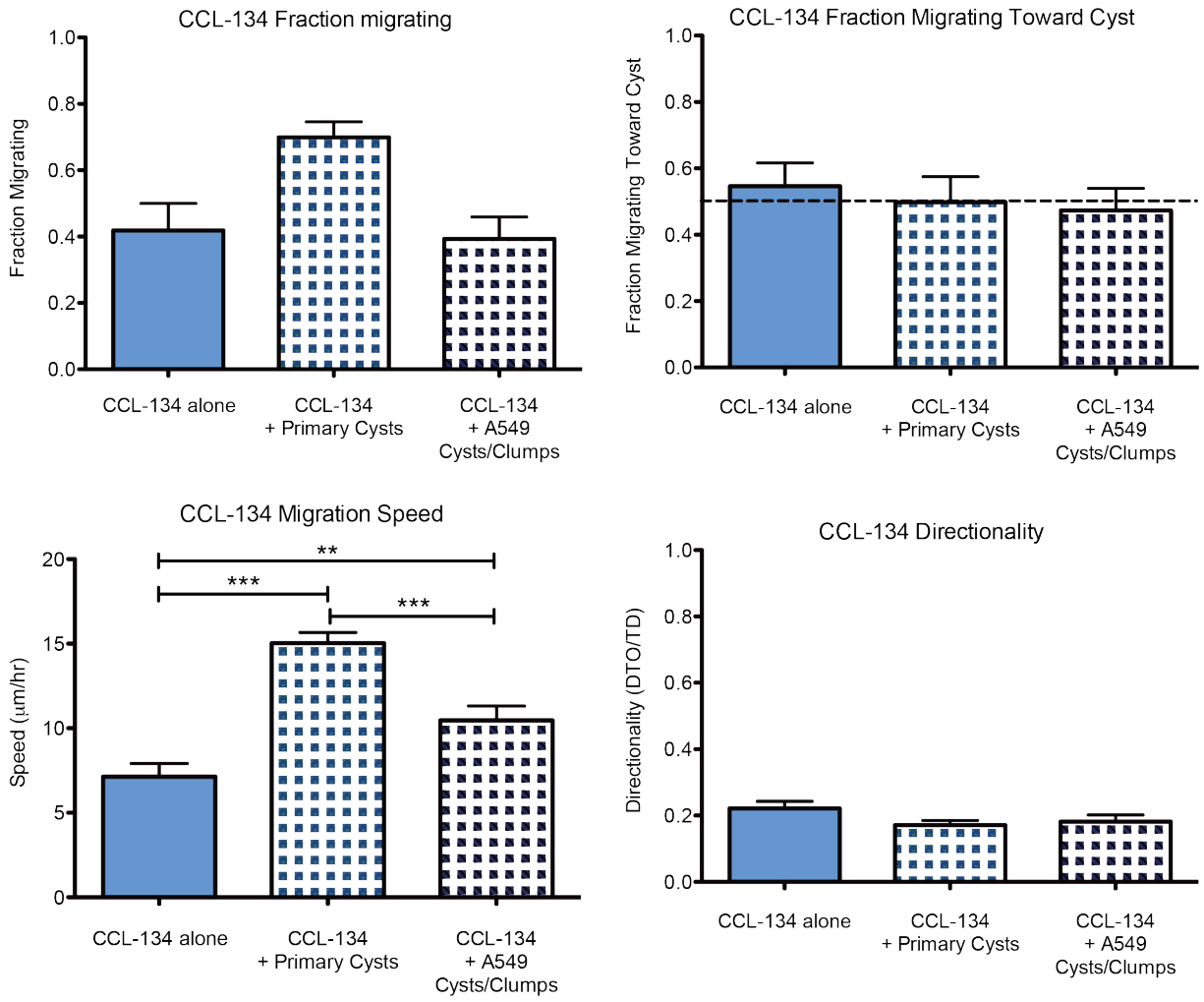

Figure 5.4 IPF fibroblast migration analysis. Plots show fraction migrating, fraction migrating toward cyst, migration speed, and directionality (Distance-To-Origin/Total Distance) of migrating IPF fibroblasts (CCL-134) in monoculture and co-culture with both epithelial cell types. Data in fraction migrating plot represent means ± SEM of cells migrating per cyst. Data in the remaining plots represent means ± SEM of all migrating cells. **p < 0.01, ***p < 0.001

significantly slower than the normal fibroblasts (10 μm/h vs. 15 μm/h). In the same A549 co-culture condition, the normal fibroblasts displayed less persistent migration than the IPF fibroblasts (directionality 0.07 vs. 0.18).

5.4.3 Epithelial-to-mesenchymal transition (EMT) markers

Hallmarks of EMT are the loss of cell junctions and onset of mesenchymal protein expression, both of which can be observed by immunostaining for key cell junction markers

(E-cadherin, ZO-1) and myofibroblast markers (vimentin, α-SMA).[7,10,41,42] In this study, we cultured primary cysts or A549 cancer cell cysts/clumps either alone or in co-culture with fibroblasts (normal or IPF) for 1, 4, and 7 days and stained for the four key proteins listed above. While the cell junction stains were inconclusive (Figure 5.S3 and Figure 5.S4), staining for the mesenchymal markers led to some unexpected observations.

As expected, primary cysts cultured alone did not express any vimentin (Fig. 5.S5A), while the cancerous A549 cells[14,43] showed strong vimentin expression at all time points (Fig. 5.S5B). In co-culture with normal fibroblasts (CCL-210; Fig. 5.5A) and with IPF fibroblasts (CCL-134; Fig. 5.5B), the primary cysts did not produce vimentin over the course of seven days, while the A549 cells appeared to have a slight decrease in vimentin expression in co-culture (Fig. 5.S5C,D). The latter result would indicate no EMT in the primary cells, and perhaps a slight EMT reversal in the A549 cells. On the other hand, the myofibroblast marker, α-SMA, was clearly expressed as stress fibers in some of the primary epithelial cells when co-cultured with both normal and IPF fibroblasts, beginning as early as one day after encapsulation and lasting through seven days in culture (Fig. 5.5C,D). A549 cells, however, did not express α-SMA at any time either in monoculture or in co-culture (data not shown).

5.5 Discussion

Epithelial-mesenchymal crosstalk is a key regulator during lung development and normal wound healing processes, and growing evidence suggests that altered paracrine signaling between the alveolar epithelium and interstitial fibroblasts may lead to disease progression in multiple pathologies.[6–9,13,15] To study these interactions, *in vitro* co-culture systems have been valuable tools for controlling the cell types present and their proximity to one another, with the

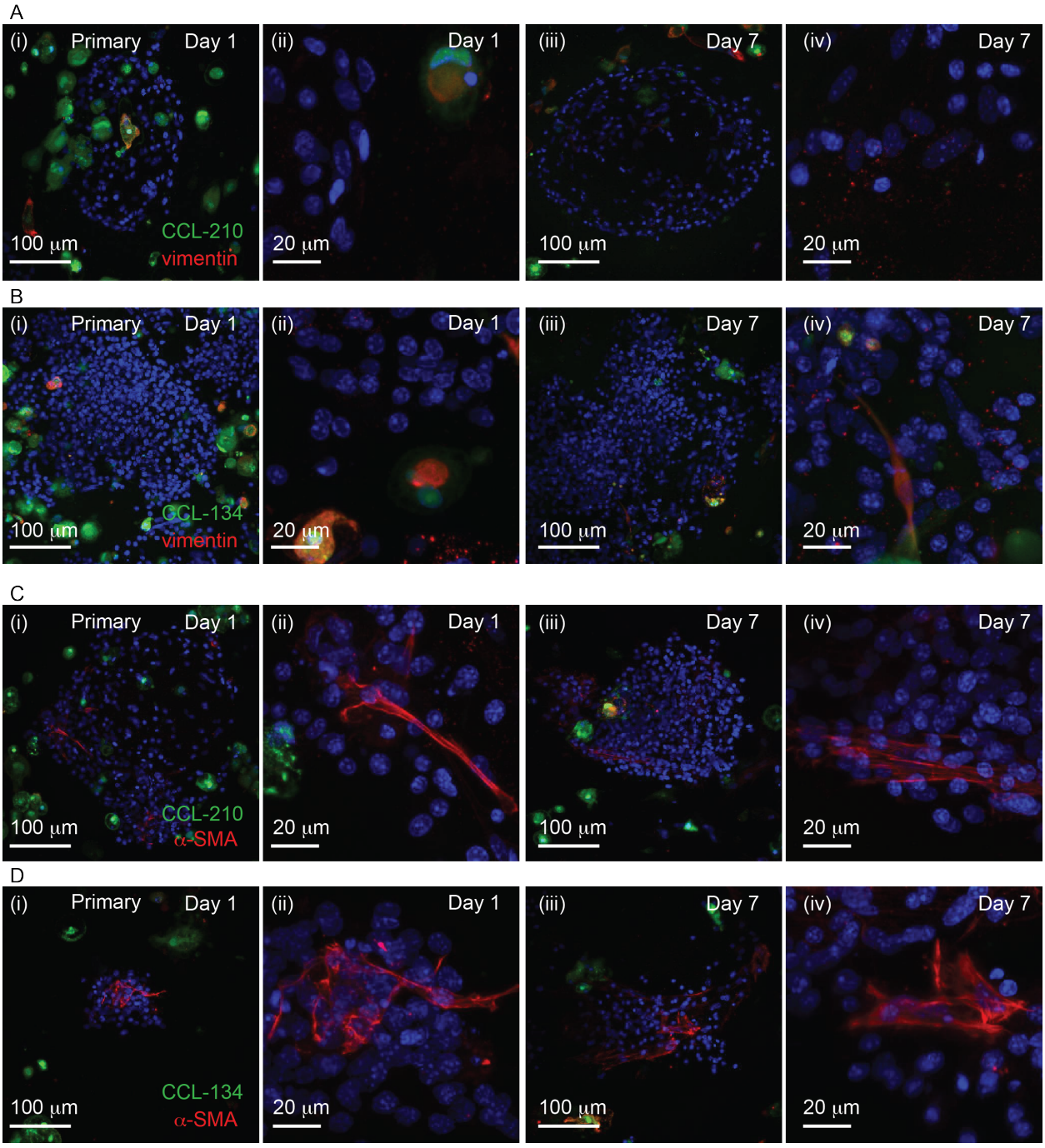

Figure 5.5 Immunostaining for mesenchymal markers. For all (i) and (ii) samples fixed one day after encapsulation. For all (iii) and (iv) samples fixed seven days after encapsulation. For all (i) and (iii) 20x objective, max z-projection of confocal image stack of whole cyst. For all (ii) and (iv) 20x objective with 4x zoom, max z-projection of confocal image stack of cyst section. (A) Primary epithelial cysts with normal fibroblasts. Green = Cell Tracker (CCL-210). Red = vimentin. Blue = nuclei. (B) Primary epithelial cysts with IPF fibroblasts. Green = Cell Tracker (CCL-134). Red = vimentin. Blue = nuclei. (C) Primary epithelial cysts with normal fibroblasts. Green = Cell Tracker (CCL-210). Red = α-SMA. Blue = nuclei. (D) Primary epithelial cysts with IPF fibroblasts. Green = Cell Tracker (CCL-134). Red = α-SMA. Blue = nuclei.

ability to mix healthy with diseased cells.[14,18–21] In the 3D model system presented here, alveolar epithelial cysts surrounded by pulmonary fibroblasts in an encapsulating hydrogel matrix recapitulate aspects of the basic tissue architecture of the distal lung. Compliant 3D culture networks have been shown to more closely represent cell behavior i*n vivo* than a traditional flat, stiff surface, especially in the areas of contact-inhibited growth[44,45] and migration mechanisms,[46,47] relevant to this work. Advantageously, the spatial arrangement of cells in this platform better recapitulates the *in vivo* tissue structure, but this also limits the types of analysis that can be performed on individual cell populations. Assessments such as RT-PCR and western blots would give global mRNA and protein levels from all the cells in the gel, and any spatial information would be lost. Therefore, we chose imaging-based measurements to visualize and quantify individual cell type proliferation, migration, and protein expression.

In the healthy adult lung alveolar epithelial cell, turnover is slow compared to many other tissues, reported to be approximately 1 month.[1,48,49] During wound healing, proliferation increases dramatically to repopulate the epithelium in a few days, followed by cell cycle arrest and apoptosis of undifferentiated cells.[1,49,50] Tumor cells, on the other hand, exhibit unchecked proliferation, and the ATCC reports that the adenocarcinoma cell line A549 has a doubling time of 22 hours. Therefore, it is not surprising that in our culture system the percent of nuclei positive for EdU one day after encapsulation was significantly higher for A549 cysts than primary cysts. Both epithelial cell types demonstrated a dramatic decrease in proliferation over time, which we attribute to contact inhibition[45,51] and physical constraint by the encapsulating hydrogel. While the gel network is degradable by various matrix-metalloproteinases (MMPs; including 1, 2, 3, 8, and 9),[52,53] their expression by these cells appears to be low, and limited outgrowth into the surrounding hydrogel is observed. The fibroblasts exhibit very low levels of

proliferation, which does not change over time or in the presence of epithelial cells, matching the normally quiescent phenotype seen *in vivo*.[1,2,8]

The exception to these trends is seen in the A549/CCL-210 co-culture condition, which shows significantly higher proliferation of both cell types four days after encapsulation, as well as higher proliferation of the normal fibroblasts on day 1. Profibrotic factors secreted from the A549 epithelial cells (osteopontin, platelet-derived growth factor PDGF, TGFβ, etc.)[5,6,54] may be one cause of this immediate increase in fibroblast proliferation. The increase in fibroblast cell numbers could then lead to increased protease levels in the gel, which would allow for network degradation and A549 outgrowth and increased proliferation on day 4. In addition, it has been shown that A549 co-culture with CCL-210 fibroblasts causes an increase in protease production by the CCL-210 cells, including MMP-2, 9, and 11, supporting the hypothesis that increased gel degradation may contribute to the increase in A549 proliferation.[15] Alternatively, the normal fibroblasts may be producing the paracrine signal HGF, which has been shown to be a potent stimulator of epithelial proliferation and whose production is greatly reduced in IPF fibroblasts, accounting for the continued decrease in A549 proliferation on day 4 with CCL-134 cells.[8,50] However, this effect is not seen in the primary epithelial cysts. Further investigation of the signaling mechanisms involved in the A549/CCL-210 co-culture condition would clearly be valuable to form a better understanding of tumor cell influence on the surrounding fibroblast population.

Normally, the alveolar epithelium produces paracrine signals, such as prostaglandin E-2 (PGE2), that keep the interstitial fibroblasts in a quiescent state, suppressing migration, proliferation, and ECM-production.[9] Conversely, in IPF the production of profibrotic signals, such as osteopontin, PDGF, TGFβ, tumor necrosis factor-alpha TNFα, and connective tissue

growth factor CTGF, is upregulated in the alveolar epithelium, and these signals are thought to contribute to increased fibroblast migration, proliferation, and collagen production seen in IPF patients.[5,6,54] In the migration studies presented here, the most significant differences were seen with the primary epithelial cyst/CCL-134 co-culture and the A549/CCL-210 co-culture. The IPF fibroblasts migrated faster than normal fibroblasts in culture with primary cysts and faster than they moved in monoculture or co-culture with tumor-derived epithelial cells, and potentially a higher fraction of IPF fibroblasts migrated per primary cyst than in the other conditions. Conversely, the normal fibroblasts migrated faster than IPF fibroblasts in culture with A549 cells and faster than they moved in monoculture, although this faster motion was significantly less persistent than in the other conditions. As with the increased proliferation seen in the A549/CCL-210 condition, increased protease activity may contribute to faster migration of fibroblasts, due to local degradation of the matrix. It is also possible that some unidentified signal from the IPF fibroblasts caused an increase in production in one or many of the profibrotic signals listed above by the primary epithelial cells and/or a decrease in production of the quiescent signal PGE2. Similarly, the cancerous A549 cells may already be producing these profibrotic signals or secreting less PGE2. More in-depth exploration of pertinent signaling molecules is required to elucidate the mechanism responsible for this increased migration speed.

Finally, epithelial-to mesenchymal transition (EMT) is thought to be a major contributor to both pulmonary fibrosis and lung tumor invasion.[6,7] Initiation of EMT is potentially regulated by paracrine signals from interstitial fibroblasts or the ECM microenvironment composition, which is produced by those fibroblasts.[10,42] In one study, *in vitro* culture of mouse alveolar epithelial primary cells on a fibronectin-coated surface was enough to induce production of myofibroblast markers (N-cadherin, α-SMA) and reduction in epithelial cell markers (surfactant

protein C), a phenomenon not observed in the same cells cultured on collagen- and laminin-rich Matrigel surfaces.[10] TGFβ is a potent stimulator of EMT both *in vivo* and *in vitro,* and has been shown to quickly stimulate production of mesenchymal markers (*e.g.,* α-SMA) by epithelial lineage cells.[10,41,42] In our co-culture system, primary epithelial cysts demonstrated clear α-SMA stress fiber formation in a few cells when in co-culture with either normal or IPF fibroblasts. The α-SMA-positive cells could be a sign of EMT initiation, although without other positive confirmations of EMT (vimentin expression, loss of cell junction proteins such as E-cadherin and ZO-1) it is difficult to determine what the α-SMA expression represents. As discussed, the appearance of α-SMA in the epithelial cysts may be caused by TGFβ signaling from the co-encapsulated fibroblasts, or by ECM signaling from the fibronectin-derived RGDS peptide incorporated into the hydrogel to facilitate cell adhesion. While our immunostaining results were inconclusive in demonstrating EMT of the primary epithelial cysts, the mechanism causing α-SMA expression and the implications for alveolar epithelial cell differentiation in this culture platform would be interesting studies to pursue.

5.6 Conclusions

The 3D *in vitro* co-culture system used in this study provided an innovative platform for studying the interactions between alveolar epithelial cysts and dispersed pulmonary fibroblasts and investigating cell functions related to disease progression. The results presented here support the growing body of evidence in the literature that crosstalk between the alveolar epithelium and interstitial fibroblasts influences their behavior in terms of proliferation, migration, and expression of protein markers. Future investigation into the signals contributing to the differences in cell behavior discovered here would provide needed insight into possible pathways

conducive to drug development. In the A549/CCL-210 co-culture condition, for example, potential targets could be found for therapeutics to reduce tumor growth by focusing on signals produced by the fibroblasts. With the primary/CCL-134 condition, one could look for signaling molecules that could be targeted to reduce the contribution of recruitment of local fibroblasts to the myofibroblast foci in IPF by limiting their migration speed. Moreover, this spatially-relevant co-culture model could be a useful starting point for drug screening trials by capturing key geometric aspects of cell behavior in alveolar tissue before moving to more complex *in vivo* models.

5.7 Acknowledgements

This work was done in collaboration with Emi Kiyotake and Jessica Hall, with intellectual input by Dr. Vivek Balasubramaniam. The authors would like to thank Sharon Ryan for teaching us the ATII mouse cell isolation procedure, and Kyle Kyburz for discussions concerning live cell tracking experiments and analysis. Funding for this work was provided by the Howard Hughes Medical Institute.

5.8 References

1. Herzog, E. L., Brody, A. R., Colby, T. V, Mason, R. & Williams, M. C. Knowns and unknowns of the alveolus. *Proc. Am. Thorac. Soc.* **5,** 778–82 (2008).

2. Hogan, B. L. M., Barkauskas, C. E., Chapman, H. A., Epstein, J. A., Jain, R., Hsia, C. C. W., *et al.* Repair and regeneration of the respiratory system: complexity, plasticity, and mechanisms of lung stem cell function. *Cell Stem Cell* **15,** 123–38 (2014).

3. Sirianni, F. E., Chu, F. S. F. & Walker, D. C. Human Alveolar Wall Fibroblasts Directly Link Epithelial Type 2 Cells to Capillary Endothelium. *Am. J. Respir. Crit. Care Med.* **168,** 1532–1537 (2003).

4. Bellusci, S., Grindley, J., Emoto, H., Itoh, N. & Hogan, B. L. Fibroblast growth factor 10 (FGF10) and branching morphogenesis in the embryonic mouse lung. *Development* **124,** 4867–78 (1997).

5. Selman, M., Thannickal, V. J., Pardo, A., Zisman, D. A., Martinez, F. J. & Lynch, J. P. Idiopathic Pulmonary Fibrosis. *Drugs* **64,** 405–430 (2004).

6. King, T. E., Pardo, A. & Selman, M. Idiopathic pulmonary fibrosis. *Lancet* **378,** 1949–61 (2011).

7. Thiery, J. P., Acloque, H., Huang, R. Y. J. & Nieto, M. A. Epithelial-mesenchymal transitions in development and disease. *Cell* **139,** 871–90 (2009).

8. Marchand-Adam, S., Marchal, J., Cohen, M., Soler, P., Gerard, B., Castier, Y., *et al.* Defect of hepatocyte growth factor secretion by fibroblasts in idiopathic pulmonary fibrosis. *Am. J. Respir. Crit. Care Med.* **168,** 1156–61 (2003).

9. Selman, M. & Pardo, A. Role of epithelial cells in idiopathic pulmonary fibrosis: from innocent targets to serial killers. *Proc. Am. Thorac. Soc.* **3,** 364–372 (2006).

10. Kim, K. K., Kugler, M. C., Wolters, P. J., Robillard, L., Galvez, M. G., Brumwell, A. N., *et al.* Alveolar epithelial cell mesenchymal transition develops in vivo during pulmonary fibrosis and is regulated by the extracellular matrix. *Proc. Natl. Acad. Sci.* **103,** 13180–13185 (2006).

11. Rock, J. R., Barkauskas, C. E., Cronce, M. J., Xue, Y., Harris, J. R., Liang, J., *et al.* Multiple stromal populations contribute to pulmonary fibrosis without evidence for epithelial to mesenchymal transition. *Proc. Natl. Acad. Sci.* **108,** E1475–E1483 (2011).

12. Kumarswamy, R., Mudduluru, G., Ceppi, P., Muppala, S., Kozlowski, M., Niklinski, J., *et al.* MicroRNA-30a inhibits epithelial-to-mesenchymal transition by targeting Snai1 and is downregulated in non-small cell lung cancer. *Int. J. Cancer* **130,** 2044–53 (2012).

13. Bhowmick, N., Neilson, E. & Moses, H. Stromal fibroblasts in cancer initiation and progression. *Nature* **432,** 332–337 (2004).

14. Amann, A., Zwierzina, M., Gamerith, G., Bitsche, M., Huber, J. M., Vogel, G. F., *et al.* Development of an innovative 3D cell culture system to study tumour--stroma interactions in non-small cell lung cancer cells. *PLoS One* **9,** e92511 (2014).

15. Fromigué, O., Louis, K., Dayem, M., Milanini, J., Pages, G., Tartare-Deckert, S., *et al.* Gene expression profiling of normal human pulmonary fibroblasts following coculture with non-small-cell lung cancer cells reveals alterations related to matrix degradation, angiogenesis, cell growth and survival. *Oncogene* **22,** 8487–97 (2003).

16. Wang, W., Li, Q., Yamada, T., Matsumoto, K., Matsumoto, I., Oda, M., *et al.* Crosstalk to stromal fibroblasts induces resistance of lung cancer to epidermal growth factor receptor tyrosine kinase inhibitors. *Clin. Cancer Res.* **15,** 6630–8 (2009).

17. Prasad, S., Hogaboam, C. M. & Jarai, G. Deficient repair response of IPF fibroblasts in a co-culture model of epithelial injury and repair. *Fibrogenesis Tissue Repair* **7,** 7 (2014).

18. Wang, X. & Kaplan, D. L. Hormone-responsive 3D multicellular culture model of human breast tissue. *Biomaterials* **33,** 3411–3420 (2012).

19. Horie, M., Saito, A., Mikami, Y., Ohshima, M., Morishita, Y., Nakajima, J., *et al.* Characterization of human lung cancer-associated fibroblasts in three-dimensional in vitro co-culture model. *Biochem. Biophys. Res. Commun.* **423,** 158–63 (2012).

20. Fang, X., Sittadjody, S., Gyabaah, K., Opara, E. C. & Balaji, K. C. Novel 3D Co-Culture Model for Epithelial-Stromal Cells Interaction in Prostate Cancer. *PLoS One* **8,** 1–11 (2013).

21. Kim, S.-A., Lee, E. K. & Kuh, H.-J. Co-culture of 3D tumor spheroids with fibroblasts as a model for epithelial–mesenchymal transition in vitro. *Exp. Cell Res.* **335,** 187–196 (2015).

22. Majety, M., Pradel, L. P., Gies, M. & Ries, C. H. Fibroblasts Influence Survival and Therapeutic Response in a 3D Co-Culture Model. *PLoS One* **10,** e0127948 (2015).

23. Friedrich, J., Ebner, R. & Kunz-Schughart, L. A. Experimental anti-tumor therapy in 3-D: spheroids--old hat or new challenge? *Int. J. Radiat. Biol.* **83,** 849–871 (2007).

24. Weiswald, L.-B., Bellet, D. & Dangles-Marie, V. Spherical Cancer Models in Tumor Biology. *Neoplasia* **17,** 1–15 (2015).

25. Lewis, K. J. R., Tibbitt, M. W., Zhao, Y., Branchfield, K., Sun, X., Balasubramaniam, V., *et al.* In vitro model alveoli from photodegradable microsphere templates. *Biomater. Sci.* **3,** 821–832 (2015).

26. Lewis, K. J. R. & Anseth, K. S. Hydrogel scaffolds to study cell biology in four dimensions. *MRS Bull.* **38,** 260–268 (2013).

27. Kloxin, A. M., Kasko, A. M., Salinas, C. N. & Anseth, K. S. Photodegradable hydrogels for dynamic tuning of physical and chemical properties. *Science* **324,** 59–63 (2009).

28. Tibbitt, M. W., Han, B. W., Kloxin, A. M. & Anseth, K. S. SFB Student Award Winner in the Ph.D. Category: Synthesis and application of photodegradable microspheres for spatiotemporal control of protein delivery. *J. Biomed. Mater. Res. Part A* **100A,** 1647–1654 (2012).

29. Kloxin, A. M., Tibbitt, M. W. & Anseth, K. S. Synthesis of photodegradable hydrogels as dynamically tunable cell culture platforms. *Nat. Protoc.* **5,** 1867–87 (2010).

30. Cruise, G. M., Scharp, D. S. & Hubbell, J. a. Characterization of permeability and network structure of interfacially photopolymerized poly(ethylene glycol) diacrylate hydrogels. *Biomaterials* **19,** 1287–1294 (1998).

31. Kloxin, A. M., Lewis, K. J. R., Deforest, C. A., Seedorf, G., Tibbitt, M. W., Balasubramaniam, V., *et al.* Responsive culture platform to examine the influence of microenvironmental geometry on cell function in 3D. *Integr. Biol.* **4,** 1540–1549 (2012).

32. Gould, S. T., Darling, N. J. & Anseth, K. S. Small peptide functionalized thiol-ene hydrogels as culture substrates for understanding valvular interstitial cell activation and de novo tissue deposition. *Acta Biomater.* **8,** 3201–9 (2012).

33. Fairbanks, B. D., Schwartz, M. P., Bowman, C. N. & Anseth, K. S. Photoinitiated polymerization of PEG-diacrylate with lithium phenyl-2,4,6-trimethylbenzoylphosphinate: polymerization rate and cytocompatibility. *Biomaterials* **30,** 6702–7 (2009).

34. Schwartz, M. P., Rogers, R. E., Singh, S. P., Lee, J. Y., Loveland, S. G., Koepsel, J. T., *et al.* A quantitative comparison of human HT-1080 fibrosarcoma cells and primary human dermal fibroblasts identifies a 3D migration mechanism with properties unique to the transformed phenotype. *PLoS One* **8,** 1–24 (2013).

35. Franzdóttir, S. R., Axelsson, I. T., Arason, A. J., Baldursson, O., Gudjonsson, T. & Magnusson, M. K. Airway branching morphogenesis in three dimensional culture. *Respir. Res.* **11,** 162 (2010).

36. Choe, C., Shin, Y.-S., Kim, S.-H., Jeon, M.-J., Choi, S.-J., Lee, J., *et al.* Tumor–stromal Interactions with Direct Cell Contacts Enhance Motility of Non-small Cell Lung Cancer Cells Through the Hedgehog Signaling Pathway. *Anticancer Res.* **33,** 3715–3723 (2013).

37. Suganuma, H., Sato, A., Tamura, R. & Chida, K. Enhanced migration of fibroblasts derived from lungs with fibrotic lesions. *Thorax* **50,** 984–989 (1995).

38. Vuorinen, K., Gao, F., Oury, T. D., Kinnula, V. L. & Myllärniemi, M. Imatinib mesylate inhibits fibrogenesis in asbestos-induced interstitial pneumonia. *Exp. Lung Res.* **33,** 357–373 (2007).

39. Crosby, L. M. & Waters, C. M. Epithelial Repair Mechanisms in the Lung. *Am. J. Physiol. Lung Cell. Mol. Physiol.* **298,** 715–731 (2010).

40. Kyburz, K. A. & Anseth, K. S. Three-dimensional hMSC motility within peptide-functionalized PEG-based hydrogels of varying adhesivity and crosslinking density. *Acta Biomater.* **9,** 6381–92 (2013).

41. Willis, B. C. & Borok, Z. TGF-beta-induced EMT: mechanisms and implications for fibrotic lung disease. *Am. J. Physiol. Lung Cell. Mol. Physiol.* **293,** L525–34 (2007).

42. Willis, B. C., Liebler, J. M., Luby-Phelps, K., Nicholson, A. G., Crandall, E. D., du Bois, R. M., *et al.* Induction of epithelial-mesenchymal transition in alveolar epithelial cells by transforming growth factor-beta1: potential role in idiopathic pulmonary fibrosis. *Am. J. Pathol.* **166,** 1321–1332 (2005).

43. Carterson, A., Bentrup, K. zu, Ott, C., Clarke, M., Pierson, D., Vanderburg, C., *et al.* A549 Lung Epithelial Cells Grown as Three-Dimensional Aggregates : Alternative Tissue Culture Model for Pseudomonas aeruginosa Pathogenesis. *Infect. Immun.* **73,** 1129–1140 (2005).

44. Puliafito, A., Hufnagel, L., Neveu, P., Streichan, S., Sigal, A., Fygenson, D. K., *et al.* Collective and single cell behavior in epithelial contact inhibition. *Proc. Natl. Acad. Sci.* **109,** 739–744 (2012).

45. Rejniak, K. A., Wang, S. E., Bryce, N. S., Chang, H., Parvin, B., Jourquin, J., *et al.* Linking changes in epithelial morphogenesis to cancer mutations using computational modeling. *PLoS Comput. Biol.* **6,** (2010).

46. Doyle, A. D., Wang, F. W., Matsumoto, K. & Yamada, K. M. One-dimensional topography underlies three-dimensional fi brillar cell migration. *J. Cell Biol.* **184,** 481–490 (2009).

47. Peyton, S. R., Kalcioglu, Z. I., Cohen, J. C., Runkle, A. P., Van Vliet, K. J., Lauffenburger, D. a., *et al.* Marrow-Derived stem cell motility in 3D synthetic scaffold is governed by geometry along with adhesivity and stiffness. *Biotechnol. Bioeng.* **108,** 1181–1193 (2011).

48. Guillot, L., Nathan, N., Tabary, O., Thouvenin, G., Le Rouzic, P., Corvol, H., *et al.* Alveolar epithelial cells: master regulators of lung homeostasis. *Int. J. Biochem. Cell Biol.* **45,** 2568–73 (2013).

49. Fehrenbach, H. Alveolar epithelial type II cell: defender of the alveolus revisited. *Respir. Res.* **2,** 33–46 (2001).

50. Mason, R. J. Biology of alveolar type II cells. *Respirology* **11,** S12–S15 (2006).

51. Aragona, M., Panciera, T., Manfrin, A., Giulitti, S., Michielin, F., Elvassore, N., *et al.* A mechanical checkpoint controls multicellular growth through YAP/TAZ regulation by actin-processing factors. *Cell* **154,** 1047–1059 (2013).

52. Lutolf, M. P., Lauer-Fields, J. L., Schmoekel, H. G., Metters, A. T., Weber, F. E., Fields, G. B., *et al.* Synthetic matrix metalloproteinase-sensitive hydrogels for the conduction of

tissue regeneration: engineering cell-invasion characteristics. *Proc. Natl. Acad. Sci. U. S. A.* **100,** 5413–8 (2003).

53. Fairbanks, B. D., Schwartz, M. P., Halevi, A. E., Nuttelman, C. R., Bowman, C. N. & Anseth, K. S. A Versatile Synthetic Extracellular Matrix Mimic via Thiol-Norbornene Photopolymerization. *Adv. Mater.* **21,** 5005–5010 (2009).

54. Pardo, A., Gibson, K., Cisneros, J., Richards, T. J., Yang, Y., Becerril, C., *et al.* Up-regulation and profibrotic role of osteopontin in human idiopathic pulmonary fibrosis. *PLoS Med.* **2,** 0891–0903 (2005).

5.9 Supplemental information

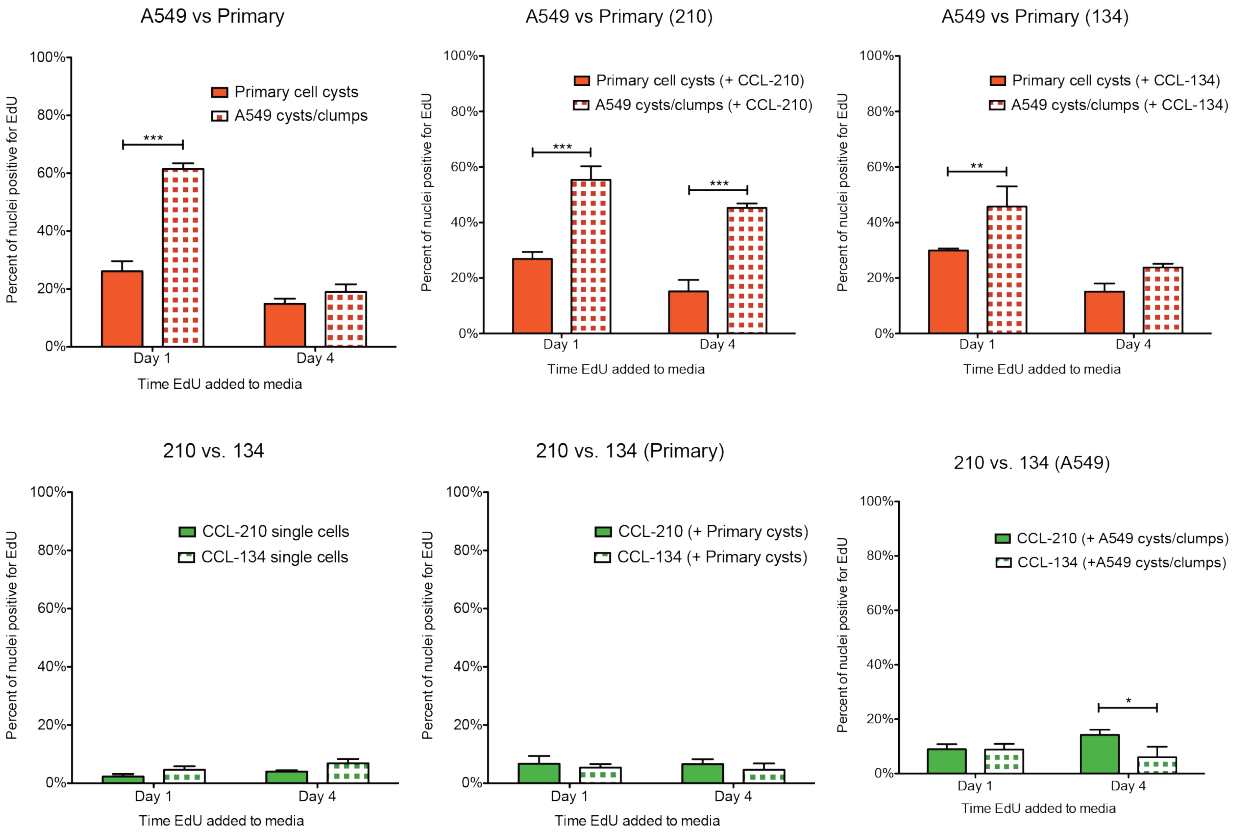

Figure 5.S1 Plots depict percent of nuclei positive for EdU at the two time points comparing healthy versus diseased cell type, separated by monoculture and co-culture condition. Results are presented as means ± SEM of three biological replicates of each condition. *$p < 0.05$, **$p < 0.01$, ***$p < 0.001$

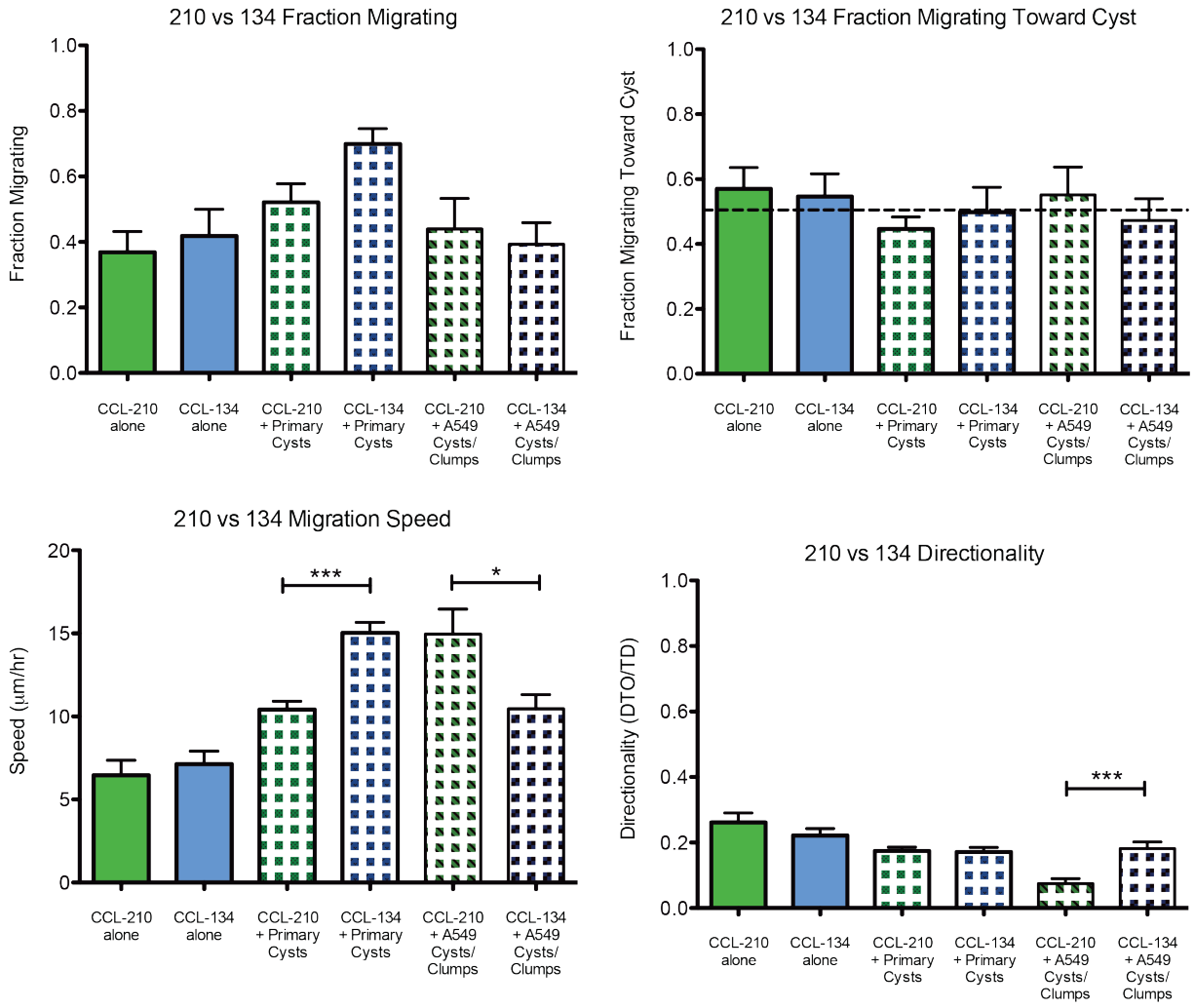

Figure 5.S2 Normal versus IPF fibroblast migration comparison. Plots show fraction migrating, fraction migrating toward cyst, migration speed, and directionality (Distance-To-Origin/Total Distance) of both fibroblasts in monoculture and co-culture with both epithelial cell types. Significance shown for paired comparison of CCL-210 and CCL-134 cells in each monoculture/co-culture condition. Data in fraction migrating plot represent means ± SEM of cells migrating per cyst. Data in the remaining plots represent means ± SEM of all migrating cells. *p <0.05, ***p < 0.001

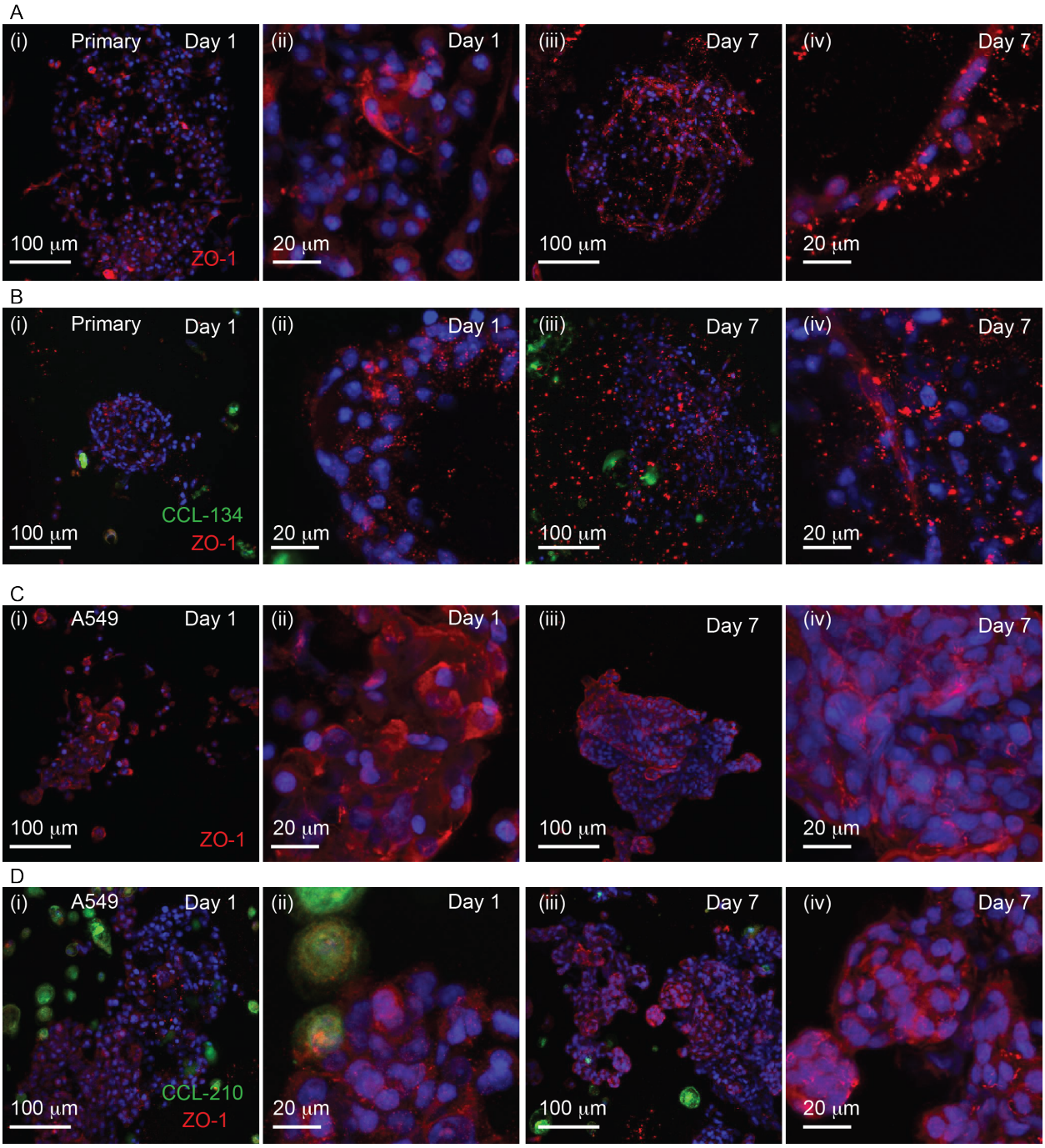

Figure 5.S3 Immunostaining for tight junction marker. For all (i) and (ii) samples fixed one day after encapsulation. For all (iii) and (iv) samples fixed seven days after encapsulation. For all (i) and (iii) 20x objective, max z-projection of confocal image stack of whole cyst. For all (ii) and (iv) 20x objective with 4x zoom, max z-projection of confocal image stack of cyst section. (A) Primary epithelial cysts in monoculture. Red = ZO-1. Blue = nuclei. (B) Primary epithelial cysts with IPF fibroblasts. Green = Cell Tracker (CCL-134). Red = ZO-1. Blue = nuclei. (C) A549 epithelial cysts in monoculture. Red = ZO-1. Blue = nuclei. (D) A549 epithelial cysts with normal fibroblasts. Green = Cell Tracker (CCL-210). Red = ZO-1. Blue = nuclei.

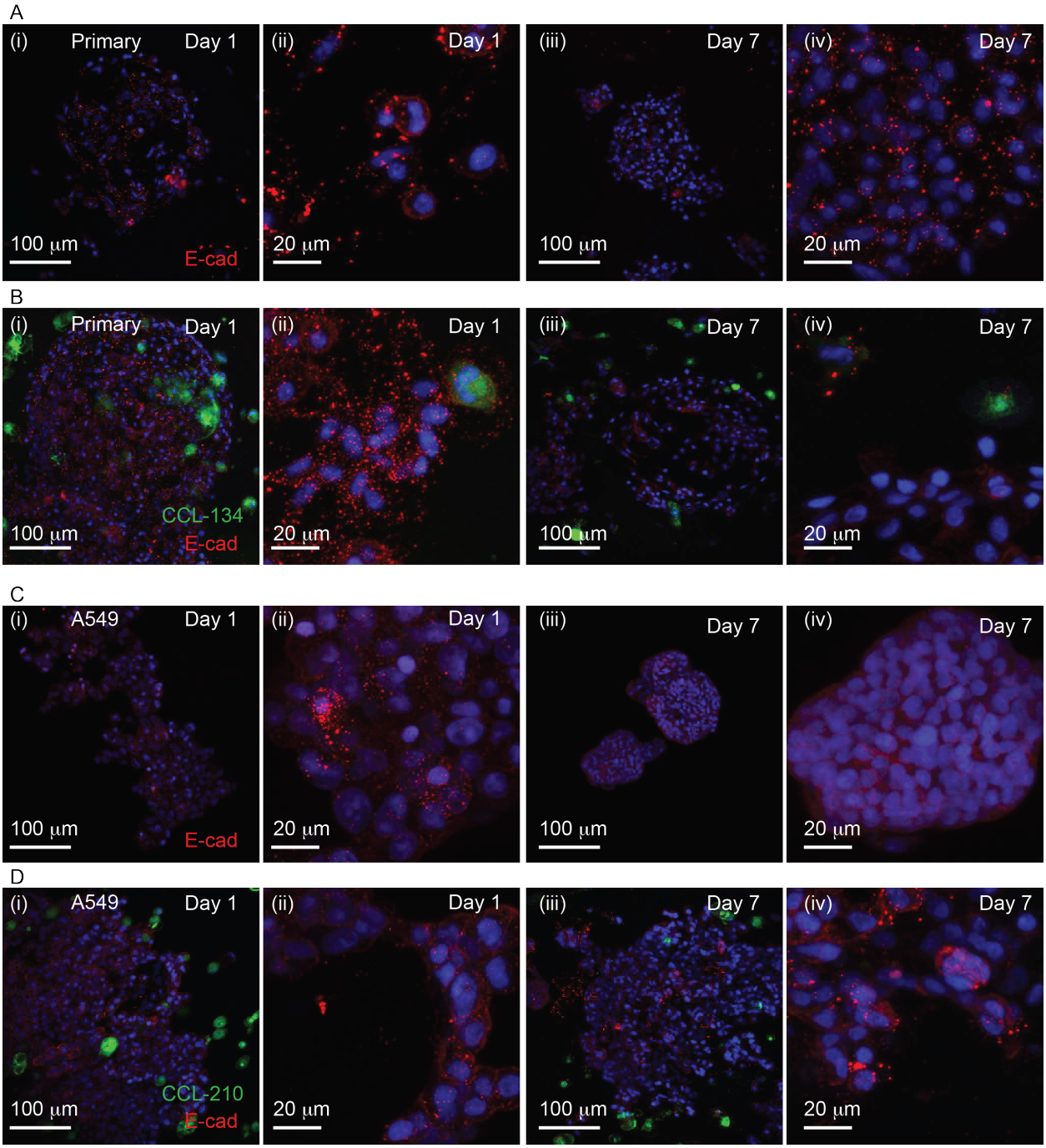

Figure 5.S4 Immunostaining for adherens junction marker. For all (i) and (ii) samples fixed one day after encapsulation. For all (iii) and (iv) samples fixed seven days after encapsulation. For all (i) and (iii) 20x objective, max z-projection of confocal image stack of whole cyst. For all (ii) and (iv) 20x objective with 4x zoom, max z-projection of confocal image stack of cyst section. (A) Primary epithelial cysts in monoculture. Red = E-cadherin. Blue = nuclei. (B) Primary epithelial cysts with IPF fibroblasts. Green = Cell Tracker (CCL-134). Red = E-cadherin. Blue = nuclei. (C) A549 epithelial cysts in monoculture. Red = E-cadherin. Blue = nuclei. (D) A549 epithelial cysts with normal fibroblasts. Green = Cell Tracker (CCL-210). Red = E-cadherin. Blue = nuclei.

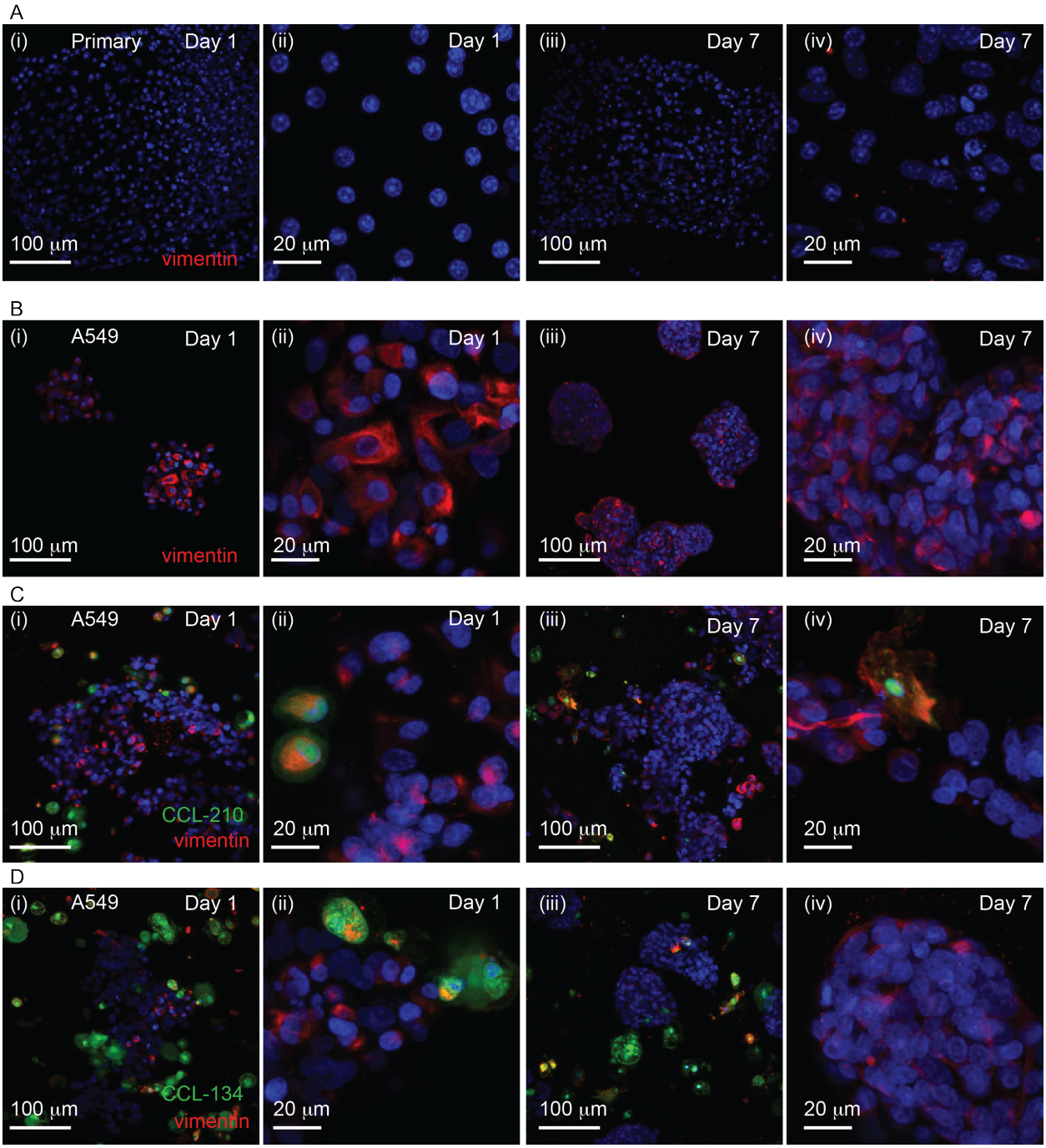

Figure 5.S5 Immunostaining for mesenchymal markers. For all (i) and (ii) samples fixed one day after encapsulation. For all (iii) and (iv) samples fixed seven days after encapsulation. For all (i) and (iii) 20x objective, max z-projection of confocal image stack of whole cyst. For all (ii) and (iv) 20x objective with 4x zoom, max z-projection of confocal image stack of cyst section. (A) Primary epithelial cysts in monoculture. Red = vimentin. Blue = nuclei. (B) A549 epithelial cysts in monoculture. Red = vimentin. Blue = nuclei. (C) A549 epithelial cysts with normal fibroblasts. Green = Cell Tracker (CCL-210). Red = vimentin. Blue = nuclei. (D) A549 epithelial cysts with IPF fibroblasts. Green = Cell Tracker (CCL-134). Red = vimentin. Blue = nuclei.

Chapter 6

Conclusions and Future Directions

Cells in the alveolar epithelium reside in a complex three-dimensional tissue architecture, where they receive a multitude of signals from the extracellular matrix (ECM), as well as from surrounding cell populations.[1–4] Disruptions in these signaling pathways can lead to diseased pathologies in alveolar tissue. In particular, abnormal communication between epithelial cells and pulmonary fibroblasts may be responsible for progression of fibrosis and tumorigenesis in the distal lung.[5,6] One hypothesis is that mutations or injury in one cell population may alter their response to normal signals from the microenvironment and/or change the signals sent to the other cell population, causing transformed cellular behavior in both.[4–6] The mechanisms involved in epithelial repair and the breakdown of normal communication pathways are complex and still largely unknown. While animal models and clinical studies are critical to this understanding, they do not allow for detailed hypothesis testing of signaling mechanisms. Therefore, development of physiologically relevant and controlled 3D culture platforms are complementary and provide critical information related to alveolar epithelial cell differentiation and epithelial-mesenchymal interactions leading to disease. Throughout this thesis, advanced polymer materials with bio-responsive peptides incorporating photosensitive addition and cleavage reactions were employed to mimic the native alveolar architecture to enable investigation of the dynamic effects of extracellular cues on cellular behavior.

In Chapter 3, a hydrogel network consisting of a poly(ethylene glycol) (PEG) backbone with enzymatically and photolytically cleavable crosslinks was utilized to study the influence of geometric confinement on differentiation and multicellular assembly of primary mouse alveolar

epithelial type II (ATII) cells. The photolabile crosslinks enabled us to erode an array of microwells of varying curvature into the base gel using standard photolithography techniques. The primary ATII cells were then seeded into the wells and covered with a top layer of hydrogel to fully encapsulate them in three-dimensional, geometrically-defined cavities. The cells were cultured in these microwells for either one or seven days, followed by fixing and immunostaining for cell phenotype markers: surfactant protein C (SPC) for ATII cells, and T1-alpha protein (T1α) for alveolar epithelial type I (ATI) cells. Spatial arrangement of the phenotypic markers within each well shape was visualized with frequency maps in both the x-y and x-z planes, using 30 wells per shape. Clustering of the nuclei was observed in the center of the wells on day 1 and near-complete filling of the wells by day 7, which was attributed either to proliferation or migration of the cells over time. Future work could readily test this hypothesis through real time tracking of cells cultured with these devices.

With regards to differentiation, limited T1α expression was observed on day 1, which was consistent with our assumption that 98-99% of the primary cells seeded into the wells were ATII-phenotypic. However, by day 7, most cells near the tops of the wells were elongated and expressed both SPC and T1α, indicating an intermediate phenotype of ATII cells in the process of differentiating to ATI-phenotype cells. There was also a population of aggregated cells deeper in the wells that were mostly SPC-positive. Interestingly, the T1α stain appeared to localize to the gel periphery, along the tops and sides of the wells, whereas the SPC was found more often near the center of the wells. This observation may suggest that cell-ECM interactions promote ATII differentiation *in vitro*. Finally, the dynamics of cell structure branching within the hydrogel platform was explored by locally eroding channels to connect neighboring wells. This was achieved by using two-photon focused light introduced at the mid-point of the culture time.

For the time course of these experiments, no migration of the primary cells was observed down these channels, and this result was attributed to the general fact that epithelial cells are typically non-migratory and no signal was added to promote motility other than the topographical channel in the gel network. These initial results with a dynamically-tunable culture system for lung epithelial cells suggested that the platform could be useful for studying evolving geometric cues critical during lung development and repair, and motivated several follow-up studies.

Although the primary cells successfully filled the microwells over time in this hydrogel platform, they formed aggregates, contrary to typical hollow alveolar tissue structures. This observation motivated us to pursue a cyst-templating technique described in Chapter 4 to create a more physiologically-relevant culture model. However, several phenomena detected in this platform may be interesting to explore further. First, the mechanism through which the cells filled the wells over time could be examined using techniques utilized in Chapter 5 to determine if proliferation or migration was the cause. For studying branching morphogenesis with the erosion of channels in the hydrogel, an attractive experiment would be to investigate the effect of the local presentation of chemotactic signals at different concentrations on migration of epithelial cells down the channels. As one example, FGF-10 has been shown to be a driving force for lung bud outgrowth during lung development,[7,8] and a gradient of this factor down the channel would be interesting to test with this system.

Of particular importance for future hydrogel development and their use with primary ATII cells, high throughput experiments are needed to understand how matrix signals (*e.g.*, integrin-binding epitopes, matrix elasticity) promote ATII differentiation toward the ATI phenotype on the gel surfaces. Ideally, an i*n vitro* model of the alveolar epithelium would include both ATI and ATII phenotypic cells; however, as has been observed many times in the

literature, most primary ATII cells in culture will differentiate toward the ATI phenotype within 4-7 days without the addition of soluble factors or specific ECM components.[1,9–11] In particular, studies have shown that keratinocyte growth factor (FGF-7) and laminin-5 are essential for maintaining the ATII phenotype in culture past one week.[10,12]

An interesting future study would be to compare phenotype marker expression of ATII cells cultured on 2D hydrogel surfaces containing different peptide sequences or full proteins, with and without soluble growth factors in the media (Figure 6.1). In preliminary work that compared collagen-coated glass, RGD-containing gels, and gels modified with three adhesive peptides (RGD, a fibronectin mimic; IKVAV, a laminin mimic; and P15, a collagen mimic[13]) all at equal levels or with a low level of RGD, results revealed that the three-peptide combination gels in conjunction with soluble FGF-7 and hepatocyte growth factor (HGF) showed the most

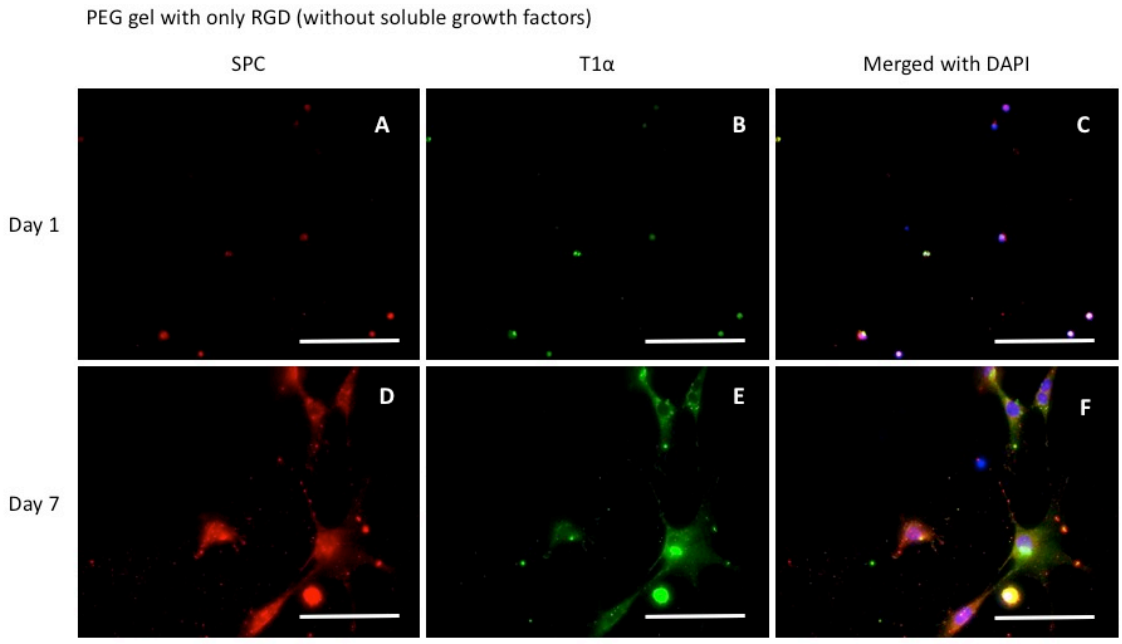

Figure 6.1 Preliminary experiment of primary ATII cells seeded on top of RGD-containing PEG hydrogels. Cells were fixed one day (A-C) and seven days (D-F) after seeding and immunostained for phenotype markers. Red = SPC (ATII phenotype). Green = T1α (ATI phenotype). Blue = DAPI (nuclei). Scale bar = 100 μm.

promise for maintaining a higher percentage of ATII phenotype cells (Figure 6.2). To confirm this result, more biological replicates would need to be performed. In addition, more peptide sequences in varying combinations, along with entrapment or conjugation of full proteins, should be tested. For example, YIGSR (also derived from laminin) has been shown to influence cell structure formation differently from IKVAV, and another laminin-specific peptide SINNR has been shown to induce cyst-like structure formation of ATII cells in culture.[14,15] To further

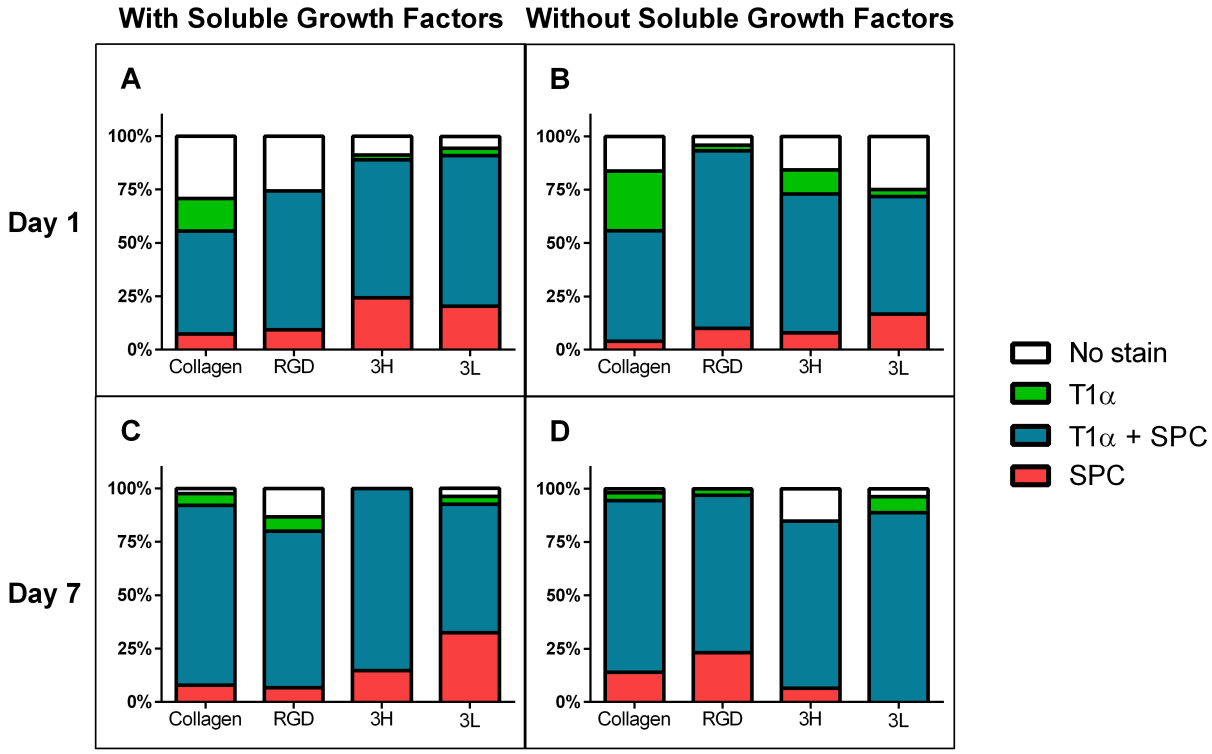

Figure 6.2 Preliminary results comparing cell phenotype marker expression over time of ATII cells seeded on top of various surfaces. Collagen = glass coated with collagen I; RGD = PEG hydrogel containing 1 mM RGD peptide; 3H = PEG hydrogel containing three peptides (RGD, IKVAV, P15) at 0.33 mM each; 3L = PEG hydrogel containing 0.05 mM RGD, 0.475 mM IKVAV, and 0.475 mM P15. Bars represent 100% of imaged nuclei, with red representing the fraction of cells expressing only SPC (ATII phenotype), blue representing cells expressing both markers (intermediate phenotype), green representing cells expressing only T1α (ATI phenotype), and white representing cells expressing neither marker. (A) Cells were cultured with soluble growth factors (FGF-7 and HGF) and fixed one day after seeding. (B) Cells were cultured without soluble growth factors and fixed one day after seeding. (C) Cells were cultured with growth factors and fixed seven days after seeding. (D) Cells were cultured without growth factors and fixed seven days after seeding.

expand the experimental space, hydrogel elastic modulus could be systematically altered to explore whether substrate stiffness influences ATII differentiation. To facilitate such a large screening process, a high-throughput setup with a liquid-handling robotic system to form the gel compositions followed by imaging and automated analysis with a high content microscope would be essential. Such a setup has been developed in our laboratory,[16] and would be simple to implement.

Chapter 4 introduced an innovative method for creating cyst-like model alveoli in a PEG hydrogel by exploiting photodegradable microspheres as templates to pattern primary ATII cells as single cell-layers cultured on the spheres. Specifically, microspheres of selected sizes (50-200 μm diameter) were polymerized as aqueous droplets in an organic phase, employing a Michael-type addition reaction between a PEG-tetrathiol macromer and a PEG-di-photodegradable-acrylate crosslinker. The microspheres were modified with a pendant CRGDS peptide to promote cellular attachment to the surface during incubation on an orbital shaker. After full microsphere coverage (24 hours for the cancer cell line A549, 3 days for the primary ATII cells), the pre-cysts were encapsulated in a second PEG hydrogel. The encapsulating hydrogel was composed of an 8-arm PEG-norbornene, which underwent photo-initiated, radical-mediated thiol-ene polymerization with a di-cysteine enzymatically-degradable peptide crosslinker (KCGPQG↓IWGQCK). Cells were cultured for one day to allow attachments to the surrounding hydrogel matrix, and then the microsphere templates were fully eroded by exposure to cytocompatible 365 nm light at ~10 mW/cm^2 for 15 minutes. The cysts were cultured for up to 7 days after encapsulation and subsequently fixed and immunostained for cell junction proteins or phenotype markers. Adherens junctions were fully formed by 4 days after encapsulation, indicated by bright β-catenin staining along the cell membranes. Tight junctions were less

pronounced on day 4, although ZO-1 was expressed in several cells. As observed in Chapter 3, the primary ATII cells mostly differentiated into ATI cells on the RGDS-functionalized microsphere surfaces, with only 2 or 3 cells per cyst staining positive for SPC on day 4. Collectively, the cyst attributes presented in Chapter 4 (size, hollow lumen, cell-cell junctions, small number of ATII cells) demonstrate that these model alveoli capture many aspects of the native alveolar epithelium and may be useful in future *in vitro* studies of this complex tissue.

While this cyst-templating technique represents a significant advancement in tunable culture platforms for studying the alveolar epithelium, there are a few aspects of the procedure that are worthy of future development. First, the microspheres formed by inverse suspension exhibit a fairly wide distribution of diameters (50-200 μm), whereas alveoli *in vivo* have roughly equivalent volumes.[17] To create uniform diameter microspheres, droplet-forming microfluidic devices were explored; specifically, the aqueous pre-polymer solution (disperse phase) was injected into a larger stream of mineral oil (carrier phase) to create droplets of constant size (Figure 6.3A-C). The droplet diameter was tuned by changing the injection aperture width or the carrier phase flow rate, and our preliminary results indicate that droplet sizes of 200 ± 5 μm were readily achieved with a 100 μm wide aperture device and 50 μL/min flow rate, and ~50 ± 5 μm diameter droplets with a 50 μm aperture device and 30 μL/min flow rate (Figure 6.3D,E). These droplet sizes correspond to the average alveolar diameter in humans and mice, respectively.[17,18]

However, the difficulty when transferring to this method of microsphere formation and polymerization is in tuning the reaction rate to achieve gelation in the resistor before the droplets leave the device without premature gelation in the disperse phase inlet area, which would clog the device. While visible-light photoinitiated systems can readily polymerize in short times with spatiotemporal specificity, the challenge has been finding such a system that leads to networks

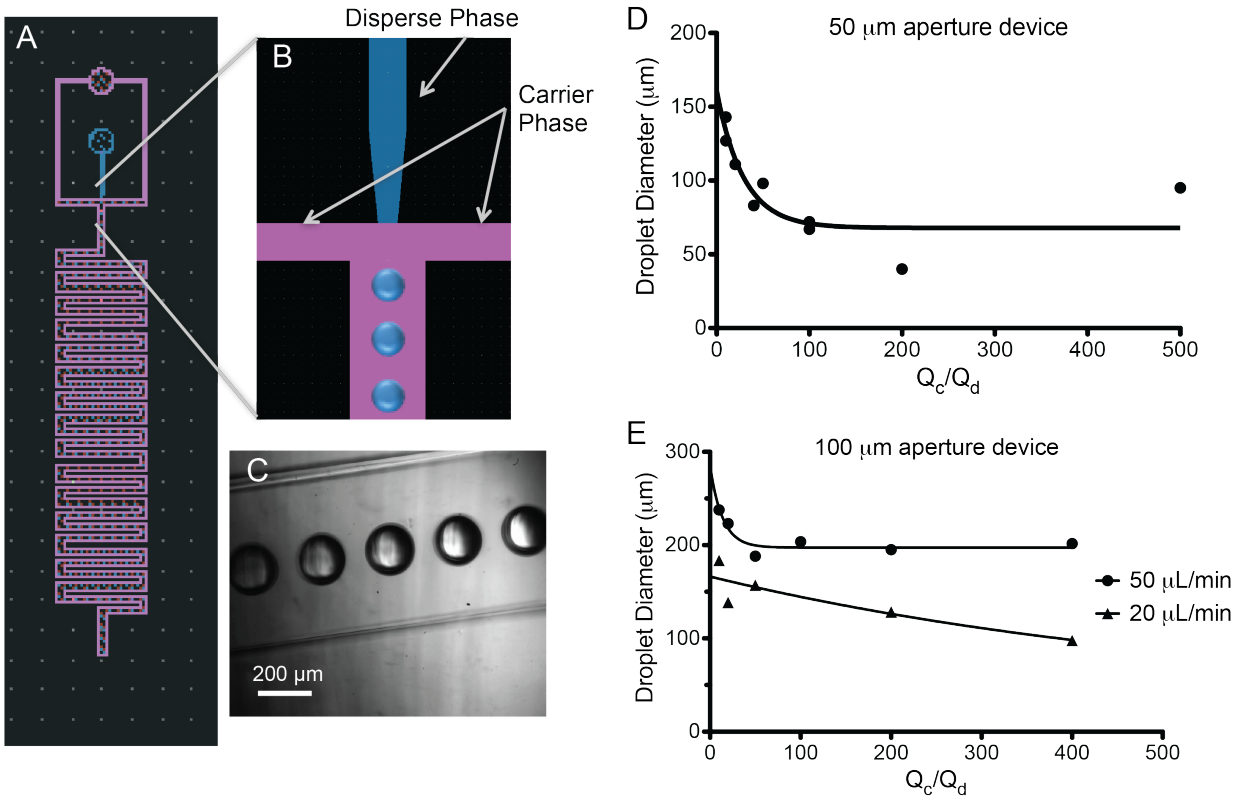

Figure 6.3 Preliminary droplet-forming microfluidic device design and droplet size results. (A) Device design with the carrier phase inlet (pink circle) at the top and the disperse phase inlet (blue circle) below it. Once the droplets are formed, they flow through the resistor to give time for polymerization before reaching the outlet at the bottom. (B) Detail view of the injection aperture where the disperse phase (blue) meets the carrier phase (pink) and forms droplets. (C) Image taken with high-speed camera (1000 fps) of aqueous gel precursor solution flowing as droplets through the resistor carried by mineral oil. (D) Plot of droplet diameter as a function of volumetric flow rate ratio (carrier phase/disperse phase; Q_c/Q_d) in a 50 µm aperture device. Qc = 30 µL/min. (E) Plot of droplet diameter as a function of flow rate ratio in a 100 µm aperture device at two different Q_c (50 µL/min and 20 µL/min). *Work done in collaboration with Dr. Nick Glass and Prof. Justin Cooper-White.

compatible with fast UV-degradation of the photocleavable crosslinker resulting in complete microsphere erosion on time scales appropriate for use with cells. However, we have seen promising results with a coumarin-caged tetramethylguanidine,[19] which can be cleaved with visible light to form a strong base that can catalyze the Michael-type addition of the same thiol- and acrylate-containing macromers used for microsphere polymerization in Chapter 4 (Figure

6.4A). Our preliminary results show that this system will polymerize in less than 5 minutes when exposed to 400-500 nm light, which is compatible with the time spent in the microfluidic device resistor (Figure 6.4B). Unfortunately, these macromers slowly and spontaneously react upon mixing to clog the inlet of the microfluidic device in approximately one hour, which necessitates the redesign of the device to include two aqueous phase inlet streams that mix within the device before reaching the droplet-forming aperture. This should be readily achievable, and then the resistor section of the device could be exposed to visible light to release the photobase and catalyze the Michael addition. Such microfluidic techniques for the formation of uniform photodegradable microspheres should prove useful for the fabrication of particles with diameters of desired sizes, allowing for the comparison of cell behavior in cysts of human versus mouse size.

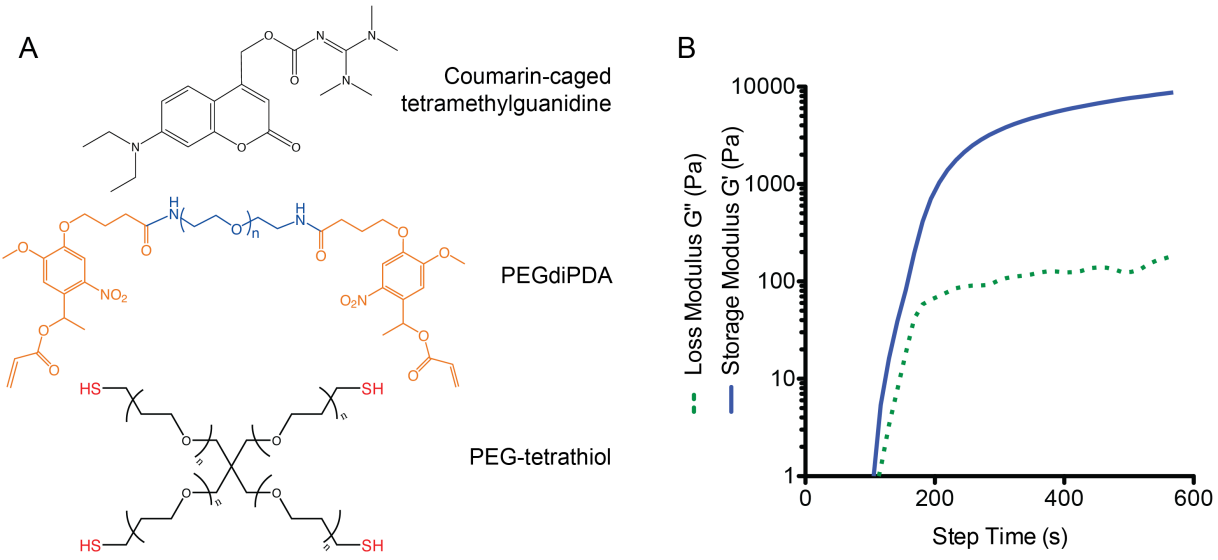

Figure 6.4 Photobase-catalyzed Michael addition polymerization. (A) System consists of catalyst (visible-light-releasable base coumarin-caged tetramethylguanidine), and gel components PEG-di-photodegradable-acrylate and PEG-tetrathiol. (B) Loss modulus (G'') and storage modulus (G') measured on a parallel-plate rheometer demonstrating gelation over time in the presence of 400-500 nm light. *Work done in collaboration with Weixian Xi and Prof. Chris Bowman.

Another major improvement to the cyst templating method would be to select for fully covered microspheres before encapsulation to reduce the number of single cells, cell aggregates, and blank microspheres co-encapsulated with the desired pre-cysts. One technique that might be employed would be to remove the preferred pre-cysts from the wells under a dissection microscope with careful pipetting. This approach is routinely used for selecting cell aggregates of defined sizes (*e.g.*, islets). An added advantage to this method would be control over the number of cysts encapsulated per gel, which is lacking in the current approach.

Finally, confirmation of epithelial cell polarization is important to establish true reproduction of the native alveolar tissue. Typically, spontaneously formed alveolus-like structures *in vitro* consist of small numbers of cuboidal ATII phenotype cells, and immunostaining for basolateral markers (β-catenin, α6-integrin) and apical markers (ZO-1, actin) is easily identified on the exterior and interior surfaces of the cysts, respectively.[20,21] More thorough examination by electron microscopy reveals microvilli on the apical surface.[15,21–23] However, with the elongated and differentiated ATI-like cells in our model alveoli, apical-basal orientation of immunostaining markers (ZO-1 and β-catenin) was not clear. While the method requires meticulous sample preparation, electron microscopy methods for imaging cell structure are now routine and could confirm the presence of microvilli on the apical surface of the cysts. This would likely be the best method to demonstrate polarity of cells in the cyst model.

In Chapter 5, the model alveoli method developed in Chapter 4 was utilized to create co-cultures of pulmonary fibroblasts encapsulated with epithelial cysts to investigate the interplay between the two cell types in a spatially relevant context. It is important to culture cells in 3D and control their density, diffusion distances, and spatial proximity when studying hypotheses related to lung disease progression. Both normal and idiopathic fibrosis (IPF)

fibroblast cell lines (CCL-210 and CCL-134, respectively) were cultured with normal and tumor-derived alveolar epithelial cells (primary mouse ATII cells and A549 cell line, respectively), and key cellular actions were measured for signs of increased activation or epithelial-to-mesenchymal transition (EMT). First, proliferation of each cell type was quantified for selected time periods (day 1 and day 4 after encapsulation) with a fluorescent EdU kit, followed by confocal imaging. The cancerous and highly proliferative epithelial cell line A549 had a significantly higher percentage of EdU-positive nuclei one day after encapsulation compared with the normally quiescent primary epithelial cells in all conditions. Interestingly, both epithelial cell types exhibited a marked decrease in proliferation by day 4, which was mainly attributed to contact inhibition within the hydrogel scaffold. Both types of fibroblasts embedded in the hydrogel system had consistently low levels of proliferation on both days, indicating a quiescent phenotype. The exception to these observations was the A549/CCL-210 co-culture condition, in which the normal fibroblasts showed increased proliferation on day 1 over monoculture and both the fibroblasts and the cancerous epithelial cells had significantly increased proliferation on day 4 over the other conditions. We hypothesized that this increase in proliferation might be due to increased protease activity or an increase in pro-mitotic signaling molecules from one or both cell types. Next, we analyzed fibroblast migration through the hydrogel scaffold using a fluorescent live-cell tracking technique. In this 24-hour experiment, normal fibroblasts (CCL-210) were observed to migrate faster when co-cultured with either epithelial cell type (compared to monoculture), but the fibroblasts moved with less directionality when co-cultured with A549 cells. The IPF fibroblasts (CCL-134) also migrated faster when co-cultured with the A549 cells, but their speed was even higher when co-cultured with primary

epithelial cysts. We hypothesized that the increased migration in co-culture may also be related to increased protease activity or an increase in pro-migratory signals from the epithelial cells.

Finally, immunostaining of key EMT-related proteins was performed to visualize differences in their expression between the co-culture systems. While the mesenchymal marker vimentin did not appear in any of the primary cysts in co-culture with fibroblasts, surprisingly, the myofibroblast marker α-SMA was expressed by a subset of primary epithelial cells in both co-cultures, as early as one day after encapsulation. The expression of α-SMA in the epithelial cells may be a result of TGF-β signaling from the fibroblasts or caused by ECM interactions with the fibronectin-derived RGD peptide in the hydrogel scaffold, since fibronectin-coated surfaces have been shown to cause expression of α-SMA in cultured primary ATII cells, in direct contrast with collagen and laminin surfaces.[24] While the mechanisms causing the differences in cell behavior seen in these experiments remain unknown, these phenomenological observations provide key results for future hypothesis testing. In summary, the co-culture model utilized in Chapter 5 provides compelling evidence that supports the role of epithelial-mesenchymal crosstalk in disease progression and identifies particular combinations of cell co-culture conditions that warrant more detailed study.

As explained in Chapter 5, there are several potential signaling mechanisms revealed by these experiments that motivate additional exploration to better understand how the epithelium interacts with the surrounding fibroblasts. First, increased protease activity may be involved in the increased proliferation and migration seen in co-cultures.[25,26] To test this hypothesis, a fluorescent sensor peptide sensitive to matrix metalloproteinase (MMP) cleavage (Figure 6.5A) could be used to measure an increase in MMP activity when epithelial cells and fibroblasts are co-encapsulated.[27,28] The sensor peptide can be tethered to the gel network, and simple area scans

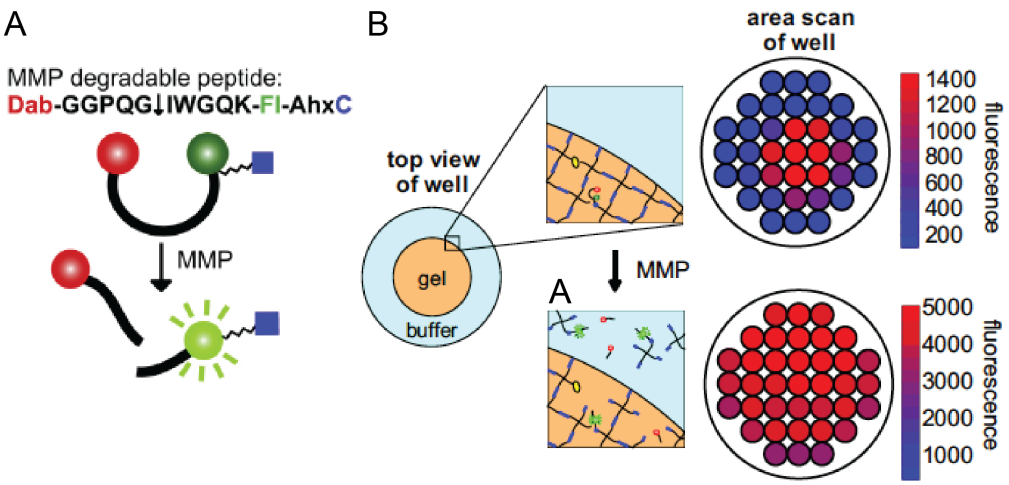

Figure 6.5 Matrix metalloproteinase (MMP) sensor peptide. (A) Peptide sequence is sensitive to cleavage by MMP-1, 2, 3, 7, 8, and 9 and includes a cysteine residue on one end to facilitate thiol-ene addition into the gel network. Fluorescein is incorporated into the cysteine end of the peptide and a quenching dabcyl moiety is added to the free end. Upon cleavage, the quencher diffuses away, leaving a fluorescent signal attached to the gel. (B) Gels containing the sensor peptide are formed in a well plate. With no MMP activity (no cells present), and area scan reveals a low fluorescence signal localized to the gel. With increased MMP activity (cells encapsulated in gels), the fluorescence signal increases in intensity and is spread more evenly throughout the well as the sensor peptide is cleaved and gel components are eroded through enzymatic degradation.

on a plate reader measure the relative intensity of the fluorescence signal in the well (Figure 6.5B). In addition, several commercially-available fluorometric assays are available that measure global protease activity in tissue supernatant (*e.g.,* Pierce, Sigma-Aldrich, Abcam). Alternatively, the proliferation and migration increases may be due to an increase in pro-mitotic and pro-migratory signaling molecules from either the fibroblasts or the epithelium.[5,29–32] For example, CCL-210 cells could be cultured in the presence of conditioned media from A549 cells and then observed for increased proliferation and migration. If a soluble signal appears to influence the CCL-210 cells, potential mediators such as platelet-derived growth factor (PDGF) or osteopontin[5,29] could be added to normal co-culture media, and CCL-210 proliferation and migration could be checked for similar increases. Similar experiments could be conducted with

the other fibroblast/epithelial cell co-culture conditions, which all showed increased migration over the culture of single fibroblast populations.

To explore the influence of paracrine signaling on the increase in A549 proliferation with CCL-210 cells, conditioned media from CCL-210 cells could be used with A549 cells and proliferation on day 4 checked for a similar increase over monoculture. If a soluble signal is implicated in this result, then the potential regulator HGF[25] could be added to the media and A549 proliferation measured again. Finally, the appearance of α-SMA in the primary cysts co-cultured with both fibroblast cell lines is particularly intriguing, especially without concurrent expression of vimentin. To test if this expression is related to ECM signaling from the hydrogel, primary cysts should be cultured alone and immunostained for α-SMA. If it appears without the fibroblasts, then other adhesive peptide mimics or matrix elasticities could be tested to probe which matrix properties might be involved in causing stress fiber formation in these epithelial cells. If α-SMA is absent in the primary cyst monoculture, then that would implicate signaling from the co-cultured fibroblasts. One potential signal known to induce α-SMA expression in primary ATII cells is TGF-β,[24,33] so that could be added to the media or covalently tethered to the hydrogel[34] and primary cysts could be checked for α-SMA expression by immunostaining.

Examining each potential soluble cue one-by-one would prove to be tedious; therefore, longer-term studies could delve further into the signaling pathways involved in epithelial-fibroblast crosstalk by examining the composition of conditioned media. In addition to the growth factors mentioned previously, components associated with microsomes may be influential in disease progression as well. Microsomes are 80-120 nm vesicles that contain membrane-associated enzymes such as microsomal prostaglandin E synthase-1, which has been shown to be involved in both IPF and lung cancer progression.[35–38] Growth factors could be

separated from microsomes through differential ultracentrifugation and the resulting fractions could be used with cells to inspect resulting cell behavior.[35] To follow up, ELISA assays for specific proteins could be performed to identify key factors present in conditioned media.[39] Continuing with the study of fibrogenesis and tumorigenesis, normal disease progression starts with only a few transformed cells, either from age-related mutations or repeated injury, and entire cell populations do not become diseased at once. To mimic this in our co-culture model, healthy and diseased fibroblasts and/or epithelial cysts could be mixed at different ratios to determine if there is a critical point at which the number of transformed cells leads to altered cell behavior in the entire system. In related studies, the density of fibroblasts with respect to epithelial cysts could be varied to establish whether the number and proximity of fibroblasts matters during the development of these diseases. Given the large experimental space defined here, a high-throughput system like the one described earlier with a liquid-handling robot and high-content microscope, along with reporter cell lines for key proteins such as α-SMA, could be useful in screening many conditions and identifying the most interesting combinations.

Moving beyond the epithelial-mesenchymal co-culture model, other cell types are important in alveolar tissue during lung development and disease, including immune cells and capillary endothelial cells.[4] Similar to the fibroblasts studied in Chapter 5, immune cells or endothelial cells could be co-encapsulated with epithelial cysts to study the interactions of these cell types in the context of disease-related soluble cues or diseased cell lines. For example, injury to the apical surface of model alveoli could be accomplished by entrapping a commonly used inflammatory stimulant lipopolysaccharide (LPS)[31,40] in the microsphere templates, which could then be released upon template erosion and interact with the interior surface of the epithelial layer. Epithelial response to this stimulant, especially with immune cells and/or fibroblasts

present in the model, would be interesting to measure. Culturing structurally-relevant vasculature in synthetic hydrogels has been notoriously difficult, although recent advances in micropatterning of endothelial cell cords surrounding a collagen core have generated excitement in the tissue engineering field.[41] An intriguing extension of the cyst templating model described in Chapter 4 would be to create photodegradable fibers of the appropriate size (5-10 μm diameter),[42] seed them with endothelial cells and co-encapsulate them with epithelial cysts. Erosion of the templates with light would leave hollow lumen reminiscent of native vasculature. Combining multiple cell types in the alveolar model system would complicate analysis of cellular behavior, but it might better recapitulate the tissue microenvironment for complex interaction studies or as a first step for drug screening trials.

In summary, we exploited photo-cleavable crosslinking molecules in PEG hydrogel networks to create spatially-relevant, tunable *in vitro* culture platforms for studying primary alveolar epithelial cell differentiation and communication with neighboring mesenchymal cells. In photopatterned microwells, we found that primary ATII cells differentiate into ATI-like cells on gel surfaces, but form unnatural aggregates in the wells. Consequently, we developed a cy-templating method using photodegradable microspheres, which created stable, physiologically-relevant model alveoli embedded in a tunable PEG hydrogel scaffold. This cyst model was expanded to introduce pulmonary fibroblasts in co-culture with epithelial cysts using combinations of healthy and diseased cell types to study the interplay between the epithelium and mesenchyme during disease progression. We found that signaling between the two cell types led to increased proliferation and migration when cancerous epithelial cells were combined with normal fibroblasts, primary epithelial cysts also encouraged increased migration of both healthy and IPF fibroblasts, and an as yet unidentified signal induced α-SMA expression in a subset of

primary epithelial cysts when co-cultured with fibroblasts. We believe the techniques developed in this thesis represent a significant advancement in alveolar tissue-specific *in vitro* platforms available to study the signaling mechanisms involved in lung development and disease, both from the ECM and from intercellular communication. Beyond lung epithelial cysts, the methods presented here to control spatial location of cells within synthetic hydrogels may prove useful for many other tissue applications requiring 3D resolution of cultured cell populations.

6.1 References

1. Fehrenbach, H. Alveolar epithelial type II cell: defender of the alveolus revisited. *Respir. Res.* **2,** 33–46 (2001).

2. Herzog, E. L., Brody, A. R., Colby, T. V, Mason, R. & Williams, M. C. Knowns and unknowns of the alveolus. *Proc. Am. Thorac. Soc.* **5,** 778–82 (2008).

3. Crosby, L. M. & Waters, C. M. Epithelial Repair Mechanisms in the Lung. *Am. J. Physiol. Lung Cell. Mol. Physiol.* **298,** 715–731 (2010).

4. Hogan, B. L. M., Barkauskas, C. E., Chapman, H. A., Epstein, J. A., Jain, R., Hsia, C. C. W., *et al.* Repair and regeneration of the respiratory system: complexity, plasticity, and mechanisms of lung stem cell function. *Cell Stem Cell* **15,** 123–38 (2014).

5. King, T. E., Pardo, A. & Selman, M. Idiopathic pulmonary fibrosis. *Lancet* **378,** 1949–61 (2011).

6. Thiery, J. P., Acloque, H., Huang, R. Y. J. & Nieto, M. A. Epithelial-mesenchymal transitions in development and disease. *Cell* **139,** 871–90 (2009).

7. Bellusci, S., Grindley, J., Emoto, H., Itoh, N. & Hogan, B. L. Fibroblast growth factor 10 (FGF10) and branching morphogenesis in the embryonic mouse lung. *Development* **124,** 4867–78 (1997).

8. Park, W. Y., Miranda, B., Lebeche, D., Hashimoto, G. & Cardoso, W. V. FGF-10 is a chemotactic factor for distal epithelial buds during lung development. *Dev. Biol.* **201,** 125–34 (1998).

9. Bhaskaran, M., Kolliputi, N., Wang, Y., Gou, D., Chintagari, N. R. & Liu, L. Trans-differentiation of Alveolar Epithelial Type II Cells to Type I Cells Involves Autocrine

Signaling by Transforming Growth Factor beta1 through the Smad Pathway. *J. Biol. Chem.* **282,** 3968–3976 (2006).

10. Qiao, R., Yan, W., Clavijo, C., Mehrian-Shai, R., Zhong, Q., Kim, K.-J., *et al.* Effects of KGF on alveolar epithelial cell transdifferentiation are mediated by JNK signaling. *Am. J. Respir. Cell Mol. Biol.* **38,** 239–46 (2008).

11. Isakson, B. E., Lubman, R. L., Seedorf, G. J. & Boitano, S. Modulation of pulmonary alveolar type II cell phenotype and communication by extracellular matrix and KGF. *Am. J. Physiol. Cell Physiol.* **281,** C1291–C1299 (2001).

12. Isakson, B., Lubman, R., Seedorf, G. & Boitano, S. Modulation of pulmonary alveolar type II cell phenotype and communication by extracellular matrix and KGF. *Am J Physiol Cell Physiol* **281,** C1291–C1299 (2001).

13. Gould, S. T., Darling, N. J. & Anseth, K. S. Small peptide functionalized thiol-ene hydrogels as culture substrates for understanding valvular interstitial cell activation and de novo tissue deposition. *Acta Biomater.* **8,** 3201–9 (2012).

14. Ali, S., Saik, J. E., Gould, D. J., Dickinson, M. E. & West, J. L. Immobilization of Cell-Adhesive Laminin Peptides in Degradable PEGDA Hydrogels Influences Endothelial Cell Tubulogenesis. *Biores. Open Access* **2,** 241–249 (2013).

15. Matter, M. L. & Laurie, G. W. A novel laminin E8 cell adhesion site required for lung alveolar formation in vitro. *J. Cell Biol.* **124,** 1083–90 (1994).

16. Mabry, K. M. P. The Role of Matrix Properties in Directing Valvular Interstitial Cell Phenotype. (2015).

17. Ochs, M., Nyengaard, J. R., Jung, A., Knudsen, L., Voigt, M., Wahlers, T., *et al.* The number of alveoli in the human lung. *Am. J. Respir. Crit. Care Med.* **169,** 120–4 (2004).

18. Stone, K. C., Mercer, R. R., Gehr, P., Stockstill, B. & Crapo, J. D. Allometric relationships of cell numbers and size in the mammalian lung. *Am. J. Respir. Cell Mol. Biol.* **6,** 235–43 (1992).

19. Zhang, X., Xi, W., Chatani, S., Podgorski, M. & Bowman, C. Light controlled thiol-Michael addition initiated by photocaged superbases. in *Abstr. Pap. 249th ACS Natl. Meet. Expo. Denver, CO, United States, March 22-26, 2015* POLY–303 (American Chemical Society, 2015).

20. Gill, B. J., Gibbons, D. L., Roudsari, L. C., Saik, J. E., Rizvi, Z. H., Roybal, J. D., *et al.* A synthetic matrix with independently tunable biochemistry and mechanical properties to study epithelial morphogenesis and EMT in a lung adenocarcinoma model. *Cancer Res.* **72,** 6013–23 (2012).

21. Yu, W., Fang, X., Ewald, A., Wong, K., Hunt, C. A., Werb, Z., *et al.* Formation of cysts by alveolar type II cells in three-dimensional culture reveals a novel mechanism for epithelial morphogenesis. *Mol. Biol. Cell* **18,** 1693 (2007).

22. Sugihara, H., Toda, S., Miyabara, S., Fujiyama, C. & Yonemitsu, N. Reconstruction of alveolus-like structure from alveolar type II epithelial cells in three-dimensional collagen gel matrix culture. *Am. J. Pathol.* **142,** 783–92 (1993).

23. Mondrinos, M. J., Koutzaki, S., Jiwanmall, E., Li, M., Dechadarevian, J.-P., Lelkes, P. I., *et al.* Engineering three-dimensional pulmonary tissue constructs. *Tissue Eng.* **12,** 717–28 (2006).

24. Kim, K. K., Kugler, M. C., Wolters, P. J., Robillard, L., Galvez, M. G., Brumwell, A. N., *et al.* Alveolar epithelial cell mesenchymal transition develops in vivo during pulmonary fibrosis and is regulated by the extracellular matrix. *Proc. Natl. Acad. Sci.* **103,** 13180–13185 (2006).

25. Bhowmick, N., Neilson, E. & Moses, H. Stromal fibroblasts in cancer initiation and progression. *Nature* **432,** 332–337 (2004).

26. Fromigué, O., Louis, K., Dayem, M., Milanini, J., Pages, G., Tartare-Deckert, S., *et al.* Gene expression profiling of normal human pulmonary fibroblasts following coculture with non-small-cell lung cancer cells reveals alterations related to matrix degradation, angiogenesis, cell growth and survival. *Oncogene* **22,** 8487–97 (2003).

27. Leight, J. L., Alge, D. L., Maier, A. J. & Anseth, K. S. Direct measurement of matrix metalloproteinase activity in 3D cellular microenvironments using a fluorogenic peptide substrate. *Biomaterials* **34,** 7344–52 (2013).

28. Leight, J. L., Tokuda, E. Y., Jones, C. E., Lin, A. J. & Anseth, K. S. Multifunctional bioscaffolds for 3D culture of melanoma cells reveal increased MMP activity and migration with BRAF kinase inhibition. *Proc. Natl. Acad. Sci.* **112,** 201505662 (2015).

29. Pardo, A., Gibson, K., Cisneros, J., Richards, T. J., Yang, Y., Becerril, C., *et al.* Up-regulation and profibrotic role of osteopontin in human idiopathic pulmonary fibrosis. *PLoS Med.* **2,** 0891–0903 (2005).

30. Selman, M., Thannickal, V. J., Pardo, A., Zisman, D. A., Martinez, F. J. & Lynch, J. P. Idiopathic Pulmonary Fibrosis. *Drugs* **64,** 405–430 (2004).

31. Mason, R. J. Biology of alveolar type II cells. *Respirology* **11,** S12–S15 (2006).

32. Marchand-Adam, S., Marchal, J., Cohen, M., Soler, P., Gerard, B., Castier, Y., *et al.* Defect of hepatocyte growth factor secretion by fibroblasts in idiopathic pulmonary fibrosis. *Am. J. Respir. Crit. Care Med.* **168,** 1156–61 (2003).

33. Willis, B. C., Liebler, J. M., Luby-Phelps, K., Nicholson, A. G., Crandall, E. D., du Bois, R. M., *et al.* Induction of epithelial-mesenchymal transition in alveolar epithelial cells by transforming growth factor-beta1: potential role in idiopathic pulmonary fibrosis. *Am. J. Pathol.* **166,** 1321–1332 (2005).

34. McCall, J. D., Luoma, J. E. & Anseth, K. S. Covalently tethered transforming growth factor beta in PEG hydrogels promotes chondrogenic differentiation of encapsulated human mesenchymal stem cells. *Drug Deliv. Transl. Res.* **2,** 305–312 (2012).

35. Jeppesen, D. K., Hvam, M. L., Primdahl-Bengtson, B., Boysen, A. T., Whitehead, B., Dyrskjøt, L., *et al.* Comparative analysis of discrete exosome fractions obtained by differential centrifugation. *J. Extracell. Vesicles* **3,** 1–16 (2014).

36. Watanabe, K., Kurihara, K., Tokunaga, Y. & Hayaishi, O. Two types of microsomal prostaglandin E synthase: glutathione-dependent and -independent prostaglandin E synthases. *Biochem. Biophys. Res. Commun.* **235,** 148–152 (1997).

37. Wei, B., Cai, L., Sun, D., Wang, Y., Wang, C., Chai, X., *et al.* Microsomal prostaglandin e synthase-1 deficiency exacerbates pulmonary fibrosis induced by bleomycin in mice. *Molecules* **19,** 4967–4985 (2014).

38. Takahashi, R., Amano, H., Satoh, T., Tabata, K., Ikeda, M., Kitasato, H., *et al.* Roles of microsomal prostaglandin E synthase-1 in lung metastasis formation in prostate cancer RM9 cells. *Biomed. Pharmacother.* **68,** 71–77 (2014).

39. Anderson, I. C., Mari, S. E., Broderick, R. J., Mari, B. P. & Shipp, M. A. The angiogenic factor interleukin 8 is induced in non-small cell lung cancer/pulmonary fibroblast cocultures. *Cancer Res.* **60,** 269–272 (2000).

40. Bedran, T. B. L., Mayer, M. P. A., Spolidorio, D. P. & Grenier, D. Synergistic Anti-Inflammatory Activity of the Antimicrobial Peptides Human Beta-Defensin-3 (hBD-3) and Cathelicidin (LL-37) in a Three-Dimensional Co-Culture Model of Gingival Epithelial Cells and Fibroblasts. *PLoS One* **9,** e106766 (2014).

41. Baranski, J. D., Chaturvedi, R. R., Stevens, K. R., Eyckmans, J., Carvalho, B., Solorzano, R. D., *et al.* Geometric control of vascular networks to enhance engineered tissue integration and function. *Proc. Natl. Acad. Sci.* **110,** 7586–7591 (2013).

42. Doerschuk, C. M., Beyers, N., Coxson, H. O., Wiggs, B. & Hogg, J. C. Comparison of neutrophil and capillary diameters and their relation to neutrophil sequestration in the lung. *J. Appl. Physiol.* **74,** 3040–3045 (1993).

Chapter 7

Bibliography

Chapter 1

1. Centers for Disease Control and Prevention. *National Vital Statistics Reports, Deaths: Final Data for 2004*. (2007).

2. King, T. E., Pardo, A. & Selman, M. Idiopathic pulmonary fibrosis. *Lancet* **378,** 1949–61 (2011).

3. Fromigué, O., Louis, K., Dayem, M., Milanini, J., Pages, G., Tartare-Deckert, S., *et al.* Gene expression profiling of normal human pulmonary fibroblasts following coculture with non-small-cell lung cancer cells reveals alterations related to matrix degradation, angiogenesis, cell growth and survival. *Oncogene* **22,** 8487–97 (2003).

4. Wang, W., Li, Q., Yamada, T., Matsumoto, K., Matsumoto, I., Oda, M., *et al.* Crosstalk to stromal fibroblasts induces resistance of lung cancer to epidermal growth factor receptor tyrosine kinase inhibitors. *Clin. Cancer Res.* **15,** 6630–8 (2009).

5. Puig, M., Lugo, R., Gabasa, M., Gimenez, A., Velasquez, A., Galgoczy, R., *et al.* Matrix Stiffening and 1 Integrin Drive Subtype-Specific Fibroblast Accumulation in Lung Cancer. *Mol. Cancer Res.* **13,** 161–173 (2015).

6. Williams, M. C. Alveolar type I cells: molecular phenotype and development. *Annu. Rev. Physiol.* **65,** 669–95 (2003).

7. Mason, R. J. Biology of alveolar type II cells. *Respirology* **11,** S12–S15 (2006).

8. Fehrenbach, H. Alveolar epithelial type II cell: defender of the alveolus revisited. *Respir. Res.* **2,** 33–46 (2001).

9. Guillot, L., Nathan, N., Tabary, O., Thouvenin, G., Le Rouzic, P., Corvol, H., *et al.* Alveolar epithelial cells: master regulators of lung homeostasis. *Int. J. Biochem. Cell Biol.* **45,** 2568–73 (2013).

10. Uhal, B. D. Cell cycle kinetics in the alveolar epithelium. *Am. J. Physiol. Cell. Mol. Physiol.* **272,** L1031–1045 (1997).

11. Hogan, B. L. M., Barkauskas, C. E., Chapman, H. A., Epstein, J. A., Jain, R., Hsia, C. C. W., *et al.* Repair and regeneration of the respiratory system: complexity, plasticity, and mechanisms of lung stem cell function. *Cell Stem Cell* **15,** 123–38 (2014).

12. Barkauskas, C., Cronce, M., Rackley, C., Bowie, E., Keene, D., Stripp, B., *et al.* Type 2 alveolar cells are stem cells in adult lung. *J. Clin. Invest.* **123,** 3025–3036 (2013).

13. Park, W. Y., Miranda, B., Lebeche, D., Hashimoto, G. & Cardoso, W. V. FGF-10 is a chemotactic factor for distal epithelial buds during lung development. *Dev. Biol.* **201,** 125–34 (1998).

14. Bellusci, S., Grindley, J., Emoto, H., Itoh, N. & Hogan, B. L. Fibroblast growth factor 10 (FGF10) and branching morphogenesis in the embryonic mouse lung. *Development* **124,** 4867–78 (1997).

15. Tang, N., Marshall, W. F., McMahon, M., Metzger, R. J. & Martin, G. R. Control of Mitotic Spindle Angle by the RAS-Regulated ERK1/2 Pathway Determines Lung Tube Shape. *Science* **333,** 342–345 (2011).

16. Perl, A.-K. T. & Gale, E. FGF signaling is required for myofibroblast differentiation during alveolar regeneration. *Am. J. Physiol. Lung Cell. Mol. Physiol.* **297,** L299–308 (2009).

17. Yano, T., Mason, R. J., Pan, T., Deterding, R. R., Nielsen, L. D. & Shannon, J. M. KGF regulates pulmonary epithelial proliferation and surfactant protein gene expression in adult rat lung. *Am. J. Physiol. Lung Cell. Mol. Physiol.* **279,** L1146–58 (2000).

18. Sugahara, K., Tokumine, J., Teruya, K. & Oshiro, T. Alveolar epithelial cells: differentiation and lung injury. *Respirology* **11,** S28–31 (2006).

19. Crosby, L. M. & Waters, C. M. Epithelial Repair Mechanisms in the Lung. *Am. J. Physiol. Lung Cell. Mol. Physiol.* **298,** 715–731 (2010).

20. Prasad, S., Hogaboam, C. M. & Jarai, G. Deficient repair response of IPF fibroblasts in a co-culture model of epithelial injury and repair. *Fibrogenesis Tissue Repair* **7,** 7 (2014).

21. Shannon, J. M., Gebb, S. A. & Nielsen, L. D. Induction of alveolar type II cell differentiation in embryonic tracheal epithelium in mesenchyme-free culture. *Development* **126,** 1675–88 (1999).

22. Steiling, H. & Werner, S. Fibroblast growth factors: key players in epithelial morphogenesis, repair and cytoprotection. *Curr. Opin. Biotechnol.* **14,** 533–537 (2003).

23. Warburton, D., Wuenschell, C., Flores-Delgado, G. & Anderson, K. Commitment and differentiation of lung cell lineages. *Biochem. cell Biol.* **76,** 971–995 (1998).

24. Isakson, B. E., Seedorf, G. J., Lubman, R. L. & Boitano, S. Heterocellular cultures of pulmonary alveolar epithelial cells grown on laminin-5 supplemented matrix. *In Vitro Cell. Dev. Biol. Anim.* **38,** 443–9 (2002).

25. Wang, J., Edeen, K., Manzer, R., Chang, Y., Wang, S., Chen, X., *et al.* Differentiated human alveolar epithelial cells and reversibility of their phenotype in vitro. *Am. J. Respir. Cell Mol. Biol.* **36,** 661–8 (2007).

26. Herzog, E. L., Brody, A. R., Colby, T. V, Mason, R. & Williams, M. C. Knowns and unknowns of the alveolus. *Proc. Am. Thorac. Soc.* **5,** 778–82 (2008).

27. Thiery, J. P., Acloque, H., Huang, R. Y. J. & Nieto, M. A. Epithelial-mesenchymal transitions in development and disease. *Cell* **139,** 871–90 (2009).

28. Willis, B. C. & Borok, Z. TGF-beta-induced EMT: mechanisms and implications for fibrotic lung disease. *Am. J. Physiol. Lung Cell. Mol. Physiol.* **293,** L525–34 (2007).

29. Marchand-Adam, S., Marchal, J., Cohen, M., Soler, P., Gerard, B., Castier, Y., *et al.* Defect of hepatocyte growth factor secretion by fibroblasts in idiopathic pulmonary fibrosis. *Am. J. Respir. Crit. Care Med.* **168,** 1156–61 (2003).

30. Kumarswamy, R., Mudduluru, G., Ceppi, P., Muppala, S., Kozlowski, M., Niklinski, J., *et al.* MicroRNA-30a inhibits epithelial-to-mesenchymal transition by targeting Snai1 and is downregulated in non-small cell lung cancer. *Int. J. Cancer* **130,** 2044–53 (2012).

31. Amann, A., Zwierzina, M., Gamerith, G., Bitsche, M., Huber, J. M., Vogel, G. F., *et al.* Development of an innovative 3D cell culture system to study tumour--stroma interactions in non-small cell lung cancer cells. *PLoS One* **9,** e92511 (2014).

32. Horie, M., Saito, A., Mikami, Y., Ohshima, M., Morishita, Y., Nakajima, J., *et al.* Characterization of human lung cancer-associated fibroblasts in three-dimensional in vitro co-culture model. *Biochem. Biophys. Res. Commun.* **423,** 158–63 (2012).

33. Bhowmick, N., Neilson, E. & Moses, H. Stromal fibroblasts in cancer initiation and progression. *Nature* **432,** 332–337 (2004).

34. Dobbs, L. G. Isolation and culture of alveolar type II cells. *Am. J. Physiol.* **258,** L134–47 (1990).

35. Bhaskaran, M., Kolliputi, N., Wang, Y., Gou, D., Chintagari, N. R. & Liu, L. Trans-differentiation of Alveolar Epithelial Type II Cells to Type I Cells Involves Autocrine Signaling by Transforming Growth Factor beta1 through the Smad Pathway. *J. Biol. Chem.* **282,** 3968–3976 (2006).

36. Qiao, R., Yan, W., Clavijo, C., Mehrian-Shai, R., Zhong, Q., Kim, K.-J., *et al.* Effects of KGF on alveolar epithelial cell transdifferentiation are mediated by JNK signaling. *Am. J. Respir. Cell Mol. Biol.* **38,** 239–46 (2008).

37. Matter, M. L. & Laurie, G. W. A novel laminin E8 cell adhesion site required for lung alveolar formation in vitro. *J. Cell Biol.* **124,** 1083–90 (1994).

38. Umino, T., Wang, H., Zhu, Y., Liu, X., Manouilova, L. S., Spurzem, J. R., *et al.* Modification of type I collagenous gels by alveolar epithelial cells. *Am. J. Respir. Cell Mol. Biol.* **22,** 702–707 (2000).

39. Mondrinos, M. J., Koutzaki, S., Jiwanmall, E., Li, M., Dechadarevian, J.-P., Lelkes, P. I., *et al.* Engineering three-dimensional pulmonary tissue constructs. *Tissue Eng.* **12,** 717–28 (2006).

40. Bissell, M. J., Kenny, P. A. & Radisky, D. C. Microenvironmental regulators of tissue structure and function also regulate tumor induction and progression: the role of extracellular matrix and its degrading enzymes. *Cold Spring Harb. Symp. Quant. Biol.* **70,** 343–56 (2005).

41. Griffith, L. G. & Swartz, M. A. Capturing complex 3D tissue physiology in vitro. *Nat. Rev. Mol. Cell Biol.* **7,** 211–24 (2006).

42. Sugihara, H., Toda, S., Miyabara, S., Fujiyama, C. & Yonemitsu, N. Reconstruction of alveolus-like structure from alveolar type II epithelial cells in three-dimensional collagen gel matrix culture. *Am. J. Pathol.* **142,** 783–92 (1993).

43. Mondrinos, M. J., Koutzaki, S., Lelkes, P. I. & Finck, C. M. A tissue-engineered model of fetal distal lung tissue. *Am. J. Physiol. Lung Cell. Mol. Physiol.* **293,** L639–50 (2007).

44. Yu, W., Fang, X., Ewald, A., Wong, K., Hunt, C. A., Werb, Z., *et al.* Formation of cysts by alveolar type II cells in three-dimensional culture reveals a novel mechanism for epithelial morphogenesis. *Mol. Biol. Cell* **18,** 1693 (2007).

45. Lwebuga-Mukasa, J. S., Ingbar, D. H. & Madri, J. A. Repopulation of a Human Alveolar Matrix by Adult Rat Type II Pneumocytes In Vitro. *Exp. Cell Res.* **162,** 423–435 (1986).

46. Gill, B. J., Gibbons, D. L., Roudsari, L. C., Saik, J. E., Rizvi, Z. H., Roybal, J. D., *et al.* A synthetic matrix with independently tunable biochemistry and mechanical properties to study epithelial morphogenesis and EMT in a lung adenocarcinoma model. *Cancer Res.* **72,** 6013–23 (2012).

47. Carterson, A., Bentrup, K. zu, Ott, C., Clarke, M., Pierson, D., Vanderburg, C., *et al.* A549 Lung Epithelial Cells Grown as Three-Dimensional Aggregates : Alternative Tissue Culture Model for Pseudomonas aeruginosa Pathogenesis. *Infect. Immun.* **73,** 1129–1140 (2005).

48. Reginato, M. J., Mills, K. R., Paulus, J. K., Lynch, D. K., Sgroi, D. C., Debnath, J., *et al.* Integrins and EGFR coordinately regulate the pro-apoptotic protein Bim to prevent anoikis. *Nat. Cell Biol.* **5,** 733–40 (2003).

49. Magnusson, M. K. & Mosher, D. F. Fibronectin : Structure, Assembly, and Cardiovascular Implications. *Arterioscler. Thromb. Vasc. Biol.* **18,** 1363–1370 (1998).

50. Parsons, J. T., Martin, K. H., Slack, J. K., Taylor, J. M. & Weed, S. A. Focal adhesion kinase: a regulator of focal adhesion dynamics and cell movement. *Oncogene* **19,** 5606–13 (2000).

51. Tibbitt, M. W. & Anseth, K. S. Hydrogels as extracellular matrix mimics for 3D cell culture. *Biotechnol. Bioeng.* **103,** 655–63 (2009).

52. Taipale, J. & Keski-Oja, J. Growth factors in the extracellular matrix. *FASEB J.* **11,** 51–59 (1997).

53. Jorma, A., Taipale, J. & Keski-Oja, J. Growth factors in the extracellular matrix. *FASEB J.* **11,** 51–59 (1997).

54. Kim, S.-H., Turnbull, J. & Guimond, S. Extracellular matrix and cell signalling: the dynamic cooperation of integrin, proteoglycan and growth factor receptor. *J. Endocrinol.* **209,** 139–51 (2011).

55. Bacac, M. & Stamenkovic, I. Metastatic cancer cell. *Annu. Rev. Pathol.* **3,** 221–47 (2008).

56. Daley, W. P., Peters, S. B. & Larsen, M. Extracellular matrix dynamics in development and regenerative medicine. *J. Cell Sci.* **121,** 255–64 (2008).

57. Ingber, D. Tensegrity: the architectural basis of cellular mechanotransduction. *Annu. Rev. Physiol.* **59,** 575–599 (1997).

58. Levental, I., Georges, P. C. & Janmey, P. A. Soft biological materials and their impact on cell function. *Soft Matter* **3,** 299–306 (2007).

59. Engler, A. J., Sen, S., Sweeney, H. L. & Discher, D. E. Matrix elasticity directs stem cell lineage specification. *Cell* **126,** 677–89 (2006).

60. Paszek, M. J., Zahir, N., Johnson, K. R., Lakins, J. N., Rozenberg, G. I., Gefen, A., *et al.* Tensional homeostasis and the malignant phenotype. *Cancer Cell* **8,** 241–54 (2005).

61. Rosso, F., Marino, G., Giordano, A., Barbarisi, M., Parmeggiani, D. & Barbarisi, A. Smart materials as scaffolds for tissue engineering. *J. Cell. Physiol.* **203,** 465–70 (2005).

62. Lutolf, M. P. & Hubbell, J. A. Synthetic biomaterials as instructive extracellular microenvironments for morphogenesis in tissue engineering. *Nat. Biotechnol.* **23,** 47–55 (2005).

63. Peppas, N. A., Hilt, J. Z., Khademhosseini, A. & Langer, R. Hydrogels in Biology and Medicine: From Molecular Principles to Bionanotechnology. *Adv. Mater.* **18,** 1345–1360 (2006).

64. Cushing, M. C. & Anseth, K. S. Materials science. Hydrogel cell cultures. *Science* **316,** 1133–4 (2007).

65. Sawhney, A., Pathak, C. & Hubbell, J. Bioerodible Hydrogels Based on Photopolymerized Poly(ethylene glycol)-co-poly(a-hydroxy acid) Diacrylate Macromers. *Macromolecules* **26,** 581–587 (1993).

66. Bryant, S. J., Nuttelman, C. R. & Anseth, K. S. Cytocompatibility of UV and visible light photoinitiating systems on cultured NIH/3T3 fibroblasts in vitro. *J. Biomater. Sci. Polym. Ed.* **11,** 439–57 (2000).

67. Bryant, S. J. & Anseth, K. S. Hydrogel properties influence ECM production by chondrocytes photoencapsulated in poly(ethylene glycol) hydrogels. *J. Biomed. Mater. Res.* **59,** 63–72 (2002).

68. Weber, L. M., He, J., Bradley, B., Haskins, K. & Anseth, K. S. PEG-based hydrogels as an in vitro encapsulation platform for testing controlled beta-cell microenvironments. *Acta Biomater.* **2,** 1–8 (2006).

69. Cordey, M., Limacher, M., Kobel, S., Taylor, V. & Lutolf, M. P. Enhancing the reliability and throughput of neurosphere culture on hydrogel microwell arrays. *Stem Cells* **26,** 2586–94 (2008).

70. Rice, M. A. & Anseth, K. S. Encapsulating chondrocytes in copolymer gels: bimodal degradation kinetics influence cell phenotype and extracellular matrix development. *J. Biomed. Mater. Res. A* **70,** 560–8 (2004).

71. Nuttelman, C. R., Henry, S. M. & Anseth, K. S. Synthesis and characterization of photocrosslinkable, degradable poly(vinyl alcohol)-based tissue engineering scaffolds. *Biomaterials* **23,** 3617–26 (2002).

72. Bryant, S. J. & Anseth, K. S. Controlling the spatial distribution of ECM components in degradable PEG hydrogels for tissue engineering cartilage. *J. Biomed. Mater. Res. A* **64,** 70–9 (2003).

73. Lutolf, M. P., Lauer-Fields, J. L., Schmoekel, H. G., Metters, A. T., Weber, F. E., Fields, G. B., *et al.* Synthetic matrix metalloproteinase-sensitive hydrogels for the conduction of

tissue regeneration: engineering cell-invasion characteristics. *Proc. Natl. Acad. Sci. U. S. A.* **100,** 5413–8 (2003).

74. Salinas, C. N. & Anseth, K. S. The enhancement of chondrogenic differentiation of human mesenchymal stem cells by enzymatically regulated RGD functionalities. *Biomaterials* **29,** 2370–7 (2008).

75. Kloxin, A. M., Kasko, A. M., Salinas, C. N. & Anseth, K. S. Photodegradable hydrogels for dynamic tuning of physical and chemical properties. *Science* **324,** 59–63 (2009).

76. Bryant, S. & Anseth, K. in *Scaffolding Tissue Eng.* (Ma, P. X. & Elisseeff, J.) 71–90 (CRC Press, 2005). doi:10.1201/9781420027563.ch6

77. Metters, A. & Hubbell, J. Network formation and degradation behavior of hydrogels formed by Michael-type addition reactions. *Biomacromolecules* **6,** 290–301 (2005).

78. Tibbitt, M. W. & Anseth, K. S. Dynamic Microenvironments: The Fourth Dimension. *Sci. Transl. Med.* **4,** 160ps24–160ps24 (2012).

79. Kloxin, A. M., Tibbitt, M. W., Kasko, A. M., Fairbairn, J. A. & Anseth, K. S. Tunable Hydrogels for External Manipulation of Cellular Microenvironments through Controlled Photodegradation. *Adv. Mater.* **22,** 61–66 (2010).

80. Benton, J. A., Kern, H. B. & Anseth, K. S. Substrate Properties Influence Calcification in Valvular Interstitial Cell Culture. *J Hear. Valve Dis* **17,** 689–699 (2008).

81. Yip, C. Y. Y., Chen, J.-H., Zhao, R. & Simmons, C. A. Calcification by valve interstitial cells is regulated by the stiffness of the extracellular matrix. *Arterioscler. Thromb. Vasc. Biol.* **29,** 936–42 (2009).

82. Wang, H., Tibbitt, M. W., Langer, S. J., Leinwand, L. a & Anseth, K. S. Hydrogels preserve native phenotypes of valvular fibroblasts through an elasticity-regulated PI3K/AKT pathway. *Proc. Natl. Acad. Sci.* **110,** 19336–19341 (2013).

83. Kloxin, A. M., Benton, J. A. & Anseth, K. S. In situ elasticity modulation with dynamic substrates to direct cell phenotype. *Biomaterials* **31,** 1–8 (2010).

84. Wang, H., Haeger, S. S. M., Kloxin, A. M. A., Leinwand, L. A. & Anseth, K. S. Redirecting Valvular Myofibroblasts into Dormant Fibroblasts through Light-mediated Reduction in Substrate Modulus. *PLoS One* **7,** e39969 (2012).

85. Engler, A., Bacakova, L., Newman, C., Hategan, A., Griffin, M. & Discher, D. Substrate compliance versus ligand density in cell on gel responses. *Biophys. J.* **86,** 617–28 (2004).

86. Tse, J. R. & Engler, A. J. Stiffness gradients mimicking in vivo tissue variation regulate mesenchymal stem cell fate. *PLoS One* **6,** e15978 (2011).

87. Zaari, N., Rajagopalan, P., Kim, S. K., Engler, A. J. & Wong, J. Y. Photopolymerization in Microfluidic Gradient Generators: Microscale Control of Substrate Compliance to Manipulate Cell Response. *Adv. Mater.* **16,** 2133–2137 (2004).

88. Kloxin, A. M., Kasko, A. M., Salinas, C. N. & Anseth, K. S. Photodegradable hydrogels for dynamic tuning of physical and chemical properties. *Science* **324,** 59–63 (2009).

89. DeForest, C. A. & Tirrell, D. A. A photoreversible protein-patterning approach for guiding stem cell fate in three-dimensional gels. *Nat. Mater.* **14,** 523–531 (2015).

90. Gandavarapu, N. R., Azagarsamy, M. A. & Anseth, K. S. Photo-Click Living Strategy for Controlled, Reversible Exchange of Biochemical Ligands. *Adv. Mater.* **26,** 2521–2526 (2014).

91. Ruoslahti, E. & Pierschbacher, M. D. New perspectives in cell adhesion: RGD and integrins. *Science* **238,** 491–7 (1987).

92. Hubbell, J. Biomaterials in Tissue Engineering. *Nat. Biotechnol.* **13,** 565–576 (1995).

93. Burdick, J. A. & Anseth, K. S. Photoencapsulation of osteoblasts in injectable RGD-modified PEG hydrogels for bone tissue engineering. *Biomaterials* **23,** 4315–23 (2002).

94. Tavella, S., Bellese, G., Castagnola, P., Martin, I., Piccini, D., Doliana, R., *et al.* Regulated expression of fibronectin, laminin and related integrin receptors during the early chondrocyte differentiation. *J. Cell Sci.* **110,** 2261–70 (1997).

95. DeLise, A. M., Fischer, L. & Tuan, R. S. Cellular interactions and signaling in cartilage development. *Osteoarthr. Cartil.* **8,** 309–34 (2000).

96. Fairbanks, B. D., Schwartz, M. P., Halevi, A. E., Nuttelman, C. R., Bowman, C. N. & Anseth, K. S. A Versatile Synthetic Extracellular Matrix Mimic via Thiol-Norbornene Photopolymerization. *Adv. Mater.* **21,** 5005–5010 (2009).

97. Hoyle, C. E. & Bowman, C. N. Thiol-ene click chemistry. *Angew. Chem. Int. Ed. Engl.* **49,** 1540–73 (2010).

98. Lutolf, M. P., Tirelli, N., Cerritelli, S., Cavalli, L. & Hubbell, J. A. Systematic modulation of Michael-type reactivity of thiols through the use of charged amino acids. *Bioconjug. Chem.* **12,** 1051–6 (2001).

99. Elbert, D. L. & Hubbell, J. A. Conjugate addition reactions combined with free-radical cross-linking for the design of materials for tissue engineering. *Biomacromolecules* **2,** 430–41 (2001).

100. Lutolf, M. P. & Hubbell, J. A. Synthesis and physicochemical characterization of end-linked poly(ethylene glycol)-co-peptide hydrogels formed by Michael-type addition. *Biomacromolecules* **4,** 713–22 (2003).

101. Lutolf, M. P., Raeber, G. P., Zisch, A. H., Tirelli, N. & Hubbell, J. A. Cell-Responsive Synthetic Hydrogels. *Adv. Mater.* **15,** 888–892 (2003).

102. Polizzotti, B. D., Fairbanks, B. D. & Anseth, K. S. Three-dimensional biochemical patterning of click-based composite hydrogels via thiolene photopolymerization. *Biomacromolecules* **9,** 1084–7 (2008).

103. Anderson, S. B., Lin, C.-C., Kuntzler, D. V & Anseth, K. S. The performance of human mesenchymal stem cells encapsulated in cell-degradable polymer-peptide hydrogels. *Biomaterials* **32,** 3564–74 (2011).

104. Benton, J. A., Fairbanks, B. D. & Anseth, K. S. Characterization of valvular interstitial cell function in three dimensional matrix metalloproteinase degradable PEG hydrogels. *Biomaterials* **30,** 6593–603 (2009).

105. Mann, B. K., Gobin, A. S., Tsai, A. T., Schmedlen, R. H. & West, J. L. Smooth muscle cell growth in photopolymerized hydrogels with cell adhesive and proteolytically degradable domains: synthetic ECM analogs for tissue engineering. *Biomaterials* **22,** 3045–51 (2001).

106. Codelli, J. A., Baskin, J. M., Agard, N. J. & Bertozzi, C. R. Second-generation difluorinated cyclooctynes for copper-free click chemistry. *J. Am. Chem. Soc.* **130,** 11486–93 (2008).

107. DeForest, C. A., Polizzotti, B. D. & Anseth, K. S. Sequential click reactions for synthesizing and patterning three-dimensional cell microenvironments. *Nat. Mater.* **8,** 659–64 (2009).

108. DeForest, C. A., Sims, E. A. & Anseth, K. S. Peptide-Functionalized Click Hydrogels with Independently Tunable Mechanics and Chemical Functionality for 3D Cell Culture. *Chem. Mater.* **22,** 4783–4790 (2010).

109. DeForest, C. A. & Anseth, K. S. Cytocompatible click-based hydrogels with dynamically tunable properties through orthogonal photoconjugation and photocleavage reactions. *Nat. Chem.* **3,** 925–931 (2011).

Chapter 2

1. Hogan, B. L. M., Barkauskas, C. E., Chapman, H. A., Epstein, J. A., Jain, R., Hsia, C. C. W., *et al.* Repair and regeneration of the respiratory system: complexity, plasticity, and mechanisms of lung stem cell function. *Cell Stem Cell* **15,** 123–38 (2014).

2. Mason, R. J. Biology of alveolar type II cells. *Respirology* **11,** S12–S15 (2006).

3. Sirianni, F. E., Chu, F. S. F. & Walker, D. C. Human Alveolar Wall Fibroblasts Directly Link Epithelial Type 2 Cells to Capillary Endothelium. *Am. J. Respir. Crit. Care Med.* **168,** 1532–1537 (2003).

4. Herzog, E. L., Brody, A. R., Colby, T. V, Mason, R. & Williams, M. C. Knowns and unknowns of the alveolus. *Proc. Am. Thorac. Soc.* **5,** 778–82 (2008).

5. Tibbitt, M. W. & Anseth, K. S. Hydrogels as extracellular matrix mimics for 3D cell culture. *Biotechnol. Bioeng.* **103,** 655–63 (2009).

6. Lutolf, M. P. & Hubbell, J. A. Synthesis and physicochemical characterization of end-linked poly(ethylene glycol)-co-peptide hydrogels formed by Michael-type addition. *Biomacromolecules* **4,** 713–22 (2003).

7. Fairbanks, B. D., Schwartz, M. P., Halevi, A. E., Nuttelman, C. R., Bowman, C. N. & Anseth, K. S. A Versatile Synthetic Extracellular Matrix Mimic via Thiol-Norbornene Photopolymerization. *Adv. Mater.* **21,** 5005–5010 (2009).

8. Kloxin, A. M., Kasko, A. M., Salinas, C. N. & Anseth, K. S. Photodegradable hydrogels for dynamic tuning of physical and chemical properties. *Science* **324,** 59–63 (2009).

9. Warburton, D., Schwarz, M., Tefft, D., Flores-Delgado, G., Anderson, K. D. & Cardoso, W. V. The molecular basis of lung morphogenesis. *Mech. Dev.* **92,** 55–81 (2000).

10. Yu, W., Fang, X., Ewald, A., Wong, K., Hunt, C. A., Werb, Z., *et al.* Formation of cysts by alveolar type II cells in three-dimensional culture reveals a novel mechanism for epithelial morphogenesis. *Mol. Biol. Cell* **18,** 1693 (2007).

11. Sugihara, H., Toda, S., Miyabara, S., Fujiyama, C. & Yonemitsu, N. Reconstruction of alveolus-like structure from alveolar type II epithelial cells in three-dimensional collagen gel matrix culture. *Am. J. Pathol.* **142,** 783–92 (1993).

12. King, T. E., Pardo, A. & Selman, M. Idiopathic pulmonary fibrosis. *Lancet* **378,** 1949–61 (2011).

13. Thiery, J. P., Acloque, H., Huang, R. Y. J. & Nieto, M. A. Epithelial-mesenchymal transitions in development and disease. *Cell* **139,** 871–90 (2009).

14. Kim, K. K., Kugler, M. C., Wolters, P. J., Robillard, L., Galvez, M. G., Brumwell, A. N., *et al.* Alveolar epithelial cell mesenchymal transition develops in vivo during pulmonary fibrosis and is regulated by the extracellular matrix. *Proc. Natl. Acad. Sci.* **103,** 13180–13185 (2006).

15. Rock, J. R., Barkauskas, C. E., Cronce, M. J., Xue, Y., Harris, J. R., Liang, J., *et al.* Multiple stromal populations contribute to pulmonary fibrosis without evidence for epithelial to mesenchymal transition. *Proc. Natl. Acad. Sci.* **108,** E1475–E1483 (2011).

Chapter 3

1. (a) D. E. Discher, P. Janmey, Y. L. Wang, *Science* 2005, **310**, 1139; (b) V. Vogel, M. P. Sheetz, *Curr. Opin. Cell Biol.* 2009, **21**, 38; (c) M. A. Wozniak, C. S. Chen, *Nat. Rev. Mol. Cell Biol.* 2009, **10**, 34; (d) N. Wang, J. D. Tytell, D. E. Ingber, *Nat. Rev. Mol. Cell Biol.* 2009, **10**, 75; (e) A. J. Keung, S. Kumar, D. V. Schaffer, in *Annual Review of Cell and Developmental Biology, Vol 26*. Annual Reviews: Palo Alto, 2010, vol. 26, pp 533-556.

2. P. Tayalia, D. J. Mooney, *Adv. Mater.* 2009, **21**, 3269.

3. (a) R. A. Marklein, J. A. Burdick, *Adv. Mater.* 2010, **22**, 175; (b) M. P. Lutolf, P. M. Gilbert, H. M. Blau, *Nature* 2009, **462**, 433.

4. (a) D. Warburton, M. Schwarz, D. Tefft, G. Flores-Delgado, K. D. Anderson, W. V. Cardoso, *Mech. Dev.* 2000, **92**, 55; (b) S. Huang, D. E. Ingber, *Nat. Cell Biol.* 1999, **1**, E131; (c) N. Gjorevski, C. M. Nelson, *Birth Defects Res. Part C-Embryo Today-Rev.* 2010, **90**, 193.

5. F. Guilak, D. M. Cohen, B. T. Estes, J. M. Gimble, W. Liedtke, C. S. Chen, *Cell Stem Cell* 2009, **5**.

6. (a) R. McBeath, D. M. Pirone, C. M. Nelson, K. Bhadriraju, C. S. Chen, *Dev. Cell* 2004, **6**, 483; (b) S. Khetan, J. A. Burdick, *Biomaterials* 2010, **31**, 8228.

7. (a) C. M. Nelson, *Biochim. Biophys. Acta-Mol. Cell Res.* 2009, **1793**, 903; (b) C. M. Nelson, M. M. VanDuijn, J. L. Inman, D. A. Fletcher, M. J. Bissell, *Science* 2006, **314**.

8. (a) C. M. Nelson, M. J. Bissell, *Annu. Rev. Cell Dev. Biol.* 2006, **22**; (b) R. Xu, A. Boudreau, M. Bissell, *Cancer Metastasis Rev.* 2009, **28**.

9. (a) C. Moraes, Y. Sun, C. A. Simmons, *Integrative Biology* 2011, **3**; (b) D. H. Kim, P. K. Wong, J. Park, A. Levchenko, Y. Sun, in *Annu. Rev. Biomed. Eng.* Annual Reviews: Palo Alto, 2009, vol. 11, pp 203-233; (c) D. E. Ingber, *Int. J. Dev. Biol.* 2006, **50**, 255.

10. (a) C. S. Chen, M. Mrksich, S. Huang, G. M. Whitesides, D. E. Ingber, *Science* 1997, **276**, 1425; (b) C. M. Nelson, R. P. Jean, J. L. Tan, W. F. Liu, N. J. Sniadecki, A. A. Spector, C. S. Chen, *Proc. Natl. Acad. Sci. U. S. A.* 2005, **102**, 11594; (c) K. A. Kilian, B. Bugarija, B. T. Lahn, M. Mrksich, *Proc. Natl. Acad. Sci. U. S. A.* 2010, **107**, 4872.

11. (a) T. Gudjonsson, L. Ronnov-Jessen, R. Villadsen, M. J. Bissell, O. W. Petersena, *Methods* 2003, **30**, 247; (b) M. J. Bissell, A. Rizki, I. S. Mian, *Curr. Opin. Cell Biol.* 2003, **15**, 753; (c) G. Y. Lee, P. A. Kenny, E. H. Lee, M. J. Bissell, *Nat. Methods* 2007, **4**.

12. N. Gjorevski, C. M. Nelson, *Integrative Biology* 2010, **2**, 424.

13. E. W. Gomez, Q. K. Chen, N. Gjorevski, C. M. Nelson, *J. Cell. Biochem.* 2010, **110**, 44.

14. (a) S. A. Ruiz, C. S. Chen, *Stem Cells* 2008, **26**, 2921; (b) L. Gao, R. McBeath, C. S. Chen, *Stem Cells* 2010, **28**, 564.

15. C. M. Nelson, J. L. Inman, M. J. Bissell, *Nat. Protoc.* 2008, **3**.

16. (a) M. Nikkhah, F. Edalat, S. Manoucheri, A. Khademhosseini, *Biomaterials* 2012, **33**, 5230; (b) O. Z. Fisher, A. Khademhosseini, R. Langer, N. A. Peppas, *Accounts Chem. Res.* 2010, **43**.

17. (a) D. R. Albrecht, V. L. Tsang, R. L. Sah, S. N. Bhatia, *Lab Chip* 2005, **5**, 111; (b) D. R. Albrecht, G. H. Underhill, T. B. Wassermann, R. L. Sah, S. N. Bhatia, *Nat. Methods* 2006, **3**, 369.

18. R. J. Mason, *Respirology* 2006, **11**, S12.

19. C. A. DeForest, K. S. Anseth, *Nat. Chem.* 2011, **3**.

20. (a) C. P. Holmes, *Journal Of Organic Chemistry* 1997, **62**, 2370; (b) J. A. Johnson, J. M. Baskin, C. R. Bertozzi, J. T. Koberstein, N. J. Turro, *Chemical Communications* 2008, 3064; (c) M. Alvarez, A. Best, S. Pradhan-Kadam, K. Koynov, U. Jonas, M. Kreiter, *Adv. Mater.* 2008, **20**, 4563; (d) Y. R. Zhao, Q. Zheng, K. Dakin, K. Xu, M. L. Martinez, W. H. Li, *Journal Of The American Chemical Society* 2004, **126**, 4653; (e) D. Y. Wong, D. R. Griffin, J. Reed, A. M. Kasko, *Macromolecules* 2010, **43**, 2824; (f) A. M. Kloxin, A. M. Kasko, C. N. Salinas, K. S. Anseth, *Science* 2009, **324**, 59; (g) A. M. Kloxin, M. W. Tibbitt, K. S. Anseth, *Nat. Protoc.* 2010, **5**.

21. (a) M. P. Lutolf, J. L. Lauer-Fields, H. G. Schmoekel, A. T. Metters, F. E. Weber, G. B. Fields, J. A. Hubbell, *Proc. Natl. Acad. Sci. U. S. A.* 2003, **100**, 5413; (b) B. D. Fairbanks, M. P. Schwartz, A. E. Halevi, C. R. Nuttelman, C. N. Bowman, K. S. Anseth, *Adv. Mater.* 2009, **21**; (c) J. Patterson, J. A. Hubbell, *Biomaterials* 2010, **31**, 7836; (d) H. Nagase, G. B. Fields, *Biopolymers* 1996, **40**, 1996.

22. C. A. DeForest, B. D. Polizzotti, K. S. Anseth, *Nat. Mater.* 2009, **8**.

23. (a) D. M. Walba, C. A. Liberko, E. Korblova, M. Farrow, T. E. Furtak, B. C. Chow, D. K. Schwartz, A. S. Freeman, K. Douglas, S. D. Williams, A. F. Klittnick, N. A. Clark, *Liq. Cryst.* 2004, **31**, 481; (b) B. J. Adzima, Y. H. Tao, C. J. Kloxin, C. A. DeForest, K. S. Anseth, C. N. Bowman, *Nat. Chem.* 2011, **3**, 256.

24. H. A. Simms, C. A. Bowman, K. S. Anseth, *Biomaterials* 2008, **29**, 2228.

25. (a) A. M. Kloxin, M. W. Tibbitt, A. M. Kasko, J. F. Fairbairn, K. S. Anseth, *Adv. Mater.* 2010, **22**; (b) M. W. Tibbitt, A. M. Kloxin, K. U. Dyamenahalli, K. S. Anseth, *Soft Matter* 2010, **6**.

26. A. E. Rydholm, S. K. Reddy, K. S. Anseth, C. N. Bowman, *Polymer* 2007, **48**.

27. (a) P. J. Flory, J. Rehner, *J. Chem. Phys.* 1943, **11**, 512; (b) P. J. Flory, *Principles of Polymer Chemistry*. Cornell University: 1953; p 672.

28. A. B. Bernard, C. C. Lin, K. S. Anseth, *Tissue Eng.* 2012, **18**, 1.

29. (a) T. Yano, R. J. Mason, T. L. Pan, R. R. Deterding, L. D. Nielsen, J. M. Shannon, *Am. J. Physiol.-Lung Cell. Mol. Physiol.* 2000, **279**, L1146; (b) W. Y. Park, B. Miranda, D. Lebeche, G. Hashimoto, W. V. Cardoso, *Dev. Biol.* 1998, **201**, 125.

30. A. Pardo, K. Ridge, B. Uhal, J. Iasha Sznajder, M. Selman, *The International Journal of Biochemistry & Cell Biology* 1997, **29**, 901.

31. G. P. Raeber, M. P. Lutolf, J. A. Hubbell, *Biophys. J.* 2005, **89**, 1374.

32. S. B. Anderson, C. C. Lin, D. V. Kuntzler, K. S. Anseth, *Biomaterials* 2011, **32**.

33. J. A. Benton, B. D. Fairbanks, K. S. Anseth, *Biomaterials* 2009, **30**.

34. M. Ehrbar, A. Sala, P. Lienemann, A. Ranga, K. Mosiewicz, A. Bittermann, S. C. Rizzi, F. E. Weber, M. P. Lutolf, *Biophys. J.* 2011, **100**, 284.

35. B. K. Mann, A. S. Gobin, A. T. Tsai, R. H. Schmedlen, J. L. West, *Biomaterials* 2001, **22**.

36. C. A. DeForest, E. A. Sims, K. S. Anseth, *Chemistry Of Materials* 2010, **22**.

37. C. A. DeForest, K. S. Anseth, *Angew. Chem.-Int. Edit.* 2011, **51**, 1816.

38. M. C. Williams, *Annu. Rev. Physiol.* 2003, **65**, 669.

39. M. J. Mondrinos, S. Koutzaki, E. Jiwanmall, M. Y. Li, J. P. Dechadarevian, P. I. Lelkes, C. M. Finck, *Tissue Eng.* 2006, **12**, 717.

40. M. Ochs, L. R. Nyengaard, A. Lung, L. Knudsen, M. Voigt, T. Wahlers, J. Richter, H. J. G. Gundersen, *Am. J. Respir. Crit. Care Med.* 2004, **169**, 120.

41. A. Tsuda, N. Filipovic, D. Haberthur, R. Dickie, Y. Matsui, M. Stampanoni, J. C. Schittny, *J. Appl. Physiol.* 2008, **105**, 964.

42. E. L. Herzog, A. R. Brody, T. V. Colby, R. J. Mason, M. C. Williams, *Proceedings of the American Thoracic Society* 2008, **5**, 778.

43. H. Fehrenbach, *Respir. Res.* 2001, **2**, 33.

44. S. Bellusci, J. Grindley, H. Emoto, N. Itoh, B. L. M. Hogan, *Development* 1997, **124**, 4867.

Chapter 4

1. Yu, W., Fang, X., Ewald, A., Wong, K., Hunt, C. A., Werb, Z., *et al.* Formation of cysts by alveolar type II cells in three-dimensional culture reveals a novel mechanism for epithelial morphogenesis. *Mol. Biol. Cell* **18,** 1693 (2007).

2. Sugihara, H., Toda, S., Miyabara, S., Fujiyama, C. & Yonemitsu, N. Reconstruction of alveolus-like structure from alveolar type II epithelial cells in three-dimensional collagen gel matrix culture. *Am. J. Pathol.* **142,** 783–92 (1993).

3. Mondrinos, M. J., Koutzaki, S., Jiwanmall, E., Li, M., Dechadarevian, J.-P., Lelkes, P. I., *et al.* Engineering three-dimensional pulmonary tissue constructs. *Tissue Eng.* **12,** 717–28 (2006).

4. Matter, M. L. & Laurie, G. W. A novel laminin E8 cell adhesion site required for lung alveolar formation in vitro. *J. Cell Biol.* **124,** 1083–90 (1994).

5. Gill, B. J., Gibbons, D. L., Roudsari, L. C., Saik, J. E., Rizvi, Z. H., Roybal, J. D., *et al.* A synthetic matrix with independently tunable biochemistry and mechanical properties to study epithelial morphogenesis and EMT in a lung adenocarcinoma model. *Cancer Res.* **72,** 6013–23 (2012).

6. Sharp, J. A., Cane, K. N., Mailer, S. L., Oosthuizen, W. H., Arnould, J. P. Y. & Nicholas, K. R. Species-specific cell-matrix interactions are essential for differentiation of alveoli like structures and milk gene expression in primary mammary cells of the Cape fur seal (Arctocephalus pusillus pusillus). *Matrix Biol.* **25,** 430–42 (2006).

7. Montesano, R. & Soulié, P. Retinoids induce lumen morphogenesis in mammary epithelial cells. *J. Cell Sci.* **115,** 4419–4431 (2002).

8. Paszek, M. J., Zahir, N., Johnson, K. R., Lakins, J. N., Rozenberg, G. I., Gefen, A., *et al.* Tensional homeostasis and the malignant phenotype. *Cancer Cell* **8,** 241–54 (2005).

9. Bissell, M. J., Rizki, A. & Mian, I. S. Tissue architecture: the ultimate regulator of breast epithelial function. *Curr. Opin. Cell Biol.* **15,** 753–762 (2003).

10. Schumacher, K. M., Phua, S. C., Schumacher, A. & Ying, J. Y. Controlled formation of biological tubule systems in extracellular matrix gels in vitro. *Kidney Int.* **73,** 1187–92 (2008).

11. Martín-Belmonte, F., Yu, W., Rodríguez-Fraticelli, A. E., Ewald, A., Werb, Z., Alonso, M. A., *et al.* Cell-polarity dynamics controls the mechanism of lumen formation in epithelial morphogenesis. *Curr. Biol.* **18,** 507–13 (2008).

12. O'Brien, L., Zegers, M. & Mostov, K. Building epithelial architecture: insights from the three-dimensional culture models. *Nat. Rev. Mol. Cell* **3,** 531–537 (2002).

13. Burri, P. H. Structural aspects of postnatal lung development - Alveolar formation and growth. *Biol. Neonate* **89,** 313–322 (2006).

14. Kitaoka, H., Nieman, G. F., Fujino, Y., Carney, D., DiRocco, J. & Kawase, I. A 4-dimensional model of the alveolar structure. *J. Physiol. Sci.* **57,** 175–185 (2007).

15. Williams, M. C. Alveolar type I cells: molecular phenotype and development. *Annu. Rev. Physiol.* **65,** 669–95 (2003).

16. Mason, R. J. Biology of alveolar type II cells. *Respirology* **11,** S12–S15 (2006).

17. Guillot, L., Nathan, N., Tabary, O., Thouvenin, G., Le Rouzic, P., Corvol, H., *et al.* Alveolar epithelial cells: master regulators of lung homeostasis. *Int. J. Biochem. Cell Biol.* **45,** 2568–73 (2013).

18. Uhal, B. D. Cell cycle kinetics in the alveolar epithelium. *Am. J. Physiol. Cell. Mol. Physiol.* **272,** L1031–1045 (1997).

19. Hogan, B. L. M., Barkauskas, C. E., Chapman, H. A., Epstein, J. A., Jain, R., Hsia, C. C. W., *et al.* Repair and regeneration of the respiratory system: complexity, plasticity, and mechanisms of lung stem cell function. *Cell Stem Cell* **15,** 123–38 (2014).

20. Barkauskas, C., Cronce, M., Rackley, C., Bowie, E., Keene, D., Stripp, B., *et al.* Type 2 alveolar cells are stem cells in adult lung. *J. Clin. Invest.* **123,** 3025–3036 (2013).

21. Park, W. Y., Miranda, B., Lebeche, D., Hashimoto, G. & Cardoso, W. V. FGF-10 is a chemotactic factor for distal epithelial buds during lung development. *Dev. Biol.* **201,** 125–34 (1998).

22. Bellusci, S., Grindley, J., Emoto, H., Itoh, N. & Hogan, B. L. Fibroblast growth factor 10 (FGF10) and branching morphogenesis in the embryonic mouse lung. *Development* **124,** 4867–78 (1997).

23. Tang, N., Marshall, W. F., McMahon, M., Metzger, R. J. & Martin, G. R. Control of Mitotic Spindle Angle by the RAS-Regulated ERK1/2 Pathway Determines Lung Tube Shape. *Science* **333,** 342–345 (2011).

24. Perl, A.-K. T. & Gale, E. FGF signaling is required for myofibroblast differentiation during alveolar regeneration. *Am. J. Physiol. Lung Cell. Mol. Physiol.* **297,** L299–308 (2009).

25. Yano, T., Mason, R. J., Pan, T., Deterding, R. R., Nielsen, L. D. & Shannon, J. M. KGF regulates pulmonary epithelial proliferation and surfactant protein gene expression in adult rat lung. *Am. J. Physiol. Lung Cell. Mol. Physiol.* **279,** L1146–58 (2000).

26. Sugahara, K., Tokumine, J., Teruya, K. & Oshiro, T. Alveolar epithelial cells: differentiation and lung injury. *Respirology* **11,** S28–31 (2006).

27. Crosby, L. M. & Waters, C. M. Epithelial Repair Mechanisms in the Lung. *Am. J. Physiol. Lung Cell. Mol. Physiol.* **298,** 715–731 (2010).

28. Prasad, S., Hogaboam, C. M. & Jarai, G. Deficient repair response of IPF fibroblasts in a co-culture model of epithelial injury and repair. *Fibrogenesis Tissue Repair* **7,** 7 (2014).

29. Isakson, B. E., Seedorf, G. J., Lubman, R. L. & Boitano, S. Heterocellular cultures of pulmonary alveolar epithelial cells grown on laminin-5 supplemented matrix. *In Vitro Cell. Dev. Biol. Anim.* **38,** 443–9 (2002).

30. Bhaskaran, M., Kolliputi, N., Wang, Y., Gou, D., Chintagari, N. R., Liu, L., *et al.* Trans-differentiation of Alveolar Epithelial Type II Cells to Type I Cells Involves Autocrine Signaling by Transforming Growth Factor ␤1 through the Smad Pathway *. *J. Biol. Chem.* **282,** 3968 –3976 (2007).

31. Qiao, R., Yan, W., Clavijo, C., Mehrian-Shai, R., Zhong, Q., Kim, K.-J., *et al.* Effects of KGF on alveolar epithelial cell transdifferentiation are mediated by JNK signaling. *Am. J. Respir. Cell Mol. Biol.* **38,** 239–46 (2008).

32. Wang, J., Edeen, K., Manzer, R., Chang, Y., Wang, S., Chen, X., *et al.* Differentiated human alveolar epithelial cells and reversibility of their phenotype in vitro. *Am. J. Respir. Cell Mol. Biol.* **36,** 661–8 (2007).

33. Umino, T., Wang, H., Zhu, Y., Liu, X., Manouilova, L. S., Spurzem, J. R., *et al.* Modification of type I collagenous gels by alveolar epithelial cells. *Am. J. Respir. Cell Mol. Biol.* **22,** 702–707 (2000).

34. Bissell, M. J., Kenny, P. A. & Radisky, D. C. Microenvironmental regulators of tissue structure and function also regulate tumor induction and progression: the role of extracellular matrix and its degrading enzymes. *Cold Spring Harb. Symp. Quant. Biol.* **70,** 343–56 (2005).

35. Griffith, L. G. & Swartz, M. A. Capturing complex 3D tissue physiology in vitro. *Nat. Rev. Mol. Cell Biol.* **7,** 211–24 (2006).

36. Ochs, M., Nyengaard, J. R., Jung, A., Knudsen, L., Voigt, M., Wahlers, T., *et al.* The number of alveoli in the human lung. *Am. J. Respir. Crit. Care Med.* **169,** 120–4 (2004).

37. Carterson, A., Bentrup, K. zu, Ott, C., Clarke, M., Pierson, D., Vanderburg, C., *et al.* A549 Lung Epithelial Cells Grown as Three-Dimensional Aggregates : Alternative Tissue Culture Model for Pseudomonas aeruginosa Pathogenesis. *Infect. Immun.* **73,** 1129–1140 (2005).

38. Tibbitt, M. W. & Anseth, K. S. Hydrogels as extracellular matrix mimics for 3D cell culture. *Biotechnol. Bioeng.* **103,** 655–63 (2009).

39. Lewis, K. J. R. & Anseth, K. S. Hydrogel scaffolds to study cell biology in four dimensions. *MRS Bull.* **38,** 260–268 (2013).

40. Salinas, C. N. & Anseth, K. S. The enhancement of chondrogenic differentiation of human mesenchymal stem cells by enzymatically regulated RGD functionalities. *Biomaterials* **29,** 2370–7 (2008).

41. Benton, J. A., Fairbanks, B. D. & Anseth, K. S. Characterization of valvular interstitial cell function in three dimensional matrix metalloproteinase degradable PEG hydrogels. *Biomaterials* **30,** 6593–603 (2009).

42. Kloxin, A. M., Lewis, K. J. R., Deforest, C. A., Seedorf, G., Tibbitt, M. W., Balasubramaniam, V., *et al.* Responsive culture platform to examine the influence of microenvironmental geometry on cell function in 3D. *Integr. Biol.* **4,** 1540–1549 (2012).

43. McKinnon, D. D., Kloxin, A. M. & Anseth, K. S. Synthetic hydrogel platform for three-dimensional culture of embryonic stem cell-derived motor neurons. *Biomater. Sci.* **1,** 460 (2013).

44. Fairbanks, B. D., Schwartz, M. P., Halevi, A. E., Nuttelman, C. R., Bowman, C. N. & Anseth, K. S. A Versatile Synthetic Extracellular Matrix Mimic via Thiol-Norbornene Photopolymerization. *Adv. Mater.* **21,** 5005–5010 (2009).

45. Kloxin, A. M., Kasko, A. M., Salinas, C. N. & Anseth, K. S. Photodegradable hydrogels for dynamic tuning of physical and chemical properties. *Science* **324,** 59–63 (2009).

46. Kloxin, A. M., Tibbitt, M. W. & Anseth, K. S. Synthesis of photodegradable hydrogels as dynamically tunable cell culture platforms. *Nat. Protoc.* **5,** 1867–87 (2010).

47. Tibbitt, M. W., Han, B. W., Kloxin, A. M. & Anseth, K. S. SFB Student Award Winner in the Ph.D. Category: Synthesis and application of photodegradable microspheres for spatiotemporal control of protein delivery. *J. Biomed. Mater. Res. Part A* **100A,** 1647–1654 (2012).

48. Tibbitt, M., Kloxin, A., Sawicki, L. & Anseth, K. Mechanical Properties and Degradation of Chain and Step- Polymerized Photodegradable Hydrogels. *Macromolecules* **46,** 2785–2792 (2013).

49. Michalet, X. Mean square displacement analysis of single-particle trajectories with localization error: Brownian motion in an isotropic medium. *Phys. Rev. E* **82,** 041914 (2010).

50. Ernst, D. & Köhler, J. Measuring a diffusion coefficient by single-particle tracking: statistical analysis of experimental mean squared displacement curves. *Phys. Chem. Chem. Phys.* **15,** 845–9 (2013).

51. Shenoy, R., Tibbitt, M. W., Anseth, K. S. & Bowman, C. N. Formation of Core-Shell Particles by Interfacial Radical Polymerization Initiated by a Glucose Oxidase-Mediated Redox System. *Chem. Mater.* **25,** 761–767 (2013).

52. Gould, S. T., Darling, N. J. & Anseth, K. S. Small peptide functionalized thiol-ene hydrogels as culture substrates for understanding valvular interstitial cell activation and de novo tissue deposition. *Acta Biomater.* **8,** 3201–9 (2012).

53. Fairbanks, B. D., Schwartz, M. P., Bowman, C. N. & Anseth, K. S. Photoinitiated polymerization of PEG-diacrylate with lithium phenyl-2,4,6-trimethylbenzoylphosphinate: polymerization rate and cytocompatibility. *Biomaterials* **30,** 6702–7 (2009).

54. Herzog, E. L., Brody, A. R., Colby, T. V, Mason, R. & Williams, M. C. Knowns and unknowns of the alveolus. *Proc. Am. Thorac. Soc.* **5,** 778–82 (2008).

55. Soutiere, S. E., Tankersley, C. G. & Mitzner, W. Differences in alveolar size in inbred mouse strains. *Respir. Physiol. Neurobiol.* **140,** 283–91 (2004).

56. Lutolf, M. P., Lauer-Fields, J. L., Schmoekel, H. G., Metters, A. T., Weber, F. E., Fields, G. B., *et al.* Synthetic matrix metalloproteinase-sensitive hydrogels for the conduction of tissue regeneration: engineering cell-invasion characteristics. *Proc. Natl. Acad. Sci. U. S. A.* **100,** 5413–8 (2003).

57. Kyburz, K. A. & Anseth, K. S. Three-dimensional hMSC motility within peptide-functionalized PEG-based hydrogels of varying adhesivity and crosslinking density. *Acta Biomater.* **9,** 6381–92 (2013).

58. Cavalcante, F. S. A., Ito, S., Brewer, K., Sakai, H., Alencar, A. M., Almeida, M. P., *et al.* Mechanical interactions between collagen and proteoglycans: implications for the stability of lung tissue. *J. Appl. Physiol.* **98,** 672–9 (2005).

59. Levental, I., Georges, P. C. & Janmey, P. A. Soft biological materials and their impact on cell function. *Soft Matter* **3,** 299–306 (2007).

60. Foster, K. A., Oster, C. G., Mayer, M. M., Avery, M. L. & Audus, K. L. Characterization of the A549 cell line as a type II pulmonary epithelial cell model for drug metabolism. *Exp. Cell Res.* **243,** 359–66 (1998).

61. Isakson, B., Lubman, R., Seedorf, G. & Boitano, S. Modulation of pulmonary alveolar type II cell phenotype and communication by extracellular matrix and KGF. *Am J Physiol Cell Physiol* **281,** C1291–C1299 (2001).

Chapter 5

1. Herzog, E. L., Brody, A. R., Colby, T. V, Mason, R. & Williams, M. C. Knowns and unknowns of the alveolus. *Proc. Am. Thorac. Soc.* **5,** 778–82 (2008).

2. Hogan, B. L. M., Barkauskas, C. E., Chapman, H. A., Epstein, J. A., Jain, R., Hsia, C. C. W., *et al.* Repair and regeneration of the respiratory system: complexity, plasticity, and mechanisms of lung stem cell function. *Cell Stem Cell* **15,** 123–38 (2014).

3. Sirianni, F. E., Chu, F. S. F. & Walker, D. C. Human Alveolar Wall Fibroblasts Directly Link Epithelial Type 2 Cells to Capillary Endothelium. *Am. J. Respir. Crit. Care Med.* **168,** 1532–1537 (2003).

4. Bellusci, S., Grindley, J., Emoto, H., Itoh, N. & Hogan, B. L. Fibroblast growth factor 10 (FGF10) and branching morphogenesis in the embryonic mouse lung. *Development* **124,** 4867–78 (1997).

5. Selman, M., Thannickal, V. J., Pardo, A., Zisman, D. A., Martinez, F. J. & Lynch, J. P. Idiopathic Pulmonary Fibrosis. *Drugs* **64,** 405–430 (2004).

6. King, T. E., Pardo, A. & Selman, M. Idiopathic pulmonary fibrosis. *Lancet* **378,** 1949–61 (2011).

7. Thiery, J. P., Acloque, H., Huang, R. Y. J. & Nieto, M. A. Epithelial-mesenchymal transitions in development and disease. *Cell* **139,** 871–90 (2009).

8. Marchand-Adam, S., Marchal, J., Cohen, M., Soler, P., Gerard, B., Castier, Y., *et al.* Defect of hepatocyte growth factor secretion by fibroblasts in idiopathic pulmonary fibrosis. *Am. J. Respir. Crit. Care Med.* **168,** 1156–61 (2003).

9. Selman, M. & Pardo, A. Role of epithelial cells in idiopathic pulmonary fibrosis: from innocent targets to serial killers. *Proc. Am. Thorac. Soc.* **3,** 364–372 (2006).

10. Kim, K. K., Kugler, M. C., Wolters, P. J., Robillard, L., Galvez, M. G., Brumwell, A. N., *et al.* Alveolar epithelial cell mesenchymal transition develops in vivo during pulmonary fibrosis and is regulated by the extracellular matrix. *Proc. Natl. Acad. Sci.* **103,** 13180–13185 (2006).

11. Rock, J. R., Barkauskas, C. E., Cronce, M. J., Xue, Y., Harris, J. R., Liang, J., *et al.* Multiple stromal populations contribute to pulmonary fibrosis without evidence for epithelial to mesenchymal transition. *Proc. Natl. Acad. Sci.* **108,** E1475–E1483 (2011).

12. Kumarswamy, R., Mudduluru, G., Ceppi, P., Muppala, S., Kozlowski, M., Niklinski, J., *et al.* MicroRNA-30a inhibits epithelial-to-mesenchymal transition by targeting Snai1 and is downregulated in non-small cell lung cancer. *Int. J. Cancer* **130,** 2044–53 (2012).

13. Bhowmick, N., Neilson, E. & Moses, H. Stromal fibroblasts in cancer initiation and progression. *Nature* **432,** 332–337 (2004).

14. Amann, A., Zwierzina, M., Gamerith, G., Bitsche, M., Huber, J. M., Vogel, G. F., *et al.* Development of an innovative 3D cell culture system to study tumour--stroma interactions in non-small cell lung cancer cells. *PLoS One* **9,** e92511 (2014).

15. Fromigué, O., Louis, K., Dayem, M., Milanini, J., Pages, G., Tartare-Deckert, S., *et al.* Gene expression profiling of normal human pulmonary fibroblasts following coculture with non-small-cell lung cancer cells reveals alterations related to matrix degradation, angiogenesis, cell growth and survival. *Oncogene* **22,** 8487–97 (2003).

16. Wang, W., Li, Q., Yamada, T., Matsumoto, K., Matsumoto, I., Oda, M., *et al.* Crosstalk to stromal fibroblasts induces resistance of lung cancer to epidermal growth factor receptor tyrosine kinase inhibitors. *Clin. Cancer Res.* **15,** 6630–8 (2009).

17. Prasad, S., Hogaboam, C. M. & Jarai, G. Deficient repair response of IPF fibroblasts in a co-culture model of epithelial injury and repair. *Fibrogenesis Tissue Repair* **7,** 7 (2014).

18. Wang, X. & Kaplan, D. L. Hormone-responsive 3D multicellular culture model of human breast tissue. *Biomaterials* **33,** 3411–3420 (2012).

19. Horie, M., Saito, A., Mikami, Y., Ohshima, M., Morishita, Y., Nakajima, J., *et al.* Characterization of human lung cancer-associated fibroblasts in three-dimensional in vitro co-culture model. *Biochem. Biophys. Res. Commun.* **423,** 158–63 (2012).

20. Fang, X., Sittadjody, S., Gyabaah, K., Opara, E. C. & Balaji, K. C. Novel 3D Co-Culture Model for Epithelial-Stromal Cells Interaction in Prostate Cancer. *PLoS One* **8,** 1–11 (2013).

21. Kim, S.-A., Lee, E. K. & Kuh, H.-J. Co-culture of 3D tumor spheroids with fibroblasts as a model for epithelial–mesenchymal transition in vitro. *Exp. Cell Res.* **335,** 187–196 (2015).

22. Majety, M., Pradel, L. P., Gies, M. & Ries, C. H. Fibroblasts Influence Survival and Therapeutic Response in a 3D Co-Culture Model. *PLoS One* **10,** e0127948 (2015).

23. Friedrich, J., Ebner, R. & Kunz-Schughart, L. A. Experimental anti-tumor therapy in 3-D: spheroids--old hat or new challenge? *Int. J. Radiat. Biol.* **83,** 849–871 (2007).

24. Weiswald, L.-B., Bellet, D. & Dangles-Marie, V. Spherical Cancer Models in Tumor Biology. *Neoplasia* **17,** 1–15 (2015).

25. Lewis, K. J. R., Tibbitt, M. W., Zhao, Y., Branchfield, K., Sun, X., Balasubramaniam, V., *et al.* In vitro model alveoli from photodegradable microsphere templates. *Biomater. Sci.* **3,** 821–832 (2015).

26. Lewis, K. J. R. & Anseth, K. S. Hydrogel scaffolds to study cell biology in four dimensions. *MRS Bull.* **38,** 260–268 (2013).

27. Kloxin, A. M., Kasko, A. M., Salinas, C. N. & Anseth, K. S. Photodegradable hydrogels for dynamic tuning of physical and chemical properties. *Science* **324,** 59–63 (2009).

28. Tibbitt, M. W., Han, B. W., Kloxin, A. M. & Anseth, K. S. SFB Student Award Winner in the Ph.D. Category: Synthesis and application of photodegradable microspheres for spatiotemporal control of protein delivery. *J. Biomed. Mater. Res. Part A* **100A,** 1647–1654 (2012).

29. Kloxin, A. M., Tibbitt, M. W. & Anseth, K. S. Synthesis of photodegradable hydrogels as dynamically tunable cell culture platforms. *Nat. Protoc.* **5,** 1867–87 (2010).

30. Cruise, G. M., Scharp, D. S. & Hubbell, J. a. Characterization of permeability and network structure of interfacially photopolymerized poly(ethylene glycol) diacrylate hydrogels. *Biomaterials* **19,** 1287–1294 (1998).

31. Kloxin, A. M., Lewis, K. J. R., Deforest, C. A., Seedorf, G., Tibbitt, M. W., Balasubramaniam, V., *et al.* Responsive culture platform to examine the influence of microenvironmental geometry on cell function in 3D. *Integr. Biol.* **4,** 1540–1549 (2012).

32. Gould, S. T., Darling, N. J. & Anseth, K. S. Small peptide functionalized thiol-ene hydrogels as culture substrates for understanding valvular interstitial cell activation and de novo tissue deposition. *Acta Biomater.* **8,** 3201–9 (2012).

33. Fairbanks, B. D., Schwartz, M. P., Bowman, C. N. & Anseth, K. S. Photoinitiated polymerization of PEG-diacrylate with lithium phenyl-2,4,6-trimethylbenzoylphosphinate: polymerization rate and cytocompatibility. *Biomaterials* **30,** 6702–7 (2009).

34. Schwartz, M. P., Rogers, R. E., Singh, S. P., Lee, J. Y., Loveland, S. G., Koepsel, J. T., *et al.* A quantitative comparison of human HT-1080 fibrosarcoma cells and primary human dermal fibroblasts identifies a 3D migration mechanism with properties unique to the transformed phenotype. *PLoS One* **8,** 1–24 (2013).

35. Franzdóttir, S. R., Axelsson, I. T., Arason, A. J., Baldursson, O., Gudjonsson, T. & Magnusson, M. K. Airway branching morphogenesis in three dimensional culture. *Respir. Res.* **11,** 162 (2010).

36. Choe, C., Shin, Y.-S., Kim, S.-H., Jeon, M.-J., Choi, S.-J., Lee, J., *et al.* Tumor–stromal Interactions with Direct Cell Contacts Enhance Motility of Non-small Cell Lung Cancer Cells Through the Hedgehog Signaling Pathway. *Anticancer Res.* **33,** 3715–3723 (2013).

37. Suganuma, H., Sato, A., Tamura, R. & Chida, K. Enhanced migration of fibroblasts derived from lungs with fibrotic lesions. *Thorax* **50,** 984–989 (1995).

38. Vuorinen, K., Gao, F., Oury, T. D., Kinnula, V. L. & Myllärniemi, M. Imatinib mesylate inhibits fibrogenesis in asbestos-induced interstitial pneumonia. *Exp. Lung Res.* **33,** 357–373 (2007).

39. Crosby, L. M. & Waters, C. M. Epithelial Repair Mechanisms in the Lung. *Am. J. Physiol. Lung Cell. Mol. Physiol.* **298,** 715–731 (2010).

40. Kyburz, K. A. & Anseth, K. S. Three-dimensional hMSC motility within peptide-functionalized PEG-based hydrogels of varying adhesivity and crosslinking density. *Acta Biomater.* **9,** 6381–92 (2013).

41. Willis, B. C. & Borok, Z. TGF-beta-induced EMT: mechanisms and implications for fibrotic lung disease. *Am. J. Physiol. Lung Cell. Mol. Physiol.* **293,** L525–34 (2007).

42. Willis, B. C., Liebler, J. M., Luby-Phelps, K., Nicholson, A. G., Crandall, E. D., du Bois, R. M., *et al.* Induction of epithelial-mesenchymal transition in alveolar epithelial cells by transforming growth factor-beta1: potential role in idiopathic pulmonary fibrosis. *Am. J. Pathol.* **166,** 1321–1332 (2005).

43. Carterson, A., Bentrup, K. zu, Ott, C., Clarke, M., Pierson, D., Vanderburg, C., *et al.* A549 Lung Epithelial Cells Grown as Three-Dimensional Aggregates : Alternative Tissue Culture Model for Pseudomonas aeruginosa Pathogenesis. *Infect. Immun.* **73,** 1129–1140 (2005).

44. Puliafito, A., Hufnagel, L., Neveu, P., Streichan, S., Sigal, A., Fygenson, D. K., *et al.* Collective and single cell behavior in epithelial contact inhibition. *Proc. Natl. Acad. Sci.* **109,** 739–744 (2012).

45. Rejniak, K. A., Wang, S. E., Bryce, N. S., Chang, H., Parvin, B., Jourquin, J., *et al.* Linking changes in epithelial morphogenesis to cancer mutations using computational modeling. *PLoS Comput. Biol.* **6,** (2010).

46. Doyle, A. D., Wang, F. W., Matsumoto, K. & Yamada, K. M. One-dimensional topography underlies three-dimensional fi brillar cell migration. *J. Cell Biol.* **184,** 481–490 (2009).

47. Peyton, S. R., Kalcioglu, Z. I., Cohen, J. C., Runkle, A. P., Van Vliet, K. J., Lauffenburger, D. a., *et al.* Marrow-Derived stem cell motility in 3D synthetic scaffold is governed by geometry along with adhesivity and stiffness. *Biotechnol. Bioeng.* **108,** 1181–1193 (2011).

48. Guillot, L., Nathan, N., Tabary, O., Thouvenin, G., Le Rouzic, P., Corvol, H., *et al.* Alveolar epithelial cells: master regulators of lung homeostasis. *Int. J. Biochem. Cell Biol.* **45,** 2568–73 (2013).

49. Fehrenbach, H. Alveolar epithelial type II cell: defender of the alveolus revisited. *Respir. Res.* **2,** 33–46 (2001).

50. Mason, R. J. Biology of alveolar type II cells. *Respirology* **11,** S12–S15 (2006).

51. Aragona, M., Panciera, T., Manfrin, A., Giulitti, S., Michielin, F., Elvassore, N., *et al.* A mechanical checkpoint controls multicellular growth through YAP/TAZ regulation by actin-processing factors. *Cell* **154,** 1047–1059 (2013).

52. Lutolf, M. P., Lauer-Fields, J. L., Schmoekel, H. G., Metters, A. T., Weber, F. E., Fields, G. B., *et al.* Synthetic matrix metalloproteinase-sensitive hydrogels for the conduction of tissue regeneration: engineering cell-invasion characteristics. *Proc. Natl. Acad. Sci. U. S. A.* **100,** 5413–8 (2003).

53. Fairbanks, B. D., Schwartz, M. P., Halevi, A. E., Nuttelman, C. R., Bowman, C. N. & Anseth, K. S. A Versatile Synthetic Extracellular Matrix Mimic via Thiol-Norbornene Photopolymerization. *Adv. Mater.* **21,** 5005–5010 (2009).

54. Pardo, A., Gibson, K., Cisneros, J., Richards, T. J., Yang, Y., Becerril, C., *et al.* Up-regulation and profibrotic role of osteopontin in human idiopathic pulmonary fibrosis. *PLoS Med.* **2,** 0891–0903 (2005).

Chapter 6

1. Fehrenbach, H. Alveolar epithelial type II cell: defender of the alveolus revisited. *Respir. Res.* **2,** 33–46 (2001).

2. Herzog, E. L., Brody, A. R., Colby, T. V, Mason, R. & Williams, M. C. Knowns and unknowns of the alveolus. *Proc. Am. Thorac. Soc.* **5,** 778–82 (2008).

3. Crosby, L. M. & Waters, C. M. Epithelial Repair Mechanisms in the Lung. *Am. J. Physiol. Lung Cell. Mol. Physiol.* **298,** 715–731 (2010).

4. Hogan, B. L. M., Barkauskas, C. E., Chapman, H. A., Epstein, J. A., Jain, R., Hsia, C. C. W., *et al.* Repair and regeneration of the respiratory system: complexity, plasticity, and mechanisms of lung stem cell function. *Cell Stem Cell* **15,** 123–38 (2014).

5. King, T. E., Pardo, A. & Selman, M. Idiopathic pulmonary fibrosis. *Lancet* **378,** 1949–61 (2011).

6. Thiery, J. P., Acloque, H., Huang, R. Y. J. & Nieto, M. A. Epithelial-mesenchymal transitions in development and disease. *Cell* **139,** 871–90 (2009).

7. Bellusci, S., Grindley, J., Emoto, H., Itoh, N. & Hogan, B. L. Fibroblast growth factor 10 (FGF10) and branching morphogenesis in the embryonic mouse lung. *Development* **124,** 4867–78 (1997).

8. Park, W. Y., Miranda, B., Lebeche, D., Hashimoto, G. & Cardoso, W. V. FGF-10 is a chemotactic factor for distal epithelial buds during lung development. *Dev. Biol.* **201,** 125–34 (1998).

9. Bhaskaran, M., Kolliputi, N., Wang, Y., Gou, D., Chintagari, N. R. & Liu, L. Trans-differentiation of Alveolar Epithelial Type II Cells to Type I Cells Involves Autocrine Signaling by Transforming Growth Factor beta1 through the Smad Pathway. *J. Biol. Chem.* **282,** 3968–3976 (2006).

10. Qiao, R., Yan, W., Clavijo, C., Mehrian-Shai, R., Zhong, Q., Kim, K.-J., *et al.* Effects of KGF on alveolar epithelial cell transdifferentiation are mediated by JNK signaling. *Am. J. Respir. Cell Mol. Biol.* **38,** 239–46 (2008).

11. Isakson, B. E., Lubman, R. L., Seedorf, G. J. & Boitano, S. Modulation of pulmonary alveolar type II cell phenotype and communication by extracellular matrix and KGF. *Am. J. Physiol. Cell Physiol.* **281,** C1291–C1299 (2001).

12. Isakson, B., Lubman, R., Seedorf, G. & Boitano, S. Modulation of pulmonary alveolar type II cell phenotype and communication by extracellular matrix and KGF. *Am J Physiol Cell Physiol* **281,** C1291–C1299 (2001).

13. Gould, S. T., Darling, N. J. & Anseth, K. S. Small peptide functionalized thiol-ene hydrogels as culture substrates for understanding valvular interstitial cell activation and de novo tissue deposition. *Acta Biomater.* **8,** 3201–9 (2012).

14. Ali, S., Saik, J. E., Gould, D. J., Dickinson, M. E. & West, J. L. Immobilization of Cell-Adhesive Laminin Peptides in Degradable PEGDA Hydrogels Influences Endothelial Cell Tubulogenesis. *Biores. Open Access* **2,** 241–249 (2013).

15. Matter, M. L. & Laurie, G. W. A novel laminin E8 cell adhesion site required for lung alveolar formation in vitro. *J. Cell Biol.* **124,** 1083–90 (1994).

16. Mabry, K. M. P. The Role of Matrix Properties in Directing Valvular Interstitial Cell Phenotype. (2015).

17. Ochs, M., Nyengaard, J. R., Jung, A., Knudsen, L., Voigt, M., Wahlers, T., *et al.* The number of alveoli in the human lung. *Am. J. Respir. Crit. Care Med.* **169,** 120–4 (2004).

18. Stone, K. C., Mercer, R. R., Gehr, P., Stockstill, B. & Crapo, J. D. Allometric relationships of cell numbers and size in the mammalian lung. *Am. J. Respir. Cell Mol. Biol.* **6,** 235–43 (1992).

19. Zhang, X., Xi, W., Chatani, S., Podgorski, M. & Bowman, C. Light controlled thiol-Michael addition initiated by photocaged superbases. in *Abstr. Pap. 249th ACS Natl. Meet. Expo. Denver, CO, United States, March 22-26, 2015* POLY–303 (American Chemical Society, 2015).

20. Gill, B. J., Gibbons, D. L., Roudsari, L. C., Saik, J. E., Rizvi, Z. H., Roybal, J. D., *et al.* A synthetic matrix with independently tunable biochemistry and mechanical properties to study epithelial morphogenesis and EMT in a lung adenocarcinoma model. *Cancer Res.* **72,** 6013–23 (2012).

21. Yu, W., Fang, X., Ewald, A., Wong, K., Hunt, C. A., Werb, Z., *et al.* Formation of cysts by alveolar type II cells in three-dimensional culture reveals a novel mechanism for epithelial morphogenesis. *Mol. Biol. Cell* **18,** 1693 (2007).

22. Sugihara, H., Toda, S., Miyabara, S., Fujiyama, C. & Yonemitsu, N. Reconstruction of alveolus-like structure from alveolar type II epithelial cells in three-dimensional collagen gel matrix culture. *Am. J. Pathol.* **142,** 783–92 (1993).

23. Mondrinos, M. J., Koutzaki, S., Jiwanmall, E., Li, M., Dechadarevian, J.-P., Lelkes, P. I., *et al.* Engineering three-dimensional pulmonary tissue constructs. *Tissue Eng.* **12,** 717–28 (2006).

24. Kim, K. K., Kugler, M. C., Wolters, P. J., Robillard, L., Galvez, M. G., Brumwell, A. N., *et al.* Alveolar epithelial cell mesenchymal transition develops in vivo during pulmonary fibrosis and is regulated by the extracellular matrix. *Proc. Natl. Acad. Sci.* **103,** 13180–13185 (2006).

25. Bhowmick, N., Neilson, E. & Moses, H. Stromal fibroblasts in cancer initiation and progression. *Nature* **432,** 332–337 (2004).

26. Fromigué, O., Louis, K., Dayem, M., Milanini, J., Pages, G., Tartare-Deckert, S., *et al.* Gene expression profiling of normal human pulmonary fibroblasts following coculture with non-small-cell lung cancer cells reveals alterations related to matrix degradation, angiogenesis, cell growth and survival. *Oncogene* **22,** 8487–97 (2003).

27. Leight, J. L., Alge, D. L., Maier, A. J. & Anseth, K. S. Direct measurement of matrix metalloproteinase activity in 3D cellular microenvironments using a fluorogenic peptide substrate. *Biomaterials* **34,** 7344–52 (2013).

28. Leight, J. L., Tokuda, E. Y., Jones, C. E., Lin, A. J. & Anseth, K. S. Multifunctional bioscaffolds for 3D culture of melanoma cells reveal increased MMP activity and migration with BRAF kinase inhibition. *Proc. Natl. Acad. Sci.* **112,** 201505662 (2015).

29. Pardo, A., Gibson, K., Cisneros, J., Richards, T. J., Yang, Y., Becerril, C., *et al.* Up-regulation and profibrotic role of osteopontin in human idiopathic pulmonary fibrosis. *PLoS Med.* **2,** 0891–0903 (2005).

30. Selman, M., Thannickal, V. J., Pardo, A., Zisman, D. A., Martinez, F. J. & Lynch, J. P. Idiopathic Pulmonary Fibrosis. *Drugs* **64,** 405–430 (2004).

31. Mason, R. J. Biology of alveolar type II cells. *Respirology* **11,** S12–S15 (2006).

32. Marchand-Adam, S., Marchal, J., Cohen, M., Soler, P., Gerard, B., Castier, Y., *et al.* Defect of hepatocyte growth factor secretion by fibroblasts in idiopathic pulmonary fibrosis. *Am. J. Respir. Crit. Care Med.* **168,** 1156–61 (2003).

33. Willis, B. C., Liebler, J. M., Luby-Phelps, K., Nicholson, A. G., Crandall, E. D., du Bois, R. M., *et al.* Induction of epithelial-mesenchymal transition in alveolar epithelial cells by transforming growth factor-beta1: potential role in idiopathic pulmonary fibrosis. *Am. J. Pathol.* **166,** 1321–1332 (2005).

34. McCall, J. D., Luoma, J. E. & Anseth, K. S. Covalently tethered transforming growth factor beta in PEG hydrogels promotes chondrogenic differentiation of encapsulated human mesenchymal stem cells. *Drug Deliv. Transl. Res.* **2,** 305–312 (2012).

35. Jeppesen, D. K., Hvam, M. L., Primdahl-Bengtson, B., Boysen, A. T., Whitehead, B., Dyrskjøt, L., *et al.* Comparative analysis of discrete exosome fractions obtained by differential centrifugation. *J. Extracell. Vesicles* **3,** 1–16 (2014).

36. Watanabe, K., Kurihara, K., Tokunaga, Y. & Hayaishi, O. Two types of microsomal prostaglandin E synthase: glutathione-dependent and -independent prostaglandin E synthases. *Biochem. Biophys. Res. Commun.* **235,** 148–152 (1997).

37. Wei, B., Cai, L., Sun, D., Wang, Y., Wang, C., Chai, X., *et al.* Microsomal prostaglandin e synthase-1 deficiency exacerbates pulmonary fibrosis induced by bleomycin in mice. *Molecules* **19,** 4967–4985 (2014).

38. Takahashi, R., Amano, H., Satoh, T., Tabata, K., Ikeda, M., Kitasato, H., *et al.* Roles of microsomal prostaglandin E synthase-1 in lung metastasis formation in prostate cancer RM9 cells. *Biomed. Pharmacother.* **68,** 71–77 (2014).

39. Anderson, I. C., Mari, S. E., Broderick, R. J., Mari, B. P. & Shipp, M. A. The angiogenic factor interleukin 8 is induced in non-small cell lung cancer/pulmonary fibroblast cocultures. *Cancer Res.* **60,** 269–272 (2000).

40. Bedran, T. B. L., Mayer, M. P. A., Spolidorio, D. P. & Grenier, D. Synergistic Anti-Inflammatory Activity of the Antimicrobial Peptides Human Beta-Defensin-3 (hBD-3) and Cathelicidin (LL-37) in a Three-Dimensional Co-Culture Model of Gingival Epithelial Cells and Fibroblasts. *PLoS One* **9,** e106766 (2014).

41. Baranski, J. D., Chaturvedi, R. R., Stevens, K. R., Eyckmans, J., Carvalho, B., Solorzano, R. D., *et al.* Geometric control of vascular networks to enhance engineered tissue integration and function. *Proc. Natl. Acad. Sci.* **110,** 7586–7591 (2013).

42. Doerschuk, C. M., Beyers, N., Coxson, H. O., Wiggs, B. & Hogg, J. C. Comparison of neutrophil and capillary diameters and their relation to neutrophil sequestration in the lung. *J. Appl. Physiol.* **74,** 3040–3045 (1993).

Chapter 8

Appendix: Epithelial-mesenchymal crosstalk influences cellular behavior in a 3D alveolus-fibroblast model system

As submitted to *Biomaterials*, 2016

8.1 Abstract

Interactions between lung epithelium and interstitial fibroblasts are increasingly recognized as playing a major role in the progression of several lung pathologies, including cancer. Three-dimensional *in vitro* co-culture systems offer tissue-relevant platforms that spatially position cells at physiologically relevant distances for studying the signaling interplay between diseased and healthy cell types. Such systems provide a controlled environment in which to probe the mechanisms involved in epithelial-mesenchymal crosstalk. To recapitulate the native alveolar tissue architecture, we employed a cyst templating technique to culture alveolar epithelial cells on photodegradable microspheres and subsequently encapsulated the cell-laden spheres within poly(ethylene glycol) (PEG) hydrogels containing dispersed pulmonary fibroblasts. A normal fibroblast cell line was co-cultured with either normal mouse alveolar epithelial primary cells or a cancerous alveolar epithelial cell line to probe the influence of tumor-stromal proximity on cell behavior. Using this 3D co-culture model, cancerous epithelial cells and normal fibroblasts had significantly higher proliferation rates in co-culture (45% and 12%, respectively) compared to single cells or any other cell combination, indicating a potential reciprocal relationship between their signaling pathways. When examining fibroblast motility, the normal fibroblasts migrated significantly faster when co-cultured with cancerous A549 cells (15 μm/h) compared to monoculture (7 μm/h). Finally, a fluorescent peptide reporter for matrix metalloproteinase (MMP) activity revealed a synergistic increase when epithelial tumor cells and

normal fibroblasts were co-cultured in this model. When MMP activity was reduced by a chemical inhibitor or when cells were cultured in gels with a non-degradable crosslinker, fibroblast migration was dramatically suppressed, and the increase in cancer cell proliferation in co-culture was abrogated. Together, this evidence supports the idea that there is an exchange between the alveolar epithelium and surrounding fibroblasts during cancer progression and points to potential signaling routes that merit further inspection to discover potential targets for therapeutic development.

8.2 Introduction

In the lungs, hollow, cyst-like alveoli consist of a polarized epithelial layer attached to a thin basement membrane and surrounded by capillaries and interstitial stromal cells, in particular a population of alveolar fibroblasts commonly found in the collagen- and elastin-rich septa dividing neighboring alveoli.[1,2] Gaps in the basement membrane allow for direct communication between the epithelium and these alveolar fibroblasts.[3] Normal epithelial-mesenchymal signaling is essential during lung development and is thought to play a role in adult alveolar homeostasis.[1,4] For example, during repair of the wounded alveolar epithelium, interstitial fibroblasts secrete extracellular matrix (ECM) proteins that enable migration of proliferating and differentiating epithelial cells, followed by matrix degradation and apoptosis of activated fibroblasts (*i.e.*, myofibroblasts).[5] However, disruption of this signaling has been implicated in the progression of lung diseases, such as idiopathic pulmonary fibrosis (IPF) and cancer.[6,7]

In cancer, the local microenvironment has been shown to be a key regulator in tumor formation and invasion, especially mesenchymal cells and the ECM proteins and cytokines that they secrete.[8–10] As in many carcinomas, there appears to be a reciprocal exchange of signals

between pulmonary fibroblasts and epithelial-derived lung cancer cells. On one hand, an alveolar epithelium-derived adenocarcinoma cell line (A549) has been shown to increase α-SMA production in normal fibroblasts and increase their matrix metalloproteinase (MMP) production, influencing matrix remodeling and tumor invasion.[11,12] On the other hand, an increase in paracrine signals secreted by cancer-associated fibroblasts (CAFs) has been shown to increase epithelial tumor proliferation, migration, and drug resistance.[8,13] These CAFs are heterogeneous in phenotype and arise from a variety of sources, including circulating bone-marrow derived cells, tissue-resident mesenchymal stem cells, and local fibroblasts.[9,10] The resident normal fibroblasts are the first to respond to the tumor wound site, activating into myofibroblasts. Tumor-secreted factors, such as TGFβ, PDGF, and IL-1, lead to further transformation of the myofibroblasts into perpetually activated, tumor-promoting CAFs.[9,10] Matrix destruction caused by an imbalance between MMPs and tissue inhibitors of metalloproteinases (TIMPs) produced by both tumor and stromal cells in lung tissue is associated with cancer progression, and MMP inhibitors are being explored as potential therapeutics, although there is still a need for MMP-specific knowledge and targeted delivery options.[14]

Much still remains to be discovered about the intricacies of epithelial-mesenchymal crosstalk during disease progression, and *in vitro* co-culture models have proven to be useful tools for studying such questions.[11,15–23] One advantage of these systems is the researcher's ability to control the density and spatial proximity of healthy cell types in co-culture with diseased cell types to probe the influence of one on the other and propose mechanisms by which injury or mutations in one type may lead to progression of disease in the overall tissue. Given the three-dimensional architecture of alveolar tissue and tumor masses, more physiologically relevant models must employ ECM mimics that support the growth and culture of 3D

multicellular tissue structures. While many techniques exist to form dense tumor spheroids (*e.g.,* the hanging drop method),[24,25] the cyst-like alveolus structure is notoriously difficult to achieve and manipulate *in vitro* with primary alveolar epithelial cells, especially in synthetic ECM mimics. Recently, our lab demonstrated the use of photolabile microspheres as templates for patterning hollow, spherical model alveoli within peptide-modified poly(ethylene glycol) (PEG) hydrogels.[26] These hydrogels capture several key features of the native ECM (*e.g.,* high water content; lung tissue appropriate elasticity; enzymatically degradable crosslinkers that enable local remodeling by cell-secreted proteases; introduction of integrin binding sites, such as the fibronectin-derived RGDS sequence), with the added advantage of precise user control over matrix properties (*e.g.*, elastic modulus, scaffold geometry, tethered biochemical cues).[27] To complement this approach, our lab has also developed a PEG crosslinker that cleaves upon exposure to selected light wavelengths (365-420 nm) under cytocompatible conditions. These materials have been used to synthesize microspheres of discrete size ranges that are completely degradable upon exposure to light, and have found applications as depots for drug delivery (10-50 μm), as well as for templating of multicellular cyst-like structures (50-200 μm).[26,28,29]

In the work presented here, our cyst templating technique was used to create model epithelial alveoli that were subsequently encapsulated in a PEG hydrogel laden with pulmonary fibroblasts. This approach allowed the culture of two distinct lung cell types in a physiologically-relevant geometry where the density and distance of the cell types were readily controlled to test hypotheses related to paracrine signaling. The results report on two types of epithelial cells: primary mouse alveolar epithelial cells to represent a healthy epithelium and an adenocarcinoma cell line (A549) to represent lung tumor cellular structures. These epithelial cells were co-cultured with a normal pulmonary fibroblast cell line (CCL-210). The co-cultured cells were

analyzed for signs of disease progression by measuring for proliferation, migration, and MMP activity. Our goal was to test whether a diseased epithelium would influence the surrounding fibroblasts by increasing their proliferation and migration, and whether these changes might be related to overall protease activity. Interestingly, our results suggest a feedback loop between diseased and healthy cells, in which cancer cell proliferation is increased in the presence of healthy fibroblasts.

8.3 Materials and methods

8.3.1 Microsphere synthesis

Photodegradable microspheres[29] were formed by inverse suspension polymerization via base-catalyzed Michael addition of a photodegradable diacrylate (PEGdiPDA; M_n~4070 Da) with a poly(ethylene glycol) tetrathiol (PEG4SH; M_n~5000 Da). The PEGdiPDA was synthesized as previously described,[30] and PEG4SH was purchased from JenKem Technology. An aqueous phase consisting of 6.9 wt% PEGdiPDA, 4.2 wt% PEG4SH, CRGDS peptide (1.5 mM final concentration), 300mM triethanolamine (Sigma-Aldrich) in pH 8.0 phosphate buffered saline (PBS, Sigma-Aldrich) was pipetted and triturated twice into an organic phase comprised of 3:1 sorbitan monooleate (Span 80, Sigma-Aldrich) and PEG-sorbitan monooleate (Tween80, Sigma-Aldrich) dissolved at 30 mg surfactant per mL in hexanes (EMD Millipore). The aqueous droplet suspension was immediately stirred at a rate of ~200 rpm with a 1cm magnetic stir bar in a 20 mL glass scintillation vial overnight, protected from light. Polymerized particles were then retrieved via centrifugation and washed consecutively with hexanes, isopropanol, and sterile phosphate-buffered saline (PBS).

Non-degradable, fluorescently labeled microspheres were used as a control and reference point for cell tracking calculations in fibroblast migration experiments. Briefly, AlexaFluor-488 C_5 maleimide (Life Technologies; <1 mM) was pre-reacted with PEG4SH for ~30 minutes in the dark. Poly(ethylene glycol) diacrylate (PEGDA; M_n~4000) was synthesized as previously described.[31] Fluorescently tagged microspheres were synthesized as above with an aqueous phase consisting of 6.9 wt% PEGDA, 4.2 wt% AlexaFluor-488-labeled PEG4SH, 300 mM triethanolamine in pH 8.0 PBS.

8.3.2 Cell culture

A549 human adenocarcinoma cells (CCL-185, ATCC) were cultured in high glucose Dulbecco's modified Eagle's medium (DMEM, Life Technologies); and human normal lung fibroblasts (CCL-210, ATCC) were cultured in low glucose DMEM. All cell line growth medium was supplemented with 10% fetal bovine serum (FBS, Life Technologies), 1% penicillin/streptomycin (Life Technologies), and 0.2% fungizone (Life Technologies). Cells were cultured at 37 °C with 5% CO_2 and passaged until use in experiments.

8.3.3 Primary ATII cell isolation

All procedures and protocols were reviewed and approved by the Animal Care and Use Committee at the University of Colorado, Boulder. Primary mouse alveolar epithelial type II (ATII) cells were isolated as previously described.[32] Briefly, FVB/NJ mice (6 weeks old) were obtained from The Jackson Laboratories, immediately euthanized by CO_2 asphyxiation and the chest cavity was opened to expose the heart-lung block. Sterile heparin was injected into the left ventricle and the inferior vena cava was cut. The pulmonary vasculature was then flushed with 1% heparin in sterile PBS. The heart-lung block was excised, and lung tissue was carefully dissected from the heart, trachea, and connective tissue.

Lung tissue was minced and digested in 0.1% Type-1 collagenase (Worthington Biochemical) and 1 mg/mL DNase (Sigma) for 20 minutes at 37°C. Trypsin (Fisher, 0.01% final concentration) was then added and the solution was incubated for another 20 minutes at 37°C. A solution containing 1mg/mL trypsin inhibitor (Life Technologies) and 1 mg/mL DNase was added, and this final mixture was filtered through 100 μm cell strainers and through a Nitex filter with 10 μm pore diameter. The filtered solution was centrifuged for 5 minutes at 2000 rpm, and the resultant pellet was resuspended in DMEM/F-12 medium (Sigma). This cell suspension was added to tissue culture plates coated with IgG (11 mg/cm^2) and incubated for 1 hour at 37°C to separate immune cells from epithelial cells. Non-adherent cells were recovered, centrifuged for 5 minutes at 2000 rpm, resuspended in 1:1 Dulbecco's Modified Eagle Medium:Nutrient Mixture F-12 (DEMEM/F12, Corning) supplemented with 10% FBS and 1% antibiotic/antimitotic (Life Technologies), and counted. Cells were then centrifuged once more at 2000 rpm for 5 minutes and resuspended at 500,000 cells/mL in DMEM/F-12 medium supplemented with 10% FBS, 1% antibiotic/antimitotic, hepatocyte growth factor (HGF; R&D Systems; 50 ng/mL), and Fibroblast Growth Factor 7 (FGF-7; Sigma; 10 ng/mL). Primary ATII cells were immediately used in cyst experiments.

8.3.4 Microsphere seeding

A549 cells at 150,000 cells/mL or primary ATII cells at 500,000 cells/mL in appropriate growth medium were combined with 40 μL of photodegradable microspheres in an ultra-low adhesion 24-well plate (Corning). Plates containing pre-cysts were incubated at 37°C with 5% CO_2 on an orbital shaker at 45 rpm. Prior to encapsulation in hydrogel formulations, A549 pre-cysts were incubated for 18-24 hours and primary pre-cysts were incubated for 3 days to allow for attachment and optimal microsphere coverage.[26]

8.3.5 Cell labeling

For Click-it Plus EdU assays and co-culture migration experiments, fibroblasts were labeled with Cell Tracker Green CMFDA (Life Technologies) per manufacturer's instructions prior to encapsulation in hydrogels. Fibroblasts were suspended in appropriate serum-free growth medium containing Cell Tracker Green (10 μM final concentration) and incubated at 37°C for 30 minutes, after which they were centrifuged and resuspended in PBS at 5 million cells/mL for encapsulation in hydrogels. For fibroblast-only migration experiments, fibroblasts were labeled with Cell Tracker Red CMPTX (Life Technologies, 20 μM final concentration) as above.

For co-culture migration experiments epithelial pre-cysts were stained with Cell Tracker Red CMPTX (Life Technologies). Pre-cysts were carefully removed from 24 well plates after the appropriate incubation period and allowed to settle by gravity. The supernatant was removed with a pipet. Appropriate serum-free growth medium containing Cell Tracker Red (20 μM final concentration) was added, and cells were incubated for 30 minutes at 37°C. Cell Tracker Red medium was removed, and cysts were resuspended in PBS for encapsulation in hydrogels.

8.3.6 Gel formation/cell encapsulation

8.3.6.1 Materials

8-arm poly(ethylene glycol) norbornene (PEG-Nb M_w ~40,000) and photoinitiator lithium phenyl-2,4,6-trimethylbenzoylphosphinate (LAP) were both synthesized as previously published.[33,34] Briefly, 8-arm PEG-OH was reacted with 5-norbornene-2-carboxylic acid (16 eq. to PEG-OH), N,N'-diisopropylcarbodiimide (16 eq. to PEG-OH), and 4-dimethylaminopyridine (1 eq. to PEG-OH) in dichloromethane overnight on ice. The product was precipitated in cold diethyl ether, dialyzed in deionized water, and lyophilized. An enzymatically-cleavable di-cysteine peptide (KCGPQG↓IWGQCK) and an integrin-binding peptide (CRGDS) were

purchased commercially from American Peptide Company, Inc. A non-degradable di-cysteine peptide (KCGPQGI^{d}WGQCK) containing the unnatural D isoform of isoleucine was synthesized using solid phase peptide synthesis on a Tribute Protein Synthesizer (Protein Technologies) with a Rink Amide MBHA resin (Novabiochem), as previously reported.[35] A quenched MMP-cleavable fluorogenic peptide substrate (Dabcyl-GGPQG↓IWGQK-Fluorescein-AEEAcC) was synthesized using solid phase peptide synthesis as described previously.[36]

8.3.6.2 Proliferation Gels

For Click-iT Plus EdU assays, 8-arm 40 kDa PEG-Nb (5 wt%) was combined with di-cysteine peptide crosslinker (degradable or non-degradable) (0.85:1 thiol:ene), CRGDS (1mM), and LAP (0.05 wt%) in sterile PBS and mixed by vortex to form a gel precursor solution. The pH was adjusted to 6.8-7.2 with sterile 0.1 M sodium hydroxide. A fibroblast cell suspension (final concentration 1.6 million cells/mL) and/or epithelial cysts were then added to the gel precursor solution and gently mixed with a pipette. 30 μL drops of this precursor solution were placed on Sigmacote-treated glass slides and exposed to 365 nm light at ~2 mW/cm^2 for 3 minutes to initiate the radical-mediated thiol-ene polymerization reaction. Each polymerized gel was then transferred to an untreated 24-well plate (Corning) with 1 mL of DMEM/F-12 growth medium supplemented with 10% FBS and 1% antibiotic/antimitotic and incubated at 37 °C with 5% CO_2. For MMP inhibition studies, 10 μM GM6001 in DMSO (Santa Cruz Biotechnology) or 0.05% DMSO was added to the media.

8.3.6.3 Migration Gels

For migration experiments, each well in a 24-well glass-bottomed plate (Greiner Bio-One) was washed in 95% ethanol prior to surface functionalization with thiol groups in 0.5% (v/v) (3-mercaptopropyl)trimethoxysilane in 95% ethanol (pH ~5.5) for 5 minutes. Each well

was then washed in 95% ethanol and allowed to air dry. To make the gel precursor solution, 8-arm 40kDa PEG-Nb (3 wt%), di-cysteine MMP-degradable crosslinker (0.75:1), CRGDS (1 mM), and LAP (0.05 wt%) in sterile PBS were combined and mixed by vortex. Sodium hydroxide (0.1 M) was used to adjust the pH of the pre-cursor solution to 6.8-7.2. A fibroblast cell suspension (final concentration 1 million cells/mL) and either epithelial cysts or fluorescently-labeled non-degradable microspheres were added to the gel precursor solution and gently pipetted to mix. A 6 mm diameter circle was cut from square, 1 mm tall rubber gaskets with a biopsy punch. The gaskets were sealed to the bottom of the wells in the thiolated 24-well glass-bottom plate and subsequently filled with 30 μL drops of the precursor solution. To initiate the thiol-ene polymerization, the plate was exposed to 365 nm light at ~2 mW/cm^2 for 4 minutes. After polymerization, the rubber gaskets were carefully removed. To each of the wells, DMEM/F-12 growth medium supplemented with 10% FBS and 1% antibiotic/antimitotic was added and incubated at 37 °C with 5% CO_2. For MMP inhibition studies, 10 μM GM6001 (Santa Cruz Biotechnology) was added to the media.

8.3.6.4 MMP Sensor Peptide Gels

To evaluate MMP activity, single cell fibroblasts, epithelial cysts, or fibroblast/cyst combinations were encapsulated in MMP degradable hydrogels containing a quenched MMP-cleavable fluorogenic peptide substrate with the same sequence used to crosslink the hydrogels (Dabcyl-GGPQG↓IWGQK-Fluorescein-AEEAcC), as described previously.[36,37] MMP sensor gels consisted of 8-arm 40k PEG-Nb (5 wt%), di-cysteine MMP-degradable peptide crosslinker (0.85:1 thiol:ene), fluorogenic MMP sensor peptide (0.25 mM), CRGDS (1 mM), and LAP photoinitiator (0.05 wt%) in sterile PBS. The pH was adjusted to 6.8-7.2 with sterile, 0.1 M sodium hydroxide. A fibroblast cell suspension (final concentration 1.6 million cells/mL) and/or

epithelial cysts were then added to the gel precursor solution and gently mixed with a pipette. Hydrogels were polymerized on top of thiol-functionalized glass coverslips (12 mm, Fisher Scientific) to create a covalent linkage between the hydrogel and the coverslip. Glass coverslips were flame cleaned and functionalized as previously described via emersion in silane solution (0.5% (3-mercaptopropyl) trimethoxysilane (Sigma Aldrich)) in 95% ethanol/water, pH~5.5), rinsed in 95% ethanol in water, and dried. 50 μL of precursor solution was pipetted into a rubber gasket with a 6 mm inner diameter centered on a coverslip. Gels were then polymerized under 365 nm light at an intensity of ~2 mW/cm^2 for 3 minutes. Rubber gaskets were removed and gels covalently attached to coverslips were placed into wells of a 24-well plate with 1 mL DMEM/F-12 growth medium. Media was changed one hour after encapsulation to remove any excess fluorogenic peptide, and samples were incubated for 22 to 46 hours after encapsulation. For MMP inhibition studies, 10 or 100 μM GM6001 (Santa Cruz Biotechnology) or 0.5% DMSO was added to the media.

8.3.7 Microparticle template erosion

Gels containing fibroblasts and/or cysts were cultured for one day to allow cell attachment to the encapsulating hydrogel. Following this 24-hour incubation period, all samples were exposed to 365 nm light at ~10 mW/cm^2 for 15 minutes to cleave the photo-labile moiety in the microspheres and fully erode the cyst templates. Gels were then incubated for ~1 hour at 37°C with 5% CO_2 before changing growth medium. Growth medium was then exchanged daily until completion of each experiment (between 1 and 5 days).

8.3.8 Click-iT EdU assay and quantifying proliferation

Three biological replicates of each cell combination were studied, and images of the proliferating nuclei were quantified using MATLAB. Cell proliferation was detected using a

Click-iT Plus EdU AlexaFluor-594 imaging kit (Life Technologies). A copper-catalyzed covalent "click reaction" between a picolyl azide on an AlexaFluor dye and an alkyne on the thymidine nucleoside analog, 5-ethynyl-2'-deoxyuridine (EdU), allowed for fluorescent staining of proliferating nuclei. EdU was added to growth media at a final concentration of 10 μM on day 1 or day 4 after cell/cyst encapsulation. Samples were then incubated for 17 hours at 37°C with 5% CO_2 to allow for EdU incorporation into DNA during active DNA synthesis, per manufacturer instructions. Samples were then fixed with 4% paraformaldehyde in PBS for 15 minutes at room temperature and washed in 3% bovine serum albumin (BSA) in PBS. Cells were permeabilized in 1% TritonX-100 for one hour and washed with 3% BSA in PBS. Click-it Plus reaction cocktail containing the AlexaFluor 594 dye was prepared as per manufacturer instructions, added to each sample, and incubated for 3 hours at room temperature, rocking. Samples were then washed with 3% BSA in PBS. Finally, nuclei were stained with DAPI (1:2000, Life Technologies) for one hour and washed in PBS. All samples were imaged on a confocal microscope (Zeiss LSM 710) with a 20× water-dipping objective (Plan Appochromat; NA = 1.0). Image stacks (10 per condition) were taken from the top to bottom of individual cysts, or in the center of the gel for fibroblast-only conditions (z step = 10 μm, average stack size ~500 μm).

For quantification, four categories of cell nuclei were counted using MATLAB: fibroblast nuclei, epithelial nuclei, proliferating fibroblast nuclei, and proliferating epithelial nuclei. TIFF images of each z-slice in each of three channels: DAPI, AF-594, and Cell Tracker Green, were created in Image-J and processed in MATLAB. Separate masks were made of objects (nuclei) in the DAPI channel and AlexaFluor 594 channels, and objects were dilated by two pixels with a Disk Structuring Element. The mean intensity within each dilated object in the Cell Tracker

Green channel was evaluated. Objects with a mean intensity above a given threshold were counted as fibroblasts; if the mean intensity fell below this threshold, the object was counted as an epithelial cell. Cell nuclei centroids were tracked and checked for their appearance in successive slices to account for double counted nuclei. Double counts were subtracted to give final cell counts and the percent of proliferating cells. Object counts were pooled from all ten image stacks, and the mean percent positive for EdU was calculated from three biological replicates. Statistical analysis was performed using two-way ANOVA followed by Bonferroni posttests. All error bars represent standard error of the mean (SEM).

8.3.9 Tracking cell migration

The 3D migration of fibroblasts in co-culture hydrogels was observed with an Operetta High Content Imaging System (Perkin Elmer) using Harmony High Content Imaging and Analysis software (Perkin Elmer) for automated image collection in real-time. As mentioned previously, co-culture hydrogels were formed and allowed to swell for 24 hours before cyst templates were eroded and fresh growth medium was introduced. During each experiment, the 10x long WD objective was used with the optical model set to confocal. Two channels, AlexaFluor 594 and AlexaFluor 488, were selected and exposure times were adjusted for each experiment. The layout selection for the images taken in each well was defined as nine fields of view in a 3x3 square in the center of the well. 400 μm z-stacks beginning at a height of 25 μm from the glass surface were collected for each image. Images were taken at 30-minute intervals for 24 hours. A live cell chamber was used to maintain the temperature at 37 °C and 5% CO_2.

Fibroblast migration in 3D was analyzed with Volocity 3D Image Analysis Software (Perkin Elmer). The protocol tracked the fibroblasts in the appropriate channel (AlexaFluor 488 for cyst co-cultures, AlexaFluor 594 for fibroblast-only gels) within a spherical region of interest

(ROI) around a cyst or microsphere with a radius of 125 μm greater than the object. This radius was chosen to limit ROI overlap between neighboring cysts/microspheres, which were spaced about 250 μm apart, on average. Either the epithelial cyst in the AlexaFluor 594 channel or the microsphere in the AlexaFluor 488 channel was tracked as a single object to be used as a reference point. The centroids of the tracked reference point and fibroblasts were exported for subsequent analysis in MATLAB to determine cell speeds, displacements, directionality, and the percent of migrating cells. To compensate for drift in each ROI analyzed, the fibroblast centroid data was normalized to the corresponding tracked reference point. Fibroblast speeds were calculated as the average of the individual speeds between subsequent time points on the cell path. Displacement (distance between start and end points) was used to determine if a fibroblast was migrating towards or away from a cyst, where a positive displacement was traveling towards a cyst and negative displacement was traveling away from a cyst relative to the centroid of the cyst. The directionality (displacement/total distance traveled) was a measure of the straightness of a cell path analogous to persistence time, with values close to 1 indicating a perfectly linear path.[38] The fraction of migrating cells was defined as the number of fibroblasts migrating divided by the total number of fibroblasts tracked, where a cell was deemed migrating if the maximum distance away from the starting position was greater than one cell body length (15 μm) at any point during the 24 hour period, a criterion used in previous migration studies.[38] Statistical analysis was performed using the Kruskal-Wallis test followed by Dunn's Multiple Comparison test. All error bars represent standard error of the mean (SEM).

8.3.10 Quantification of MMP activity and Metabolic Activity

After 22 or 46 hours post-encapsulation, 10% PrestoBlue (Invitrogen) was added to each well to detect metabolic activity. Two hours later, fluorescence intensity readings were

conducted using a Synergy H1 microplate reader (BioTek) at 560 nm excitation/590 nm emission for PrestoBlue, and 494 nm excitation/521 nm emission for the fluorogenic peptide. After fluorescence readings, cells were immediately fixed with 4% PFA for 15 minutes and washed thrice with PBS. Cells were then stained with Hoechst (1:1000, ThermoScientific) for 1 hour and subsequently washed with PBS.

Gels were imaged using an Operetta High Content Imaging System (Perkin Elmer) using Harmony High Content Imaging software, with the 10X long WD objective in confocal mode. 300 μm z-stack images were taken (31 images 20μm apart) in 9 fields of view for each gel. Harmony Analysis software was then used to count cell nuclei. Fluorogenic peptide signal (MMP activity) and PrestoBlue signal (metabolic activity) were each normalized to cell number. Statistical analysis was preformed using two-way ANOVA with Bonferroni posttests. Error bars represent standard error of the mean (SEM).

8.4 Results

Using a previously developed cyst-forming technique,[26] a physiologically-relevant 3D co-culture system for lung cells was created with alveolar epithelial cysts embedded in a synthetic polymer hydrogel and surrounded by low-density pulmonary fibroblasts (Fig. 8.1). This *in vitro* culture system enabled us to probe cellular behavior in response to co-culture with a diseased cell type in the appropriate spatial context in an attempt to elucidate the role of epithelial-mesenchymal crosstalk in disease progression. To accomplish this goal, three cell types were used: normal alveolar epithelial cells (primary mouse cells), lung tumor epithelial cells (A549 cell line), and normal pulmonary fibroblasts (CCL-210 cell line). While the primary epithelial cells attached and spread to form single-cell layers on the microsphere templates, the

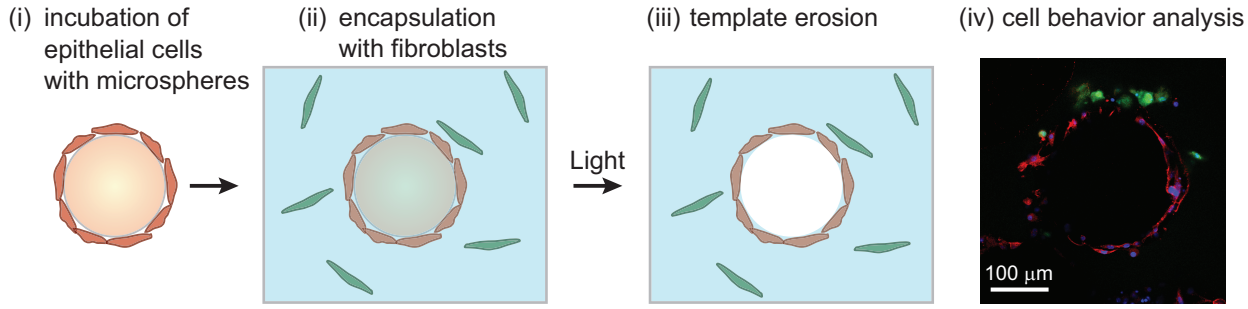

Figure 8.1 Cross-sectional schematic of the co-culture set-up. (i) Epithelial cells (red) were incubated on an orbital shaker with photodegradable microspheres (orange) containing RGDS peptides to allow for cellular attachment to the surface of the microsphere. (ii) Pre-cysts were co-encapsulated with a single cell suspension of fibroblasts (green) in a poly(ethylene glycol) (PEG) hydrogel (blue) containing pendant RGDS for cell adhesion and an enzymatically-degradable peptide crosslinker to allow for local matrix remodeling. (iii) One day after encapsulation, cytocompatible 365 nm light at ~10 mW/cm^2 for 15 minutes was applied to completely erode the microsphere templates, leaving a shell of epithelial cells surrounding a liquid-filled lumen. (iv) Cells were cultured for 1-5 days before being analyzed for proliferation, migration, or protease activity. In this confocal image slice, normal fibroblasts labeled with Cell Tracker Green were co-cultured with primary epithelial cells, which were subsequently stained for an alveolar epithelial type 1 (ATI) phenotype marker. Green = Cell Tracker (fibroblasts), Blue = DAPI (nuclei), Red = T1α (ATI).

cancerous A549 cells tended to form multilayered structures either on the microspheres or as detached aggregates, both of which were embedded in the encapsulating hydrogel. Therefore, the A549 results presented here include both the cyst-like structures, as well as the higher density aggregates, with no significant differences found between the two structure types in the assays studied here. We believe that this phenomenon is relevant to the tumor structures found in cancer progression, and many of the 3D model systems presented in the literature make use of tumor spheroids.[11,19,24,39] The advantage with the presented co-culture system is that we can study both normal alveolar epithelial cells in their native tissue structure, as well as tumor aggregates, and how they respond in the presence of fibroblasts distributed adjacent to and far from the epithelial surface.

8.4.1 Proliferation

An increase in proliferation in either epithelial cells or fibroblasts would indicate abnormal behavior potentially leading toward disease progression.[7,9] Here, we used a commercially available fluorescent EdU assay to measure the proliferation of each cell type after a 17-hour incubation period initiated on days 1 and 4 post-encapsulation. Automated analysis of confocal image slices (Fig. 8.2A) was performed to quantify the percent of nuclei positive for EdU.

The results for both epithelial cell types demonstrated a significant decrease in proliferation between day 1 and day 4, whether alone or in co-culture with fibroblasts (Fig. 8.2B). The primary epithelial cells had no difference in proliferation between co-culture and monoculture on either day, with ~28% positive on day 1 and ~15% positive on day 4. On day 1, the A549 cancer cells also showed no difference between monoculture (61%) and co-culture (55%). Remarkably, the A549 cells did exhibit significantly increased proliferation on day 4 when co-cultured with the normal fibroblasts (45%) compared with monoculture (19%). When comparing primary epithelial cell proliferation to A549 proliferation, A549 cells had significantly higher percentages of EdU-positive nuclei on day 1 for monoculture and both co-culture conditions (Supplementary Fig. 8.1). On day 4, however, A549 proliferation was significantly higher only when co-cultured with normal fibroblasts.

The fibroblasts had a much lower proliferation rate than either epithelial cell type, and this rate did not appear to change over time (Fig. 8.2B). Interestingly, the normal fibroblasts had a significantly higher percentage of EdU-positive nuclei when co-cultured with A549 cells on both days (~12%) compared to monoculture (~3%), and on day 4 when compared to co-culture with primary cysts (7%).

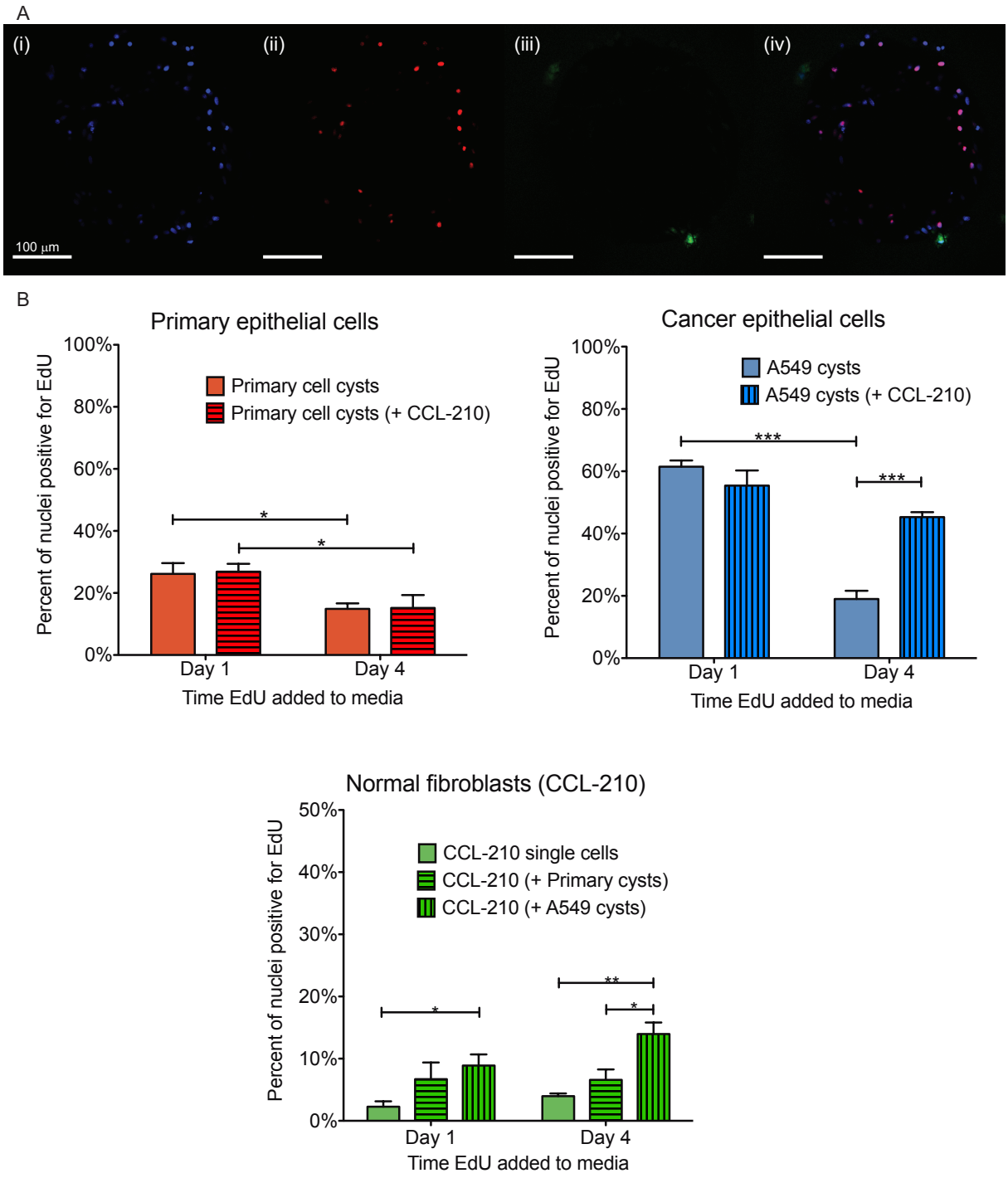

Figure 8.2 Click-iT Plus EdU proliferation assay. (A) Example confocal image slices used for automated nuclei counts. Each object found in the blue and red channels was measured for mean intensity in the green channel, and objects above a certain threshold were counted as fibroblasts. (i) Blue = DAPI (all nuclei). (ii) Red = EdU (proliferating nuclei). (iii) Green = Cell Tracker (fibroblasts). (iv) Merged image of previous three channels. (B) Plots depict percent of nuclei positive for EdU at the two time points in monoculture and both co-cultures, separated by cell type. Results are presented as means ± SEM of three biological replicates of each condition. *p < 0.05, **p < 0.01, ***p < 0.001

8.4.2 Fibroblast migration

Increased motility of both fibroblasts and epithelial cells has been used as an indicator of disease progression.[40–43] In the healthy adult lung, both cell populations remain quiescent until an injury occurs. Normal wound healing involves migration of interstitial fibroblasts to the wound site where they contribute to deposition of a provisional ECM.[5] ATII progenitor cells then migrate along this provisional matrix to repopulate the wounded epithelium.[5,44] In cancer metastasis, it has been proposed that tumor cells undergo an epithelial-to-mesenchymal transition (EMT), detach from the main tumor, and migrate through the surrounding matrix to reach the blood stream.[7] In addition, tumors are thought to recruit and transform local normal fibroblasts into activated fibroblasts that promote tumor growth.[9,10] These cancer-associated fibroblasts (CAFs) have been shown to facilitate tumor cell invasion by creating tracks through the ECM, along which cancer cells can migrate.[9,45,46] Therefore, an increase in fibroblast migration measurements would suggest activation of the wound repair response, which is over stimulated in lung cancer, while epithelial migration would indicate either wound repair or tumor metastasis.

In this study, we fluorescently labeled each cell type and used live cell microscopy to record confocal image stacks every 30 minutes for 24 hours, starting one day post-encapsulation (Fig. 8.3A). Using automated software and analysis codes, we tracked cell position in three dimensions over time and calculated key migration measurements, namely the fraction of cells migrating per analyzed cyst, the fraction of cells migrating toward the reference cyst, the speed, and the directionality. While no significant movement was detected in the epithelial cells, we did observe fibroblast migration in these gels. Cells that traveled at least one cell body length away from their starting position at any point during the 24-hour experiment were considered to

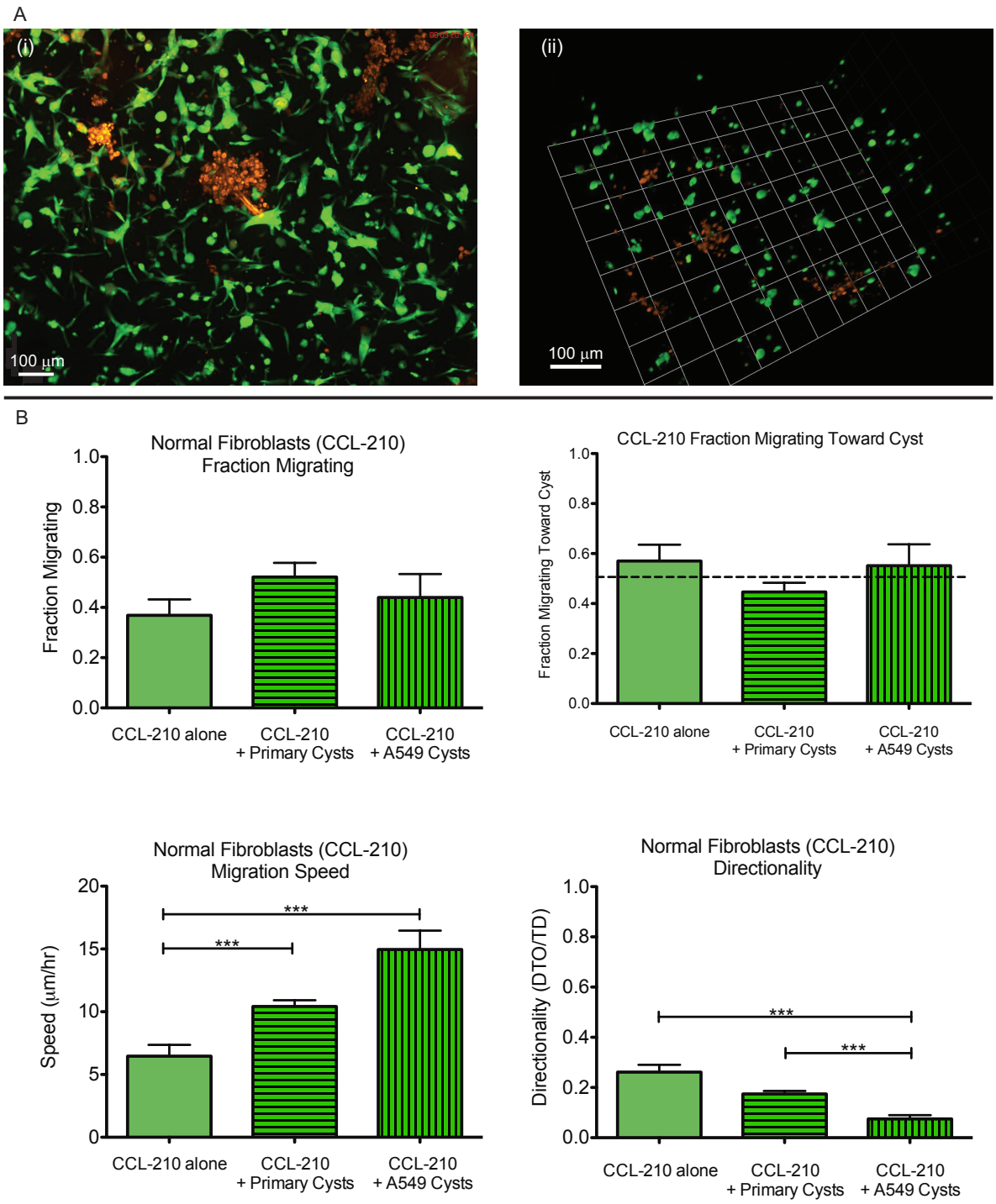

Figure 8.3 Normal fibroblast migration analysis. (A) Example images of fibroblasts (green) in co-culture with epithelial cysts (red) used in cell tracking. (i) Max z-projection of 400 μm confocal stack. (ii) 3D rendering of 200 μm confocal stack using Volocity (Perkin Elmer). (B) Plots show fraction migrating, fraction migrating toward cyst, migration speed, and directionality (Distance-To-Origin/Total Distance) of migrating normal fibroblasts (CCL-210) in monoculture and co-culture with both epithelial cell types. Data in fraction migrating plot represent means ± SEM of cells migrating per cyst. Data in the remaining plots represent means ± SEM of all migrating cells. ***$p < 0.001$

be migrating. All other measurements were calculated for the migrating cells only. Cells considered to be moving toward their reference cyst had final positions closer to the cyst than their starting positions.

The normal fibroblasts (CCL-210, Fig. 8.3B) had no statistically significant difference in cells migrating per cyst when co-cultured with either A549 cancer cells (44%) or primary cysts (52%) compared to monoculture (37%). Likewise, in all conditions the normal fibroblasts showed no directional preference toward or away from the reference cyst. Interestingly, the average speed of the migrating CCL-210 cells in monoculture was ~6 μm/h, while their speed in co-culture with either epithelial cell type was significantly faster (10 μm/h with primary cysts and 15 μm/h with A549 cells). These speeds are much slower than previously reported values for human dermal fibroblasts in similar hydrogels (~40 μm/h),[38] although migration speed is highly dependent on network properties and our gels were more highly crosslinked than these gels, which could explain the slower speeds. In addition, our migration speeds fall in the same range reported for human mesenchymal stem cells (~5-20 μm/h, depending on RGD concentration and crosslinking density).[47] With regards to directionality (distance to origin/total distance), where a value of 1 represents a completely straight path, the normal fibroblasts in all conditions exhibited relatively random migration. However, co-culture with A549 cells resulted in significantly less persistent motion (0.07) than in monoculture (0.26) or in co-culture with primary cysts (0.17).

8.4.3 Matrix metalloproteinase (MMP) activity

Increased protease activity is associated with cancer progression, enabling tumor outgrowth and angiogenesis.[14] To measure global MMP activity in our gels, a recently developed fluorogenic MMP-sensitive peptide (Dabcyl-GGPQG↓IWGQK-Fluorescein-AEEAcC) was

covalently tethered to the hydrogel network enabling fast and *in situ* measurement of MMP activity by taking a fluorescence area scan of the gel using a standard plate reader.[36,37] Overall metabolic activity was measured concurrently by adding a resazurin-based assay to each well. The fluorescence signals from the MMP sensor peptide and from the metabolic activity assay

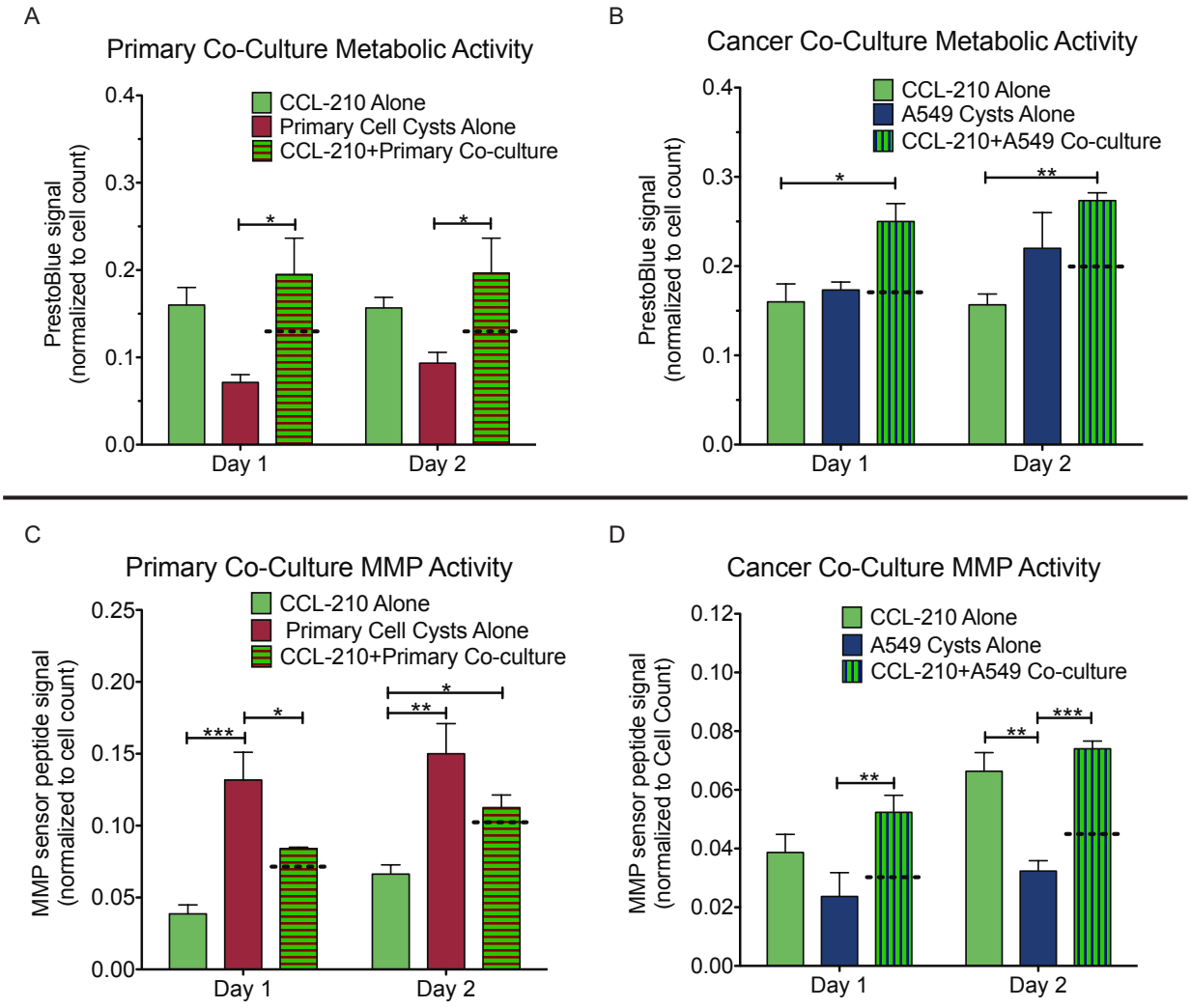

Figure 8.4 (A) Metabolic activity on days 1 and 2 after encapsulation as measured by resorufin fluorescence normalized to cell count for each cell type cultured alone and in co-culture. (B) MMP activity on days 1 and 2 after encapsulation as measured by an MMP-sensitive fluorescent sensor peptide normalized to cell count for each cell type cultured alone and in co-culture. Dotted lines represent the weighted average of the two cell types cultured alone, which would be the expected value for the co-culture barring any crosstalk. Data represents means ± SEM for 3 biological replicates of each condition. *$p < 0.05$, **$p < 0.01$, ***$p < 0.001$

were both normalized to cell count as estimated by imaging cell nuclei across the bulk of each gel.

In both co-cultures, primary epithelial cells with the normal fibroblasts and cancer epithelial cells with the normal fibroblasts, on both days overall metabolic activity appeared to be synergistically increased over the calculated weighted average of the two cell types cultured alone (Fig. 8.4A). The weighted average is the level expected in the co-culture if there were no crosstalk between the cell types influencing metabolism or MMP expression. The primary cell co-cultures had an average normalized metabolic activity on both days of 0.20 compared to a weighted average of 0.13 on both days. The cancer cell co-cultures had an average normalized metabolic activity of 0.25 and 0.27 on days 1 and 2, respectively, compared with weighted averages of 0.17 and 0.20.

In contrast, only the cancer cell co-cultures demonstrated a synergistic increase in MMP activity on both days (Fig. 8.4B). The primary cell co-cultures had an average normalized MMP activity of 0.08 and 0.11 on days 1 and 2, respectively, compared with weighted averages of 0.07 and 0.10. However, the cancer cell co-cultures had day 1 and day 2 MMP activities of 0.05 and 0.07, respectively, versus weighted averages of 0.03 and 0.04.

8.4.4 Matrix metalloproteinase (MMP) inhibition

To investigate whether the observed increase in MMP activity in the cancer cell co-culture might be influencing the increased cancer cell proliferation and fibroblast migration speed seen earlier, we tested the influence of a broad spectrum small molecule MMP inhibitor (GM6001) on proliferation and migration in our co-culture model. GM6001 binds with the zinc

active site on MMPs and has been shown to inhibit the bioactivity of MMPs 1, 2, 3, 8, and 9, among others.[14,48] Furthermore, this inhibitor has previously been used with A549 cells to effectively block invasion into a 3D matrix and has been shown to reduce the fluorescence signal from the MMP sensor peptide used in this work.[36,37,49] To confirm the effectiveness of GM6001 with our co-culture model, we repeated the MMP activity assay with 10 μM GM6001 in the media and observed a reduction by half in the normalized signal on both days compared with the DMSO control group (Supplementary Fig. 8.2).

We repeated the proliferation assay with cancer cells alone and in co-culture with normal fibroblasts and added 10 μM GM6001 to the media, comparing it to a DMSO control group as well as our original data (Fig. 8.5). In addition we performed the same assay in non-degradable gels, which contained a crosslinker with the same di-cysteine peptide sequence as before except the isoleucine at the cleavage site was switched to the unnatural D isoform, rendering it insensitive to MMP cleavage.[35] In all conditions, the cancer cells alone demonstrated statistically similar levels of proliferation on day 4, around 22%. For the co-cultures, both the original degradable gel and the DMSO control had statistically higher proliferation levels on day 4 than the cancer cells alone, around 43%. Both the MMP-inhibited and non-degradable gel co-cultures exhibited a reduction in proliferation on day 4 that was statistically lower than the co-culture controls and statistically similar to the cancer cells alone, 24% and 29% respectively.

The corresponding fibroblast proliferation results (Supplementary Fig. 8.3) on day 4 in the MMP-inhibited and DMSO control co-cultures showed no change from the original (14%) and were significantly higher than the fibroblasts alone (4%). The fibroblasts in the non-degradable gel co-cultures were not statistically different from either group (10%).

We also repeated the migration assay with MMP inhibitor in the media for both the fibroblasts alone and the fibroblasts in co-culture with the cancer epithelial cells. In both cases, the inhibitor completely blocked migration, so we were unable to calculate migration speed or directionality.

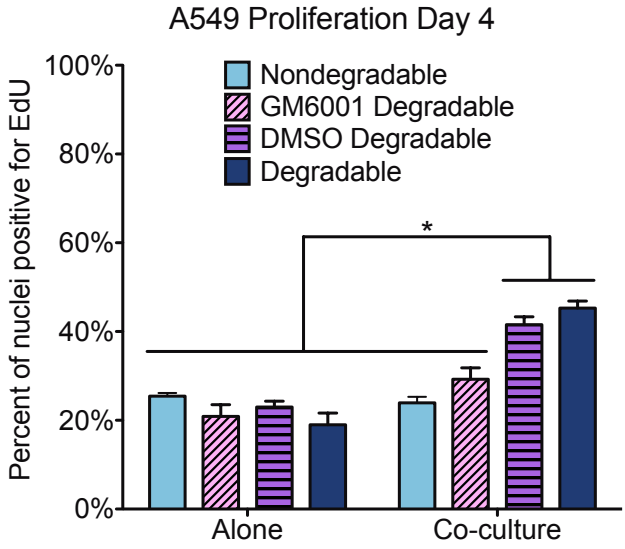

Figure 8.5 Click-iT Plus EdU proliferation assay. Plot depicts percent of A549 cell nuclei positive for EdU on day 4 in monoculture and the A549/CCL-210 co-cultures, separated by gel and media type. The nondegradable gels contained a peptide crosslinker insensitive to MMP cleavage. GM6001 was added at 10 μM, and the DMSO control media contained 0.05% DMSO. The degradable bars refer to the original experiment in MMP-degradable gels with regular growth media. Results are presented as means ± SEM of three biological replicates of each condition. *$p < 0.05$

8.5 Discussion

Epithelial-mesenchymal crosstalk is a key regulator during lung development and normal wound healing processes, and growing evidence suggests that altered paracrine signaling between the alveolar epithelium and interstitial fibroblasts may lead to disease progression in multiple pathologies.[6–8,12,50,51] To study these interactions, *in vitro* co-culture systems, and

particularly biomaterial matrices, have evolved to serve as valuable tools for controlling the cell types present and their proximity to one another, with the ability to mix healthy with diseased cells.[11,16–19] In the 3D model system presented here, alveolar epithelial cysts were surrounded by pulmonary fibroblasts in an encapsulating hydrogel matrix that recapitulates aspects of the basic tissue architecture of the distal lung. Compliant 3D culture networks have been shown to more closely represent cell behavior *in vivo* than traditional flat and typically stiff surfaces (*e.g.*, tissue culture plastic ware is ~6 orders of magnitude stiffer than lung tissue), and are especially influential in the areas of contact-inhibited growth[52,53] and migration mechanisms[54,55] relevant to this work. Advantageously, the spatial arrangement of cells in this platform better reflects many aspects of the *in vivo* lung structure, but this also limits the types of analysis that can be performed on individual cell populations. Assessments such as RT-PCR and western blots give global mRNA and protein levels from all the cells in the gel, and any spatial information is lost. Therefore, we chose imaging-based measurements to visualize and quantify individual cell type proliferation and migration.

In the healthy adult lung, alveolar epithelial cell turnover is slow compared to many other tissues; the replacement time is reported to be approximately one month.[1,56,57] During wound healing, proliferation increases dramatically to repopulate the epithelium in a few days, followed by cell cycle arrest and apoptosis of undifferentiated cells.[1,57,58] Tumor cells, on the other hand, exhibit unchecked proliferation, and the ATCC reports that the adenocarcinoma cell line A549 has a doubling time of just 22 hours. Therefore, it is not surprising that in our culture system the percent of nuclei positive for EdU one day after encapsulation was significantly higher for A549 cysts than primary cysts. Both epithelial cell types demonstrated a dramatic decrease in proliferation over time, which we attribute to contact inhibition[53,59] and physical constraint by the

encapsulating hydrogel. While the gel network is degradable by various matrix-metalloproteinases (MMPs; including 1, 2, 3, 8, and 9),[60,61] their expression by these cells appears to be low, especially for the cancer cells, and limited outgrowth into the surrounding hydrogel is observed. The fibroblasts exhibit very low levels of proliferation, which does not change over time or in the presence of healthy epithelial cells, matching the normally quiescent phenotype seen *in vivo*.[1,2,51]

The exception to these trends is seen in the A549/CCL-210 co-culture condition, which shows significantly higher proliferation of both cell types four days after encapsulation, as well as higher proliferation of the normal fibroblasts on day 1. Profibrotic factors secreted from the A549 epithelial cells (osteopontin, PDGF, TGFβ, etc.)[5,6,62] may be one cause of this immediate increase in fibroblast proliferation. Enhanced proliferation is one marker used to distinguish CAFs from normal fibroblasts in the tumor stroma.[9] Therefore, these results may indicate the onset of fibroblast transformation by the cancer cells in our co-culture model. While the cancer cells alone show a decrease in proliferation over time in our gels, co-culture with normal fibroblasts enables the cancer cells to maintain a high level of proliferation on day 4. One possible explanation is that the increased MMP activity observed in the cancer cell-fibroblast co-culture leads to increased local matrix degradation, which reduces contact inhibition and allows more space for the cancer cells to continue proliferating. This hypothesis is supported by the fact that switching to an MMP-insensitive peptide crosslinker, as well as blocking global MMP activity with a broad-spectrum small molecule MMP inhibitor, abrogates the enhanced proliferation seen on day 4 in co-culture.

Normally, the alveolar epithelium produces paracrine signals, such as prostaglandin E-2 (PGE2), that keep the interstitial fibroblasts in a quiescent state, suppressing migration,

proliferation, and ECM-production.[50] Conversely, in cancer the malignant epithelium produces a multitude of profibrotic and pro-inflammatory signals, such as PDGF, TGFβ, and IL-1, and these signals are thought to contribute to increased fibroblast migration, proliferation, and secretion of tumor-promoting signals seen in lung cancer patients.[8–10] In the migration studies presented here, the normal fibroblasts migrated faster in culture with A549 cells than they moved in monoculture, although this faster motion was significantly less directed than in the other conditions. As with the increased proliferation seen in this same co-culture condition, increased protease activity may contribute to faster migration of fibroblasts, due to local degradation of the matrix. Alternatively, the cancerous A549 cells may already be producing one or many of the profibrotic signals listed above or secreting less of the quiescent signal PGE2. Reduction of MMP activity by a broad-spectrum inhibitor was enough to prevent any migration of fibroblasts through these gels, likely due to the need for local network degradation to create space for the cells to migrate through. However, it is still unclear what influence MMPs have on fibroblast migration speed and directionality in this co-culture model. Alternative peptide crosslinkers in the gel network susceptible to cleavage by specific MMPs may enable more investigation into this mechanism.

Protease activity is important for normal ECM turnover and matrix remodeling after wound closure.[5,14] However, an imbalance in MMP and TIMP levels favoring matrix destruction has been associated with tumor invasiveness, angiogenesis, and metastasis.[8,14] Fromigué, *et al.* found an increase in RNA expression and protein levels of specific MMPs (2, 9, and 11) in the conditioned media from direct co-cultures of A549 cancer cells and CCL-210 pulmonary fibroblasts, which matches our observation of increased general MMP activity for co-cultures of the same cell lines.[12] Interestingly, this synergistic increase in MMP activity is not seen in the

healthy primary cell co-culture, suggesting that paracrine signaling from the cancer cells may be causing this increase in MMP production through pro-inflammatory signals such as TGFβ.

While the results presented here point to an increase in MMP activity as being influential in tumor-promoting cell behavior (*e.g.* increased fibroblast migration and cancer cell proliferation), the complex signaling pathways involved in this epithelial-mesenchymal crosstalk remain elusive. Targeted MMP inhibitors are actively being developed as anti-cancer drugs based on tumor cell expression profiles; however, this evidence suggests the need to probe further into the source of these MMPs (*e.g.* tumor-adjacent stromal cells) as well as the upstream signaling cues causing the increase in MMP production. *In situ* hybridization might be used in this co-culture system to determine specific MMP gene expression profiles for the two cell types and discover the origin of this upregulation in MMPs in co-culture versus monoculture. Since protease activity is essential for normal tissue homeostasis and wound healing throughout the body, further investigation of the tumor-stromal signaling pathways leading to this increase in MMPs could reveal potential targets for the development of novel therapeutics, limiting the deleterious side effects seen with current broad-spectrum MMP-inhibiting drugs. Cellular outcomes pertinent to anti-cancer drugs, such as matrix remodeling and 3D migration, inherently necessitate the engineering of 3D, adaptable environments for co-culture of multiple cell types and testing the efficacy of drugs. Therefore, once therapeutics have been identified, this unique co-culture model could provide a spatially-organized, alveolar tissue-relevant platform for screening before attempting to use more expensive and complex mouse models.

8.6 Conclusions

The 3D *in vitro* co-culture system used in this study provided an innovative platform for studying the interactions between alveolar epithelial cysts and dispersed pulmonary fibroblasts and investigating cell functions related to disease progression. The results presented here support the growing body of evidence in the literature that crosstalk between the alveolar epithelium and interstitial fibroblasts influences their behavior in terms of proliferation, migration, and protease activity. Co-culture of tumor-derived epithelial cells with normal pulmonary fibroblasts led to an increase in MMP activity, cancer cell and fibroblast proliferation, and fibroblast migration speed. Future investigation into the signals contributing to the differences in cell behavior discovered here would provide needed insight into possible pathways conducive to drug development. For example, MMP activity appears to be influential in fibroblast motility and proliferation of tumor cells, furthering the importance of developing targeted MMP inhibitors for anti-cancer therapy. Moreover, this spatially-relevant co-culture model could be a useful starting point for drug screening trials by capturing key geometric aspects of cell behavior in alveolar tissue before moving to more complex *in vivo* models.

8.7 Acknowledgements

The authors would like to thank Sharon Ryan for teaching us the ATII mouse cell isolation procedure, Kyle Kyburz for discussions concerning live cell tracking experiments and analysis, Emi Tokuda for providing the MMP sensor peptide and many helpful discussions, and Chun Yang for providing the non-degradable peptide crosslinker. Funding for this work was provided by the Howard Hughes Medical Institute and the National Science Foundation (CTS1236662).

8.8 References

1. Herzog, E. L., Brody, A. R., Colby, T. V, Mason, R. & Williams, M. C. Knowns and unknowns of the alveolus. *Proc. Am. Thorac. Soc.* **5,** 778–82 (2008).
2. Hogan, B. L. M., Barkauskas, C. E., Chapman, H. A., Epstein, J. A., Jain, R., Hsia, C. C. W., *et al.* Repair and regeneration of the respiratory system: complexity, plasticity, and mechanisms of lung stem cell function. *Cell Stem Cell* **15,** 123–38 (2014).
3. Sirianni, F. E., Chu, F. S. F. & Walker, D. C. Human Alveolar Wall Fibroblasts Directly Link Epithelial Type 2 Cells to Capillary Endothelium. *Am. J. Respir. Crit. Care Med.* **168,** 1532–1537 (2003).
4. Bellusci, S., Grindley, J., Emoto, H., Itoh, N. & Hogan, B. L. Fibroblast growth factor 10 (FGF10) and branching morphogenesis in the embryonic mouse lung. *Development* **124,** 4867–78 (1997).
5. Selman, M., Thannickal, V. J., Pardo, A., Zisman, D. A., Martinez, F. J. & Lynch, J. P. Idiopathic Pulmonary Fibrosis. *Drugs* **64,** 405–430 (2004).
6. King, T. E., Pardo, A. & Selman, M. Idiopathic pulmonary fibrosis. *Lancet* **378,** 1949–61 (2011).
7. Thiery, J. P., Acloque, H., Huang, R. Y. J. & Nieto, M. A. Epithelial-mesenchymal transitions in development and disease. *Cell* **139,** 871–90 (2009).
8. Bhowmick, N., Neilson, E. & Moses, H. Stromal fibroblasts in cancer initiation and progression. *Nature* **432,** 332–337 (2004).
9. Augsten, M. Cancer-Associated Fibroblasts as Another Polarized Cell Type of the Tumor Microenvironment. *Front. Oncol.* **4,** 62 (2014).
10. Marsh, T., Pietras, K. & McAllister, S. S. Fibroblasts as architects of cancer pathogenesis. *Biochim. Biophys. Acta - Mol. Basis Dis.* **1832,** 1070–1078 (2013).
11. Amann, A., Zwierzina, M., Gamerith, G., Bitsche, M., Huber, J. M., Vogel, G. F., *et al.* Development of an innovative 3D cell culture system to study tumour--stroma interactions in non-small cell lung cancer cells. *PLoS One* **9,** e92511 (2014).
12. Fromigué, O., Louis, K., Dayem, M., Milanini, J., Pages, G., Tartare-Deckert, S., *et al.* Gene expression profiling of normal human pulmonary fibroblasts following coculture with non-small-cell lung cancer cells reveals alterations related to matrix degradation, angiogenesis, cell growth and survival. *Oncogene* **22,** 8487–8497 (2003).
13. Wang, W., Li, Q., Yamada, T., Matsumoto, K., Matsumoto, I., Oda, M., *et al.* Crosstalk to stromal fibroblasts induces resistance of lung cancer to epidermal growth factor receptor tyrosine kinase inhibitors. *Clin. Cancer Res.* **15,** 6630–8 (2009).
14. Vandenbroucke, R. E., Dejonckheere, E. & Libert, C. Series 'Matrix metalloproteinases in lung health and disease': A therapeutic role for matrix metalloproteinase inhibitors in lung diseases? *Eur. Respir. J.* **38,** 1200–1214 (2011).
15. Prasad, S., Hogaboam, C. M. & Jarai, G. Deficient repair response of IPF fibroblasts in a co-culture model of epithelial injury and repair. *Fibrogenesis Tissue Repair* **7,** 7 (2014).
16. Wang, X. & Kaplan, D. L. Hormone-responsive 3D multicellular culture model of human breast tissue. *Biomaterials* **33,** 3411–3420 (2012).

17. Horie, M., Saito, A., Mikami, Y., Ohshima, M., Morishita, Y., Nakajima, J., *et al.* Characterization of human lung cancer-associated fibroblasts in three-dimensional in vitro co-culture model. *Biochem. Biophys. Res. Commun.* **423,** 158–63 (2012).

18. Fang, X., Sittadjody, S., Gyabaah, K., Opara, E. C. & Balaji, K. C. Novel 3D Co-Culture Model for Epithelial-Stromal Cells Interaction in Prostate Cancer. *PLoS One* **8,** 1–11 (2013).

19. Kim, S.-A., Lee, E. K. & Kuh, H.-J. Co-culture of 3D tumor spheroids with fibroblasts as a model for epithelial–mesenchymal transition in vitro. *Exp. Cell Res.* **335,** 187–196 (2015).

20. Majety, M., Pradel, L. P., Gies, M. & Ries, C. H. Fibroblasts Influence Survival and Therapeutic Response in a 3D Co-Culture Model. *PLoS One* **10,** e0127948 (2015).

21. Puperi, D. S., Balaoing, L. R., O'Connell, R. W., West, J. L. & Grande-Allen, K. J. 3-Dimensional spatially organized PEG-based hydrogels for an aortic valve co-culture model. *Biomaterials* **67,** 354–364 (2015).

22. Kim, H. J., Li, H., Collins, J. J. & Ingber, D. E. Contributions of microbiome and mechanical deformation to intestinal bacterial overgrowth and inflammation in a human gut-on-a-chip. *Proc. Natl. Acad. Sci.* **113,** E7–E15 (2016).

23. Huh, D., Matthews, B. D., Mammoto, A., Montoya-Zavala, M., Hsin, H. Y. & Ingber, D. E. Reconstituting Organ-Level Lung Functions on a Chip. *Science* **328,** 1662–1668 (2010).

24. Friedrich, J., Ebner, R. & Kunz-Schughart, L. A. Experimental anti-tumor therapy in 3-D: spheroids--old hat or new challenge? *Int. J. Radiat. Biol.* **83,** 849–871 (2007).

25. Weiswald, L.-B., Bellet, D. & Dangles-Marie, V. Spherical Cancer Models in Tumor Biology. *Neoplasia* **17,** 1–15 (2015).

26. Lewis, K. J. R., Tibbitt, M. W., Zhao, Y., Branchfield, K., Sun, X., Balasubramaniam, V., *et al.* In vitro model alveoli from photodegradable microsphere templates. *Biomater. Sci.* **3,** 821–832 (2015).

27. Lewis, K. J. R. & Anseth, K. S. Hydrogel scaffolds to study cell biology in four dimensions. *MRS Bull.* **38,** 260–268 (2013).

28. Kloxin, A. M., Kasko, A. M., Salinas, C. N. & Anseth, K. S. Photodegradable hydrogels for dynamic tuning of physical and chemical properties. *Science* **324,** 59–63 (2009).

29. Tibbitt, M. W., Han, B. W., Kloxin, A. M. & Anseth, K. S. SFB Student Award Winner in the Ph.D. Category: Synthesis and application of photodegradable microspheres for spatiotemporal control of protein delivery. *J. Biomed. Mater. Res. Part A* **100A,** 1647–1654 (2012).

30. Kloxin, A. M., Tibbitt, M. W. & Anseth, K. S. Synthesis of photodegradable hydrogels as dynamically tunable cell culture platforms. *Nat. Protoc.* **5,** 1867–87 (2010).

31. Cruise, G. M., Scharp, D. S. & Hubbell, J. a. Characterization of permeability and network structure of interfacially photopolymerized poly(ethylene glycol) diacrylate hydrogels. *Biomaterials* **19,** 1287–1294 (1998).

32. Kloxin, A. M., Lewis, K. J. R., Deforest, C. A., Seedorf, G., Tibbitt, M. W.,

Balasubramaniam, V., *et al.* Responsive culture platform to examine the influence of microenvironmental geometry on cell function in 3D. *Integr. Biol.* **4,** 1540–1549 (2012).

33. Gould, S. T., Darling, N. J. & Anseth, K. S. Small peptide functionalized thiol-ene hydrogels as culture substrates for understanding valvular interstitial cell activation and de novo tissue deposition. *Acta Biomater.* **8,** 3201–9 (2012).
34. Fairbanks, B. D., Schwartz, M. P., Bowman, C. N. & Anseth, K. S. Photoinitiated polymerization of PEG-diacrylate with lithium phenyl-2,4,6-trimethylbenzoylphosphinate: polymerization rate and cytocompatibility. *Biomaterials* **30,** 6702–7 (2009).
35. Yang, C., Mariner, P. D., Nahreini, J. N. & Anseth, K. S. Cell-mediated delivery of glucocorticoids from thiol-ene hydrogels. *J. Control. Release* **162,** 612–618 (2012).
36. Leight, J. L., Alge, D. L., Maier, A. J. & Anseth, K. S. Direct measurement of matrix metalloproteinase activity in 3D cellular microenvironments using a fluorogenic peptide substrate. *Biomaterials* **34,** 7344–7352 (2013).
37. Leight, J. L., Tokuda, E. Y., Jones, C. E., Lin, A. J. & Anseth, K. S. Multifunctional bioscaffolds for 3D culture of melanoma cells reveal increased MMP activity and migration with BRAF kinase inhibition. *Proc. Natl. Acad. Sci.* **112,** 201505662 (2015).
38. Schwartz, M. P., Rogers, R. E., Singh, S. P., Lee, J. Y., Loveland, S. G., Koepsel, J. T., *et al.* A quantitative comparison of human HT-1080 fibrosarcoma cells and primary human dermal fibroblasts identifies a 3D migration mechanism with properties unique to the transformed phenotype. *PLoS One* **8,** 1–24 (2013).
39. Franzdóttir, S. R., Axelsson, I. T., Arason, A. J., Baldursson, O., Gudjonsson, T. & Magnusson, M. K. Airway branching morphogenesis in three dimensional culture. *Respir. Res.* **11,** 162 (2010).
40. Choe, C., Shin, Y.-S., Kim, S.-H., Jeon, M.-J., Choi, S.-J., Lee, J., *et al.* Tumor–stromal Interactions with Direct Cell Contacts Enhance Motility of Non-small Cell Lung Cancer Cells Through the Hedgehog Signaling Pathway. *Anticancer Res.* **33,** 3715–3723 (2013).
41. Kumarswamy, R., Mudduluru, G., Ceppi, P., Muppala, S., Kozlowski, M., Niklinski, J., *et al.* MicroRNA-30a inhibits epithelial-to-mesenchymal transition by targeting Snai1 and is downregulated in non-small cell lung cancer. *Int. J. Cancer* **130,** 2044–53 (2012).
42. Suganuma, H., Sato, A., Tamura, R. & Chida, K. Enhanced migration of fibroblasts derived from lungs with fibrotic lesions. *Thorax* **50,** 984–989 (1995).
43. Vuorinen, K., Gao, F., Oury, T. D., Kinnula, V. L. & Myllärniemi, M. Imatinib mesylate inhibits fibrogenesis in asbestos-induced interstitial pneumonia. *Exp. Lung Res.* **33,** 357–373 (2007).
44. Crosby, L. M. & Waters, C. M. Epithelial Repair Mechanisms in the Lung. *Am. J. Physiol. Lung Cell. Mol. Physiol.* **298,** 715–731 (2010).
45. Scott, R. W., Hooper, S., Crighton, D., Li, A., König, I., Munro, J., *et al.* LIM kinases are required for invasive path generation by tumor and tumor-associated stromal cells. *J. Cell Biol.* **191,** 169–185 (2010).
46. Sanz-Moreno, V., Gaggioli, C., Yeo, M., Albrengues, J., Wallberg, F., Viros, A., *et al.* ROCK and JAK1 Signaling Cooperate to Control Actomyosin Contractility in Tumor

Cells and Stroma. *Cancer Cell* **20,** 229–245 (2011).

47. Kyburz, K. A. & Anseth, K. S. Three-dimensional hMSC motility within peptide-functionalized PEG-based hydrogels of varying adhesivity and crosslinking density. *Acta Biomater.* **9,** 6381–92 (2013).

48. Yadav, R. K., Gupta, S. P., Sharma, P. K. & Patil, V. M. Recent Advances in Studies on Hydroxamates as Matrix Metalloproteinase Inhibitors: A Review. *Curr. Med. Chem.* **18,** 1704–1722 (2011).

49. Wang, S., Li, E., Gao, Y., Wang, Y., Guo, Z., He, J., *et al.* Study on Invadopodia Formation for Lung Carcinoma Invasion with a Microfluidic 3D Culture Device. *PLoS One* **8,** (2013).

50. Selman, M. & Pardo, A. Role of epithelial cells in idiopathic pulmonary fibrosis: from innocent targets to serial killers. *Proc. Am. Thorac. Soc.* **3,** 364–372 (2006).

51. Marchand-Adam, S., Marchal, J., Cohen, M., Soler, P., Gerard, B., Castier, Y., *et al.* Defect of hepatocyte growth factor secretion by fibroblasts in idiopathic pulmonary fibrosis. *Am. J. Respir. Crit. Care Med.* **168,** 1156–61 (2003).

52. Puliafito, A., Hufnagel, L., Neveu, P., Streichan, S., Sigal, A., Fygenson, D. K., *et al.* Collective and single cell behavior in epithelial contact inhibition. *Proc. Natl. Acad. Sci.* **109,** 739–744 (2012).

53. Rejniak, K. A., Wang, S. E., Bryce, N. S., Chang, H., Parvin, B., Jourquin, J., *et al.* Linking changes in epithelial morphogenesis to cancer mutations using computational modeling. *PLoS Comput. Biol.* **6,** (2010).

54. Doyle, A. D., Wang, F. W., Matsumoto, K. & Yamada, K. M. One-dimensional topography underlies three-dimensional fi brillar cell migration. *J. Cell Biol.* **184,** 481–490 (2009).

55. Peyton, S. R., Kalcioglu, Z. I., Cohen, J. C., Runkle, A. P., Van Vliet, K. J., Lauffenburger, D. a., *et al.* Marrow-Derived stem cell motility in 3D synthetic scaffold is governed by geometry along with adhesivity and stiffness. *Biotechnol. Bioeng.* **108,** 1181–1193 (2011).

56. Guillot, L., Nathan, N., Tabary, O., Thouvenin, G., Le Rouzic, P., Corvol, H., *et al.* Alveolar epithelial cells: master regulators of lung homeostasis. *Int. J. Biochem. Cell Biol.* **45,** 2568–73 (2013).

57. Fehrenbach, H. Alveolar epithelial type II cell: defender of the alveolus revisited. *Respir. Res.* **2,** 33–46 (2001).

58. Mason, R. J. Biology of alveolar type II cells. *Respirology* **11,** S12–S15 (2006).

59. Aragona, M., Panciera, T., Manfrin, A., Giulitti, S., Michielin, F., Elvassore, N., *et al.* A mechanical checkpoint controls multicellular growth through YAP/TAZ regulation by actin-processing factors. *Cell* **154,** 1047–1059 (2013).

60. Lutolf, M. P., Lauer-Fields, J. L., Schmoekel, H. G., Metters, A. T., Weber, F. E., Fields, G. B., *et al.* Synthetic matrix metalloproteinase-sensitive hydrogels for the conduction of tissue regeneration: engineering cell-invasion characteristics. *Proc. Natl. Acad. Sci. U. S. A.* **100,** 5413–8 (2003).

61. Fairbanks, B. D., Schwartz, M. P., Halevi, A. E., Nuttelman, C. R., Bowman, C. N. & Anseth, K. S. A Versatile Synthetic Extracellular Matrix Mimic via Thiol-Norbornene Photopolymerization. *Adv. Mater.* **21,** 5005–5010 (2009).

62. Pardo, A., Gibson, K., Cisneros, J., Richards, T. J., Yang, Y., Becerril, C., *et al.* Up-regulation and profibrotic role of osteopontin in human idiopathic pulmonary fibrosis. *PLoS Med.* **2,** 0891–0903 (2005).

8.9 Supplementary data

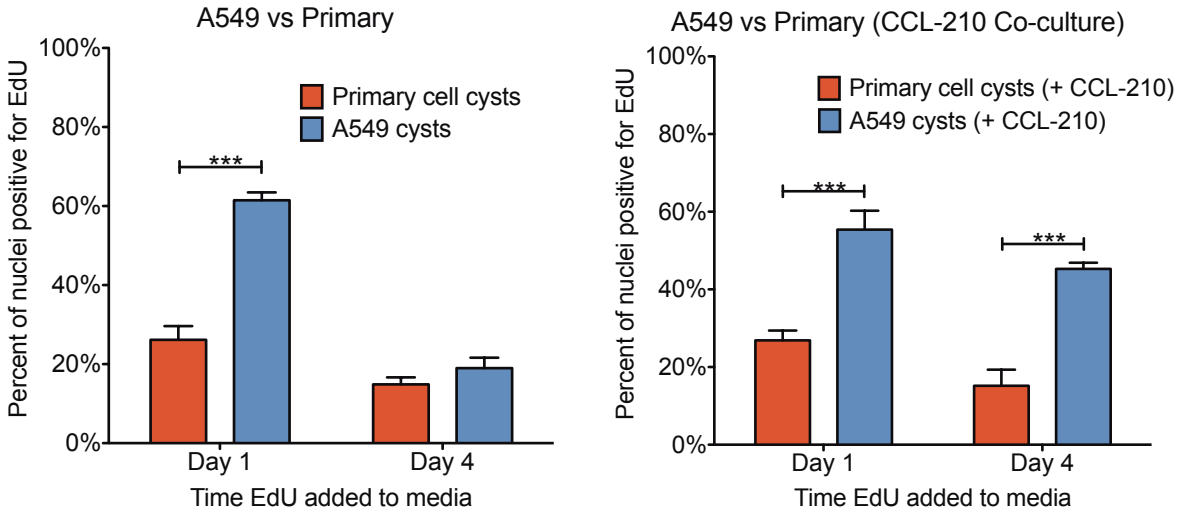

Supplementary Figure 8.1 Plots depict percent of nuclei positive for EdU at the two time points comparing healthy versus cancer epithelial cells, separated by monoculture and co-culture condition. Results are presented as means ± SEM of three biological replicates of each condition. ***$p < 0.001$

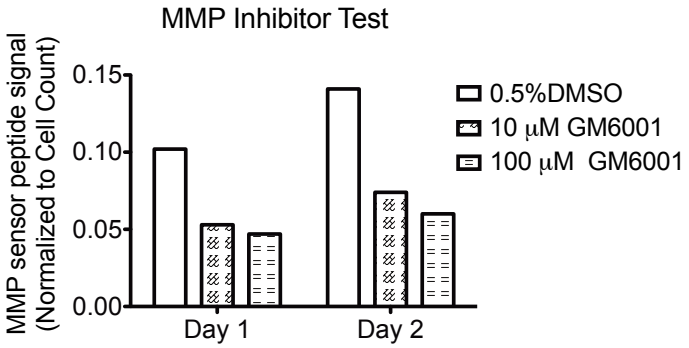

Supplementary Figure 8.2 MMP activity on days 1 and 2 after encapsulation as measured by an MMP-sensitive fluorescent sensor peptide normalized to cell count for A549/CCL-210 co-cultures exposed to either 0.5% DMSO, 10 μM GM6001 or 100 μM GM6001 in the media.

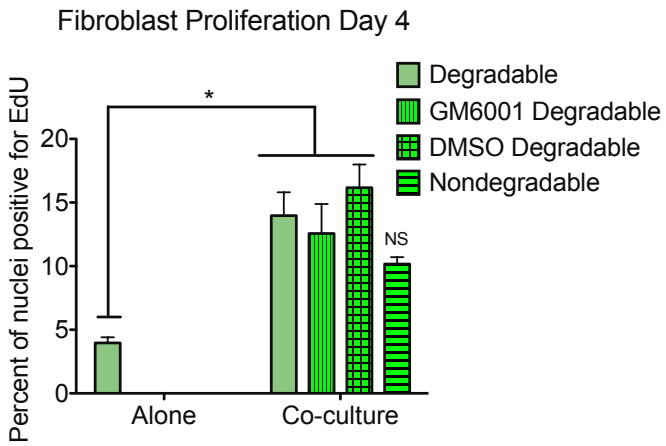

Supplementary Figure 8.3 Click-iT Plus EdU proliferation assay. Plot depicts percent of fibroblast nuclei positive for EdU on day 4 in monoculture and the A549/CCL-210 co-cultures, separated by gel and media type. The degradable bars refer to the original experiment in MMP-degradable gels with regular growth media. GM6001 was added at 10 μM, and the DMSO control media contained 0.05% DMSO. The nondegradable gels contained a peptide crosslinker insensitive to MMP cleavage. Results are presented as means ± SEM of three biological replicates of each condition. *$p < 0.05$, NS = not significant